Université de Montréal

Mechanics of cell growth and tissue architecture in plants

par
Amirhossein Jafari Bidhendi

Département de Sciences Biologiques, Institut de Recherche en Biologie Végétale
Faculté des Arts et des Sciences

Thèse présentée à la Faculté des Arts et des Sciences
en vue de l'obtention du grade de doctorat
en sciences biologiques

April 2018

Résumé

Le développement des plantes nécessite la coordination des mécanismes de différenciation des cellules méristématiques en cellules hautement spécialisées: la division, la croissance et la formation de la géométrie cellulaire. La différenciation et la morphogenèse cellulaires sont étroitement liées et régulées par les propriétés mécaniques de la paroi cellulaire. Les mécanismes conduisant à l'émergence de diverses formes et fonctions des tissus végétaux sont complexes et encore peu compris. Ma thèse de doctorat approfondie les principes mécaniques à la base de la formation des cellules épidermiques ondulées. Je me suis également penché sur l'étude des avantages mécaniques que confèrent les motifs imbriqués.

Les cellules épidermiques sont constituées de deux parois cellulaires périclines parallèles reliées par des parois anticlines. Aux jonctions, les cellules épidermiques forment des cavités et des saillies imbriquées les unes aux autres. Des images en 3D, prises en microscopie confocale, de cotylédons marqués par des fluorophores spécifiques à la cellulose montrent une déposition accrue de cellulose au niveau des cavités des parois périclines s'étendant le long des parois anticlines. Le marquage des cotylédons par COS^{488} démontre également une plus grande abondance de pectines dé-estérifiées aux mêmes sites. J'ai développé des modèles par éléments finis de la déformation de la paroi cellulaire et simulé les disparités biochimiques en alternant les régions plus rigides à travers et au long des parois périclines des deux côtés d'une paroi anticline. Le modèle montre que les parois rigidifiées non déformables se développent en cavités lorsque la pression interne étire la paroi cellulaire. Le modèle suggère également la présence de contraintes mécaniques plus élevées au niveau des saillies. Les résultats du modèle indiquent qu'une boucle de rétroaction positive entre la contrainte et la rigidité de la paroi cellulaire générerait les formes ondulées à partir de différences infinitésimales de rigidité ou de contrainte de la paroi cellulaire. En outre, le modèle suggère que des événements de flambage stochastiques peuvent initier la morphogenèse des cellules.

On a longtemps émis l'hypothèse que le motif imbriqué de cellules épidermiques améliore l'adhérence cellule-cellule et donc la résistance de traction de l'épiderme. L'étirage des feuilles d'*Arabidopsis* de type sauvage ou du mutant *any1* (caractérisé par une réduction de l'ondulation cellulaire) n'a montré aucun détachement cellulaire en cas de rupture du tissu. J'ai

émis l'hypothèse que les jonctions des cellules ondulantes renforcent la résistance de l'épiderme contre la propagation de fissures. J'ai observé une grande anisotropie dans la réponse mécanique à la rupture de l'épiderme d'oignon selon l'orientation des cellules. Les fissures qui suivent l'alignement des cellules se propagent sans trop de résistance, entraînant une rupture fragile du tissu. Ceci découlerait de la propagation de la ligne de rupture par suite du détachement des cellules. Les fissures se propagent difficilement lorsqu'elles sont perpendiculaires à l'axe principal des cellules. En fracturant des feuilles dont les cellules épidermiques sont ondulées, j'ai remarqué que les fissures se propageaient, par intermittence, à la fois au niveau des jonctions de la cellule et de la paroi cellulaire. J'ai émis l'hypothèse que ce motif de fracture d'épiderme à cellules ondulées se caractérisait par une augmentation de la résistance à la fracture. Pour n'étudier que les effets de la géométrie des cellules sur cette résistance, j'ai éliminé le rôle que jouerait l'anisotropie des matériaux en concevant des modèles physiques macroscopiques de l'épiderme. J'ai gravé au laser des motifs cellulaires sur du poly-méthacrylate de méthyle. De cette façon, le matériau isotrope permettait d'étudier uniquement l'effet de la géométrie cellulaire. Alors que la fracturation des spécimens de contrôle sans gravure et des spécimens avec des cellules gravées longitudinalement ont démontré une rupture fragile, une fracturation transversale aux rangées cellulaires, dans les modèles mimant des cellules d'oignon ou des cellules ondulées de cotylédons d'*Arabidopsis*, a montré une résistance accrue à la fracture.

En conclusion, je démontre que la forme ondulée des cellules épidermiques est le résultat d'une distribution alternée de la rigidité dans la paroi cellulaire, un processus qui pourrait être initié par une anisotropie de stress stochastique due au flambement. De plus, ces formes cellulaires augmentent la résistance à la rupture de l'épiderme végétal en le protégeant contre la propagation des fissures; un mécanisme de défense ingénieux pour les surfaces les plus exposées.

Mots-clés: géométrie des cellules végétales, morphogenèse, mécanique cellulaire, analyse par éléments finis, cellulose, pectine, développement, ténacité à la rupture, résistance à la déchirure, biomimétique

Abstract

Plant development entails cell division, cell growth and shaping, and the differentiation of meristematic cells into highly specialized cell types. Differentiation and cell shape are closely linked and involve the regulation of the mechanical properties of the cell wall. The mechanisms leading to the generation of the diverse array of shapes and functionalities found in plant tissues are perplexing and poorly understood. In my Ph.D. research, I investigated the mechanical principles underlying the formation of wavy leaf pavement cells. Further, I studied the putative mechanical advantage that emerges from the interlocking patterns.

Epidermal pavement cells consist of two parallel periclinal walls connected by vertical anticlinal walls. At the borders, wavy pavement cells make interlocking indentations and protrusions. 3D confocal micrographs of cotyledons stained with cellulose-specific fluorophores revealed a significant accumulation of cellulose at the sites of indentation on the periclinal walls extending down the anticlinal walls. Staining the cotyledon samples with COS^{488} also suggested a higher abundance of de-esterified pectin at these sites. I developed finite element models of the cell wall deformation and simulated the biochemical inhomogeneities by assigning alternately stiffened regions across and along the periclinal walls on two sides of an anticlinal wall. It was observed that the non-deforming stiffened regions develop into sites of indentations when the internal pressure stretches the cell wall. The model also suggested higher stresses to associate with the neck regions. The model results indicate that a positive feedback loop between stress and cell wall stiffness could generate wavy shapes starting from infinitesimally small differences in cell wall stiffness or stress. Further, the model suggests that stochastic buckling events can initiate the cell shaping process.

It has been long hypothesized that the interlocking pattern of pavement cells improves cell-cell adhesion and thus the tensile strength of the epidermis. Stretching to rupture the leaf samples of wild-type *Arabidopsis* or *any1* mutant with reduced cell waviness did not show any cell detachment upon failure. However, I hypothesized the undulating cell borders could enhance the resistance of the epidermis against the propagation of damage. I observed a considerable anisotropy in the tear behavior of onion epidermis parallel and perpendicular to the cells' main axis. Tears along the cell lines propagated without much resistance resulting in brittle

failure of the tissue. This was observed to originate from tears propagating by cell detachment. Perpendicular to the cells' main axis, tears had considerable difficulty in propagating. Fracturing the leaf samples with wavy epidermal cells, I noticed the cracks propagated in both the cell borders and the cell wall intermittently. I hypothesized that this pattern of fracture in the epidermis with wavy cells indicates an increase in the fracture toughness. To untangle the influence of material anisotropy from the cell geometry on fracture toughness, I designed macroscopic physical models of the epidermis by laser engraving the cell patterns on polymethylmethacrylate. This way, the isotropic material would allow studying only the effect of cell geometry. While fracturing the control specimens with no engraving and the specimens with longitudinally placed cells demonstrated a brittle fracture, fractures transverse to cell lines in the onion cell patterns or across the *Arabidopsis* cotyledon wavy cell pattern showed an increased fracture toughness.

I suggest the wavy shape of pavement cells in the epidermis results from the alternate placement of stiffer regions in the cell wall, a process that can initiate from a stochastic stress anisotropy due to buckling. Further, these shapes increase the fracture toughness of the plant epidermis protecting it against the spread of damage; an ingenious defense mechanism at the most exposed surfaces.

Keywords: plant cell shape, morphogenesis, cell mechanics, finite element analysis, cellulose, pectin, development, fracture toughness, tear resistance, biomimetic

Table of contents

List of figures

expansion to simulate higher growth rate; the right end of the wall may move in space. **B)** Differential expansion of the layers results in the formation of a curvature with the faster-expanding layer forming a convex curve. **C)** Finite element model of the walls of two adjacent cells. Only anticlinal walls are considered; loads are applied on internal surfaces of the walls. **D)** In the presence of differential pressures and uniform anticlinal wall stiffness the anticlinal wall forms a second order curve into the cell with lower pressure. Heatmap represents stress. **E)** A spatially confined region (green) in the anticlinal wall is assigned a softer value than the default stiffness (gray). **F)** A turgor differential results in the formation of a local protrusion into the cell with lower turgor. **G)** Periclinal walls are added to the model. **H)** When periclinal walls have isotropic material properties, the cell with the higher turgor pressure forms a more pronounced swelling in Z pulling the anticlinal walls inwards. **I)** Anticlinal wall model designed to possess alternating zones of stiffening across and along the wall. At one end of the geometry a fixed boundary condition is set while the other end is stretched. **J)** For a stiffness ratio of 100:1 between the stiff and soft segments, slight waves appear in the anticlinal wall when stretched. The strain and stresses shown in the magnified top view demonstrate that the waves are produced due to local moments produced by the abrupt change in the material stiffness. The magnitude of a wave does not exceed 0.3 times the cell wall thickness. The maximum is observed at small strains. At higher strain values the minute bends flatten out. In this model, the stress (shown as von Mises stress) is higher in the lobe (protrusion) side of the wall. 70

Figure 4-3. Finite element simulation of stresses and resulting deformations upon load application through turgor pressure. **A)** Multicell finite element model used to assess stress pattern in the anticlinal walls between hexagonal cells. The red square marks the anticlinal wall that is shown isolated in B and C to reveal stresses. In this wall, stress components in vertical direction **(B)** are significantly larger than in horizontal direction (**C**). **B-1)** Color-coded distribution of vertical (Z direction) component of wall stress. **B-2)** The arrows indicate the magnitude and direction of the vertical stress. **C-1)** Color-coded distribution of axial (X direction) component of wall stress. **C-2)** The arrows indicating axial stress in horizontal direction show the compressive stresses resulting from the vertical expansion. Stress values are relative as normalized input values are used in models (see modeling procedures and supplemental information). **D)** Position of segment crossing two adjacent cells modeled in **E-N**. Segment comprising sections of the periclinal walls of the two adjacent cells and the shared

inhomogeneity in the periclinal wall can cause locally elevated stress in the connected wall transmitting the stresses between the inner and outer cell walls. **C)** Oblique view of a z-stack 3D reconstruction of pavement cells from *Arabidopsis thaliana* GFP-MAP4 line excluding periclinal walls demonstrating cortical anticlinal microtubules. **D)** Dual channel image of propidium iodide (green) and GFP-MAP4 (orange) showing that cortical anticlinal microtubules appear more abundantly on the neck side of the undulations. **E** and **F)** Cortical periclinal microtubules visualized in cotyledons of the *Arabidopsis thaliana* GFP-MAP4 line 4 (**E**) and 1 DAG (**F**). At both stages, microtubule density on the opposite sides of corresponding lobe-neck pairs is different with higher density at the neck side. However, this difference is less pronounced in earlier developmental stages (white arrows in **F)**. At 4 DAG microtubules appear to be bundled in necks while they are scarce in lobes. Occasionally microtubule bundles reach the tips of a lobe. The images do not correspond to the same cotyledon. Scale bars = 10 μm. **G) G-1)** A closed-box model of a hollow cell with turgor pressure applied to inner face of the outer periclinal wall. Turgor pressure was not applied to lateral walls as equal pressures were shown in previous models to cancel each other out from two sides in a multicell context and only result in compression of the wall thickness. Inner periclinal wall was prevented from out or inward displacement to simulate attachment to mesophyll layer. **G-2)** A buckling mode from the linear buckling analysis demonstrating folding of the cell border in both periclinal and anticlinal walls. Interestingly, the model suggests the location of indentation on periclinal walls to bulge out of plane which is consistent with microscopic observations of pavement cells. **H)** A schematic of the model with mechanical buckling acting as a morphogenetic cue initiating the mechanical and growth anisotropy. **H-1)**. Compressive stress in anticlinal walls arises due to internal pressure bulging out periclinal walls or from the growth in the cellular environment such as by matrix swelling. **H-2)** Stress inhomogeneities arisen due to buckling mark stress hotspots that trigger local bundling of microtubules (**H-3)** and reinforcement of the cell wall by cellulose deposition and alterations in pectin esterification in necks. This further develops the protrusions at undulating borders (**H-4)**. 93

Figure 4-8S. Finite element models designed to investigate the effect of anticlinal wall stiffness modulation and turgor pressure differential on cell shape. **A)** Relative dimensions in the model focusing on anticlinal wall between adjacent cells; only half of each cell is modeled with symmetry boundary conditions. **B)** Deformation of two cells with isotropic material properties

perpendicular to the original cut. All following figures are for type (A) loading scenario, although similar outcomes were observed in type (B) loading. **C)** SEM micrographs showing a local change of tear path from transverse (to cell axis) to longitudinal. **D)** Tear oriented along the cell axis continues a fairly straight path. **E)** Micrograph depicting a transverse blade notch immediately turning close to 90° and then continuing in an oblique path. **F)** and **G)** Transverse tear becoming oblique and later aligning with cells long axis. **H)** In a few rare cases, transverse tears did not deviate or reorient but continued a straight path transversely to cell axes. In these cases, a rough tear surface could be observed with tissue segments bridging the crack. The dotted red arrows mark the tear path. The beginning of the arrows marked with a red-rhombus show the direction, orientation but not the exact distance of the original blade-cut with respect to the image frame. The stars in (E) mark the location of a sharp tear reorientation. Scale bars = 1 mm except for (G, H) = 500 μm and (C) = 100 μm. 132

List of abbreviations

AFM: atomic force microscopy

any1: *anisotropy1*

ARP: actin-related protein

ASTM: American Society for Testing and Materials

AUX1: Auxin resistant 1

CAD: computer aided design

CESA: cellulose synthases

CGA: 1-cyclohexyl-5-(2,3,4,5,6-pentafluorophenoxy)-1λ4,2,4,6-thiatriazin-3-amine

COS^{488}: chitosan oligosaccharides conjugate with Alexa ^{488}

CSI1: cellulose synthase interactive protein 1

CT: compact tension

DAG: days after germination

DIC: digital image correlation

DMSO: dimethyl sulfoxide

FE/FEM/FEA: finite element/ finite element method/ finite element analysis

GFP: green fluorescent protein

GPa: gigapascal

HG: homogalacturonan

ISO: International Organization of Standardization

LFM: lateral force microscopy

LVDT: linear variable differential transformer

MAP: microtubule-associated protein

MEMS: microelectromechanical systems

mg: milligram

min: minute

mL: milliliter

mm: millimeter

mM: millimolar

MPa: megapascal

MS: Murashige and Skoog

nm: nanometer

PBS: phosphate buffer saline

PDMS: polydimethylsiloxane

PFS: pontamine Fast Scarlet 4B

PG: polygalacturonase

PIN1: Peptidyl-prolyl cis-trans isomerase NIMA-interacting 1

PME: pectin methylesterases

PMEI: pectin Methylesterase Inhibitor

PMEIoe: pectin Methylesterase Inhibitor overexpression

PMMA: polymethylmethacrylate

PPI: pixels per inch

RGI: rhamnogalacturonan I

RGII: rhamnogalacturonan II

ROS: reactive oxygen species

RVE: representative volume element;

S4B: Pontamine Fast Scarlet 4B

SEM: scanning electron microscope

TUB: tubulin

v/v: volume/volume

w/v: weight/volume

XET: xyloglucan endotransglycosylases

μm: micrometer

μM: micromolar

To my family

Acknowledgements

I would like to express my heartfelt gratitude to my supervisor, Dr. Anja Geitmann for setting me in the road of the research I did, for her patience, for believing in me and supporting me for all these years. By trusting me at her lab, Anja opened to me the gates toward the fantastic world of molecular cell biology. This profoundly transformed my life perspectives. With her profound insight in both biology and mechanics, she instructed me how to do research, and how to convey my thoughts. She has continuously been a role model for me inspiring me in many aspects of academic and non-academic life.

I thank Dr. Frédérick Gosselin from the Polytechnique Montréal. He graciously accepted to advise me as a member of my committee. I frequented Frédérick 's office many times throughout the years and discussed many aspects of my projects with him. I always enjoyed and appreciated his valuable insight. I am thankful to Dr. Mario Cappadocia for his kind, fatherly support, and advice. Mario enlightened me in so many ways, on academic life, opera and life.

I would like to thank Ms. Louise Pelletier for her patience and help. Louise provided me with valuable insight in sample preparation and imaging sessions with the scanning and transmission electron microscopes in my initial years of Ph.D. study. I enjoyed working with her and wish her all the best. I thank Mss. Anne-Marie Gagné and Annie Aubin for their friendly support throughout my Ph.D. years. They greatly helped me with the administrative matters in all these years.

I thank my teammates and friends in the lab; the ones that have left the lab and those that are present. Their support and amity made the years of my stay in the lab a gratifying experience. I have learned abundantly from everyone throughout these years. I thank Dr. Youssef Chebli for always being there to help with the issues related to the lab and answering my numerous questions on various procedures and protocols. Similarly, I would like to thank Bara Altartouri, for the countless hours of fruitful and unforgettable talks on the project. Many late working hours and commutes back home were made greatly pleasurable due to his company and the exchange of ideas we had. I learned considerably from Bara regarding sample preparation and the lab works and relished his friendship for all these years. I would like to thank Dr. Shafayet Zamil. Shafayet with his high spirits and insight on various technical topics inspired me in many

cases. He is always a positive force in difficult times. I would also like to thank Dr. Hana Rakusova and Dr. Yuki Hamamura, two of my best colleagues for their support in these years.

I would especially like to thank my dear partner, Anahid. Anahid stood by my side and supported me in the years of my Ph.D. despite many late nights of coming back from the laboratory and my very odd working hours. Without her love, support, and patience this work could never be completed. I am always grateful to my parents and my little sister, Leila, the never-diminishing lights in my life. Forever, I will be indebted to their non-ending love and encouragement. I cannot thank them sufficiently.

Chapter 1: General Introduction

The cell wall, a polysaccharide-rich layer that envelopes plant cells, is the dominant feature distinguishing plant and animal cell attributes. The significance of the cell wall in determining the physical properties of plant cells is evident from the convergence of rheologies across kingdoms upon removal of the cell wall (Durand-Smet et al., 2014). Depending on cell type and developmental stage, the cell wall can comprise multiple layers. The primary cell wall is produced at the surface of the plasma membrane in young cells and in soft tissues such as fruit parenchyma. In harder tissues such as wood, a secondary cell wall is added between the primary cell wall and the plasma membrane. The secondary wall is deposited only in maturing cells once cell expansion has ceased. Therefore, any investigation of cell shaping and morphogenesis focuses on the primary cell wall. Unlike animal cells that can move propelled by forces generated by the cytoskeleton, the stiffness of the cell wall prevents cytoskeletal forces from affecting cell shape directly. The small forces required to stall the polymerization of actin (Footer et al., 2007), although adequate to deform the plasma membrane, are unlikely to be of a magnitude capable of affecting the plant cell wall. Instead, to shape the cell or to move, the plant cell relies on deformation of the cell wall under a sustained internal pressure. Thus, the wall gives plant cells more permanent shapes compared to their pliable animal counterparts. Growth along a particular axis is realized by anisotropies in the mechanical properties of the cell wall (Bidhendi and Geitmann, 2016; Geitmann and Ortega, 2009). Growth of the plant cell has been thought to result from cell wall loosening (e.g., by expansin proteins) and relaxation under turgor maintained by water uptake. Plant cell shape change is also strictly governed by the cell wall mechanics. This is demonstrated in both short-range reversible deformation of guard cells, long-range invasive growth of pollen tubes, or high-speed deformations and of the pericarp in ballistochory (Amsbury et al., 2016; Bidhendi and Geitmann, 2018a; Chebli et al., 2012; Cooke et al., 1976; Cosgrove, 2018; Hofhuis et al., 2016). Mechanical properties of the cell wall are regulated by its biochemical composition. In chapter 2, I provide an overview of the main constituents of the primary cell wall and their mechanical implications for cell wall and cell growth. I include in these considerations the material that connects plant cells in a tissue—the middle lamella, a thin layer formed mostly from pectins during the generation of the cell plate

and acting as glue preventing the relative displacement of cells. Cell-cell adhesions have to be overcome in situations where plant cells have to separate, such as in the pistil to accommodate the penetration of the pollen tube (Cheung et al., 2010). On the other hand, cell adhesion must be sufficiently strong to secure the integrity of the tissue.

The cell wall also plays a role in the ability of plant cells to sense and respond to mechanical cues. Mechanical forces act as signals that can trigger subcellular events such as cytoskeletal polarization, cell division or ion channel activity (Bringmann and Bergmann, 2017; Buckingham et al., 2005; Elliott and Shaw, 2018; Hamant et al., 2008; Maathuis, 2011). For external mechanical triggers to initiate an intracellular response, the cell wall acts as an intermediary, as its deformation or physical damage are the mechanical events that are translated into an effect at the membrane level. Cell wall mechanics, therefore, has gained considerable attention with regard to plant development and reproduction.

The understanding of plant cell mechanics has benefited from an interdisciplinary approach combining cell biology, micro-manipulation and theoretical modeling. Models are physical or mathematical representations of a system aimed at simplifying the problem focusing on the aspects vital to the phenomenon being investigated. Mathematical modeling of plant cells has taken various levels of complexity. Models vary from versions of the Lockhart equation trying to correlate the cell growth to wall extensibility and water uptake, to 3D representations incorporating realistic shapes and sophisticated material behaviors exploring cell and tissue mechanics (Amsbury et al., 2016; Bidhendi and Geitmann, 2018a; Carter et al., 2017; Cooke et al., 1976; Fayant et al., 2010; Geitmann and Ortega, 2009; Hofhuis et al., 2016; Majda et al., 2017; Sapala et al., 2018). Predictive modeling is employed to test the influence of one or more parameters on the outcome of a virtual experiment and allows resolving the contributions of intertwined factors. For instance, Fayant et al. (2010) studied how the stiffness gradients at the tip of the growing pollen tube affect its morphology, and the authors were able to validate the predictions using novel experimental data on the biochemical profile of the cell wall. Similarly, Yanagisawa et al. (2015) studied how mechanical anisotropy is expected to be regulated in a trichome branch to achieve the microscopically observed branch shapes. The value of such models lies in their predictive power allowing experimental validation, and their ability to guide biologists into novel ways of interpreting their data and in the design of future experiments.

Furthermore, these models can be used to study parameters that cannot or are impractical to be addressed empirically. Modeling can also be employed to interpret the outcomes of experimental techniques. Application of engineering principles and techniques has improved our knowledge of plant cell biology. They have helped clarify the effect of hydrolytic enzymes on cell wall extensibility, how the cell wall of a pollen tube maintains its shape or how pectin and cell wall mechanics change during organogenesis (Bolduc et al., 2006; Braybrook and Peaucelle, 2013; Cameron and Geitmann, 2018; Cosgrove, 1997, 2015; Milani et al., 2013; Sanati Nezhad et al., 2013). The mechanical techniques adapted to the study of plant cells are diverse in scope and in the nature of their measurements and their working environment. These methods range from indentation techniques to micro and nanofabrication-based microelectromechanical systems (MEMS) and lab-on-chip devices that allow for mechanical characterization of cells at micron scales. Models are needed to interpret the results obtained with these techniques, and the outcome of these experiments can be used to inform the predictive models. In Annex 1, I outline the mechanical methods relevant for the investigation of the mechanics of plant cells. One of the principal methods of mechanical characterization is tensile testing. This technique is employed in my research and is not technically trivial when used on tiny and soft plant samples. I provide an overview of this technique with regard to its application for the mechanical characterization of the plant cell wall in Annex 2. Several mathematical approaches are used to solve the boundary values problems arising in describing the behavior of the materials. The finite element method is a powerful mathematical approach that is widely applied to solve nonlinear mechanical and structural problems with complex geometries (Baker, 2012). This numerical technique has been used in predictive modeling and interpretation of mechanical tests on plant cells. In chapter 3, I provide an overview of the state-of-the-art in finite element modeling as it has been employed to investigate the mechanics and morphogenesis of the plant cells.

The plant epidermis is the most conspicuous plant tissue. Aside from the various considerations pertaining to its specific function, it makes an ideal tissue for fundamental research on plant cell functioning in general. This is simply due to being the most accessible layer facilitating observations and treatments. As a result, multiple mechanical and modeling attempts have been focused on exploring the mechanics of the epidermis. The plant epidermis

develops during embryogenesis and covers the plant organs throughout development. How the cells in the outer layer of the embryo differentiate and acquire properties distinct from the inner layers is not well understood. In *Arabidopsis*, epidermis differentiation is partly attributed to genes such as *AtML1* and *PDF2* with their expressions restricted to the outer cells in later stages of embryonic development (Javelle et al., 2011; Ogawa et al., 2015; Takada et al., 2013). The protective role of the epidermis, as the plant skin, is intuitive. The properties of the epidermis are dynamic and can be affected by the environmental cues through its development. For instance, *AtML1* and *PDF2,* suggested to be governed by AtDEK1, are speculated to be influenced by extracellular signals (Javelle et al., 2011; Johnson et al., 2005; Ogawa et al., 2015). Even cell fate in the epidermis is affected by environmental factors such as the development of guard cells which is influenced by light intensity and CO_2 concentration (Casson and Gray, 2008). The protective functions of the epidermis are achieved through a variety of mechanical and chemical features. Plant trichomes, for example, are employed for defense purposes against biotic and abiotic stress. They protect from drought by contributing to moisture retention, and they are used to deter herbivores through either their mechanical or chemical features (Amada et al., 2017; Oelschlägel et al., 2009). The cuticle, a lipid-rich hydrophobic layer is a natural secretion of the epidermis produced by most aerial plant organs. While the protective role of the cuticle specifically against water-soluble contaminants is intuitive, its many functions may also include signaling (Fernández et al., 2016; Javelle et al., 2011; Serrano et al., 2014; Yeats and Rose, 2013). The epidermal tissue is also implicated in the control of growth of the underlying layers as evinced by the existence of tissue stress due to growth differentials between the epidermis and the layers underneath (Baskin and Jensen, 2013; Peters and Tomos, 2000). Depending on species and organ these roles may differ as both roles of restriction and promotion of growth have been suggested (Savaldi-Goldstein et al., 2007). Therefore, mechanical investigation of how the epidermis grows and how it affects the mechanics of the whole plant is vital in a developmental context. On the leaf epidermis of many plants, the epidermal cell borders form wavy outlines that generate interlocking patterns. The genesis of these shapes in pavement cells is not well understood. Further, the correlation between these shapes and the cells' functions has remained elusive. These have instigated much interest, resulting in intense biological and mechanical research in the past few years (Armour et al., 2015; Fu et al., 2005; Jacques et al., 2014; Majda et al., 2017; Panteris and Galatis, 2005; Sampathkumar et al., 2014a;

Sapala et al., 2018; Zhang et al., 2011). In chapter 4, using microscopic observations of the cell wall composition and the finite element-based mechanical models of the cell wall, I scrutinize the mechanical basis of shape formation in pavement cells. In chapter 5, I examine how the wavy interdigitating shape of pavement cells can act to protect the leaf surface.

Chapter 2: Relating the mechanics of the primary plant cell wall to morphogenesis

Amir J Bidhendi[1], Anja Geitmann[1,2,*]

[1]Institut de Recherche en Biologie Végétale, Département de sciences biologiques

Université de Montréal, Montreal, Quebec, H1X 2B2, Canada

[2]Department of Plant Science, McGill University, Macdonald Campus, 21111 Lakeshore, Ste-Anne-de-Bellevue, Québec H9X 3V9, Canada

*Address correspondence to: Anja Geitmann (geitmann.aes@mcgill.ca)

This is a pre-copyedited, author-produced version of an article by Bidhendi and Geitmann (2016) published in Journal of Experimental Botany following peer review. The version of record is available online at: https://academic.oup.com/jxb/article/67/2/449/2884961/Relating-the-mechanics-of-the-primary-plant-cell, doi.org/10.1093/jxb/erv535

2.1 Abstract

Regulation of the mechanical properties of the cell wall is a key parameter used by plants to control the growth behavior of individual cells and tissues. Modulation of the mechanical properties occurs through the control of the biochemical composition and the degree and nature of interlinking between cell wall polysaccharides. Preferentially oriented cellulose microfibrils restrict cellular expansive growth, but recent evidence suggests that this may not be the trigger for anisotropic growth. Instead, non-uniform softening through the modulation of pectin chemistry may be an initial step that precedes stress-induced stiffening of the wall through cellulose. Here we briefly review the major cell wall polysaccharides and their putative contributions to primary cell wall mechanics.

2.2 Introduction

The plant cell is encapsulated in a more or less stiff extracellular matrix, the cell wall. While the physical properties of mammalian cells and their interactions with their environment are largely determined by the cytoskeletal network, in plants the cell wall dominates the mechanical behavior of the cell—even in the case of young and undifferentiated cells. This is readily demonstrated by the fact that once the cell wall is removed from a plant protoplast, the rheological properties of the latter are similar to those of animal cells (Durand-Smet et al., 2014). Even rapidly growing cells with thin, primary cell walls such as pollen tubes can exhibit an apparent stiffness that is orders of magnitude higher than that of animal cells (Jones et al., 1999; Nguyen et al., 2010; Sanati Nezhad et al., 2013). It should be noted, however, that while plant cells are stiffer, a substantial portion of the apparent cellular stiffness in walled cells may derive from the turgor pressure that acts as a hydroskeleton (Deng et al., 2011; Forouzesh et al., 2013). The measurement of apparent cellular stiffness therefore does not allow for straightforward deduction of the material properties of the wall.

The differences in mechanical behavior between plant and animal cells have significant implications for the mechanics of processes such as cellular growth and morphogenesis that occur during tissue differentiation. In plant cells these processes are governed by the mechanical properties of the wall which serve as modulating parameters. While plant cell expansion *per se* is driven by turgor pressure, the spatio-temporal control of the process relies on the mechanics

of the cell wall (Geitmann and Ortega, 2009). The cell wall not only confines the growth behavior of the individual cell but also regulates the development of the entire tissue, since neighboring cells are tightly connected at their shared walls. Generally, plant cells do not detach, slide, or move past each other, and the architecture of a plant tissue is therefore much less malleable than that of an animal organ in which cells can migrate over significant distances. Exceptions exist; for example, invasively growing plant cells can separate cell-cell connections in order to pass through the created spaces; and tissues with developmentally generated air spaces require locally controlled cell detachment. In the present review we will focus on the mechanics of the primary cell wall in early phases of plant cell morphogenesis and organogenesis when cells are tightly attached to each other. The contribution of individual cell wall components to the mechanical behavior of the overall wall material is reviewed in the context of plant morphogenetic processes.

2.3 The degree of pectin methylesterification cannot be used as a proxy to predict cell wall mechanical properties

Plant cell walls consist of a network of interconnected polymers with diverse biochemical and mechanical properties. Because of its complex structure, the cell wall has been compared with a composite material, underscoring the fact that different polymers play different roles in terms of mechanical behavior of the overall structure. The behavior of isolated polymers has only very limited predictive power in terms of the behavior of the complex and heterogeneous structure enveloping the living cell, however. Cross-links and other interactions between biopolymers render the behavior of the material both complex and also versatile. Nevertheless, general principles can be deciphered by characterizing the functionalities of its individual wall components.

An important group of polymers in the primary plant cell wall are pectins. These polymers have been considered to act as a gel, forming an amorphous substrate into which a structural network consisting of cellulose and hemicelluloses is embedded. The principal pectin species are homogalacturonan (HG), rhamnogalacturonan I (RG-I), and rhamnogalacturonan II (RG-II) that can be covalently linked to each other (Caffall and Mohnen, 2009; Ridley et al.,

2001). Pectins are synthesized in the Golgi apparatus and transferred to the extracellular space by secretion (Mohnen, 2008).

HG pectin is a linear polymer with 1,4-linked α-D-galacturonic acid residues and is the most abundant type, representing more than 60% of pectins in the cell wall (Caffall and Mohnen, 2009). HG pectins are secreted in highly methylated form (Micheli, 2001; Wolf et al., 2009). De-esterification by pectin methylesterases (PMEs) typically occurs *in muro* (in the wall), and this process changes the mechanical properties of pectin because it enables cross-linking by positively charged calcium ions. Paradoxically, the de-esterification of pectin has been linked with both increased and decreased cell wall stiffness *in vivo* (Palin and Geitmann, 2012). In the pollen tube, the apical end of the cell displays highly methylesterified pectin which has been correlated with softer mechanics and is consistent with the physical requirements of the rapid growth behavior of this subcellular region (Chebli et al., 2012; Vogler et al., 2013; Zerzour et al., 2009). In the *Arabidopsis thaliana* shoot apical meristem, on the other hand, decreased stiffness was found in locations displaying de-methylesterified pectins and is reported as a necessary prerequisite for organogenesis (Braybrook and Peaucelle, 2013; Kierzkowski et al., 2012; Peaucelle et al., 2011; Wolf et al., 2012). This apparent contradiction may be explained by different actions of the respective PMEs involved. The molecular pattern of pectin demethylation can occur in a blockwise or non-blockwise manner, and parameters such as pH, initial stage of methylesterification, and cation concentration are thought to influence the mode of HG de-esterification (Osorio et al., 2008). In blockwise de-esterification, PME acts continuously on galacturonic acid residues, removing the methoxyl group, resulting in a continuous region of de-esterified pectin. It is suggested that continuous demethylation of more than nine galacturonic acid residues allows strands of pectin to be linked more efficiently by Ca^{2+} bonds, leading to gelation and enhanced stiffness of the material (Willats et al., 2001a; Wolf and Greiner, 2012). This is supported by experimental evidence, showing that the application of exogenous calcium to onion scale cell walls and to cell wall fractions of herbaceous peony inflorescence stem results in increased stiffness in the cell walls (Li et al., 2012a; Xi et al., 2015). Elevated calcium concentrations also result in the cessation of pollen tube growth—presumably because of increased cell wall rigidity—whereas removal of calcium from the medium causes pollen tubes to burst due to compromised structural integrity of the cell

wall (Hepler and Winship, 2010; Picton and Steer, 1983). In non-blockwise mode demethylation, PME acts discontinuously on a pectic domain, resulting in less effective Ca^{2+} bridging over a given region. Moreover, when not bonded together via Ca^{2+} bridges, the de-esterified pectic chains might be more susceptible to degradation by polygalacturonases (PGs), which might be the process that eventually results in cell wall softening (Arancibia and Motsenbocker, 2006; Wakabayashi et al., 2003; Willats et al., 2001b). Further, the increased porosity resulting from the lack of cross-linking may facilitate the access of degrading/loosening enzymes as speculated in the case of fruit ripening (Brummell, 2006). Several studies have suggested the action of PMEs to precede that of PGs in cell wall softening during fruit ripening, although Redgwell *et al*. observed no causality between de-esterification and PG action (Arancibia and Motsenbocker, 2006; Redgwell et al., 1990; Wakabayashi et al., 2003). The authors speculate that rather than providing the PGs with a substrate, de-esterification may lead to cell wall loosening by decreasing the pH through the release of protons (Bosch and Hepler, 2005; Hall et al., 1993). The lowered pH is thought to activate wall loosening enzymes and agents such as expansins, resulting in increased extensibility of the cell wall and promotion of growth/creep (Suslov et al., 2015). Additional studies are clearly warranted to shed light on the modes of action of PME and PG in the context of pectin de-esterification and cell wall mechanics. Finally, demethylation can also promote hydration, and therefore reduction in cell wall stiffness (Wolf and Greiner, 2012), presumably through facilitating the relative slippage and unfolding of other cell wall polysaccharides. The challenge is to correlate the methylesterification status of pectin to the mechanics of the cell wall, implying that using standard molecular probes or pectin-specific antibodies to localize the methylated or de-esterified pectin domains *per se* is not a reliable proxy for the mechanical behavior of the specific region, but that actual mechanical tests are required to this end.

2.4 Alterations in the ratio of arabinan and galactan side chains in RG-Is affect the mechanical behavior of the cell wall

RG-Is are very complex, structurally heterogeneous, branched glycan domains with repeating units of [→2)-α-L-Rhap-(1→4)-α-D-GalpA-(1→] in the backbone. RG-I structure is highly versatile, even in a given tissue, and is sometimes thought to act as a scaffold to which other

pectic polysaccharides of HG and RG-II covalently bind, forming the pectin matrix (Vincken et al., 2003). In the primary cell wall, the side chains of RG-I may contain galactan, arabinan, and arabinogalactan, while RG-I found in seed mucilage is unbranched (Caffall and Mohnen, 2009). The relative abundance of RG-I compared with HG pectin depends on the source and extraction method (Yapo, 2011). Potato tuber walls are reported to consist of 36% dry weight RG-I, while suspension-cultured sycamore walls contain only ~7% (Caffall and Mohnen, 2009). The function of RG-I in determining the mechanical properties of the plant cell wall is only poorly understood even if it has been implicated in cell wall extensibility and firmness. Using RG-I-specific antibodies, McCartney et al. (2000) observed that in pea cotyledons galactan-rich RG-I appears at the inner face of the cell wall at later stages of development, while arabinan-rich RG-I as well as HG are present throughout development. Compression tests on pea cotyledons before and after appearance of galactan-rich RG-I revealed that cotyledons with galactan-rich cell walls were twice as stiff as those without detectable galactan-rich RG-I. However, it should be noted that in this study the contribution of galactan-rich RG-I to the observed increased stiffness was not clearly distinguished from potential changes in the content of cellulose or other cell wall polysaccharides. Further, (1→4)-β-D-galactan was observed to be associated with de-esterified HG. Since (1→4)-β-D-galactans are flexible chains, whether the increased stiffness is imparted by its interaction with other wall polysaccharides or by its effect on the hydration state of the cell wall is not clear. Jones et al. (2003) suggested that arabinan provides the stomatal wall with the flexibility required for its deformation, by preventing tight packing of HG pectin. Degradation of cell wall arabinan locks the stomatal movement which can be reversed experimentally by removal of HG pectin. This phenomenon may also be explained by the effect of RG-I side chains on the hydration status of the matrix, which I will discuss in the following sections. This is consistent with the observation that arabinan side chains extracted by enzymatic debranching of intact RG-I from potato can be hydrated more readily than galactan side chains (Larsen et al., 2011). Ulvskov et al. (2005) studied the mechanical properties of potato tuber tissues under compression in two transgenic lines with truncation in either the arabinan or galactan side chains. The authors suggested that the changes in structure of RG-I can affect the hydration status of the cell wall. Further, the line with affected galactan side chains was more prone to fail under compression, was more brittle, and had a shorter relaxation time in stress relaxation experiments when compared to the arabinan affected line and the wild-type.

The faster relaxation was speculated to be a result of depletion of a slow relaxing component of the cell wall, namely galactan. Although the pectic network has often been neglected in terms of its load-bearing capacity when compared with cellulose microfibrils, it can undeniably transmit and distribute loads through the cell wall in connections with the cellulose-hemicellulose network (McCann and Roberts, 1994) and might have higher sensitivity than the latter. Studying the behavior of the cell wall network in the epidermis of onion using two-dimensional Fourier-transform infrared spectroscopy, Wilson et al. (2000) showed that while pectin and cellulose-hemicellulose networks act relatively independently under mechanical stress, the pectin network is the first to sense the mechanical oscillations, rather than the more rigid cellulose fibers. A recent *in vitro* study of the interaction between cellulose from *Gluconacetobacter xylinus* and pectins with different neutral sugar contents suggests that in fact both pectin and cellulose contribute to load bearing during compression tests (Lin et al., 2016). Importantly, the authors suggest that binding of pectins with a high content of neutral sugar side chains to cellulose microfibrils is stronger than that of HG to cellulose, although the bonds were reversible upon washing or mechanical compression. In stress-strain curves of compression tests, for equivalent strains, pectin-cellulose composites tolerated higher stresses compared with pure cellulose specimens, indicating a contribution of pectins to load bearing. Nevertheless, it is not clear if the contribution of the pectin in resisting compressive loads is solely due to structural reinforcement of the cellulose composite or to the formation of a denser porous matrix that slows the flow of fluid within the material towards the outside. Interestingly, when compared with pure cellulose composite, the pectin-cellulose composites with higher compressive stiffness compared with released the highest amount of pectin under compression. This could be due to higher fluid pressure gradients within the specimens and resulting detachment of pectins. Further, considering that the cell wall in living plants is mainly under tension rather than other modes of mechanical deformation, it is interesting to know how tensile properties of these composites may relate to their compressive behavior. A recent study seems to suggests that pectin gels from RG-I can form hyperelastic hydrogels with nearly incompressible bulk behavior and stiffening under large deformations (Mikshina et al., 2015). If the RG-I network does indeed exhibit strain stiffening, its contribution in distributing the mechanical loads to the network of cellulose and other wall polysaccharides could be critical since it might have the ability to control cell wall expansion under large pressure and strain

conditions. RG-Is are a very complex class of polysaccharides with diverse functions that certainly deserve more attention in future studies as their influence on cell mechanics and growth might be more dramatic than we thought.

2.5 RG-II-borate cross-linking may be essential for polar growth

RG-II is a highly branched domain of pectin polysaccharides and constitutes <10% of primary cell walls in eudicots and is found in all vascular plants. RG-II is a highly complex structure with a HG backbone and (A–D) substituted side chains of oligosaccharides. Borate cross-links apiosyl residues in side chain A of RG-II monomers and forms apiose-borate-apiose diesters, increasing the stiffness of the wall as well as decreasing its porosity (Caffall and Mohnen, 2009; Dumont et al., 2014; Fleischer et al., 1999; Funakawa and Miwa, 2015). Interestingly, a recent study suggests that dimerization can occur in protoplasmic or newly secreted RG-IIs but not in those already existing in the cell wall (Chormova et al., 2014). Borate cross-linking is essential for the successful expansive growth of cells by providing the cell wall with proper mechanical strength. In the cell wall of *Arabidopsis* rosette leaves, >90% of RG-II content exists in dimer form. In plants of the *mur1* mutant, deficient in L-fucose, a monosaccharide found in RG-II, this percentage drops to 56%. This mutant exhibits dwarfed growth, reduced rosette leaf expansion, and reduced tensile strength of the stem due to a possible truncation of side chain A in RG-II (O'Neill et al., 2001; Ryden et al., 2003). Watering these plants with boric acid enhances leaf expansion by promoting dimerization of RG-II (O'Neill et al., 2001). The tensile modulus and tensile strength of hypocotyls of *mur1-1* grown in the presence of 2.6 mM boric acid are rescued by promoting dimerization of RG-II (Ryden et al., 2003). The tensile modulus and tensile strength correspond to the slope of the elastic portion and to the failing point of the stress-strain curve in a tensile test, respectively. In pollen tubes, changing the concentration of boric acid affects the growth rate in a similar fashion to Ca^{2+} (Holdaway-Clarke et al., 2003), consistent with the notion that the ion is necessary to stabilize the cell wall during cellular expansive growth. Interestingly, Koshiba et al. (2010) found that under boron deficiency, BY-2 cells display increased Ca^{2+}uptake. We speculate that this occurs at least partly to compensate for loss of RG-II dimerization and to control the pectin network properties including the mechanics of the network and pore size through Ca^{2+} cross-linking. Mutation in

Arabidopsis SIA2 encoding a sialyltransferase-like protein possibly involved in the transfer of Dha and Kdo (Dumont et al., 2014), two disaccharides present in RG-II side chains, results in shorter, swollen or dichotomously branched pollen tubes and a higher frequency of bursting. As Dha and Kdo are not present in side chain A where borate bridging takes place, it seems that impairment in the assembly of other RG-II side chains can affect cell wall stability, although further studies are required to verify the impairment of RG-II structure in this situation (Holdaway-Clarke et al., 2003). *bor1-1*, a high-boron-requiring *A. thaliana* mutant, shows severe defects in the expansion of rosette leaves in low boron concentration (Noguchi et al., 1997). Interestingly, boron deficiency seems to impact meristems and reproductive tissues such as pollen and female gametophytes more than other somatic tissues (Chatterjee et al., 2014). Increasing the boron concentration rescues the phenotype of the somatic plant body, but rescuing female sterility requires more elevated boron concentrations. *bor2-1* and *bor2-2*, the loss-of-function mutants of BOR2, a boron efflux transporter located in the epidermis of the root elongation zone, on the other hand, are compromised in root elongation under boron-deficient conditions (Miwa et al., 2013). It was suggested that although the boron concentration in the root was not affected significantly compared with the wild-type, the proportion of cross-linked RG-II was significantly reduced.

Although the role of RG-II dimerization for cell wall stiffness is relatively well established, the subcellular localization of RG-II in growing cells remains a puzzle. In general, regions of softer cell wall are associated with pronounced cellular growth activity, whereas stiffer cell walls are present where the cell does not grow or has stopped doing so (Geitmann and Ortega, 2009). Consistent with this, in pollen tubes, highly methylesterified pectin is present mostly in the growing apex of the cell, whereas the non-growing shank displays de-esterified HG (Fayant et al., 2010; Geitmann and Ortega, 2009; Zerzour et al., 2009). RG-II distribution would be expected to follow the same pattern, being predominantly present in the stable, non-growing regions of the cell. However, immunolocalization showed that the opposite is the case. In pollen tubes of three plant species including *A. thaliana*, RG-II is present in all regions of the cell, both growing and non-growing (Dumont et al., 2014). In wild-type *Nicotiana tabacum* pollen tubes, RG-II concentration was even found to be higher in the growing apex (Iwai et al., 2006). While this is puzzling, the specificity of the antibody did not actually allow

the distinction to be made as to whether the RG-II was cross-linked by borate esters or not; clearly a crucial parameter for the mechanical behavior of the polymer. It has also been speculated that the HG backbone of RG-II and its side chains are resistant to fragmentation by glycanases, which maintains the integrity of the pectin network, while the framework can be enzymatically modified during cell growth (Rose, 2003).

The situation is further complicated by the fact that boron deficiency is linked to oxidative damage and cell death (Dordas and Brown, 2005). It is therefore difficult to distinguish whether RG-II dimerization is directly essential for polar growth and cell elongation or whether effects on cellular growth are mediated through the viability of the cell as a whole. Further, boron is thought to have various other functions besides cross-linking RG-II. It can act as a signaling molecule, as a stabilizer of the plasma membrane, and it also may be involved in auxin metabolism (Chatterjee et al., 2014). It has recently been reported that boron deficiency inhibits primary root growth in *A. thaliana* through putative auxin-, ethylene- or reactive oxygen species (ROS)-dependent pathways (Camacho-Cristóbal et al., 2015; Martín-Rejano et al., 2011). Auxin resistant 1 (AUX1) is reported to be involved in growth inhibition at the root tips under boron-deficient conditions (Martín-Rejano et al., 2011). How a compromised cell wall integrity and altered cell wall mechanical stresses due to impeded RG-II cross-linking may trigger an auxin-dependent response resulting in inhibition of cell expansion has not been elucidated. Clearly, RG-II localization, its degree of dimerization, and its interaction with other cell wall polysaccharides merit further investigation to determine how RG-II contributes mechanically to the whole cell wall matrix in a growing cell.

2.6 Changes in pectin status alter the biphasic properties of the cell wall

The hierarchical structure and connectedness of cell wall polymers create voids whose size affects the passage of water, ions, and macromolecules (Fig. 2-1A). The apoplastic water content in growing primary cell walls amounts to ~60% (w/v) (Jackman and Stanley, 1995; Pettolino et al., 2012). Therefore, the mechanical behavior of the plant cell wall is influenced by how easily solutes move through spaces when the wall is deformed through tensile or compressive forces. The overall behavior can be considered to be that of a poroelastic material that is greatly

influenced by the structure, size, and connectivity of its pores. In fact, like a sponge, the response of a poroelastic substrate to application of a load is a combination of the deformation behavior of the solid phase and the resistance of the porous structure to movement of the intrinsic fluid (Fig. 2-1B, C). Interestingly, even if the putatively non-linear and viscous response of the porous solid scaffold is neglected, the retarded movement of fluid through voids and cavities can exhibit a time-dependent response similar to viscoelasticity. Decoupling the relative contributions of these two behaviors in the deformation of a biological material is not a trivial task (Galli et al., 2009; Strange et al., 2013; Wang et al., 2014). The poroelastic behavior of the plant cell wall is significantly influenced by configurational changes in cell wall polymers and their interconnections. One of the parameters that influence porosity of the plant cell wall is the degree of methylesterification of HG pectin. *In vitro* compression tests on lime pectin gels with different levels and modes of de-esterification revealed a reduction in the water-holding capability of the pectin gel with the degree of de-esterification (Willats et al., 2001b). Metal ions such as aluminum or copper are known to affect further the hydraulic conductivity of the pectic matrix as well as water uptake of the plant by saturating the polymer cavities and affecting the porosity of the composite (Blamey et al., 1993; McKenna et al., 2010). McKenna *et al*. used bacterial cellulose-pectin composites as plant cell wall analogs to study the changes in hydraulic conductivity of the cell wall due to ions. They found that the hydraulic conductivity of the cell wall analogs correlates with changes observed in pectin network porosity revealed by scanning electron microscopy. Pectin methylesterification therefore not only affects the stiffness of the solid component of the wall by altering polymer cross-linking, but also influences the degree of porosity and hence the movement of liquid.

Plant organs with rapid movement requirements such as the Venus flytrap rely on rapid water exchange alongside structural instability, such as buckling, for their movement (Forterre, 2013). It is therefore plausible that in these organs, the structure of the cell wall needs to possess the porosity that facilitates the movement of water at short time scales. The variety of physical requirements suggests that the short and long time scale behavior of cell walls under load can vary significantly. With respect to the role of the hydration state for the biomechanical properties of the cell wall, Köhler and Spatz (2002) suggested that the strengthening of the secondary cell wall by lignification may be mostly due to the ability of the hydrophobic cross-linked polymers

to expel water from the cell wall rather than the strength of the polymer itself (Köhler and Spatz, 2002; Ulvskov et al., 2005).

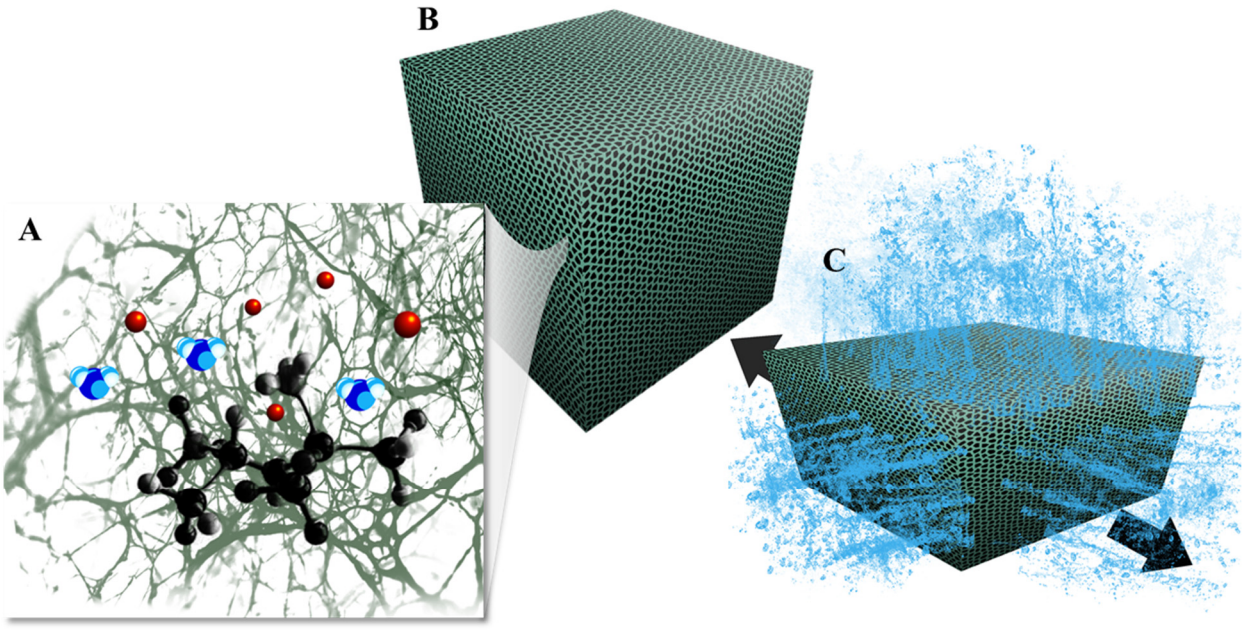

Figure 2-1. Cell wall porosity affects the mechanical properties of the material. **A)** Pore size of the cell wall polymers affects the passage of ions (red), water molecules (blue), and macromolecules (black). **B)** Schematic representation of fluid-saturated porous material. **C)** Fluid extrusion from the porous material under tensile stress.

Changes in configuration of all types of pectin polymers can affect the porosity of the cell wall. As discussed earlier, alterations in side chains of RG-I affect the hydration state and porosity of the cell wall. De-esterification of HG pectin affects the cell wall porosity (Goldberg et al., 2001). As for RG-II, within 10 min of adding boric acid to suspension-cultured *Chenopodium album* L. cells grown on a boron-deficient medium for more than a year caused dimerization of RG-II and a rapid decrease in wall porosity (Fleischer et al., 1999). It remains an open question whether borate cross-linking can occur in the pre-existing monomeric RG-II, a putative requirement for such a rapid change in the cell wall, or whether dimerization can occur only in cytoplasmic or newly secreted RG-II (Chormova et al., 2014). Either way, RG-II dimerization and changes in cell wall porosity can occur quite rapidly, and controlling cell wall porosity can therefore have implications for the transport and incorporation of new cell wall polymers into the cell wall as well as for the access of wall-modifying enzymes and proteins to their substrate (Fleischer et

al., 1999). Further, poroelastic time- and strain-rate-dependent behaviors of the cell wall not only need to be scrutinized in the context of plant cell growth, but are also relevant for the interpretation of mechanical tests carried out on cell walls. These facts emphasize the need for careful evaluation of the conditions under which mechanical testing of plant specimens is performed as dehydration of the tissues can greatly alter their mechanical properties.

2.7 Cellulose, the usual suspect of cell wall mechanical anisotropy

Cellulose microfibrils have generally been considered to be the principal load-bearing components of the cell wall and the determinant of growth anisotropy (Baskin, 2005). The reason for this is the high tensile modulus of ~140 GPa that allows the fibrils to resist cell expansion. Cellulose microfibrils are made up of β-1,4-glucan chains assembled into microfibrils by intermolecular hydrogen bonds between the oxygen atoms. Cellulose microfibrils are thought to behave more or less like cables. Parallel arranged cellulose microfibrils cannot withstand loading perpendicular to their long axis, but, through connections, the load is distributed among the cross-linking pectin and xyloglucan network (Dyson et al., 2012). When the microfibrils in a given section of cell wall are organized to display a preferential orientation, cellular expansion under the effect of turgor pressure is reduced in that direction.

Cellulose is synthesized at grouped CESA (cellulose synthase) enzymes (rosettes), each of which can synthesize a single thread of glucan (Doblin et al., 2002). Glucan chains are then packed with non-covalent hydrogen and van der Waals bonds into cellulose microfibrils (for a review, see Cosgrove, 2014). The length of the microfibrils and the shape and area of their cross-section are important in defining the type and quality of their interactions with other wall polysaccharides, such as xyloglucans, and can affect their slippage or separation during the growth of the primary wall. However, despite a large body of research on cellulose structure and interactions, surprisingly little is firmly established. Even basic characteristics such as microfibril length, number of glucan chains per cellulose microfibril, the shape of the microfibril cross-section, or the mechanism guiding CESA in the absence of a functional link to microtubules are elusive (Cosgrove, 2014; Li et al., 2012b). In land plants, the diameter of

cellulose microfibrils is suggested to be in the range of 2-5 nm (Cosgrove, 2014; Thomas et al., 2013). Cellulose microfibrils can consist of crystalline and non-crystalline domains. In crystalline regions, glucan chains are well ordered and bonded to each other by non-covalent (hydrogen) bonds. It is suggested that the crystalline and non-crystalline regions can either be placed alternately, or the amorphous non-crystalline regions can encapsulate the crystalline part, or both (Burgert and Dunlop, 2011; Salmén and Bergström, 2009). The values reported for the longitudinal elastic modulus of cellulose I range from 25 GPa to 220 GPa, depending on certain factors such as whether or not the intramolecular hydrogen bonding is considered in calculations (Cintrón et al., 2011; Diddens et al., 2008; Eichhorn and Young, 2001; Mariano et al., 2014). However, most of these studies are either based on theoretical models or carried out using X-ray diffraction or Raman spectroscopy. Only a few studies have performed relatively direct mechanical tests on cellulose, for example by employing the atomic force microscopy- (AFM) assisted three-point bending test (Cheng and Wang, 2008; Guhados et al., 2005; Iwamoto et al., 2009). Moreover, most studies are based on the crystalline portion of cellulose, and the mechanical properties of non-crystalline or amorphous cellulose are even less well defined. Some have assumed values as low as 5 GPa for non-crystalline cellulose (Eichhorn and Young, 2001; Hancock et al., 2000; Kulasinski et al., 2014). The absence of well-documented mechanical parameters becomes more significant when considering that the crystalline fraction in plant cell wall cellulose can be considerably lower compared with commonly studied cellulose from other sources such as bacteria (Mariano et al., 2014). Therefore, we think that in studies correlating the orientation of cellulose microfibrils to growth anisotropy in plant cells, complementary evidence identifying cellulose crystallinity is of utmost importance.

Recent studies suggest that some microfibrils in the plant cell wall form aggregates and exist in the form of bundles with non-covalent bonding, and that it is the orientation of these bundles and not that of individual microfibrils that defines the expansion behavior of the cell wall (Anderson et al., 2010; Thomas et al., 2013). In higher plants, individual microfibrils of ~3 nm in thickness can form aggregates of thicker fibrils with 5-10 nm and 30-50 nm thickness in primary and secondary cell walls, respectively (Fernandes et al., 2011; Li et al., 2014). However, it might be that ‘super bundles’ of greater thickness are formed, which would explain how

cellulose orientation can be resolved by common confocal microscopy that is subject to the diffraction limit of 200 nm (Fig. 2-2; Anderson et al., 2010).

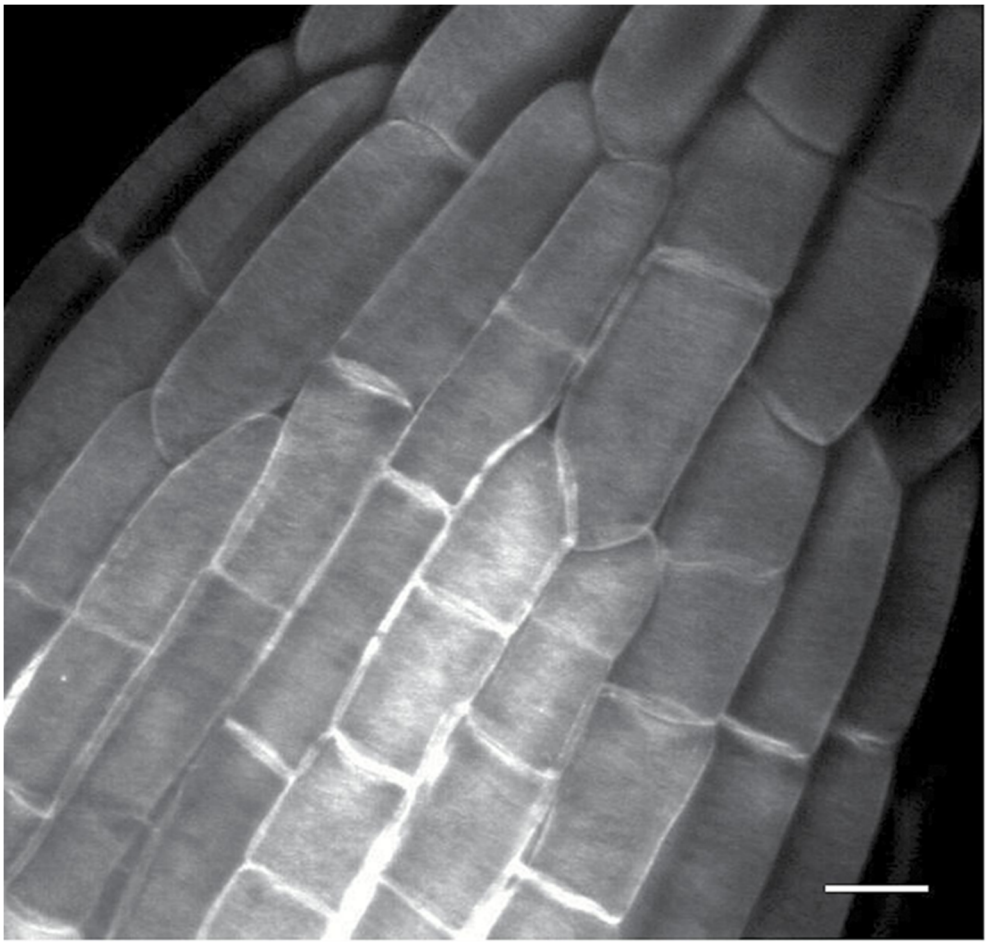

Figure 2-2. Discernible arrays of cellulose are oriented perpendicular to the growth direction in the growth region of an *Arabidopsis thaliana* root. These arrays probably correspond to 'super-bundles' of microfibrils. Staining with Pontamine Fast Scarlet (S4B). Scale bar = 10 μm.

The multinet (passive reorientation) theory termed by Roelofsen and Houwink (1953) suggests that the most recently added layer of cellulose microfibrils at the inner face of the cell wall is deposited in a direction perpendicular to the axis of cell growth. When thus oriented, the cellulose in the inner cell wall layer is therefore able to resist tension and is considered to be mechanically most influential, while microfibrils in the older layers are passively reoriented in the direction of growth (Richmond, 1991; Richmond et al., 1980). It should be noted that this hypothesis is not necessarily incompatible with other models proposed to explain the growth of

the cell wall, such as wall loosening by expansins or wall assembly by xyloglucan endotransglycosylases (XETs) (Cosgrove, 2005). Anderson et al. (2010) observed that in some layers of elongating root epidermal cell walls, cellulose reorients from transverse orientation in early stages to oblique orientations at later stages, in a trend similar to that previously reported for hypocotyl cell walls (Refrégier et al., 2004), and consistent with the multinet theory.

2.8 Microtubules, cellulose, and growth anisotropy

The movement of rosettes to lay down cellulose microfibrils in the new cell wall layer is generally accepted to be guided by cortical microtubules through microtubule-rosette links (Crowell et al., 2009). Cellulose synthase interactive protein 1 (CSI1) has been proposed as a link between microtubules and CESA (Bringmann et al., 2012; Gu et al., 2010; Schneider et al., 2012). Disruption of microtubules by drugs such as oryzalin or colchicine has been shown to adversely affect proper bundling of cellulose microfibrils and cell shape (Baskin et al., 2004; Baskin et al., 1994; Li et al., 2012b; Panteris and Galatis, 2005). Clearly the regulatory machinery that links internal structures to external cell wall polymers across the plasma membrane is of fundamental importance to plant cell morphogenesis. Microtubules are also involved in targeting of CESA to the plasma membrane (Gutierrez et al., 2009). Recent studies indicate that microtubules also participate in cell wall assembly by delivering vesicles containing non-cellulosic polysaccharides such as pectin; a role that was thus far assumed to rely mostly on the actin-myosin system (Oda et al., 2015; Zhu et al., 2015).

In anisotropically elongating cells or tissues, the orientation of the cellulose microfibrils is typically perpendicular to the main axis of growth, and is considered to be causal. However, recent evidence has shown that the relationship consists of a feedback mechanism in which the mechanical status of the cell induces the deposition of cellulose in a particular direction. This is thought to be mediated by microtubules, as their orientation is believed to respond to and align with the direction of maximal stress (for a review, see Uyttewaal et al., 2012). Experimental evidence to support this idea has been obtained both in single cell cultures and in tissues. Microtubules in suspended protoplasts exposed to centrifugal forces were shown to orient along the centrifugal force vector, resulting in growth of cells in the perpendicular direction (Wymer et al., 1996). Similar findings were carried out in cotyledon epidermal cells where stress

anisotropy due to cell shapes was linked to reorganization and alignment of microtubules in the direction of maximal stresses (Sampathkumar et al., 2014b).

It is important to realize that the action of depositing cellulose microfibrils can actually maintain or even increase stresses by causing stress concentration in a particular direction and/or at a particular location. This may sound counterintuitive as it is sometimes presumed that it is the weaker walls that undergo the largest stresses. In fact, by resisting strains and limiting the expansion of cells, aligned cellulose microfibrils can lead to the formation of geometrical discontinuities or curvatures which in turn result in higher stresses at specific locations. For instance, consider a cylindrical, thin-walled elastic shell, with uniform isotropic material properties (such as, for example, a Frankfurter sausage): because of the cylindrical geometry, inflation of this tube causes transverse stresses in the shank that can be shown to be twice as high as the stresses in the longitudinal direction in this region (Fig. 2-3A). If a spherical shell balloon has a stiffer belt-shaped band at its equator, the belt region expands less, resulting in a dumbbell shape with a narrow 'waist' region. Due to difference in deformability, this stiffer waist region is subject to the highest principal stresses (Fig. 2-3B). This is an example of how material discontinuities can generate geometrical changes that in turn cause local stress concentration. Since stress equals force per cross-section, the effect of geometrical discontinuities on the evolution of local stress can be offset partly or entirely if the wall becomes thicker at locations of elevated stress. However, often the addition of cellulose does not necessarily thicken the wall and thus locally elevated stresses can be expected at locations with higher density of cellulose.

Because of the effect of cellulose deposition on local stress patterns, microtubules can be considered to be crucial mediators of a positive feedback mechanism as they act as enhancers of growth anisotropy. The microtubule-severing protein katanin is proposed to increase the ability of microtubules to self-organize in parallel arrays in response to mechanical stress. The katanin mutant *ktn1* displays impaired microtubule dynamics, resulting in a shoot apical meristem with randomly oriented microtubules, a rather bumpy meristem surface, and decreased response of meristemic cells to mechanical stress (Uyttewaal et al., 2012), consistent with the notion that proper organ formation depends on this positive feedback mechanism.

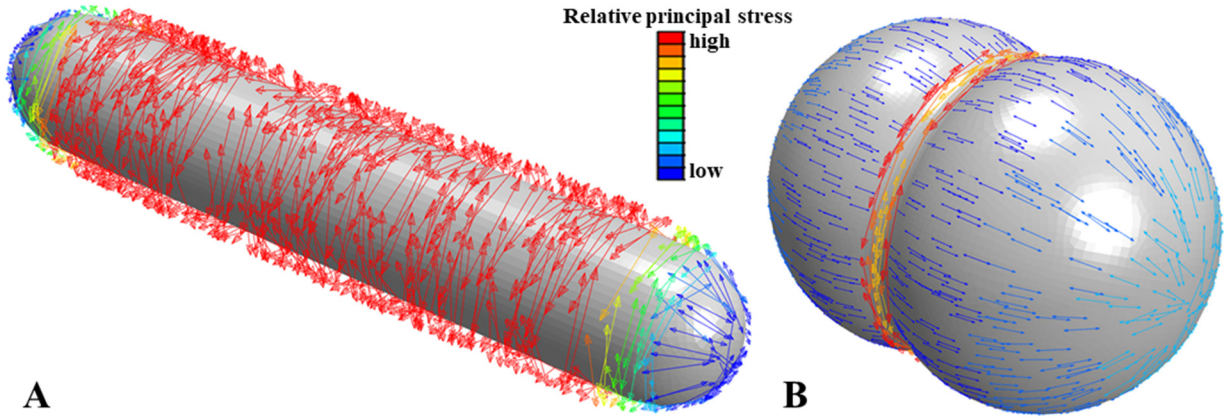

Figure 2-3. Influence of geometry and material discontinuity on wall stresses: maximum principal stresses in elastic bodies in a cylindrical shell **A)** and in an inflated balloon with a stiffened equatorial band resulting in a dumbbell shape **B)**. In (A), stress is higher in the circumferential direction than in the longitudinal direction. In (B), locally elevated stress is present in the waist region.

Sampathkumar et al. (2014a) suggested that large-scale stresses operating at the tissue rather than at the cell level act additively on local, subcellular stress in controlling the direction and orientation of microtubules. Further, Bozorg et al. (2014) showed that stress and strains in the cells are not necessarily always oriented perpendicular to each other. The authors demonstrated that stresses and strains can fall parallel in cells in a specific region of a tissue due to tissue level stresses thanks to a peculiar local shape of tissue, as in the valley between the meristem and a leaf primordium. The question is whether cellulose microfibrils orient in the direction orthogonal to the direction of positive maximum strain (growth) or whether they orient in the direction of maximal stress. Although these may seem difficult to distinguish, they are not of the same nature. Stress is the force that is experienced at any given point of a structure due to the application of a load (here the turgor pressure), whereas strain is the deformation that results from the application of the load. The amplitude of local strain depends not only on the local stress but also on the material properties determining the resistance to deformation. Strain, therefore, does not necessarily correlate with stress (Yip et al., 2013). By introducing fiber reorientation in a mechanical feedback model, Bozorg et al. (2014) observed that simulations in which microfibrils oriented in the direction of maximum stress behaved stably and similar to a fixed anisotropy direction model, suggesting that the rule can make a robust shaping cue.

However, orientation in the direction orthogonal to the maximum strain rule resulted in unstable fiber directions, and eventually the orientation of fibers became longitudinal (in the direction of maximum elongation). Based on these *in silico* simulations, the authors suggested that cellulose microfibrils orient in the direction of maximal stress (rather than strain).

2.9 Pectin: the new black?

The notion that cellulose-mediated stiffening is the result of a positive feedback mechanism raises the question of what initiates the morphogenetic process in anisotropic growth. It had long been assumed that the orientation of cellulose is both the causal and initial agent. However, this concept has recently been challenged by observations of other cell wall components that display marked inhomogeneity upon the onset of growth asymmetry and even prior to a perceivable preferential orientation of cellulose. Using AFM to map the mechanical changes in *Arabidopsis* hypocotyl epidermal cells, Peaucelle et al. (2015) observed that the longitudinal anticlinal walls (the anticlinal walls that preferentially expand during hypocotyl elongation) undergo softening prior to the onset of anisotropic elongation (Fig. 2-4). Monitoring the orientation of microtubules and CESA tracks suggests the absence of perceivable transverse alignment of cellulose at this stage. Changes in mechanical symmetry of the cell resulting in growth symmetry breaking were attributed to softening due to selective de-esterification of pectin in longitudinal walls. The authors suggest that growth symmetry breaking is controlled at the subcellular level by changes in pectin status in selected walls of a given cell. They propose that cellulose microfibril deposition in the transverse direction follows but is not an initiator. Therefore, since changes in stiffness of pectin polymers are not as pronounced when compared with substantial stiffness of cellulose microfibrils, tools with sufficient force resolution must be used to measure the mechanical properties in growing cells, especially at early stages of growth. These studies point to a relatively novel concept—the role of changes in the pectin status as the primary morphogenetic trigger. Only once these are initiated do they lead to changes in stress distribution which in turn trigger microtubule reorganization that only in a second step leads to reinforcement by cellulose in a positive feedback loop (see the previous section). In this scenario, microtubules and cellulose microfibrils play the role of mediator and enhancer of anisotropy instead of initiating it (Fig. 2-4).

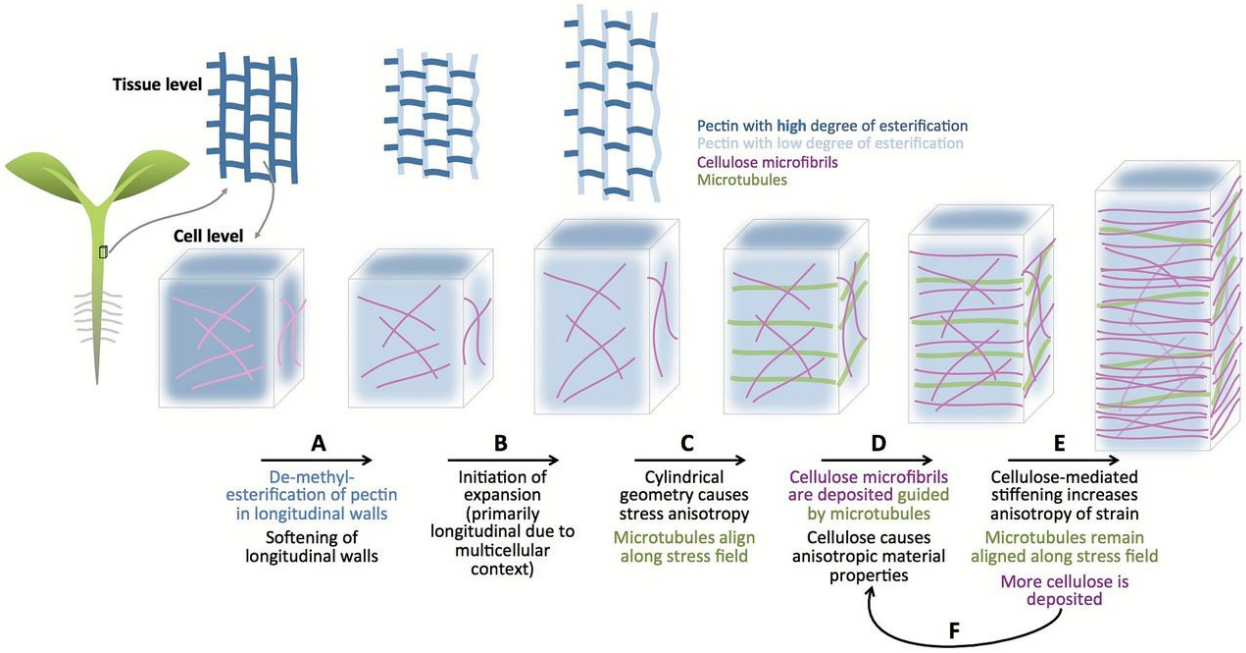

Figure 2-4. General concept of a two-step mechanism achieving anisotropic plant cell growth. **A)** Longitudinally oriented cell walls soften through pectin de-esterification [consistent with this, using AFM, Peaucelle et al. (2015) showed that longitudinal anticlinal walls in the epidermis of *Arabidopsis* hypocotyls become softer prior to the onset of cell expansion; immunohistochemistry suggests that this is correlated with de-esterification of pectin]. **B)** The difference in mechanical properties between longitudinal and transverse walls triggers expansion of the longitudinal walls. Because of tissue geometry and tight cell–cell attachments, the expansive activity in the hypocotyl tissue occurs primarily longitudinally. **C)** Due to the newly generated cylindrical geometry of the cells, the primary stress field is transverse to the growth direction. Microtubules align transversally, in the direction of maximum stress [consistent with this, Peaucelle et al. (2015) showed that microtubule alignment occurs only after softening of longitudinal walls]. **D)** Deposition of cellulose microfibrils in transverse orientation causes material of the longitudinal walls to become anisotropically reinforced. **E)** An increase in stress anisotropy maintains the transverse orientation of microtubules. **F)** Continued deposition of cellulose microfibrils reinforces the cell wall anisotropy.

To further corroborate the notion of pectin as a mechanical initiator of growth anisotropy, a feedback loop involving the phytohormone auxin and pectin de-esterification in organ formation has been proposed (Braybrook and Peaucelle, 2013; Peaucelle et al., 2011). Auxin-induced organogenesis is accompanied by a local decrease in stiffness of the tissue. In the *pin1* mutant defective in polar auxin transport, the shoot apical meristem grows but exhibits severe abnormalities in or the absence of the development of floral organs, resulting in needle-shaped apices of inflorescence stems (Okada et al., 1991). While local application of auxin to the organ

free apex of *pin1* rescues organogenesis accompanied by a detectable decrease in stiffness at the site of the emerging leaf primordium, rescue through exogenous auxin was not possible in meristems of plants overexpressing pectin methylesterase inhibitor3 (*PMEI3oe*) (Braybrook and Peaucelle, 2013). This suggests that in the shoot apical meristem auxin-induced stiffness modulation is mediated through pectin de-esterification. Interestingly, immunolocalization of PIN1 in *PMEIoe* revealed disorganized polarity of the auxin transporter (Braybrook and Peaucelle, 2013). This is indicative of a reverse mutual influence of pectin de-esterification on auxin polarity. It is speculated that altered wall mechanics actually affect the organization of PIN1 polarity.

The enduring concept of cellulose acting as the sole mediator and initiator of growth anisotropy may have originated from or been reinforced by the presumption that other wall polysaccharides, and especially pectins, do not contribute to load bearing and determination of the mechanical properties of the cell wall, due to their relatively low elastic modulus. However, it turns out that even in the presence of cellulose, pectins can affect the mechanical properties of the cell wall and act as distributors of mechanical load in the cellulose-hemicellulose-pectin network. Hydrated pectins might interact with and bind to cellulose microfibrils (Dick-Pérez et al., 2011; Dick-Perez et al., 2012). Pectin perhaps somewhat liquefies the cell wall, reducing cellulose self-association and facilitating cellulose slippage in expanding cell walls (Thimm et al., 2009). Extraction of pectin is observed to be associated with increased rigidity of the cell wall (Cosgrove, 2014; Dick-Perez et al., 2012), with microfibrils having a higher tendency to become denser and form aggregates (Thimm et al., 2009). Pectin-xyloglucan interaction might also prevent unfolding of xyloglucan chains attached to cellulose microfibrils, resulting in increased stiffness. Abasolo et al. (2009) performed tensile tests on *mur1* and *qua2* mutants of *A. thaliana*. *mur1* is deficient in L-fucose, affecting RG-II dimerization and xyloglucan fucosylation, while *qua2* has 50% HG content. The results showed considerably lower tensile stiffness for these mutants compared with the wild-type (Col-0) and *mur2* (affected xyloglucan fucosylation but no changes in pectin content). However, ultimate strengths (defined at the rupture point) showed no significant differences. Also, after the first cyclic loading of the tensile-testing protocol, all the hypocotyl specimens showed strain hardening, but this was much more pronounced in the case of *mur1* and *qua2* specimens. This may indicate that unfolding of

the xyloglucan network is easier in the case of a compromised pectin network showing a drop in tensile stiffness, whereas when the xyloglucan strands are unfolded, stiffness values tend to converge.

2.10 Conclusion

The emergence of feedback mechanisms regulating cell wall properties suggests that this cellular feature should be regarded as a dynamic self-regulating structure that continuously generates feedback on its mechanical properties and modifies itself to align with the requirement for plant cell growth and function. The cell wall fulfills this mechanical 'self-awareness' through modulation of its polysaccharides, cross-links, macromolecules, proteins, and ion contents. Cellulose microfibrils have conventionally been regarded as major cell-shaping components of the plant cell wall and they are known to determine growth anisotropy by restricting cellular expansion along their principal orientation. The fact that cellulose orientation is guided through links with microtubules, which in turn are sensitive to mechanical stresses in the cell wall, illustrates one possible way in which the cellular geometry and mechanical status can generate feedback onto cell wall assembly. However, this is only one of the mechanisms through which the cell wall senses its mechanical state and triggers the cell to respond accordingly. Pectins have gained increased attention in recent years. Changes in pectin polymer configuration can precede organogenesis, and these occur even prior to detectable changes in cellulose orientation. Pectins can loosen or stiffen the matrix and affect the stiffness of the cell wall directly, or indirectly through restricting the slippage of cellulose for instance by impeding the unfolding of xyloglucans. Modulation of pectins can presumably also increase the local stiffness of the matrix, triggering a positive feedback loop that in turn orchestrates a microtubule-guided cellulose reinforcement of mechanical and growth anisotropy. On the other hand, changes in pectin configuration through de-esterification, dimerization, and branching can affect the porosity of the cell wall. Cell wall porosity influences its permeability to macromolecules including enzymes that tune the expansive growth of the cell by breaking or creating cross-links between polymers. Further, changes in cell wall porosity influence how readily water can move through voids and cavities in the cell wall. Since expansive growth of plant cells is typically a relatively slow process, it is unclear how changes in poroelasticity of the cell wall affect its

expansive behavior, and warrants future experimental and modeling studies. However, in measurements of the cell wall mechanics that rely on rapid and substantial deformation of the cell wall, retarded water movement within the wall could play a significant role and poroelastic properties should therefore certainly be accounted for.

Chapter 3: Finite element modeling of shape changes in plant cells

Amir J Bidhendi[1], Anja Geitmann[1,2,*]

[1]Institut de Recherche en Biologie Végétale, Département de sciences biologiques

Université de Montréal, Montreal, Quebec, H1X 2B2, Canada

[2]Department of Plant Science, McGill University, Macdonald Campus, 21111 Lakeshore, Ste-Anne-de-Bellevue, Québec H9X 3V9, Canada

*Address correspondence to: Anja Geitmann (geitmann.aes@mcgill.ca)

This is a pre-copyedited, author-produced version of an article by Bidhendi and Geitmann (2018a) published in Plant Physiology following peer review. The version of record is available online at: http://www.plantphysiol.org/content/176/1/41, doi.org/10.1104/PP.17.01684

Plant cells come in a striking variety of different shapes. Shape formation in plant cells is driven by turgor pressure and controlled by tuning the cell wall polymers. Understanding the shaping aspects of plant cells requires a knowledge of the molecular players and the biophysical constraints under which they operate. Mechanical modeling has emerged as a useful tool to correlate cell wall structure, composition, and mechanics with cell and organ shape. The finite element method is a powerful numerical approach used to solve problems in continuum mechanics. This Update critically analyzes studies that have used finite element analysis for the mechanical modeling of plant cells. Focus is on models involving single cell morphogenesis or motion. Model design, validation, and predictive power are analyzed in detail to open future avenues in the field.

The cell wall is a polysaccharide-rich extracellular matrix that gives plant cells their shape at the expense of constraining their growth and movement. All cellular growth processes and shape changes involve a deformation of this extracellular matrix and are controlled by it. This control is exerted by modulating the mechanical properties of the matrix, which, in turn, are regulated by the polymers present in the wall and the state of linkages between them. The main polysaccharides of the primary cell wall are pectins, cellulose microfibrils, and xyloglucans (Bidhendi and Geitmann, 2016; Cosgrove, 2015). Cellulose microfibrils are recognized as the primary load-bearing component limiting cellular expansion (Baskin, 2005; Geitmann and Ortega, 2009). However, an increasing amount of evidence points at the pivotal function of pectins and hemicelluloses in defining the mechanics of the cell wall (Amsbury et al., 2016; Bidhendi and Geitmann, 2016; Braybrook and Peaucelle, 2013; Palin and Geitmann, 2012; Parre and Geitmann, 2005; Torode et al., 2017). To understand how modulation of the plant cell wall affects and regulates the change of cell shape, the biomechanical context must be considered; for instance, see the Update in this issue on wall structure, mechanics, and growth (Cosgrove, 2018) or previous reviews (Bidhendi and Geitmann, 2016; Geitmann and Ortega, 2009).

Biological experimentation with the goal of identifying the crucial players in determining cell mechanics is challenging. Mutational or pharmacological modifications of the cell wall biochemistry often result in pleiotropic effects through feedback mechanisms that alter

Advances

- Polar cellular morphogenesis of tip-growing structures such as pollen tubes and trichome branches involves isotropic cell wall structure at the apex, whereas the shank is transversely reinforced ensuring a tubular geometry.
- Self-similar growth of pollen tubes entails a gradient of elastic modulus increasing from tip to shank. Growth/strain anisotropy in a trichome branch is correlated with an attenuating cell wall thickness or elastic modulus toward the tip.
- Finite element (FE) modeling has been used to predict the locations of elevated stress in pavement cells revealing spatial co-localization with incidences of enhanced microtubule bundling. These FE models have also been employed to assess how tissue-level cues compete with subcellular stress.
- The formation of undulations in pavement cells is ascribed to alternating material stiffness in the anticlinal walls.
- The opening mechanism of stomatal guard cells is proposed to involve the geometry of the cell cross-section, radial cellulose reinforcement, local variations in pectin composition, and polar restriction of expansion.

other cellular processes. Therefore, mechanical modeling has proven useful in guiding biological experimentation by focusing on mechanical aspects of the behavior. Most modeling approaches in plant cell mechanics are based on the premise that the cell wall is a deformable material and that the deforming force is imposed by the turgor pressure, uniformly applied within the compartment of a single cell. This concept applies both to irreversible shape change (cell growth) and reversible shape change (stress generation or turgor-regulated motion). Since turgor is a scalar, for nonspherical cell shapes to develop during differentiation, the cell wall mechanical behavior must differ between subcellular regions. This can be achieved through the variation of wall thickness or heterogeneous distribution of the material properties (Green, 1962; Sanati Nezhad and Geitmann, 2015). The mechanical aspects of shaping or deformation processes can be explored using a variety of mathematical approaches (Dyson and Jensen,

2010). The finite element (FE) method is one of the available computational techniques particularly suited to the analysis of problems in continuum mechanics with a high degree of geometrical details and/or material complexity (Box 1). This Update analyzes examples in which this numerical tool is applied to evaluate the growth and elastic deformations of individual plant cells.

Box 1. Process involved in establishing a finite element model

Constructing a finite element model entails four principal steps. First, the geometry of the problem is defined (Fig. 3-1A). The structure is then meshed by discretizing the geometry into a finite number of subdomains called elements (Fig. 3-1B). Each element is defined by nodes at vertices. Then boundary conditions are imposed on the model to define and constrain the behavior of the structure properly. Boundary conditions are values such as displacements that are defined for certain nodes, such as those at external borders of the structure (Fig. 3-1C). Displacements, interactions between bodies and external forces applied to the system are defined at this step. FE allows for the definition of complex interactions between bodies such as friction or fluid flow at the boundaries. Different load types can be imposed on the model such as pressure, concentrated or distributed forces, or gravity (Fig. 3-1C). The final step is to assign a material model to the elements of the structure that explains how the material behaves under loads (Box 3). Upon running the simulation, the FE algorithm constructs a stiffness matrix relating the forces and displacements for each element. The matrices of all elements are assembled into global matrices for the whole model. Applying the boundary conditions and inverting the global stiffness matrix yield the load-induced displacements for each node from which various outputs such as strains and stresses are computed (Fig. 3-1D).

The uses of FE modeling for cell or tissue studies can be categorized as either forward or inverse approaches. The forward use of a model describes a deformation behavior, reversible or irreversible, inherent to the cell, such as a growth or shaping process. The purpose is to predict

or explain the mechanical behavior arising from wall properties and turgor pressure (Fig. 3-1). Models used for an inverse approach are employed for the identification of material parameters from experiments such as indentation measurements (Bidhendi and Korhonen, 2012; Bolduc et al., 2006; Forouzesh et al., 2013; Sanati Nezhad et al., 2013). In this Update, we take a critical look at selected forward modeling studies of single plant cells (Fig. 3-1).

3.1 Irreversible shape formation in growing plant cells

Plant cell growth involves an irreversible stretching of the cell wall and an increase in cell volume and surface that can be substantial in certain cell types. Biologically, this is accompanied by the continuous accretion of new cell wall material onto the existing wall. Simulating the resulting large deformations and the concomitant addition of material is a challenge for mechanical modeling that can be tackled in several ways. Typically, when using FE modeling, small, pressure-induced deformations are simulated repeatedly, and between the increments, a remeshing is performed. The geometrical structure resulting from the previous deformation step is meshed again to replace the often distorted mesh from the previous step. Stretching of the cell wall due to loading results in a reduction of cell wall thickness. To account for the addition of new material, the thickness of the wall is readjusted (e.g. set to the initial value to maintain a constant wall thickness). This principle has been used, for example, to simulate tip growth in the pollen tube, the delivery organ for the sperm cells in plants (Fayant et al., 2010).

3.1.1 FE modeling of tip growth

Tip-growing cells such as pollen tubes, root hairs, and fungal hyphae feature a spatially confined expansion zone allowing these cells to perform invasive behavior by penetrating the substrate (Bascom et al., 2018; Sanati Nezhad and Geitmann, 2015; Sanati Nezhad et al., 2013). The profile of the growing tip is radially symmetrical and remains self-similar when moving forward. Mutations or pharmacological treatments interfering with cytoskeletal functioning or cell wall composition can affect the self-similarity, resulting in either a tapered or a swollen

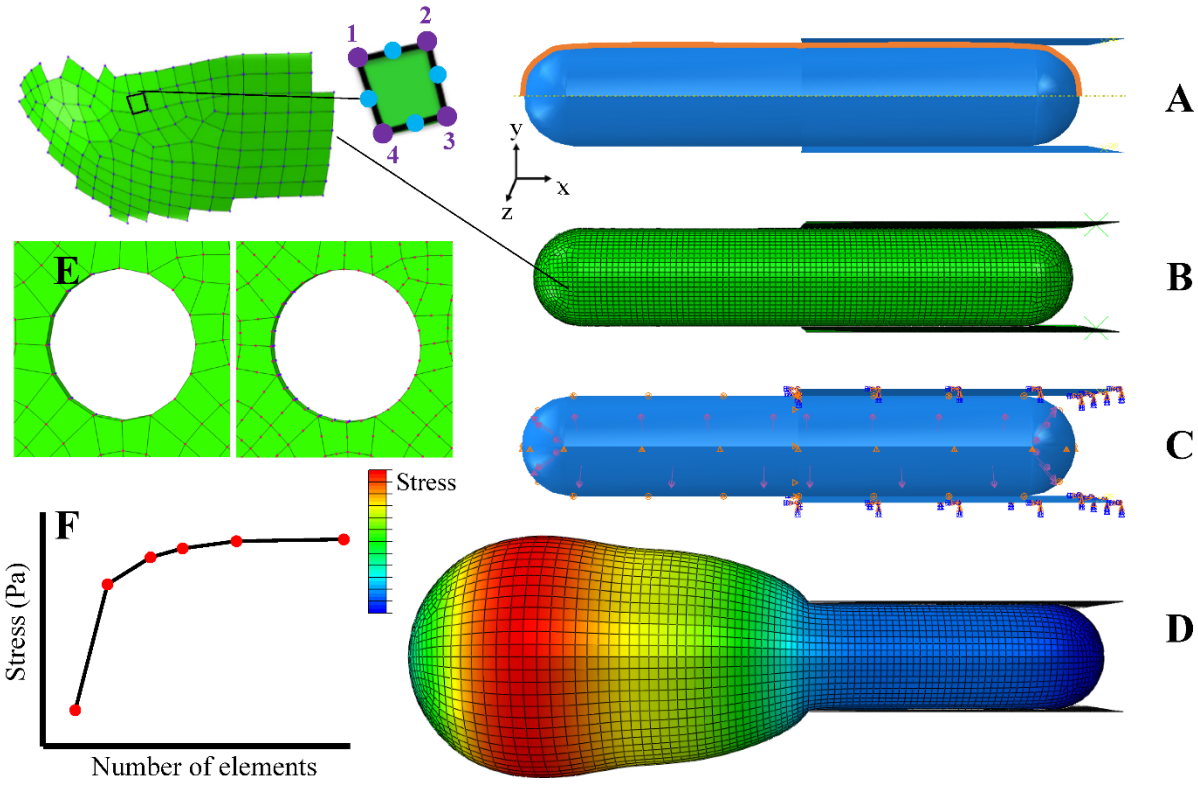

Figure 3-1. A) A closed cylindrical shell with hemispherical caps generated by the rotation of a line (orange) around a symmetry axis (yellow). The thin-shelled closed vessel is constrained on its right half by two nondeforming rigid, flat plates. **B)** The cylinder is meshed using three-dimensional quadrilateral shell elements (curved shell). The image on the left shows the first-order elements defined by four nodes (purple) used to discretize the geometry. Additional nodes (blue) would formulate the second-order elements. The elements can be regularly shaped or skewed. Excessively skewed element shapes are to be avoided. **C)** Boundary conditions are applied to the model. The rigid plates are fixed to prevent their rotation or displacement. Displacement boundary conditions are applied to prevent the cylinder moving freely in the space. The turgor pressure is applied uniformly to the internal surfaces. A sliding frictionless contact property is defined between the rigid plates and the deformable cylinder to prevent the penetration of one body into the other, while allowing their relative displacement. **D)** The isotropic closed cylinder deforms toward a spherical shape where it is not constricted by the plates. The heat map represents the von Mises stress distribution. **E)** First-order (left) and second-order (right) elements used around a discontinuity. **F)** Graph depicting the results obtained in a mesh convergence study. A value such as stress in a critical region is plotted against the total number of elements representing the structure to verify the independence of results from the mesh quality and the number of elements.

phenotype (Hwang et al., 2005; Klahre et al., 2006; Kost, 2008; Kost et al., 1999). Modeling of tip growth has been addressed using a variety of approaches (Campàs and Mahadevan, 2009; Dumais et al., 2006; Goriely and Tabor, 2003; Kroeger and Geitmann, 2011; Kroeger and Geitmann, 2012; Kroeger et al., 2008), one of which focused on the cell wall mechanical properties using the FE approach. FE modeling was used specifically to simulate how the generation of aberrant pollen tube phenotypes is mediated by changes in the cell wall mechanics (Fayant et al., 2010). The wall of the growing pollen tube was represented as a shell of uniform thickness (Box 2) but with spatially varying material properties. The apical dome was divided into hoop-shaped subregions in which the elastic modulus (Box 3; Boudaoud, 2010; Dumais, 2013; Huang et al., 2012; Julkunen et al., 2007; Kha et al., 2010; Niklas, 1992; Sun, 2006; Zerzour et al., 2009) could be assigned independently (Fig. 3-2A). Load application was performed repeatedly, and after each step, the structure was remeshed, and the wall thickness was reset to the initial value to counter thinning and simulate the addition of cell wall material (Fig. 3-2B). The goal was to predict the spatial distribution of material properties in the cell wall that would generate perfectly cylindrical and self-similar growth patterns and to identify those that result in deviations such as swelling and tapering.

Two types of biological constraints were used to validate the biological relevance of the simulations. To represent a normally growing tube, the model had to produce a self-similar shape profile, and the strain pattern resulting from the deformation of the wall had to reproduce those observed experimentally (Rojas et al., 2011). Two key mechanical parameters were analyzed for their ability to shape the tube: (1) the profile of the elastic modulus gradient from tip to shank; and (2) the degree of material anisotropy expressing how differently the material responds to loads applied in different directions. The validation suggested that isotropic behavior combined with a characteristic increase in elastic modulus, gradual from the tip to the flank and sudden from the flank to the shank, most accurately reproduce the pollen tube growth pattern. The mechanical gradients incorporated in this model were implemented as varying the elastic modulus between discrete regions rather than as a continuous and smooth function, and the values extracted were rather approximate. Despite these approximations, the model results matched well with mechanical and biochemical observations, suggesting that the simplification was not detrimental to the purpose of the study. Crucially, the gradient in elastic modulus

Box 2. Geometry, elements, and meshing

The geometry of the structure can be produced either by parametric drawing using a computer-aided design (CAD) software or reconstructed from sample images, e.g., from a 3D confocal stack. Simplification is a crucial consideration. Any feature that is not a part of the simulation or is not likely to affect the outcome is removed to minimize model development and computation times. For instance, symmetry about an axis can be used to model the 3D problem as a 2D axisymmetric model or shape symmetry can be exploited to model only a portion of the geometry. However, discretion is required to avoid eliminating any relevant information in this process. The plant cell wall is usually represented as either a 'shell' or a 'solid' model. In the 'shell' approach, the thickness of the wall is an input value while in the 'solid' approach it is directly reflected by the 3D geometry. Shell idealization is appropriate when the thickness of the cell wall is negligible compared to other dimensions (e.g., local radius of curvature). This is the case for a typical primary cell wall of 100-500 nm thickness compared to a typical cell diameter of 10-50 μm. If detailed information on stresses or strains through the thickness of the wall is needed, however, a 'solid' approach using volumetric elements is more appropriate.

Elements discretizing the body can be one-dimensional beams, two-dimensional triangles or quadrilaterals, or three-dimensional elements, depending on the dimensions and curvature of the structure. Elements can be of first, second or higher orders. Second-order elements, for instance, have additional midside nodes (Fig. 3-1B). The choice of the element type, shape and order is a critical step since it affects the computation time and the precision of the calculations. For instance, additional nodes in second-order elements, for the same number of elements, allow capturing the curvatures better (Fig. 3-1E). Therefore, there is often a compromise between using fewer second-order or more first-order elements. Similarly, shear-locking or overly stiff behavior in some of the first-order elements formulations is alleviated in quadratic elements, which enables them to calculate the deformations and stresses more accurately in bending-dominated applications (Sun, 2006). Nodes possess degrees of freedom that describe their properties. In the simplest form, this defines the displacement possibilities of the node in 2D or 3D space.

Box 2. Geometry, elements, and meshing- Cont.

In special applications, additional degrees of freedom such as pore pressure or temperature are added. The size of the elements discretizing the geometry is adjusted based on the resolution of the solution needed. While the precision can be increased by refining the element size, in practice, due to limitations such as computation time, elements are refined only locally in critical regions. These include zones where a more precise solution is needed, around discontinuities or contacts with other bodies. A mesh convergence study must be carried out to ensure that the solution of a simulation is not dependent on the number and quality of elements used. For this purpose, the number of elements is increased iteratively, and the results (e.g., critical stress at a specified location) are compared until the variation in the solution is deemed negligible (Fig. 3-1F).

Box 3. Material models

Some of the basic concepts in mechanical behavior of materials such as deformation due to loading, stress and strain, creep or relaxation, elasticity or plasticity and parameters such as Young's modulus and Poisson's ratio are covered in helpful reviews (Boudaoud, 2010; Dumais, 2013; Geitmann and Ortega, 2009; Niklas, 1992). The material model to describe plant cell mechanics can be linear or nonlinear. This choice depends on the nature of the problem being solved. When large deformations occur in the model, as in the simulation of growth, a nonlinear elastic material model (e.g., a hyperelastic formulation) is preferable. Time-dependent properties, such as viscoelasticity, can be incorporated using information gained from mechanical tests such as creep or relaxation. One of the simplest hyperelastic formulations is the Neo-Hookean model that requires defining only two material inputs. This is analogous to isotropic linear elasticity that requires two Lamé constants such as Young's modulus and Poisson's ratio to be defined. While using material models with a greater number of constants sometimes helps to achieve a better fit to an experimental observation, the lack of uniqueness of model parameters that can replicate an experimental observation can make the model unsuitable for producing meaningful predictions.

Box 3. Material models- Cont.

If material models with several independent parameters are used to define the mechanical behavior of the cell wall, several types of experiments or simplifying assumption are needed to ensure their uniqueness. Mechanical anisotropy is an important property that can be incorporated to explain the behavior of the cell wall. This parameter characterizes how the material behaves in various directions. A fully anisotropic behavior (different properties in any given direction) is impractical to define due to the many parameters required. Therefore, if suitable, material symmetry (this differs from geometrical symmetry in Box 2) is often used to idealize the material behavior. Among the useful idealizations are transverse isotropy (isotropic properties in a plane perpendicular to the axis along the fiber direction) or orthotropic behavior (with three perpendicular planes or axes of material symmetry). Transverse isotropy, for instance, is very well-suited to represent the anisotropy of the cell wall due to preferential orientation of cellulose microfibrils. Such anisotropic cases are defined by assigning different material constants along independent coordinate directions. A promising approach adopted for plant cell wall material was the use of hyperelastic models such as the Holzapfel-Gasser-Ogden model (e.g., Gasser et al., 2006) that allow for separate definition of fiber (e.g., cellulose) and matrix (e.g., pectin) phases. This model, in particular, has been used to formulate the transverse isotropy of plant cell wall material (Huang et al., 2012; Yanagisawa et al., 2015). User-defined materials can be developed and incorporated into the FE model definition to account for any further detail in behavior or interactions between cell wall constituents (e.g., refer to Julkunen et al., 2007; Kha et al., 2010; Yi and Puri, 2012).

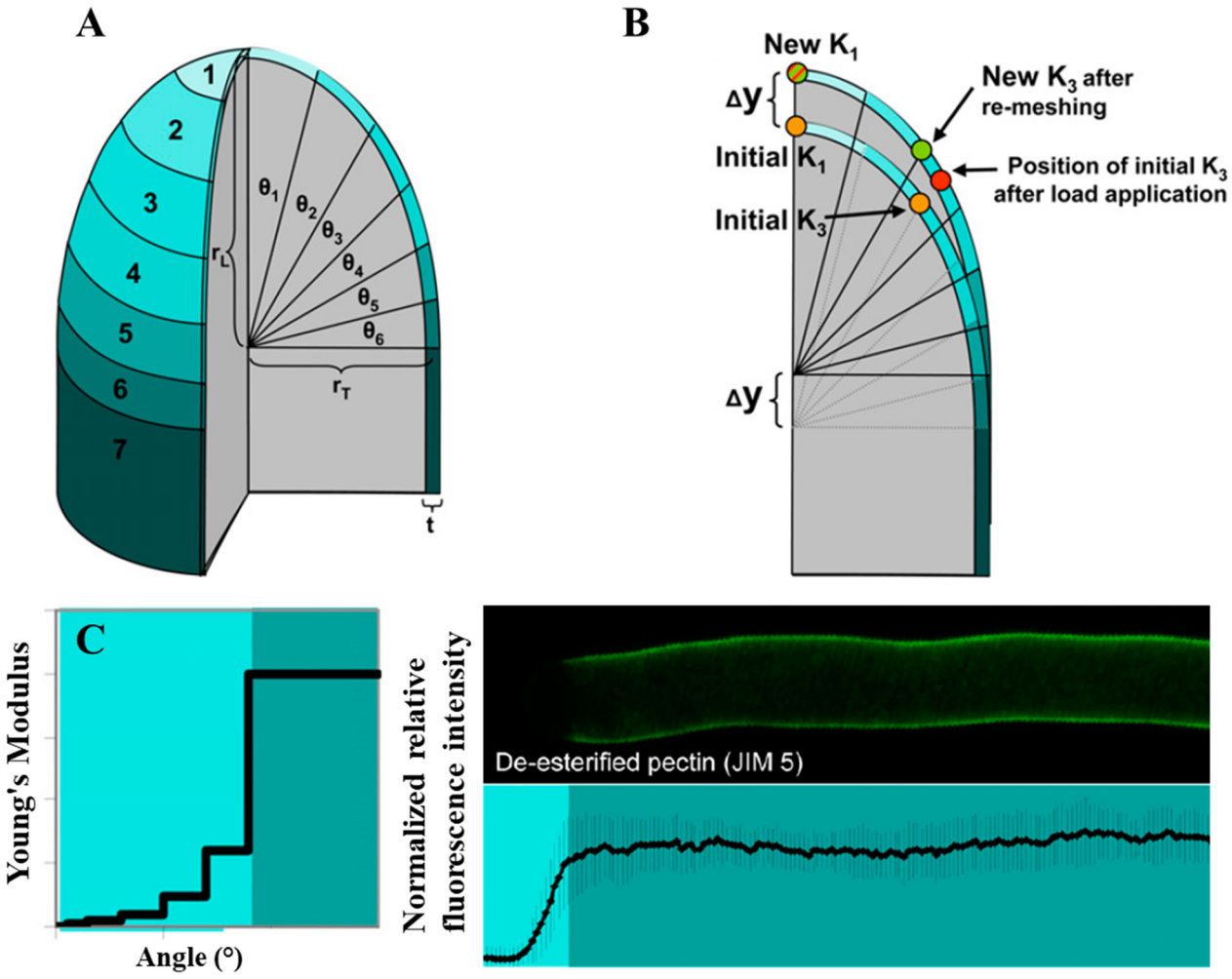

Figure 3-2. A) A pollen tube modeled as a hollow shell with uniform thickness. The apical dome is divided into subregions, allowing for the elastic properties to be adjusted in each region independently. **B)** Several key points are followed on the FE model upon each loading cycle and remeshing to mimic growth. **C)** The stiffness gradient predicted by the FE model to produce a self-similar tube closely matches the de-esterification pattern of pectin. Images were adopted from Fayant et al. (2010).

predicted by the FE model correlates well with the biochemical composition of the pollen tube wall, notably the distribution of esterified and acidic pectin (Fig. 3-2C). This result is consistent with the effect of the pectinase-mediated digestion of pectin, which results in a dramatic apical swelling of the pollen tube (Parre and Geitmann, 2005), presumably through the loss of the modulus gradient. It also accords well with mechanical measurements revealing that the cell wall at the tip of the growing pollen tube is softer and modulates its properties to generate an

oscillatory growth pattern (Zerzour et al., 2009). The reciprocation between predictions made by the *in silico* FE model, experimental validation, refinement of the model, and guidance toward further biological experimentation illustrates the value of FE in the predictive modeling of cell development.

3.1.2 FE modeling of diffuse growth during trichome branch morphogenesis

A similar yet distinct modeling approach was carried out to investigate the growth mechanics in trichomes. These epidermal cells (Fig. 3-3A) come in many shapes, sizes, and metabolic functions. They can be branched or unbranched, glandular or nonglandular (Tissier, 2012), and can be single-cell entities or comprise multiple cells. Trichome shape is intimately linked to their respective function, such as defense, pollination, or moisture retention (Amada et al., 2017; Oelschlägel et al., 2009). The unicellular trichome in *Arabidopsis* (*Arabidopsis thaliana*) forms a stellate body with three or four branches and is an excellent cell type in which to investigate the mechanics underlying complex cell morphogenesis. Actin is involved in the diffuse growth of plant cells (see Szymanski and Staiger, 2018). Disruption of cytoskeletal components is associated with the loss of branching, a needle-like phenotype, or swelling (Mathur, 2004; Mathur et al., 1999; Szymanski et al., 1999), phenotypes that can be studied using FE modeling. Branch morphogenesis in *Arabidopsis* trichomes was investigated using FE modeling in conjunction with live-cell imaging to understand the mechanics of branch growth (Yanagisawa et al., 2015). Similar to modeling of the pollen tube, the two constraints on the model to match were the shape of the branch and the growth (strain) pattern of the wall. Time-lapse imaging demonstrated that, unlike the self-similar pollen tube, the trichome tip radius tapers off while the radius of the base of the branch remains relatively constant (Fig. 3-3B). Fiducial markers were used to track the local growth pattern. To justify a choice of material model, the authors visualized the alignment of cellulose synthase (CESA) complexes and microtubules (see Elliott and Shaw, 2018), which were oriented transversely to the branch axis. Motivated by this preferential orientation inferred for cellulose that is commonly regarded as the major load-bearing polymer of the cell wall, transverse isotropy (Box 3) was incorporated in the elastic model using the Holzapfel-Gasser-Ogden hyperelastic material behavior (Gasser et al., 2006).

The critical parameters in this material model are the dispersion, fiber angle, and fiber-to-matrix stiffness ratio, which needs to be sufficiently large for anisotropy to emerge (Huang et al., 2012). The FE simulations indicated that strong transverse alignment of fibers results in the anisotropic, axial growth of the shell. The random orientation of the fibers implemented in this model produced a spherical bulge instead.

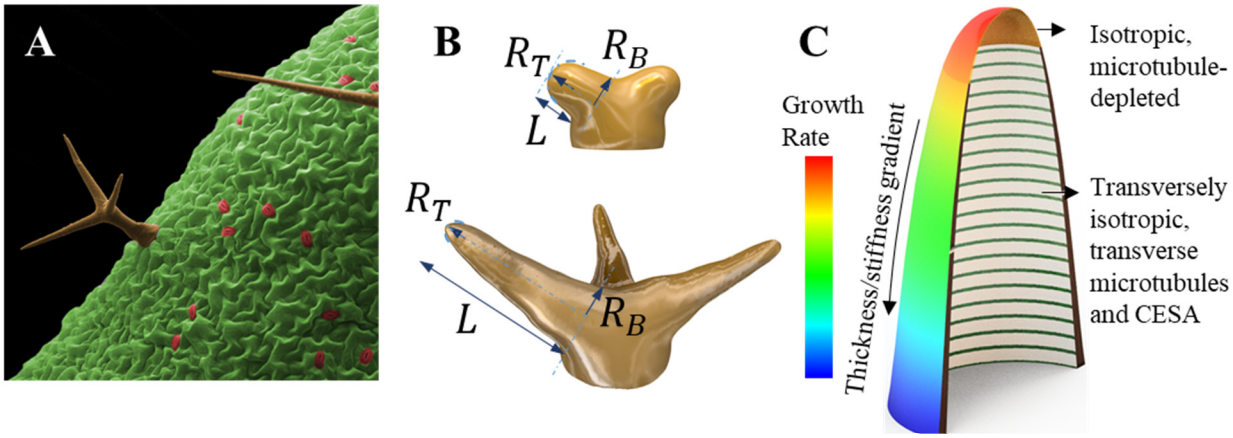

Figure 3-3. A) Epidermal cells on the adaxial surface of an *Arabidopsis* leaf feature three cell types: trichomes (brown), stomatal guard cells (red), and pavement cells (green). **B)** Development of the trichome branch embodies reduction of the tip radius of curvature, while the radius at the base of the branch remains constant. L, branch length; RT, branch radius at the tip; RB, branch radius at the base. **C)** The growth and thickness of the cell wall in a trichome branch are correlated and exhibit a gradient toward the tip of the branch. Microtubules and CESA trajectories are oriented transversely to the long axis of the branch, while the tip exhibits a microtubule-depleted zone. Image redrawn after Yanagisawa et al. (2015); (Zamil et al., 2017).

Because the tip apex of the trichomes was observed to be depleted of microtubules, it was concluded that the cell wall at the tip should be isotropic. Varying the size of the isotropic zone and comparing the evolution of the tip radius of curvature against the branch length, the FE results indicated that the size of the isotropic apical zone should vary over time to reproduce the experimentally observed tapering. This conclusion was drawn because no single value of the tip isotropic zone could produce results that fit the experimental curve. It is not clear to what extent such detailed results depend on the choice of material behavior model, and whether a different hyperelastic model would lead to a different conclusion. However, transverse isotropy alone could not reproduce the growth gradient toward the tip observed experimentally (Fig. 3-3C). Therefore, it was suggested that a thickness or elastic modulus gradient should exist along the

trichome branch. Transmission electron microscopy and light microscopy confirmed this predicted attenuation of cell wall thickness toward the tip, with a value close to but less dramatic than that predicted by the FE model. Therefore, a combination of both thickness and elastic modulus gradient parameters might be employed by the cell, although the FE model used here produced unrealistic results when combining the two. As remarked earlier, it would be interesting to investigate the dependency of simulation results on the material model employed.

In the *Arabidopsis* mutant *arpc2*/*distorted2*, trichome branch growth is impaired, the tip radius of curvature remains high compared with the wild-type, and the stalk swells (Kotchoni et al., 2009). Intriguingly, wall thickness and growth gradients were both absent in these aberrant trichome branches, further supporting a correlation between wall thickness and growth rate variations. It is unclear, however, whether the relationship is causal, and if it is, which is the cause and which the effect. While a thinner wall in the model can translate into a lower rigidity to reproduce a higher strain, a higher strain in the absence of reinforcing new wall material results in wall thinning. Likewise, the absence of a thickness gradient in *arpc2* may result from a failure to grow and a consequent lack of wall thinning. This study suggests that, while similarities exist, the growth behavior particular to trichome branches is distinct from tip growth. As the tip radius attenuates, wall thickness is not preserved, and growth occurs in the whole branch rather than a confined apical zone. Yanagisawa et al. (2015) report that the cell wall of *arpc2* is enriched in well-aligned cellulose, and microtubules are transversely oriented. Cellulose orientation was used as a proxy for transverse isotropy bringing about anisotropic (axial) growth in mutant branches. Although trichome branches in *arpc2* show impaired growth, comparing the time data provided for the branch length and tip radius for the wild-type and mutant shows that, for an equal length (e.g. at 40-µm branch length), the mutant branch has a larger tip radius of curvature, indicating that at least some degree of swelling occurs in the branch too, besides the general swelling in the stalk (see Figs. 1B and 3C in Yanagisawa et al., 2015). Whether this apparent swelling is a result of changes in the tip isotropic zone or changes in other wall polymers is not clear. While the fibrillar textures of the cell walls of the wild-type and the mutant seem unaltered, the quality of the fibers and their linkages might have undergone changes. Furthermore, other wall polymers may have been affected as a result of mutation. This emphasizes the need for experimental studies to characterize and compare the changes in

mechanical properties in a wide array of *Arabidopsis* mutants; the mechanical changes due to mutations can be manifested in ways that go beyond what can be assessed readily by visually tracing cellulose orientation.

In the studies that have modeled the shaping process of plant cells using the FE method, the geometry is loaded incrementally while cell wall thickness is adjusted to account for the thinning of material. The drawback of this strategy is that this process results in the elimination of stresses that develop in each increment. While it is possible to retain the stress information and transfer it to the next increment, it might differ from the quality of wall stresses during the insertion of wall-building materials. Attempts to describe cell growth were also been done by using viscoelastic behavior (e.g., Huang et al., 2015). However, loading to deform an elastic or viscoelastic structure may develop unique stress patterns different from those produced by the cleavage of chemical bonds and insertion of new materials. In fact, currently, we have little information on changes occurring in cell wall stress during growth or cell deformation. Additionally, in most of the available modeling studies, stress information is presented only in relative form. Absolute stress values could serve as a useful parameter to further validate the quality and relevance of a model's predictions. However, reporting absolute values based on models that are inevitably greatly simplified requires considerable experimental support, as explained below.

3.1.3 Stress development in plant cells correlates with morphogenetic phenomena

A subset of forward FE simulations of plant cells are the stress analysis models. The main variable investigated in these models is the stress developed in a single step of turgor application. The stress analysis models of plant cells or tissues published so far do not fall under irreversible FE models and are static, since they do not involve any remeshing, wall modification, stress update, or other introduction of a form of permanent deformation. While these models do not explicitly simulate irreversible material deformation, we categorize them under the irreversible use of FE models because they are sometimes employed to investigate the link between the mechanics and a physiological or morphogenetic response, such as cytoskeletal patterning, that can be linked to an irreversible biological response. Several studies use static stress analysis to

correlate the mechanical aspects with a morphogenetic problem such as gene expression, hormonal activity, and ontogeny at tissue scale (e.g., Bassel et al., 2014; Boudon et al., 2015; Bozorg et al., 2014). To illustrate the concept, however, we will discuss those that focus primarily on cell shape, namely the shape of epidermal pavement cells in relation to microtubule organization and wall biochemistry. Pavement cells in the leaf epidermis of eudicotyledons form interlocking patterns similar to pieces of a jigsaw puzzle (Fig. 3-3A and 3-4A). There have been numerous hypotheses, such as cuticle stiffening or cells being squeezed physically during growth, to explain the peculiar shaping phenomenon in these cells (Armour et al., 2015; Korn, 1976). The potential role of mechanics underlying the shaping process and the potential advantages of such cell shape for the epidermis or leaf have remained elusive (Jacques et al., 2014). Since pavement cells, as opposed to trichome branches, are tightly connected to neighboring cells, they allow studying the mechanics of cell-tissue interaction. Studies have suggested the involvement of the cytoskeleton in the shaping process downstream of an auxin-dependent pathway (Fu et al., 2005; Lin et al., 2013; Xu et al., 2010; Zhang et al., 2011). Microtubules are suggested to be associated with regions of indentation (often termed the neck), putatively resulting in anisotropic reinforcement of these regions by guiding CESA complexes and preferential deposition of cellulose microfibrils (Belteton et al., 2017; Panteris and Galatis, 2005). For simpler cell shapes, it is known that microtubules reorient in the direction of maximal mechanical stress (Hamant et al., 2008; Williamson, 1990). Whether the microtubule arrays experimentally observed in pavement cells equally correlate with stress patterns, however, was unknown for lack of information on stress distribution.

3.1.4 FE modeling of turgor-induced stresses in the periclinal pavement cell walls

The correlation between cell shape, mechanical stress, and microtubule alignment can be easily verified for simpler cell geometries, such as the tubular shapes of trichome branches or root and shoot epidermal cells. In a pressurized thin-walled cylindrical vessel with hemispherical caps, the pressure-induced transverse stress that arises due to cell shape is twice the longitudinal component. However, in the case of pavement cells, predicting the local distribution of stress is not as straightforward. Sampathkumar et al. (2014a) used FE modeling to study the effect of

cell shape and tissue-level stresses on microtubule arrangement in pavement cells. The static model developed in this study focuses on cell-level stress development and how it correlates with tissue-level mechanical and physiological responses. The FE model consists of the outer periclinal walls (the horizontal walls parallel to the plane of leaf) of pavement cells, extracted from confocal microscopy stacks, modeled as thin shells. At the borders of periclinal walls, the anticlinal walls (the vertical side walls) were modeled as 1D beam elements adding stiffness to borders. Tensile stress was generated in the cell walls upon the application of pressure to the inner face of the walls. Whether an isotropic or transversely isotropic hyperelastic material was used, the result indicated a higher stress at the indentation side of the wavy borders. The location and pattern of stress from the shell FE model matched well with the anisotropic alignment of microtubules, with a preference for bundling at sites of indentation (Armour et al., 2015; Fu et al., 2005; Zhang et al., 2011). These data suggest that stress resulting from cell shape at the subcellular scale might act as a mechanical cue for the cytoskeletal arrangement, even in cells with complex shapes.

Sampathkumar et al. (2014a) used the FE model of the pavement cells further, to predict the microtubule organization based on tissue-level stress patterns and their alterations upon the application of external forces or cell ablation. Their FE model suggested that, upon laceration, or more subtly, cell ablation, the stress pattern becomes circumferential around the vacant region (Fig. 3-4, A and C). Cell removal was reproduced in the model by gradual reduction in turgor pressure and cell wall stiffness in compromised cells. Time-lapse imaging reported an increase in microtubule bundling and a change in organization hours after laceration. Previous observations also had reported a reorientation of microtubules due to externally applied mechanical stress in *Arabidopsis* leaves (Jacques et al., 2013). The authors proposed that this indicates that changes in tissue-wide mechanical stresses can affect microtubule organization despite the initial cell-level order imposed on microtubular arrangement. However, to what degree the perturbation of mechanical stresses at tissue scale can override the cell-level control of microtubule arrangement is disputable. First, the FE model developed by Sampathkumar et al. (2014a) predicts that, upon laceration or cell removal, circumferential stress patterns would be produced in pavement cells in a region of tissue spanning over multiple cells (Fig. 3-4A). Conversely, observation of a fluorescently tagged microtubule line seems to suggest that

microtubule arrangement is affected more strongly only in cells near the afflicted region (Fig. 3-4B). Second, the study reports that the response of microtubules to changes in mechanical stress depends upon the magnitude of stress. To demonstrate this, the FE model was used to reproduce the ablation of only a few pavement cells. Similar to the case of laceration but with a lower magnitude, the FE model predicts a circumferential rearrangement of microtubules adjacent to the location of the perished cells (Fig. 3-4C). However, the experimental observation does not seem to closely match the FE prediction (Fig. 3-4, C and D). The authors argue that this observation demonstrates a stress-magnitude dependency of the microtubule rearrangement and that ablation of only a few cells does not seem to be able to strongly rearrange the microtubules circumferentially in neighboring cells. However, a closer look reveals microtubules in neighboring cells to be oriented predominantly parallel to the long axes of the cells, rather than featuring a circumferential orientation around the site of ablation (Fig. 3-4D). This might indicate that the rearrangement of microtubules due to cell ablation might at least partially occur due to other cues, such as a wound response, a mechanism shown previously (Geitmann et al., 1997). Furthermore, the microtubule response might depend upon a competition between the subcellular and supercellular cues, with a weight factor for each that depends on the homeostasis within the cell and tissue, rather than being dominated consistently by one.

3.1.5 FE modeling of wave formation in anticlinal walls of pavement cells

While the model by Sampathkumar et al (2014a) was useful to predict how stresses in fully differentiated pavement cells are distributed, it does not address the generation of the cell undulations. (Majda et al., 2017) proposed an FE model to explain the underlying mechanics of wave formation in pavement cells. Motivated by their undulating shapes, the model focuses exclusively on the anticlinal cell walls. The authors propose that wave formation results from bending of the anticlinal walls due to their stretching combined with a particular spatial distribution of mechanical properties. The FE model developed in this study purportedly demonstrates that, if segments with high and low elastic moduli are laid alternatingly along and across the anticlinal walls, stretching this structure forms bends resembling the protrusions and indentations of the pavement cell wall. A main result of the model is that the indentation side of

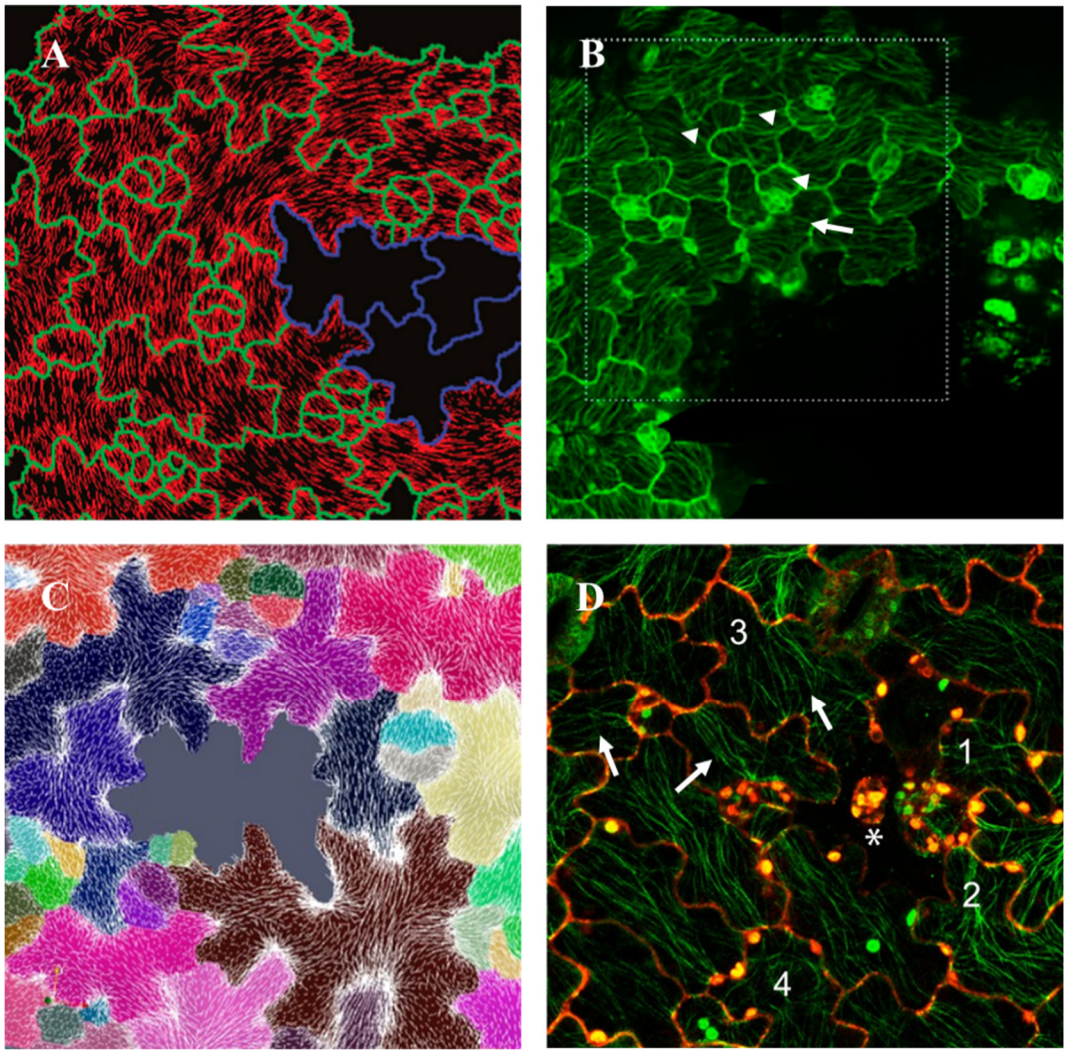

Figure 3-4. A) FE model suggesting a stress pattern in pavement cells circumferential to the site of laceration. **B)** Fluorescence-tagged microtubules demonstrate hyperbundling and a seemingly circumferential pattern around the wound site. White arrowheads show examples of noncircumferential microtubules in cells away from the site of laceration. The white arrow shows that, even in cells adjacent to laceration, there seems to be a local competition between the cell shape-dictated microtubule organization and the putative circumferential reorientation of microtubules due to tissue-level stress. **C)** FE model suggesting a stress pattern in pavement cells circumferential to removed cells. **D)** Microtubules demonstrate a change in bundling and orientation upon the small-scale wound. However, their orientations seem longitudinal to cell axes rather than being circumferential to the site of the wound. White arrows indicate examples of cells with microtubules oriented parallel to the long cell axis, inconsistent with the hypothesized circumferential orientation. The star indicates ablated cells. Numbers indicated individual cells. All these images are reprinted from Sampathkumar et al. (2014a) with permission from the authors. Bars = 25 μm (B) and 50 μm (D).

the bend of the anticlinal wall is associated with the softer material. While this result seems corroborated by the atomic force microscopy (AFM) stiffness measurements reported in this study, it is challenged by available data on the mechanics of the pavement cell wall. First, as mentioned before, well-aligned microtubules are associated with indentation sides in anticlinal and periclinal walls (Armour et al., 2015; Fu et al., 2005; Zhang et al., 2011), although whether these precede the initiation of undulations warrants further investigation (Belteton et al., 2017). It was hypothesized that this microtubular array leads to the deposition of well-aligned cellulose enrichment, thus preventing further expansion in these areas of the periclinal wall (Panteris and Galatis, 2005). This local stiffening in the periclinal wall of differentiated cells is corroborated by AFM stiffness mapping (Sampathkumar et al., 2014a). Moreover, using fiducial markers on the surface of growing pavement cells, (Armour et al., 2015) demonstrated that cell wall expansion is more pronounced on the protrusion side of undulations while the opposing indentation sides seemed restricted in their growth. This further corroborates an added stiffness at the indentation side, all of which seems to be difficult to reconcile with the results of the anticlinal wall FE model developed by Majda et al. (2017).

While the two scenarios are not mutually exclusive, reconciling them would necessitate allowing for a drastic and sudden change in the biochemical and biomechanical makeup at the border between adjacent cell wall regions. An indentation would have to feature a stiff periclinal wall (Armour et al., 2015; Panteris and Galatis, 2005; Sampathkumar et al., 2014a) directly neighboring a soft anticlinal wall (Majda et al., 2017). Only detailed analysis of the local wall biochemistry and mechanical behavior will provide conclusive answers. An additional consideration is the geometry. Given that the very narrow band of the anticlinal wall is bordered by two large sheets of periclinal wall, potentially representing significant boundary conditions limiting the freedom of displacement, one wonders whether the former can dominate the latter and whether modeling the anticlinal wall while entirely neglecting the periclinal walls can be a justifiable simplification. We posit that an FE model representing the entire 3D geometry of the cell, including all its load-bearing walls, is warranted to address the challenge of wavy pavement cell morphogenesis.

3.2 Reversible shape changes in plant cells

Reversible shape changes in plant organs and cells can be generated by modulation of the turgor pressure. As opposed to growth-related deformations, these remain mostly in the elastic range and do not involve dynamic modification of the cell wall material and biochemistry. However, these reversible movements are still governed by the mechanical properties of the cell wall material and the geometry of the cell or tissue. At the tissue level, the opening of the Venus flytrap (*Dionaea muscipula*) and other similar processes enabling seed dispersal are examples of the exploitation of turgor modulation, cell shape, and wall mechanics to accomplish actuation (Forterre et al., 2005; Geitmann, 2016; Hofhuis et al., 2016). Similarly, motion at the single cell level, such as stomatal opening and closing, is powered hydraulically.

To illustrate the application of FE modeling to reversible shape changes, the example of stomatal guard cells is examined here. Guard cells form pores in the leaf epidermis that are specialized to optimize gas exchange between the plant and the environment. The ability of these epidermal valves to respond efficiently to various stimuli, such as light and aridity, is crucial for photosynthesis, water retention, and thus, for survival. Stomatal opening is driven by an increase in turgor pressure in the guard cells. The pressure in subsidiary cells, the specialized epidermal cells immediately surrounding the guard cells, resists this process; so that together these two antagonistic effects regulate stomatal dynamics (Edwards et al., 1976; Franks and Farquhar, 1998; Von Mohl, 1856). The shape and structure of guard cells vary among species. Stomata in graminaceous monocots have guard cells that are typically narrow and dumbbell shaped, whereas those of dicots are kidney shaped. Here, we focus on the latter. The increase in the width of the stomatal aperture by inflation of the guard cells is suggested to occur in two stages. The guard cells in the closed state of the pore display a nearly elliptical cross-section that becomes circular when pressurized (Fig. 3-5A). The first stage of the pore opening or increase in volume of guard cells is suggested to be governed mainly by an inflation-driven change in the cross-sectional shape of guard cells with little stretch in the wall. The further increase in cell volume is attributed to stretching of the cell wall accompanied by its thinning and expansion at the poles (Sharpe and Wu, 1978). How the swelling of the two guard cells, their specific design, and their wall mechanics enable pore opening has been the subject of multiple studies with somewhat antithetical outcomes (Amsbury et al., 2016; Carter et al., 2017;

Cooke et al., 1976; Cooke et al., 2008; DeMichele and Sharpe, 1973; Raschke, 1975; Sharpe and Wu, 1978; Woolfenden et al., 2017). Several cell features have been hypothesized to be critical for pore opening when guard cell pressure rises: (1) the increased thickness of the ventral walls of guard cells (Fig. 3-5A); (2) the radial reinforcement by cellulose microfibrils, resulting in anisotropy of the cell wall (Fig. 3-5B); (3) the elliptical cross-section of guard cells under low turgor pressure; and (4) the constraint on polar expansion of guard cells due to pectin de-esterification.

3.2.1 Reversible changes in guard cell cross-sectional shape may underlie stomatal pore opening

FE studies by Cooke and colleagues were among the first to consider a realistic closed-cell geometry for guard cells. The comprehensive analyses carried out in these studies produced results that remain cogent to date (Cooke et al., 1976; Cooke et al., 2008. More information available under 'Stomatal Control System': hdl.handle.net/1813/45423; Lee, 1986). Cooke et al. (1976) modeled a generic stomate with a doubly elliptical toroidal shell by rotating an ellipse forming the transverse cross-section about another ellipse that lies in the horizontal plane (Fig. 3-5A; videos demonstrating the data for the guard cell model and results, for shell and solid, can be accessed at the following links: hdl.handle.net/1813/43793 and hdl.handle.net/1813/43794). The parameters investigated were the effects of guard cell geometry, wall thickness, radial cellulose reinforcement, and the turgor pressure in both guard and subsidiary cells. Thickening of the ventral wall has long been proposed to underlie pore opening (Meidner and Mansfield, 1968). Considering a nonuniform wall thickness, Cooke et al. (1976) found that opening of aperture width is virtually the same as in a model with uniform wall thickness, suggesting that the wall thickness gradient is irrelevant for stomatal opening. These results indicated that the geometry of guard cells is paramount in their function. If the torus was set to be doubly circular in this model, or if the cross-section was defined to be elliptical with the major axis perpendicular to the leaf surface (dotted ellipse in Fig. 3-5A), the pore was shown to close upon pressure application unless some physiologically implausible criteria were enforced. In these cases, the guard cell deformation consisted largely of cell wall stretching rather than change in cell cross-sectional shape. In contrast to other geometries, the authors determined that a doubly

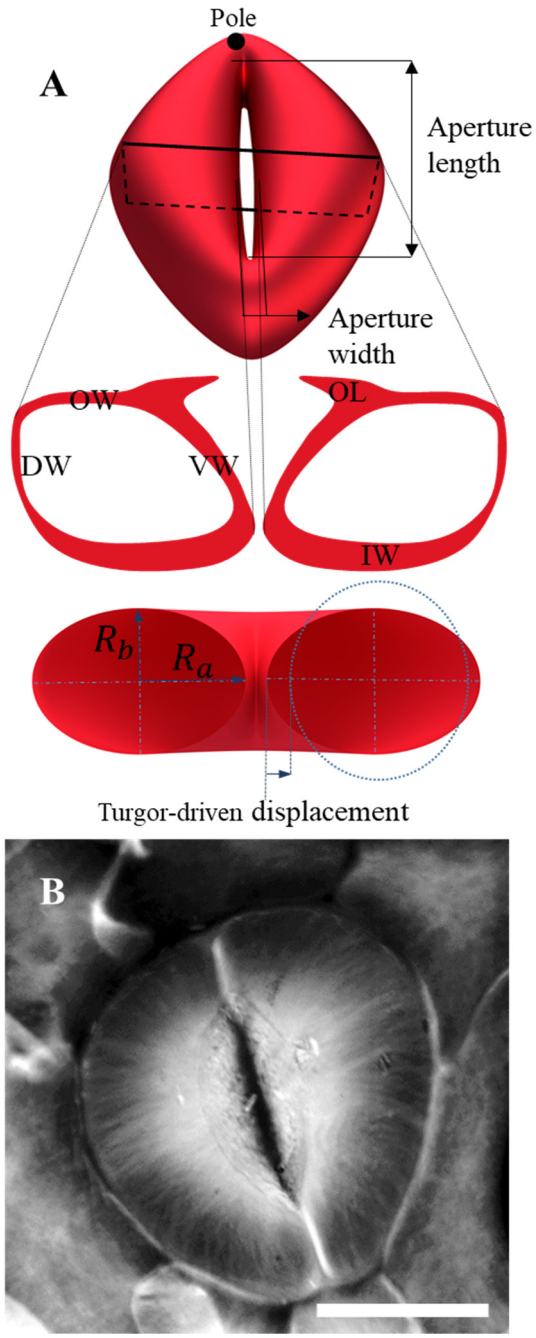

Figure 3-5. A) Cross-sectional view of guard cells composed of ventral wall (VW), dorsal wall (DW), inner wall (IW), and outer wall (OW). R_a and R_b refer to the horizontal and vertical radii of the elliptical cross-section, respectively. Only the outer ledge (OL) is shown. Inflation of the guard cells causes a change of the elliptical cross-section to circular and then to an ellipse with the major axis perpendicular to the plane of the leaf. **B)** Confocal micrograph of guard cells in an *Arabidopsis* cotyledon, stained with Calcofluor White to reveal cellulose. Bar = 15 µm.

elliptical geometry opens upon the application of turgor pressure and disturbs the neighboring cells minimally when inflated. These simulations indicated that, during deformation and pore opening, the cells bulge out of the leaf plane. While the width of the guard-cell pair increases as a result of pore opening, the width of a single guard cell can decrease slightly because of the out-of-plane bulge of the inner and outer walls. Interestingly, the aperture length was observed to remain virtually constant during pore opening, without necessitating a displacement restraint to be imposed a priori on guard cell poles.

Parametric studies carried out by Cooke et al. (1976) revealed that aperture width is a multilinear function of the pressures in the guard cells and subsidiary cells. An antagonism ratio was defined to express the contribution of each cell type in aperture opening. The radial orientation of cellulose microfibrils in mature guard cells (Fig. 3-4B) has long been known (Ziegenspeck, 1955), and the resulting transverse isotropy has been considered a crucial feature promoting stomatal opening. An early study even made a physical model of stomatal opening by radially reinforcing a pair of elongated balloons using adhesive tape (Aylor et al., 1973). On the other hand, simulations by Cooke et al. (1976) suggest that circumferential cellulose reinforcement acts to impede aperture opening driven by guard cell inflation. *Ceteris paribus*, their model, predicted that increasing the elastic modulus of the wall in the radial direction, representing a higher anisotropy ratio imposed by radial cellulose bundles, diminishes the effect of a unit increase in guard cell pressure on pore opening while it increases the contribution of a unit increase in the pressure of subsidiary cells in closing it. From this, the authors concluded that radial cellulose anisotropy is not a mechanism to open but, conversely, a leverage to close the pore. Interestingly, a recent study by Rui and Anderson (2016) has demonstrated that guard cells in a mutant with reduced cellulose content and anisotropy exhibit a wider aperture, which seems to, at least partly, support the findings of the model by Cooke et al. (1976). Assessing the dynamics of pore opening and the effect of subsidiary cells will require further investigation. The emergence of such complex and nonlinear control on the Watergate (stomatal pore) by relying only on geometry and mechanics is a spectacularly simple strategy and may be, in part, how plants can respond rapidly and reliably to environmental cues (Franks and Farquhar, 2007; Raven, 2014; Roelfsema and Hedrich, 2005). Together, Cooke et al. (1976); (Cooke et al., 2008) and Lee (1986) conclude that opening of the stomatal pore is influenced predominantly by the

elliptical geometry of the guard cell cross-section. They suggest that nonuniform wall thickening or anisotropic material properties are not required *per se*, although they might regulate the dynamic response of guard cells.

3.2.2 Reassessing the contribution of cellulose-induced radial anisotropy to stomatal opening

The role of cellulose orientation and cell wall anisotropy was reassessed in a recent study by Woolfenden et al. (2017), who used nonlinear elasticity with a transversely isotropic material behavior to represent the guard cell wall, similar to studies by (Cooke et al., 1976). The authors observed that, using isotropic material properties, increasing the turgor pressure causes the stomatal pore to close rather than open. A radially reinforced version of their model engendered pore opening. They concluded that circumferentially oriented cellulose microfibrils are crucial for stomatal opening. However, these results were based on a structure with an idealized circular cross-section for the guard cells, whereas the base model in the study by Cooke et al. (1976) was elliptical in cross-section (Fig. 3-5A). While Woolfenden et al. (2017) did simulate this situation as well, they stated that, at higher 'correct' pressures, the pore closes in the absence of anisotropic properties. The study does not explicitly state a caveat that cannot be neglected, however. Many of the model inputs, including the cell wall thickness, cross-sectional shape, and material model parameters including the elastic moduli, are significantly simplified, and idealized or arbitrary values are used, as is inevitable in the absence of biomechanical data. It is hardly possible to expect the model to reliably predict anything more than general tendencies, even if biologically relevant absolute pressure values are used. A small change in, say, the assumed Young's modulus of the cell wall or the use of a different nonlinear elastic model has the potential to significantly alter the observed threshold values or even the trends at which the model opens or closes. Arguing that one model more accurately reflects reality when neither uses better quality input parameters, warrants substantiation. Similar caveats apply to attempts aimed at quantitatively identifying material constants from such models; many approaches should remain qualitative. This points to a limitation of the current state of modeling in plant cell mechanics in general. In the absence of detailed quantitative information, many of the parameters required to define a given model must be input based on educated guesses; and

whether the predictions made by the model hold up in experimental conditions remains to be shown. That a given combination of material and geometrical parameters produces results resembling the biological situation is seductive but does not prove this combination to be the one reflecting the reality. Other solutions often are possible. This caveat should at least be acknowledged.

Another example is the observation that the aperture is least sensitive to turgor pressure at higher pore width (the curve moves toward a plateau; Franks and Farquhar, 1998). This led Woolfenden et al. (2017) to conclude that a strain stiffening must occur in the cell wall matrix. While this explanation is reasonable, it may not be the only one. Annexing increasing numbers of parameters to the model to match an observed behavior, without proper substantiation, risks appearing opportunistic if not arbitrary. The nonlinear behavior observed in experiments (Franks and Farquhar, 1998) also could be caused by a two-step opening mechanism, similar to the one described before and demonstrated in the FE model put forward by Cooke et al. (1976, 2008). This would entail an initial turgor-induced change in geometry from elliptical to circular (inflation), followed by an accommodation of any further increase in pressure by cell wall stretching, a process that requires higher turgor differentials to produce visible results. Therefore, the matrix strain-stiffening conjecture proffered by Woolfenden et al. (2017), while consistent with polymer chemistry (Bidhendi and Geitmann, 2016), could be a secondary mechanism responsible for the apparent low sensitivity of aperture opening at high pressures. These concepts certainly merit further validation. Woolfenden et al. (2017), furthermore, did not explore the effect of subsidiary cells in their model in any depth. They suggested that, in the presence of cellulose-mediated anisotropy in the guard cell walls, the effect of pressure in the subsidiary cells becomes negligible. This result is in clear contrast to that of Cooke et al. (1976), who reported the guard cell anisotropy to augment the effect of subsidiary cells in closing the stomata. Further investigations must address this discrepancy.

3.2.3 Correlating the mechanics and phenotype of genotypes: the devil may lie in the ultrastructural details

While cell wall mechanical studies often focus on cellulose orientation, parameters such as cell wall thickness, cross-section shape, and other cell wall polymers seem to have the potential to

influence the mechanics and function of guard cells. However, since a multitude of parameters may interplay, isolating the role of each may not always be straightforward. It has been reported that pectin chemistry is correlated with the ability of guard cells to function correctly (Amsbury et al., 2016; Merced and Renzaglia, 2014). *pme6-1* (a mutant of pectin methylesterase *PME6*) was shown to have a decreased dynamic range and a defect in stomatal opening. Interestingly, the results of immunolabeling suggest that, in wild-type *Arabidopsis*, unesterified pectin (antibody, LM19) is present in all cell wall regions of guard cells. Highly methylated pectin (antibody, LM20), on the other hand, is absent from guard cell walls, as also reported previously by Merced and Renzaglia (2014), and is limited to cell junctions, as is calcium-bridged pectin (antibody, 2F4). This means that unesterified pectin in the guard cell walls, although negatively charged, does not seem to be gelated by calcium ions. In *pme6-1*, the pectin distribution was reversed: highly esterified pectin was reported in the entire guard cell wall. The authors concluded that pectin determines the mechanics of the cell wall and that lack of a functioning pectin methylesterase causes the wall to become too rigid and lose the deformability required to open the pore (Amsbury et al., 2016).

While this is a reasonable hypothesis (Bidhendi and Geitmann, 2016), the study provides no evidence for the fact that the weakly esterified pectin was gelated by calcium or whether the mechanical properties of the cell wall materials were altered in any way. The antibody 2F4 was not used on the mutant, let alone micromechanical testing of cell wall properties. More importantly, the study fails to ascertain whether other parameters are also changed in the mutant. While the authors claim a lack of any noticeable difference in ultrastructure between the wild-type and the mutant, transmission electron microscopy cross-section micrographs of the guard cells of *pme6-1* and the wild-type provided in their study seem to reveal an interesting, yet conflicting, phenomenon (see Supplemental Fig. S2, G and H, of Amsbury et al., 2016). In cross-sections, the guard cell walls of the mutant appear considerably thicker than those of the wild-type, relative to the area of the lumen. This seems especially the case for the inner walls. Whether the images in this paper are representative remains an open question. However, compensation mechanisms are common when a normal process of the cell is disturbed and can cause a chain of events. Here, in response to a disturbed function of pectin methylesterase, an increase in cell rigidity may have occurred through abnormal wall thickening. If this were to be

confirmed, the change in cell wall dimensions or cross-sectional shape, rather than biochemical processes, would be the factor altering the mechanics of the unit surface of the wall (see Supplemental Fig. S2, G and H, of Amsbury et al., 2016). The irregular cell shape as viewed in the cross-section, and inner wall thickness may explain the anomaly in stomatal opening. It should be noted that an earlier study on the chemical alteration of the guard cell wall during development in *Funaria hygrometrica* by Merced and Renzaglia (2014) reserves a special role for rhamnogalacturonan I distribution in guard cell walls, in addition to the role of homogalacturonan. Further assessment of the potential contribution of other types of pectin in guard cell mechanics may provide answers to some of these outstanding questions.

3.2.4 The roles of pectin-induced stiffening and adjacent subsidiary cells in the polar prevention of guard cell elongation and stomatal opening

Pectin biochemistry was also the focus of a modeling study that suggests de-esterification of pectin at poles of guard cells to underlie pore opening (Carter et al., 2017). Ventral walls of guard cells are generally thicker compared with dorsal walls (Meidner and Mansfield, 1968; Renzaglia et al., 2017). Using AFM stiffness measurements, Carter et al. (2017) suggested that ventral wall thickening does not occur in young guard cells, while the stomata are still as functional as in mature guard cells. This is consistent with predictions made by an FE model developed in the same article, similar to the model by Woolfenden et al. (2017), suggesting the effect of ventral wall thickening to be minimal in stomatal opening, as also proposed by Cooke et al. (1976). Interestingly, Carter et al. (2017) showed that pectin is unesterified in guard cell poles and that the application of polygalacturonases rendered guard cells incapable of opening the aperture. Probing the stiffness of the enzyme-treated guard cells with AFM, the authors suggested that the guard cells' dysfunction arises from the removal of polar stiffening due to polygalacturonase treatment. However, from the image provided, it seems that, rather than the removal of stiffness from poles, the enzyme treatment had caused the relative apparent stiffness to spread over a broader region of the guard cell walls (see Fig. 4I of Carter et al., 2017). Furthermore, it should be considered that the enzyme treatment also might change the turgor pressure in the guard cells or subsidiary cells. Neither of these possible collateral effects nor any possible changes in cell ultrastructure resulting from pectin modification were verified.

The simulations predicted that, whether or not the cells are fixed at the poles, a threshold pressure (1 MPa) is required to initiate aperture opening. A threshold pressure has indeed been observed in biological samples. This lag in response was found to be due to the antagonizing effect of turgid subsidiary cells (Franks and Farquhar, 1998). As the pressure in these cells approaches zero, for example due to damage, the threshold pressure vanishes and the pore opens at guard cell pressures close to zero. The role of subsidiary cells is not spelled out in the model by Carter et al. (2017), but the modeling equivalent of an external constraining obstacle was nevertheless incorporated, only motivated by an unrelated biological feature. Carter et al. (2017) used the experimental finding of the stiffened guard cell poles to hypothesize that polar stiffening augments the pore opening at a given turgor pressure. They argued that the stiffened polar cell wall fixes the cell ends in place, and this concept was implemented by adding a boundary condition to the Woolfenden et al. (2017) FE model, on which the model by Carter et al. (2017) is based. This boundary condition consisted of fixing the poles in place. The problem of this translation of a biological concept into the FE model is that, to replicate the polar stiffening due to pectin de-esterification, it should have been implemented as a property (e.g. locally elevated Young's modulus) of the guard cell wall. Instead, the constrained displacement boundary condition removes displacement degrees of freedom at the poles, which biologically can only reflect an external constraint such as the above-mentioned surrounding subsidiary cells. Therefore, while the simulations are consistent with the findings by Franks and Farquhar (1998), the biological justification used by Carter et al. (2017) to implement the boundary condition merits reassessing. It is important to note that, as mentioned before, the model developed by Cooke et al. (1976; videos are available under hdl.handle.net/1813/43793 and hdl.handle.net/1813/43794) did not demonstrate a considerable polar expansion even though the poles were free to displace. Clearly, the choice of the model geometry is a crucial step in model construction.

Future studies to address these questions, specifically the effects of cell cross-sectional shape and subsidiary cells on the stomatal complex, have the potential to further elucidate the functioning of pectin in stomatal mechanics. Suffice it to say that the scenarios proposed by various groups, even if seemingly inconsistent, provide food for further thought. We wonder whether guard cells use different mechanisms redundantly, or distinctly at different stages of

development. An observation reinforcing this hypothesis may be the change from semicircular to elliptical cross-section between early-stage and mature guard cells (Merced and Renzaglia, 2014).

Outstanding Questions

- Transverse isotropy and restriction of lateral expansion are attributed mainly to cellulose microfibrils. Why then does depolymerization or disturbed actin functioning cause swelling in some cells although cellulose microfibrils may have remained seemingly intact?
- How do the mechanical stresses evolve in the cell wall during the cell growth?
- Is the reorganization of microtubules in cells located adjacent to a tissue injury or a perturbation a consequence of a change in the mechanical stress status or a response to a biological/chemical signal triggered due to loss of homeostasis?
- How can the softening proposed at the convex side of anticlinal walls in pavement cells be reconciled with the proposed stiffening suggested due to cellulose reinforcement at adjacent periclinal walls?
- What are the linking components between mechanical stress and strain in the wall and a biological response such as microtubule realignment? Do they function based on network tension or compression?
- Contradictory reports on the mechanics of guard cell deformation point to the necessity to judiciously assess the influence of parameters such as cell geometry, microfibril-mediated radial anisotropy, and pectin. Further, do guard cells employ different, and perhaps redundant, mechanical strategies to open the pore throughout their development?
- Are dumbbell-shaped guard cells in monocots mechanically similar to their kidney-shaped dicot counterparts?

3.3 Remark

FE modeling is a powerful tool that has been employed successfully to simulate the behavior of geometrically complex plant cells. The modeling technique has been used to localize and predict stress and strain in cells with the purpose to understand the underlying biological mechanisms, and it has been applied to both reversible and irreversible processes, such as guard cell movement and cell growth events, respectively. Despite, or because, the rapid adoption of FE modeling by the plant cell community, care must be taken in interpreting FE results. FE modeling, as with any modeling strategy, is subject to a dependency on the quality of inputs; flawed inputs result in flawed outcomes. Oversimplification or misrepresentation of the model components, ranging from the geometry, material behavior, or boundary conditions, has the potential to bear misleading results or to reinforce a bias as a self-fulfilling prophecy (see Outstanding Questions). Good modeling practice is to experiment with and eliminate the parameters that may affect the outcome before accepting the remaining ones. It is the responsibility of the user to ascertain that the inputs agree well with the physics of the problem and that the output is biologically relevant, which requires a proper understanding of both the physics and the biology of the problem.

3.4 Footnotes

www.plantphysiol.org/cgi/doi/10.1104/pp.17.01684

A.J.B. and A.G. wrote the manuscript; A.J.B. prepared the figures.

Research in the Geitmann lab is funded by Discovery and Accelerator Grants from the National Science and Engineering Research Council of Canada and by the Canada Research Chair program.

[OPEN] Articles can be viewed without a subscription

Received November 27, 2017.

Accepted December 7, 2017.

Published December 11, 2017.

Chapter 4: Mechanics of wavy shape formation in plant epidermal cells

Amir J Bidhendi[1], Bara Altartouri[1], Frédérick P Gosselin[2], Anja Geitmann[1,3,*]

[1]Institut de Recherche en Biologie Végétale, Département de sciences biologiques

Université de Montréal, Montreal, Quebec, H1X 2B2, Canada

[2]Laboratoire de mécanique multi-échelles, Département de génie mécanique, École Polytechnique de Montréal, C.P. 6079, Succ. Centre-ville, Montreal, Quebec, H3C 3A7, Canada

[3]Department of Plant Science, McGill University, Macdonald Campus, 21111 Lakeshore, Ste-Anne-de-Bellevue, Québec H9X 3V9, Canada

*Address correspondence to: Anja Geitmann (geitmann.aes@mcgill.ca)

Author contributions

A.J.B. and A.G. designed the study, A.J.B. performed the modeling and the experiments. B.A. provided the CGA treatment results. A.J.B., F.P.G., and A.G. analyzed the data, A.J.B. and A.G. wrote the manuscript.

4.1 Summary

Plant cell shape is governed by the mechanical properties of the cell wall and is intimately related to the specific function of the cell. Pavement cells covering the surface of plant leaves form wavy interlocking patterns in many plants. We use computational mechanics to simulate the morphogenetic process based on experimentally assessed cell shapes, growth dynamics, and cell wall chemistry. The simulations suggest a multi-step process underlying the morphogenesis of pavement cells. The mechanical shaping process relies on spatially confined, feedback-augmented stiffening of the cell wall in the periclinal walls, an effect that correlates with experimentally observed deposition patterns of cellulose and de-esterified pectin. Furthermore, we provide evidence for mechanical buckling of the pavement cell walls that can robustly initiate patterns and may precede chemical and geometrical anisotropy.

Keywords: Plant cell mechanics, mechanical modeling, leaf, epidermis, pavement cell, interlocking, morphogenesis, pectin, cellulose, growth, development, cell wall, finite element analysis, buckling

4.2 Highlights

- Mechanical modeling predicts that spatial variations in the cell wall mechanical properties in the periclinal walls are required for the development of interlocking cell patterns in the leaf epidermis.
- The neck (indentation) side of an undulation is characterized by bundled cortical microtubules, an accumulation of cellulose microfibrils, and de-esterified pectin in the periclinal walls.
- Modeling predicts that a stress-stiffening feedback mechanism is sufficient to generate the pronounced wavy shapes of the cell borders.
- Proof of concept is provided for mechanical buckling and the resulting formation of stress hotspots as steps preceding chemical and mechanical isotropy breaking of the cell wall.

4.3 Introduction

Differentiation of plant cells begins with simple spherical or polyhedral bodies produced by cell division in the apical or lateral meristems. The cells formed at the shoot and root apical meristems are approximately cubic whereas those deriving from lateral meristems tend to be longitudinal and brick shaped—all possess a relatively simple geometry. During differentiation of plant organs, tissue-dependent cell types emerge that exhibit a kaleidoscopic array of different morphologies, depending on location and function (Geitmann and Ortega, 2009; Mathur, 2004). In plants, the morphodynamics of differentiating cells is intimately linked to the mechanics of the extracellular matrix—the cell wall. While shaping processes are regulated by the cytoskeleton, they are not mechanically driven by it, since the forces generated by cytoskeletal arrays are too small to act against the wall (Money, 2007). The plant cell wall is a hydraulic structure that regulates the shape of the plant cell by balancing the intrinsic turgor pressure and external mechanical constraints through its compliance (Geitmann and Ortega, 2009). The turgor pressure propelling cell expansion is a scalar acting uniformly on all cellular surfaces. Therefore, to grow into complex shapes, plant cells must meticulously regulate the mechanical properties of the wall in space and time and at subcellular scale. This is important since, unlike animal cells, morphogenetic processes in plant cells are typically irreversible.

The wall of growing plant cells, the primary wall, is a composite material comprising several types of polysaccharides, proteins, ions and water. Two main structural components of the primary cell wall are pectins and cellulose microfibrils (for a recent review see Bidhendi and Geitmann, 2016). Cellulose microfibrils are generally recognized as the main load-bearing component that confer anisotropy (Anderson et al., 2010; Baskin, 2005; Bidhendi and Geitmann, 2016; Burgert and Fratzl, 2009; Crowell et al., 2011; Geitmann, 2010), whereas pectin chemistry influences the local stiffness of the wall (Bidhendi and Geitmann, 2016; Palin and Geitmann, 2012). Both cellulose microfibrils and pectins are thought to direct the local shaping of cells, but hitherto these concepts have mostly been investigated in cells with simple shapes such as pollen tubes (Fayant et al., 2010), root hairs (Shaw et al., 2000), trichome branches (Yanagisawa et al., 2015), cells of root and shoot epidermis (Baskin, 2005; Peaucelle et al., 2015). How growing plant cells form complex shapes is poorly understood (Bidhendi and Geitmann, 2018a).

Some of the most intriguing manifestations of plant cell morphogenesis occur at the surface of the leaves. The three cell types composing the leaf epidermis—guard cells, trichomes and pavement cells—are geometrically very different from one another. In the leaf epidermis of many plants, pavement cells interlock by generating alternately placed protrusions (lobes) and indents (necks) (Vőfély et al., 2018). The resulting pattern resembles a jigsaw puzzle (Figs. 4-1A and B). This complex growth pattern of leaf pavement cells makes them an ideal model to study mechanisms underlying the formation of complex shapes in plant cells (Bidhendi and Geitmann, 2018a; Geitmann and Ortega, 2009; Mathur, 2004; Szymanski, 2014). Various biomechanical concepts have been proposed to explain the formation of lobes in pavement cells (Jacques et al., 2014; Korn, 1976; Korn and Spalding, 1973; Majda et al., 2017; Watson, 1942). Hypotheses range from buckling of the cell walls resulting from the growth of cells in a confined space, inhibition of pavement cell expansion due to forces from cuticle or inner mesophyll layers to localized outgrowth of the anticlinal cell walls (Korn, 1976). The 'localized outgrowth' hypothesis is the most widely accepted explanation for shape generation in pavement cells. It states that regions of localized outgrowth penetrate into neighboring cells (Korn, 1976). The orchestrated formation of alternate necks and lobes in adjacent cells implies that a signaling mechanism must exist that operates across the walls connecting neighboring cells. The concept of local growth activities has been correlated with well-organized microtubule bundles in neck regions and accumulation of actin microfilaments at sites of lobes both of which had been proposed to be regulated by auxin-mediated antagonistic pathways (Fu et al., 2005; Fu et al., 2002; Xu et al., 2010), but these notions warrant further investigation (Belteton et al., 2017). Although their exact roles in this context are poorly defined, actin microfilaments and microtubules are key players in determining pavement cell shape (Mathur, 2004, 2006; Smith, 2003; Smith and Oppenheimer, 2005; Zhang et al., 2011). Evidence for this has been provided by pharmacological and mutation-mediated interference with cytoskeletal functioning which affects pavement cell shape (Baskin et al., 2004; Baskin et al., 1994; Mathur, 2004). Actin microfilament patches in lobes are suggested to promote local outgrowth through exocytotic delivery of new wall-building materials and wall-loosening agents such as expansins (Cosgrove, 2005; Fu et al., 2002; Panteris and Galatis, 2005; Smith, 2003). Microtubules are generally thought to regulate plant cell wall mechanics by determining the orientation of newly deposited cellulose microfibrils (Crowell et al., 2009; Gu et al., 2010). This is accomplished by guiding

the location of insertion and trajectory of cellulose synthase (CESA) enzymes at the surface of the plasma membrane (Hamant and Traas, 2010). Cellulose microfibrils are therefore thought to mimic the orientation of microtubules and, inversely, microtubules have been used as a proxy to infer the localization of cellulose microfibrils (Eng and Sampathkumar, 2018; Fu et al., 2005; Zhang et al., 2011).

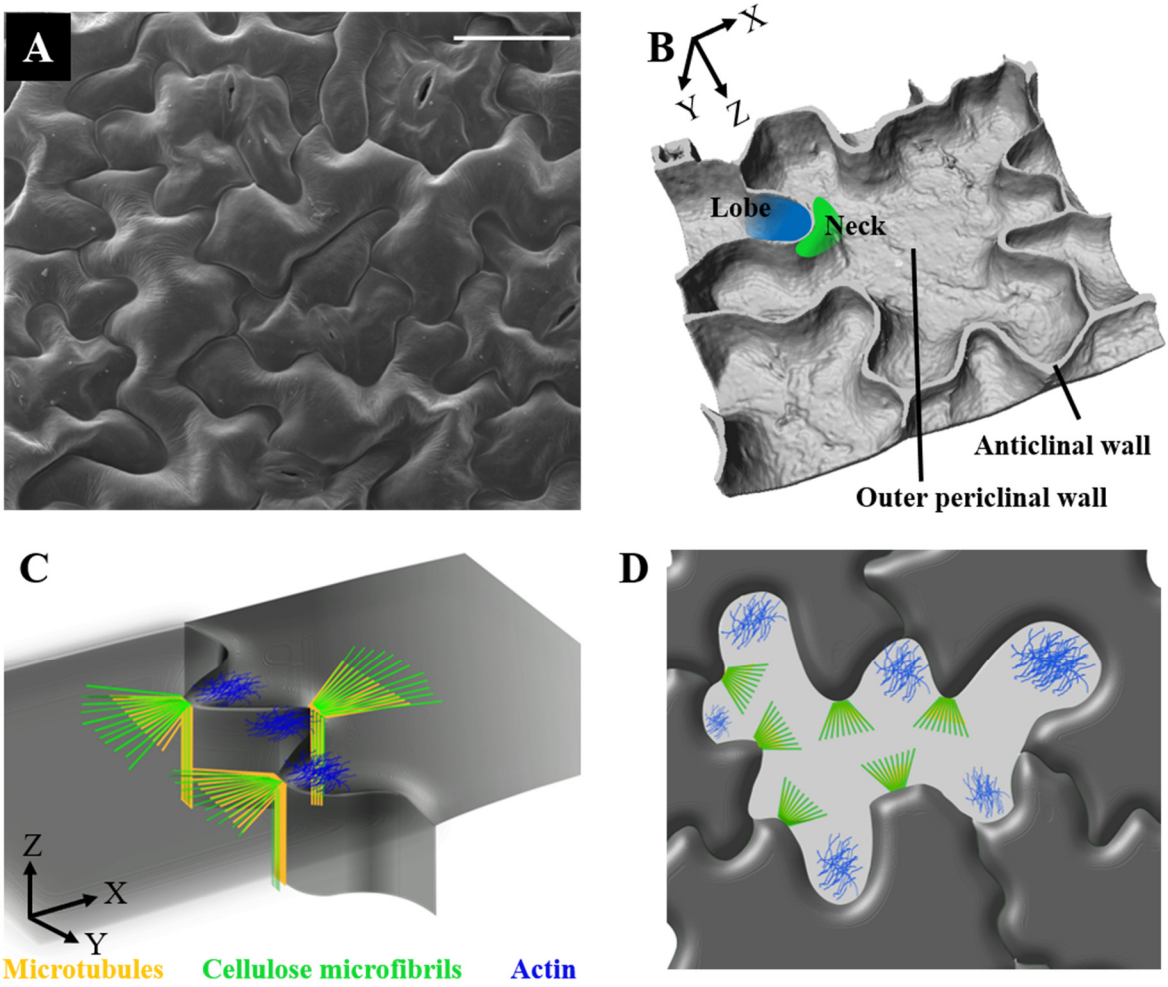

Figure 4-1. Pavement cells in the leaf epidermis of *Arabidopsis thaliana*. **A)** Scanning electron micrograph showing jigsaw puzzle shaped pavement cells (Scale bar = 30 µm). **B)** 3D reconstruction of confocal microscope z-stack of a pavement cell consisting of the outer periclinal and anticlinal cell walls. **C)** Local deposition of cellulose microfibrils (red) guided by microtubules (green) on anticlinal and periclinal walls proposed by (Panteris and Galatis, 2005). Tips of lobes display actin arrays (blue) as shown by (Armour et al., 2015; Fu et al., 2005) **D)** Paradermal view of pavement cells showing localization of microtubules, cellulose microfibrils, and actin microfilaments.

In pavement cells, two effective microtubule arrays are suggested to be involved in the formation of a neck region and add cellulose microfibrils at these locations. In an influential paper, Panteris and Galatis (2005) proposed that a cortical array underlies the anticlinal wall of a neck and is contiguous with a cortical array that spreads out beneath the adjacent periclinal wall (Fig. 4-1C and D). Actin filaments are suggested to be present mostly in lobe regions promoting expansion (Panteris and Galatis, 2005) (Figs. 4-1C and D). Panteris and Galatis proposed that the essence of shape formation in pavement cells involves a distinct cellulose configuration on the neck side of the undulations and a resulting stiffening of the cell wall, but mechanical validation of this concept is absent (Jacques et al., 2014). The role of the wall polysaccharides in mediating the mechanical conditions has not been investigated in detail. Further, cellulose orientation has not been directly visualized in pavement cells using fluorescence techniques. In a recent study by Sampathkumar et al. (2014a), the effect of pavement cell shape on the stress state of the cell wall and microtubule reorganization was modeled mechanically. However, while this relationship may constitute one step of a patterning mechanism governing development, it does not explain the initiation of polarized shapes and lobe formation *de novo*. Importantly, however, in this study a convincing causal link is made from cell shape to spatial orientation of microtubules, but the reverse question of the effect of microtubule orientation (or of cellulose microfibrils) on shape development remains unexplored. Recently, Majda et al. (2017) proposed a role for differential polysaccharide distribution in the anticlinal walls, a 2D morphogenetic concept that we tested further in the context of our own simulations.

We developed 2D and 3D finite element (FE) models to explore the pavement cell mechanics and elucidate how undulating patterns initiate and how they progress starting from simple polygonal geometries. We validated the predictions made by the simulation experimentally by monitoring the spatial distribution of putative mechanical players including pectin, cellulose microfibrils, and microtubules to validate their predicted behavior in cell morphogenesis.

4.4 Results

4.4.1 Verifiable predictions on cell wall deformation through finite element modeling

Finite element modeling was used to simulate the deformation of the cell wall under the application of internal pressure (turgor) as the deforming force. The finite element method is a mathematical tool widely used in structural mechanics and allows for solving problems involving complex material behaviors and geometries. The results of the mechanical model were used to interpret the experimentally acquired data on cell wall composition and microtubule arrangement to identify the mechano-structural requirements for the formation of interdigitations in pavement cells. Details about the parameters used in models are referenced to and explained in the supplemental information where applicable.

4.4.2 Generating cellular protrusions based on anticlinal wall modification requires differential turgor pressure

The undulations in epidermal pavement cells as seen from above correspond to the edge forming the junction between the anticlinal and periclinal walls. We term these undulating edges the *superficial cell borders* (*superficial outer* or *inner* corresponding to outer and inner periclinal walls of a cell, respectively). Since the undulations in the superficial borders of leaf pavement cells correspond to bends in the anticlinal wall, the putative differential expansion of this wall structure has been the primary focus of various experimental or modeling studies (for instance refer to Jacques et al., 2014; Majda et al., 2017). To determine which mechanical conditions would be required to generate a bend in the anticlinal wall resulting in the protrusion of one cell into the neighboring cell, we isolated the problem and developed a finite element model of a section of anticlinal wall between two adjacent cells (Fig. 4-2A). For this isolated approach, periclinal walls were neglected. The anticlinal wall was constructed to consist of two layers (the primary walls of the two adjacent cells) that are glued together (by the middle lamella, a pectin-rich, thin layer that connects cells in a plant tissue).

The first hypothesis we tested assumes that the curvature in the anticlinal wall is generated because of different growth rates of the two layers, similar to a temperature controlled

actuator consisting of two layers with different thermal expansion properties or in curling of thin bilayers (Pezzulla et al., 2016) (Fig. 4-2A). Relative displacement between the layers is not allowed to mimic the role of the middle lamella. One layer is set to expand at a higher rate by assigning a higher coefficient of thermal expansion—our modeling equivalent of adding new cell wall material. The simulations show that the layer at the convex (neck) side of the forming bend is the one with the higher rate of expansion (Fig. 4-2B). However, this contradicts our understanding of the biology of pavement cells. An actin array at the concave (lobe) side of undulations (Fig. 4-1D) suggests that delivery of new cell wall material by exocytosis occurs predominantly on this side of the double wall (Armour et al., 2015; Panteris and Galatis, 2005). The finite element model based on asymmetric anticlinal wall expansion predicts the opposite—addition of new cell wall material on the convex side of the undulation.

The second hypothesis we tested is not based on modulation of wall growth behavior, but on that of the acting forces. We examined whether differential turgor in neighboring cells can generate a bend in the anticlinal wall. For modeling, the cell geometry is hexagonal (Figs. 4-2C and 4-8SA). As above, non-slipping non-separable contact is considered between the anticlinal wall layers in contact. This is to reflect the adhesion between the cell wall layers at the middle lamella. Turgor pressure is exerted on the internal surfaces of both cells, and the model allows for independent adjustment of the turgor pressure in each cell. At equal turgor pressures in the two neighboring cells, the overall shape and the relative position of the midline of the anticlinal wall in contact between two cells does not change as the forces acting on the two sides cancel each other out. If differential turgor pressures are applied, the cell with the higher pressure curves into the cell with lower pressure (Fig. 4-2D). A more spatially confined deformation similar to a lobe protrusion can be achieved if the anticlinal wall layers are made softer on a limited length, combined with the application of differential pressure (Figs. 4-2E and F). To produce a local protrusion, this locally reduced stiffness must be applied to both wall layers in the same region (although not necessarily at the same magnitude). If only one wall layer is softened, the deformation resulting from the differential pressure application causes an overall bend of the entire wall section rather than a spatially confined protrusion.

4.4.3 Mechanical changes confined to anticlinal walls cannot reproduce cell growth

To investigate whether the predictions made by the isolated anticlinal wall model remain valid in the presence of the periclinal walls, these are added to the finite element model (Figs. 4-2G and H). The aspect ratios for cell wall dimensions are adopted from average values obtained from pavement cells in *Arabidopsis* cotyledons at early stages of development (e.g., Fig. 4-12SH). Periclinal wall thickness is set to be identical to that of the anticlinal walls, and the material is configured to be isotropic with uniform stiffness. The pressure in the right cell is set 10:1 compared to the cell on the left. The simulations show that upon application of the turgor pressure the cells swell out of the plane, the free anticlinal walls displace inward, reducing the in-plane cell surface (Fig. 4-2H). The anticlinal wall shared with the neighboring cell displaces toward the cell with higher pressure (Figs. 4-8SB and D). Softening of the whole anticlinal wall in the contact region between the cells results mainly in an upward stretch of this wall, a displacement toward the cell with a higher pressure with a bulge in the mid-depth of the anticlinal walls toward the cell with lower pressure. However, the borders of the anticlinal and periclinal walls remain relatively straight (Fig. 4-8SC). A high ratio of turgor pressures (100:1) was used to produce a discernible behavioral trend. Even at this unphysiologically high pressure differential, the protrusion remains isolated to the anticlinal wall and forms no visible wave at the superficial borders of the cells. Similar results are obtained when the softening is confined to an isolated region of the contact anticlinal wall. Therefore, unlike the isolated anticlinal wall model, if cell walls are isotropic, pressurization of a cell does not generate behavior expected from a differentiating epidermal cell. It neither increases the area of the cell in plane nor does it generate anticlinal curvatures into the adjacent cells. These results can be explained considering the respective surface areas of the periclinal and anticlinal walls. Since the combined inner and outer periclinal walls of a cell possess a higher surface area compared to the combined anticlinal walls of the same cell (see for instance Fig. 4-12SH), the force of the turgor pressure acting

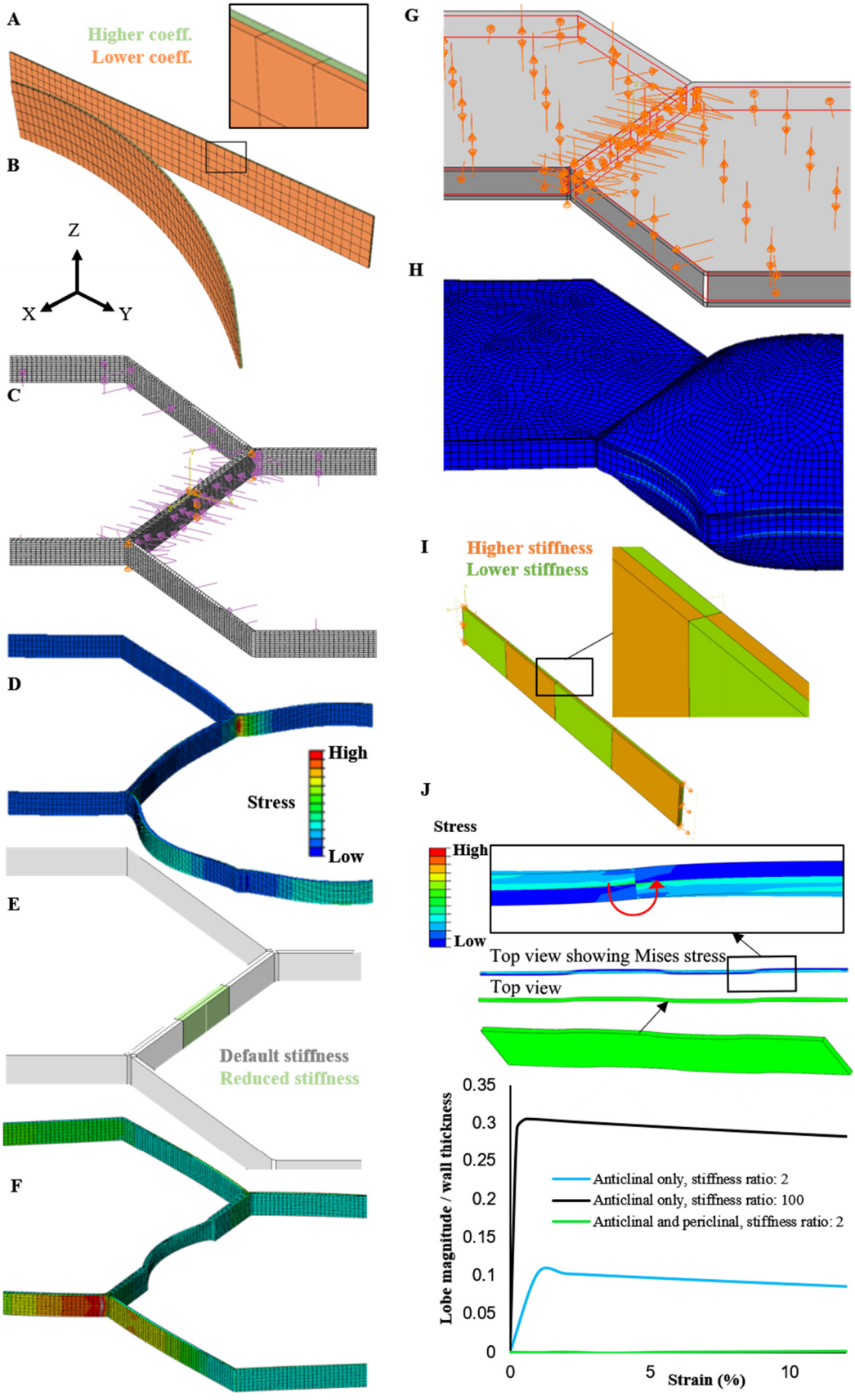
A
Higher coeff.
Lower coeff.
B
Z
X
Y
C
D
High
Stress
Low
E
Default stiffness
Reduced stiffness
F
G
H
I
Higher stiffness
Lower stiffness
J
Stress
High
Low
Top view showing Mises stress
Top view
Lobe magnitude / wall thickness
0.35
0.3
0.25
0.2
0.15
0.1
0.05
0
0
5
10
Strain (%)
Anticlinal only, stiffness ratio: 2
Anticlinal only, stiffness ratio: 100
Anticlinal and periclinal, stiffness ratio: 2

Figure 4-2. Finite element model simulating the differential growth of anticlinal cell wall layers. **A)** Representation of anticlinal wall separating adjacent cells by two material layers glued together at their interface. One layer (green) is given a higher coefficient of thermal expansion to simulate higher growth rate; the right end of the wall may move in space. **B)** Differential expansion of the layers results in the formation of a curvature with the faster-expanding layer forming a convex curve. **C)** Finite element model of the walls of two adjacent cells. Only anticlinal walls are considered; loads are applied on internal surfaces of the walls. **D)** In the presence of differential pressures and uniform anticlinal wall stiffness the anticlinal wall forms a second order curve into the cell with lower pressure. Heatmap represents stress. **E)** A spatially confined region (green) in the anticlinal wall is assigned a softer value than the default stiffness (gray). **F)** A turgor differential results in the formation of a local protrusion into the cell with lower turgor. **G)** Periclinal walls are added to the model. **H)** When periclinal walls have isotropic material properties, the cell with the higher turgor pressure forms a more pronounced swelling in Z pulling the anticlinal walls inwards. **I)** Anticlinal wall model designed to possess alternating zones of stiffening across and along the wall. At one end of the geometry a fixed boundary condition is set while the other end is stretched. **J)** For a stiffness ratio of 100:1 between the stiff and soft segments, slight waves appear in the anticlinal wall when stretched. The strain and stresses shown in the magnified top view demonstrate that the waves are produced due to local moments produced by the abrupt change in the material stiffness. The magnitude of a wave does not exceed 0.3 times the cell wall thickness. The maximum is observed at small strains. At higher strain values the minute bends flatten out. In this model, the stress (shown as von Mises stress) is higher in the lobe (protrusion) side of the wall.

upon them ($F = P \times A$, where P is the pressure and A is the surface area on which the pressure is exerted) is greater and results in a net out-of-plane deformation of the cell. This is not to consider that, regardless of the difference in surface area, the effect of turgor pressure on anticlinal walls can be cancelled out when the pressure inside neighboring cells are equal. The resulting deformation of the periclinal walls leads to a contraction of the in-plane dimensions of the cell. These simulations therefore suggest that isotropic softening of the anticlinal walls does not cause epidermal plant cells to grow in plane. This strongly suggests that attention must be focused on the periclinal walls.

From the above, it seems that the control of lobe expansion may not lie with the anticlinal wall, but we wanted to assess whether possibly the initiation of lobes could be triggered by processes in the anticlinal wall. Recently, Majda et al. (2017) proposed a mechanical model that suggests this might be the case. The authors propose that alternate placement of stiffness along and across the anticlinal walls results in wavy anticlinal walls upon stretching. Based on their simulations the authors propose that the stiff and soft segments in the anticlinal wall form the

lobes (protrusions) and necks (indents), respectively, when the anticlinal wall is stretched by 'tissue forces'. To further assess the predictive power of this model, we reproduced the finite element models of the proposed mechanism. As proposed by Majda et al. (2017), we simulated an isolated anticlinal wall placing alternating stiff and soft regions along and across the anticlinal wall (Fig. 4-2I, 4-14S). Majda et al. (2017) had used a linear elastic material model for investigating the cell wall behavior. Details of our model construct can be found in the supplemental information, and Figs. 4-2I, J and 4-14S. Using the same stiffness ratio of 2 that was used by Majda et al. (2017) we were not able to produce any discernably wavy shapes. Upon very slight stretching (strains∼1%), the anticlinal wall made a quantitatively detectable deformation that, however, did not surpass 0.1 times its own thickness (Fig. 4-14SC). In other words, in an anticlinal wall of 1 μm thickness, the amplitude of this curvature would be 100 nm, significantly less than its own thinnest dimension. Upon further stretch, this minute deformation disappeared and the band straightened. The minute bend is generated by the moment at the abrupt transition between opposing stiffness changes in the model. In an attempt to reproduce discernible waves similar to those presented by Majda et al. (2017), we increased the stiffness ratio to 100:1, keeping all other parameters constant. While this led to a small increase in the maximum wall bending, the deformation remained extremely shallow and did not surpass 0.3 times the thickness of the wall (Fig. 4-2J and 4-14SE).

Even minute deformations might represent an initial trigger that could lead to undulation formation if enhanced by a subsequent amplification mechanism. Therefore, we wanted to test whether the minute deformations generated in the anticlinal wall by the Majda et al. (2017) model would still be produced once the periclinal wall is considered. To this end, we added the upper and lower periclinal walls to the finite element model. With all the parameters kept constant, the minute deformations observed earlier virtually disappeared (Figs. 4-2J, and 4-14SD, E). Whether or not turgor pressure is applied to the periclinal walls did not affect the outcome. In our hands, the model proposed by Majda et al. (2017) is, therefore, unable to generate any undulations when the periclinal walls are included.

Two additional features of the model by Majda et al. (2017) discouraged us from pursuing this approach further. Firstly our simulations of the model proposed by Majda et al. (2017) showed that the lobe side of the anticlinal undulation experiences higher stress compared

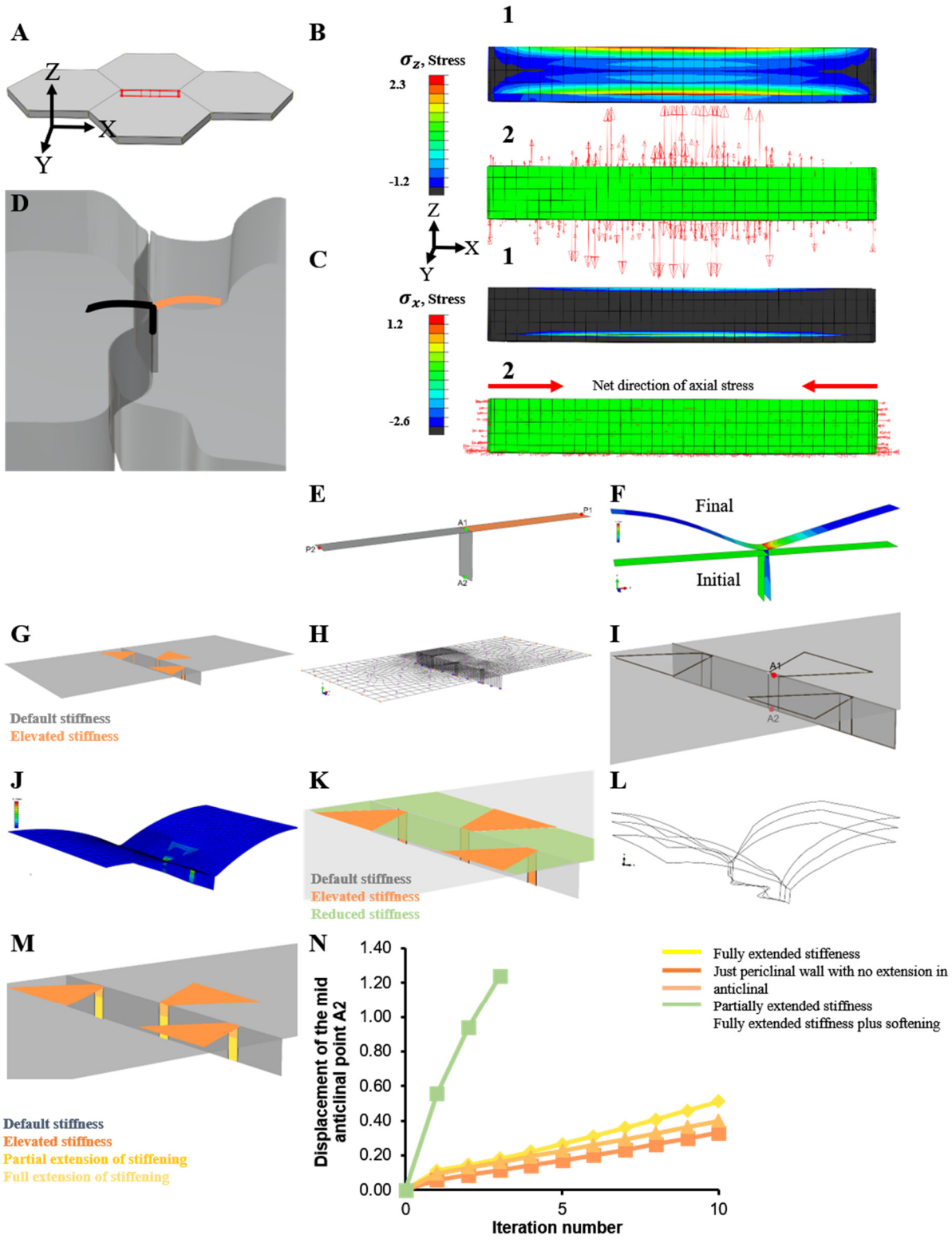
A
Z
X
Y
B
1
σ_Z, Stress
2.3
-1.2
2
Z
X
Y
C
1
σ_X, Stress
1.2
-2.6
2
Net direction of axial stress
D
E
A1
P1
P2
A2
F
Final
Initial
G
Default stiffness
Elevated stiffness
H
I
A1
A2
J
K
Default stiffness
Elevated stiffness
Reduced stiffness
L
M
Default stiffness
Elevated stiffness
Partial extension of stiffening
Full extension of stiffening
N
Displacement of the mid anticlinal point A2
1.40
1.20
1.00
0.80
0.60
0.40
0.20
0.00
0
5
10
Iteration number
Fully extended stiffeness
Just periclinal wall with no extension in anticlinal
Partially extended stiffness
Fully extended stiffness plus softening

Figure 4-3. Finite element simulation of stresses and resulting deformations upon load application through turgor pressure. **A)** Multicell finite element model used to assess stress pattern in the anticlinal walls between hexagonal cells. The red square marks the anticlinal wall that is shown isolated in B and C to reveal stresses. In this wall, stress components in vertical direction **(B)** are significantly larger than in horizontal direction (**C**). **B-1)** Color-coded distribution of vertical (Z direction) component of wall stress. **B-2)** The arrows indicate the magnitude and direction of the vertical stress. **C-1)** Color-coded distribution of axial (X direction) component of wall stress. **C-2)** The arrows indicating axial stress in horizontal direction show the compressive stresses resulting from the vertical expansion. Stress values are relative as normalized input values are used in models (see modeling procedures and supplemental information). **D)** Position of segment crossing two adjacent cells modeled in **E-N**. Segment comprising sections of the periclinal walls of the two adjacent cells and the shared anticlinal wall. **E)** Shell model of wall segments. Pressure load is applied on lower surface of the periclinal walls, similar to loading in 2D beam model shown in Fig. 4-9SA. **F)** Deformation in the shell model is similar to the beam model. **G)** Finite element model with alternate placement of stiffened regions on the periclinal and anticlinal walls of two adjacent cells. **H)** Turgor pressure is applied to inner surface of the periclinal walls (no pressure on the anticlinal wall as the acting forces cancel each other out). **I)** Position of fiducial markers used to monitor shape formation by measuring the displacement of the anticlinal wall. **J)** Initiation of undulations in the first iteration of the model. Heatmap represents von Mises stress. **K)** Finite element model with alternate placement of stiffened regions on the periclinal and anticlinal walls of two adjacent cells with cell wall softening in areas between the incipient necks. **L)** Evolution of undulations for three iterative load applications. **M)** Stiffening extensions on the anticlinal wall extending into different depths. **N)** Displacement of the anticlinal wall mid-point (A2) under different wall stiffening-softening scenarios reveals that fully extended stiffening leads to more pronounced undulation, but the effect is small compared to that of a softening in the periclinal wall.

to the neck side (Fig. 4-2J). As will be discussed later, this is incompatible with the rest of our knowledge on the mechanics of wavy epidermal cells. Secondly, the model by Majda et al. (2017) is conceptually unable to produce first order bends observed in many young cells (see simple bends in early-stage cells and our contraction-based models, e.g., Figs. 4-6H, 4-7F, 4-12SH and 4-8S). Since for generation of lobes and necks in the model by Majda et al. (2017) a stiffness transition along the wall is needed, the minimum number of peaks that could be generated in a single segment of anticlinal wall would be a pair, each curve being on one side of the transition point. All evidence combined, we decided that any further approach cannot focus solely on the anticlinal wall but should include the periclinal walls in the simulations to be relevant.

An important consequence of the presence of the periclinal walls is the tensile force that is exerted on the anticlinal walls through the pressure that causes the periclinal wall to bulge out of the epidermal plane. To assess the resulting stresses generated in the anticlinal wall, the FE model was extended to represent four cells (Fig. 4-3A). The pressure is set equal in all cells. The anticlinal wall to be analyzed is the one in the center between the four cells. Boundary conditions are applied to the corners of the lower periclinal walls to simulate an attachment to the underlying mesophyll layer. In the anticlinal walls, the vertical component of the stress was considerably larger (σ_z against σ_x, Figs. 4-3B and C), revealing the net direction of stress in these walls. Consistent with the results mentioned above, the results indicate that the transverse component of the stress (σ_x) can become locally negative (compressive). These findings indicate that forces with the potential to induce buckling in the anticlinal walls can arise simply from cell geometry.

4.4.4 Differential stiffness in the periclinal wall can generate cell border undulations

Given that spatial variations in the mechanical properties of anticlinal walls cannot yield wall undulations similar to those seen in pavement cells, we hypothesize that considering the mechanical properties of periclinal walls might be crucial in growth and shaping of cells. We postulate that to form undulating borders, the mechanical properties of the periclinal wall must vary in alternatingly arranged, spatially confined regions as initially proposed by (Panteris and Galatis, 2005) (Fig. 4-1C). We first consider the generation of an isolated bend in the cell border by focusing on a transverse segment including both anticlinal and periclinal wall segments. In this one-dimensional approach, the periclinal walls of two adjacent cells are modeled with beam elements with a shared anticlinal wall as a vertical beam (Fig. 4-3D). The periclinal walls of the two adjacent cells are assigned different initial stiffness values, and then turgor pressure is applied to the beam elements (Fig. 4-9SA). The boundary conditions imposed on this model, as with the 2D shell model of Fig. 4-3E, enable horizontal (in X direction) movement for the end-point of the anticlinal wall (A2) which represents the midway point of the entire anticlinal wall depth. The periclinal end-points (P1 and P2) can only move in the Y direction. The point corresponding to the connection of the anticlinal wall with the periclinal walls (A1) may move

in all directions. Similar boundary conditions are applied to all models henceforth. The 2D thin shell model of the same situation yields the same results confirming the robustness of the predictions independently of the modeling tools (Fig. 4-3E, F, and 4-9SD). The simulations show that upon application of equal pressure in both cells, the periclinal walls bulge out (in the Z direction), but the wall with the higher stiffness deforms less than the periclinal wall of the neighboring cell. Consequently, the anticlinal wall moves from the mid-point towards the cell with the stiffer periclinal wall. This displacement of the mid-point connecting the two cells could be considered to represent the formation of a protrusion with the lobe being formed by the cell with the lower periclinal wall stiffness (Fig. 4-9SB).

In these simulations, the stiffness differential is implemented *ab initio*; prior to application of the turgor pressure (*ab initio* stiffening). To assess whether the order of the events affects the final state of cell wall deformation, stiffening is implemented in cells already under turgor pressure (*cum tempore* stiffening). Simulations reveal that it does not matter for the outcome whether the cells are under turgor or relaxed when the stiffening of one of the periclinal cell walls is implemented (Figs. 4-9SC-F). In a biological sense, this means that when a segment of the periclinal wall is reinforced, either by deposition of cellulose or by changes in other cell wall polysaccharides, a shift of the relative position of the anticlinal wall toward the cell with the stiffened periclinal wall can be expected upon the next step in development. This does not depend on whether or not the cell wall is under stress when the stiffening occurs.

4.4.5 Differential turgor does not steer pavement cell morphogenesis in the presence of a stiffness differential in the periclinal wall

To verify the influence of turgor pressure on the formation of necks, differential turgor is applied to the two neighboring cells as detailed in the previous section. The results show that in all cases, regardless of the relative turgor pressures in the two cells, the anticlinal wall is displaced toward the cell with the stiffer periclinal wall (Figs. 4-10SA-F) as it stretches less under tension compared to the softer side. In extreme conditions, when the pressure on the stiffened side approaches zero, the horizontal (in X direction) displacement of the anticlinal wall becomes negligible (Figs. 4-10SE and F). This means that the mechanical and geometrical properties of

the cell wall are so dominant that they seem to largely override the effect of pressure differentials.

Further, it is observed that when the anticlinal wall is stiffer than the default value (i.e., the value of the non-stiffened periclinal wall), the displacement of mid-points corresponding to points A1 and A2 in Fig. 4-3E is enhanced as the anticlinal wall deforms less under the effect of the turgor differential (Figs. 4-10SA-F). Taken together, the simulations suggest that differential turgor pressure is not a requirement to form pavement cell undulations, but that cell wall mechanics seems to be dominant.

4.4.6 The relation between stiffness differential and undulation is non-linear

To assess how different the stiffnesses between the lobe and neck on the opposing periclinal walls must be for an undulation to evolve, different ratios of stiffness between the stiffened and default periclinal walls are examined by monitoring the resultant displacement of the anticlinal wall. As the ratio increases from 1 to 5, the displacement of the anticlinal wall increases rapidly, but beyond this value the deformation plateaus (Fig. 4-11SA). At this point, the stiffer side behaves as a rigid structure compared to the softer (lobe) side. Unless turgor pressure is increased, any additional stiffness in the stiffer wall does not result in a perceivable increase in horizontal (in X direction) displacement of the anticlinal wall.

We then wanted to test whether subtle stiffness differentials would lead to undulations if load application is repeatedly applied. Iterative load application is accomplished by re-zeroing the stress developed in shell elements following each load application and by repeating the simulation, starting off with the last deformed shape. Running the simulation for 5 iterations shows that the resulting horizontal (in X direction) displacement of the anticlinal wall is negligible compared to the vertical (out of epidermis plane, in the Z direction) deformation (Fig. 4-11SB). Therefore, when continued, the cells only balloon out of the plane, not forming discernable undulations. This demonstrates that repeated load application does not cause more pronounced wave formation if the stiffness difference is negligible, to begin with, and remains constant. A sufficiently large stiffness ratio between the two periclinal wall segments is required even when repeating the load application with stress relief (Fig. 4-11SC).

4.4.7 Reproducing an interlocking pattern of pavement cells requires alternate positioning of differential stiffness along the periclinal walls

The simulations thus far indicate that locally increased stiffness of a periclinal wall segment at one side of a cell-cell border can displace the relative position of the anticlinal wall in the presence of turgor. To verify whether the observed deformation in the periclinal segments and displacement of the anticlinal wall can reproduce alternatingly positioned necks and lobes, finite element models of larger wall segments are developed to incorporate multiple, alternatingly placed regions of cell wall stiffening (Fig. 4-3G). To follow experimental observations on microtubule distribution, which presumably are translated to enhanced cellulose deposition, the stiffening regions on periclinal walls are extended in the depth of the anticlinal walls. Equal turgor pressures are applied in both cells (Fig. 4-3H). To assess the magnitude of the shape forming effect, horizontal (in X direction) displacement of the mid-point of the anticlinal wall (A2) is recorded in each simulation (Fig. 4-3I). The results of the simulations show that one iteration of pressure application will cause a displacement of the anticlinal wall that simulates the initiation of lobes and necks (Fig. 4-3J). The distribution of stresses reveals that regions of higher stress correspond to the regions with higher cell wall stiffness. To attain more pronounced lobes and necks, the process of turgor application is repeated. After each iteration, the deformed geometry (output) is used as initial geometry (input) for the next iteration, and wall stresses are readjusted to zero. The subsequent simulation is performed with all other parameters kept constant (Fig. 4-11SE). This model shows how continuous deformation of the cell wall with localized alternatingly placed stiffness on two sides under turgor pressure can develop into lobes and necks. To verify the general validity of the model predictions, independently of implementing isotropic or anisotropic stiffness, an anisotropic model of similar construct was developed. The results confirmed those of the existing isotropic model (refer to supplemental information and Fig. 4-11SD for more details).

4.4.8 Loosening of the cell wall promotes lobe outgrowth

It is thought that the delivery of new wall material and wall loosening enzymes on the lobe side of an undulation, facilitates the expansion of lobe protrusions into the neighboring cells. The provision of this material is presumably mediated by arrays of actin microfilaments (Mathur and

Hülskamp, 2002; Panteris and Galatis, 2005). To examine the effectiveness of wall loosening in generation of interdigitations, the finite element model was modified to allow for spatially confined softening of the cell wall. Similar to the stiffening, the softening is implemented either *ab initio* or *cum tempore*. The location of these softening regions is limited to the zones of the periclinal walls between the stiffened regions (Fig. 4-3K). As above, the triangular stiffened regions on periclinal walls are extended by narrow bands in the depth of the anticlinal wall. Simulations show that softening in the 'inter-neck' regions facilitates greater extension of the wall interdigitation in X-Y plane while the 'ballooning' of the periclinal walls in the Z direction is less pronounced compared to the simulations without the softening (Fig. 4-3L).

4.4.9 Extension of stiffening in the depth of the anticlinal walls enhances but cannot generate pavement cell lobes *de novo*

In the simulations above, the triangular stiffening regions in the inner and outer periclinal walls are connected by extensions of stiffened bands in the anticlinal walls. To investigate the influence of anticlinal wall stiffness extension, we modified this stiffening in the anticlinal wall to be only partially extended or absent and compared the displacement results with the full extension of the stiffened band (Fig. 4-3M). The simulations indicate that in the presence of periclinal wall stiffenings, undulations can be generated without stiffening in the anticlinal wall, but the magnitude of the undulations remain smaller compared to simulations with partially or fully extended stiffened bands in the anticlinal wall (Fig 4-3I, N). Keeping all the other variables constant, the extension of stiffening into the anticlinal wall increases the magnitude of the formed lobe as measured by the relative displacement of point A2.

The presence of anticlinal wall stiffening in the absence of local stiffening in the periclinal walls produces no deformation under application of turgor pressure. This is consistent with the simulations made using the isolated anticlinal wall model. This simulation, therefore, further emphasizes the dominant role of the periclinal wall in the formation of interdigitations.

4.4.10 Multi-cell simulation confirms that local stiffening and turgor-driven stretch of the cell wall can form interlocking pattern in the tissue context

To assess whether the concepts identified above hold for a multicellular context, a multicell finite element model was developed based on an arrangement of multiple, identical whole cell modules with hexagonal geometry and alternatingly located stiffness and softening zones on the periclinal walls (Fig. 4-4A). The periclinal stiffening regions in inner and outer walls are connected by stiffened bands extending in the depth of the anticlinal walls (Figs. 4-4B and C).

As in the previous sections, in this class of models a turgor pressure difference in adjacent cells is not necessary to generate the protrusions. The results indicate that highest stresses correspond to regions with a higher stiffness (neck). Interestingly, the model predicts that stress lines extend between adjacent necks and cross each other in the center of the periclinal cell wall (Figs. 4-4F and 4-11SG).

To investigate the effect of the geometry resulting from the local stiffening and softening of the periclinal walls on the stress pattern in the cell wall, we use the output geometry of the previous simulation as a new input model, but we implement isotropic and uniform material properties. The result of the subsequent load (turgor) application indicates that after the lobes and necks are formed, the geometry itself results in stress anisotropy with higher stresses in necks, even if their stiffness is the same as that of the lobe (Fig. 4-11SG). This confirms the validity in 3D of predictions that had been made previously on a surface model focusing only on the periclinal walls (Sampathkumar et al., 2014a).

4.4.11 A positive mechanical feedback loop based on stress-induced stiffening and lateral inhibition can shape pavement cells

Previously, we showed that if the stiffness ratio between the opposing necks and lobes is not sufficiently large, iterating the simulation with repeated load application cannot produce discernable displacements on cell borders if the stiffness ratio remains constant. However, a living cell is dynamic; it can increase cell wall stiffness by adding cellulose. The deposition of cellulose microfibrils is guided by microtubules, and microtubules orient along stress fields (Landrein and Hamant, 2013; Uyttewaal et al., 2012). In the previous section, we observed that,

even if the cell material possesses a uniform stiffness value in all regions after the lobes and necks are initiated, the shape itself generates higher stresses at the convex sides of the undulations on the periclinal walls. We, therefore, investigated the effect of stress-driven microtubule bundling on the cell shaping process if a feedback mechanism is implemented in which the cell wall is gradually stiffened in regions with locally elevated stress. This is implemented over several iterations starting with an infinitesimally small initial stiffness difference in the periclinal wall segments (4E and F). After each iteration, the model is set to update local stiffness values based on the presence of local stress (Fig. 4-13SA). For this purpose, a Python code was developed to extract the stresses present at each element of the structure at the end of each iteration (output). Based on the local elemental stress, each element is assigned a new stiffness value calculated based on the previous stiffness value and the output stress resulting from the previous iteration.

The initial stiffness difference ratio implemented for this test is 1.01. The results indicate that the deformation upon the first iteration is relatively small and during subsequent iterations, the displacement of the lobe does not increase considerably but reaches a plateau with a negligible displacement. Stresses resulting from a single load application are not local enough to produce undulations through the feedback mechanism (Fig. 4-4E). Essentially, stresses are leveled out over the distances relevant here, and the feedback loop causes an increase in overall stiffness at the border of the two periclinal walls rather than sharpening the differences between neighboring lobe and neck regions.

We, therefore, tested whether adding an inhibitory mechanism could cause an augmentation in stiffness differential during feedback iterations. To implement this, feedback-driven stiffening is prevented in regions between the incipient necks, given as an input to the feedback model (Fig. 4-4F). Lobe formation is amplified by the feedback mechanism even when starting with very small stiffness differences between future necks and lobes (ratio 1.01) (Figs. 4-13SB and 4-4F). These results suggest that while a feedback loop starting from infinitesimally small stiffness differences does produce realistic results, it cannot be based on stress stiffening alone but needs to incorporate a mechanism that prevents stiffening at selected locations.

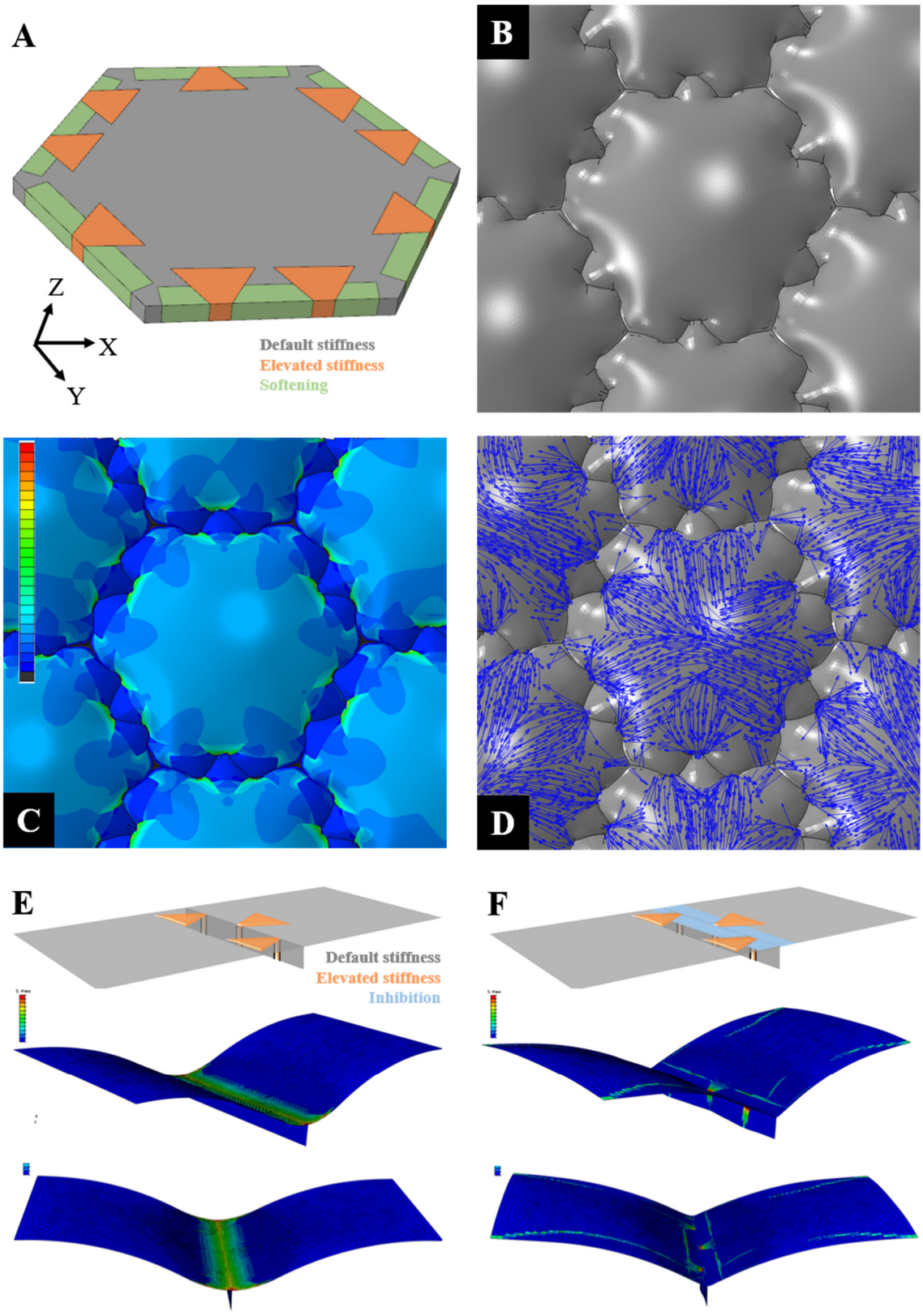
A
Z
X
Y
Default stiffness
Elevated stiffness
Softening
B
C
D
E
Default stiffness
Elevated stiffness
Inhibition
F

Figure 4-4. Shape and stress development in pavement cells based on inhomogeneity in cell wall stiffness. **A)** Whole cell model considering local, alternating stiffening and softening of the inner and outer periclinal walls as well as extension of the stiffened regions in the anticlinal walls. **B-D)** Simulation of turgor induced deformation and stress in a model composed of multiple single-cell units as shown in **A**. The turgor pressure was set equal in all cells. **B)** Shaping of undulations. **C)** Stress pattern generated by turgor application in the periclinal walls and at periphery of tricellular junctions. Heatmap represents maximum principal stresses. **D)** Orientation of stress lines in periclinal walls. **E-F)** Incorporation of positive stress-stiffening feedback mechanism that amplifies stiffness based on local stress conditions starting from minute stiffness differential (ratio 1.01) in periclinal and anticlinal walls. Deformation and stress pattern after hundred iterations of load application. Heatmap represents von Mises stress. **E)** Without inhibition mechanism stiffness differentials even out. **F)** Inhibition of stiffening at alternating locations allows for stiffness differentials to amplify and undulations to form.

4.4.12 Experimental validation of *in silico* predictions

The models above predict that alternating changes in material properties of the cell wall at the site of undulations can produce an interlocking pattern in pavement cells. Changes in material properties suggest that variations in the biochemical composition of the cell wall are involved. To experimentally validate the predictions made by the simulations, we studied the spatial distribution of two major cell wall components known to modulate the mechanical properties of primary plant cell walls: cellulose microfibrils and homogalacturonan pectin (Bidhendi and Geitmann, 2016). This was performed in the epidermis of *Arabidopsis* cotyledons.

4.4.13 Pectin is weakly esterified in neck regions

Our model predicts that the mechanical properties along the cell border vary in space, but it does not specify which biochemical component of the cell wall is responsible for this effect. Pectin de-esterification has been linked to changes in mechanical stiffness of the plant cell wall (Bidhendi and Geitmann, 2016; Braybrook and Peaucelle, 2013; Chebli et al., 2012). We used COS^{488}, an oligosaccharide probe conjugated with Alexa Fluor 488 recently synthesized and reported to be highly specific for de-esterified HG pectin (Mravec et al., 2014). COS^{488} staining typically exhibits higher signals at tips of undulations at the anticlinal walls (Fig. 4-5A). Maximum intensity projections of z-stacks were used to capture all wall areas despite different z-positions in lobes and necks. The results indicate a pattern of de-esterification in the periclinal walls with neck (indentation) side of a curvature exhibiting a higher signal (Fig. 4-5C, D and

E). Interestingly, COS^{488} staining also showed bright spots at cell junctions (Fig. 4-5A). We hypothesize that de-esterification of pectin in the middle lamella might be employed at the junctions to strongly attach the neighboring cells to each other.

A recent study has shown that propidium iodide, a common chemical probe for cell wall staining, has a higher affinity for weakly esterified pectin compared to its highly esterified form (Rounds et al., 2011). We exploited this affinity of propidium iodide to investigate the variations in pectin chemistry in the walls of pavement cells. Living cotyledons of wild-type *Arabidopsis thaliana* taken from seedlings at 2-3, 4 and 5 days after germination (DAG) were stained using propidium iodide and observed under the confocal laser scanning microscope. At this developmental stage, pavement cells have already acquired wavy shapes but continue to grow (Zhang et al., 2011). In the anticlinal wall, the fluorescent signal intensity was typically higher at the tips of the undulations compared to the straight wall segments between two undulations (Fig. 4-12SA). Maximum projections of z-stacks showed that in the periclinal walls higher signal intensities were present on the neck sides of the undulations while at the lobe sides the signal was often dim (Fig. 4-12SB). Comparison of the signal intensity difference between neck and lobe pairs ($n>100$) of different cells ($n=19$) of several cotyledons ($n=5$), showed a significant statistical difference ($p<0.00001$). The same result was obtained when analyzing orthogonal views (Fig. 4-5B). Based on the higher affinity of propidium iodide to de-esterified pectin, we hypothesized that pectin is weakly esterified at neck side of undulations.

Both with the specific de-esterified pectin marker COS^{488} and propidium iodide, the neck side showed a higher fluorescence signal indicating enrichment of de-esterified pectin. While in this study we mainly focused on pavement cells between 2-5 DAG, this association was not limited to larger cells or already wavy wall segments. Indeed, we observed that walls with even a slight curvature in 2-5 DAG stage (Fig. 4-5D) or early stage pavement cells at 1 DAG (Fig. 4-5E) both exhibit a similar pattern on the neck side. However, due to challenges of working with early-stage cells such as staining the periclinal walls, we focused on day 2 after germination onwards. Even at this stage, cells are growing and new cells continue to appear as a result of cell division.

4.4.14 Cellulose microfibrils and microtubules form organized bundles at the neck sides

The pattern of stiffening in the periclinal and anticlinal walls of pavement cells can be mediated through coordinated positioning of cellulose microfibrils which in turn is thought to be controlled by microtubules. We, therefore, wanted to investigate the orientation of microtubules in pavement cells and used cotyledons of GFP lines MAP4 and TUB6 of seedlings between 3-5 DAG. Visualizing the microtubules beneath the outer periclinal wall down to half the thickness of the anticlinal wall showed strong bundling of microtubules in association with necks (Figs. 4-12SC, 4-6A and B). While in lobes microtubules could occasionally be observed, their occurrence in this location was scarce compared to necks. It seems that in central regions of cells, where bundles of microtubules arriving from multiple necks converge, the overall distribution of microtubules becomes random. A similar pattern for stress lines was observed in the multicell models as discussed earlier (Fig. 4-4D). As the GFP-MAP4 line is suggested to be prone to microtubule over-bundling, we used GFP-TUB6 line to confirm the observations (Fig. 4-6C). The results from GFP-TUB6 on microtubule distribution in the outer periclinal wall support the previous results for GFP-MAP4 pavement cells. The fan-shaped orientation of microtubules is more evident in GFP-TUB6 results compared to crowded GFP-MAP4. Interestingly, at some locations, microtubules appear to form bundles while the borderline of cells appears to be relatively straight. These sites were also associated with marked accumulations of microtubule label at the anticlinal walls (arrowheads in Fig. 4-6C). The inner periclinal walls showed a similar trend for the microtubules at locations of fully developed necks as well as for the relatively straight regions corresponding to arrowheads in Fig. 4-6C with a marked bundling of microtubules (Fig. 4-6D). We hypothesize that these regions may mark the onset of new oncoming necks but do not further investigate this in this study. Further, away from the tip of the lobes, bundles of microtubules radiating from two adjacent necks form transverse bundles on the shank of the tube-like lobe (Figs. 4-6A and B). These arrays seem to connect regions of greatest stress which the FE model predicts will develop in the necks. If this results in increased cellulose deposition at these locations, this stiffening would restrict the widening of lobes and instead allows for their elongation. A finite element model shows that

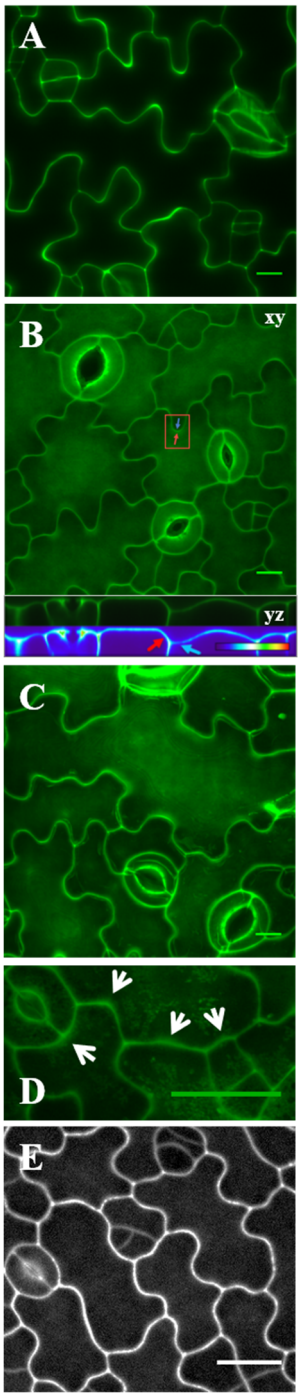

Figure 4-5. Staining for pectins in *Arabidopsis thaliana* cotyledons sampled 3 to 5 DAG. **A)** COS^{488} stain shows varying signal intensity through the length of cell borders and dots at tri-cellular cell junctions. **B)** Propidium iodide and **C)** COS^{488} show higher signal intensity at the neck side of the periclinal walls also visible in the YZ orthogonal section taken at the location of the inset identified by the red rectangle in **B**, shown in monochrome and heatmap. **D)** COS^{488} staining shows that in smaller cells and relatively straight lines and **E)** cells at earlier stages (1 DAG) higher signal appears on the neck side. Scale bars = 10 µm (**A, B and C)** and 20 µm (**D** and **E)**.

placement of stiffened necks produces stress fields that can eventually result in the orientation of microtubules that connect the opposing necks (Fig. 4-4D).

These conjectures on growth behavior of cells based on the orientation of microtubules are based on the presumption that cellulose microfibrils are deposited in the same orientation as microtubules. In the majority of the earlier studies, microtubule orientation has therefore been used as a proxy for cellulose-mediated wall stiffening, although direct evidence was rarely provided. The reason for this is mostly technical since fluorescent labeling of cellulose in living cells covered by a cuticle remains a challenge. To study the distribution and organization of cellulose microfibrils in pavement cells, we used calcofluor white and Pontamine Fast Scarlet 4B (PFS) (Anderson et al., 2010) to stain the living cotyledons. PFS is reported to be highly specific for cellulose and is used in high-resolution imaging of cellulose (Anderson et al., 2010; Liesche et al., 2013).

In confocal images of pavement cells stained with PFS or calcofluor white, a notable concentration of cellulose microfibrils was observed in the neck regions from where they form a divergent fan-shaped configuration in the outer periclinal walls (Figs. 4-12SD, E and 4-6E). Tips of lobes displayed considerably weaker signal and generally seemed devoid of organized microfibrils. However, similar to the organization of microtubules, microfibrils appear to connect neighboring necks (Fig. 4-6F). Similar to the organization of microtubules, in most pavement cells of seedlings between 2-5 DAG, the orientation of cellulose microfibrils in outer periclinal walls away from the undulations were mostly random in mid-regions exhibiting lower aspect ratios or dominantly transverse in narrow cell regions that were axially elongated (Figs. 4-6E, F and N). The association of cellulose bundles with neck (indentation) sides was not limited to pavement cells that display pronounced lobes. We observed that even in pavement cells of cotyledons acquired by removing the seed coat or just germinated, slight cell shape curvatures are already associated with radiating cellulose bundles (Fig. 4-6H).

To investigate the mechanical impact of the observed spatial distribution of cellulose microfibrils on wavy cell shape development, we experimentally reduced cellulose crystallinity and monitored the shape of the same cells in a time-lapse study. Reducing cellulose crystallinity

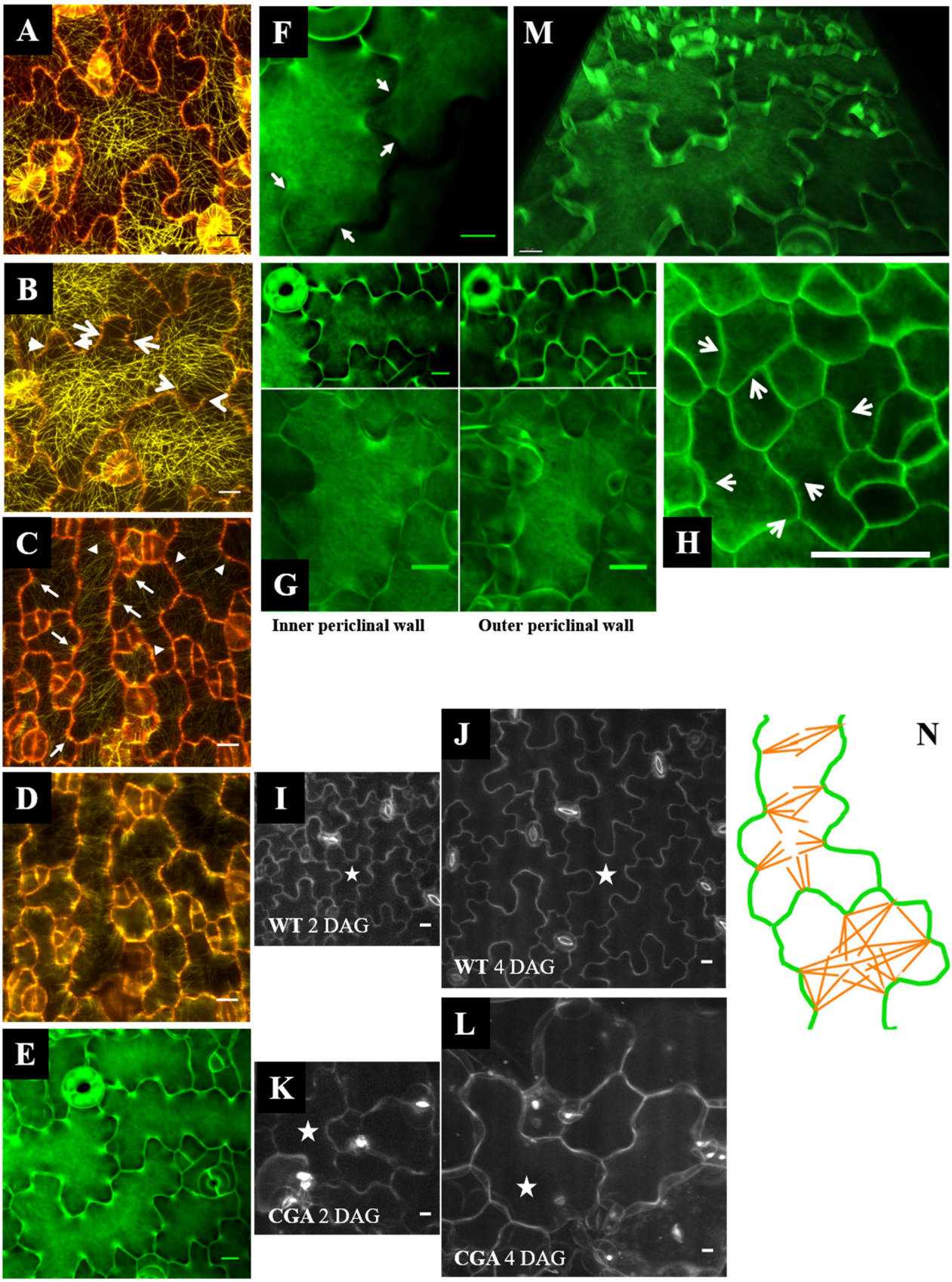
A
F
M
B
G
H
C
Inner periclinal wall
Outer periclinal wall
D
I
J
N
WT 2 DAG
WT 4 DAG
E
K
L
CGA 2 DAG
CGA 4 DAG

Figure 4-6. Organization of microtubules and bundles of cellulose microfibrils in pavement cells. **A)** Microtubules labeled by GFP-MAP4 are abundant in association with the neck sides of undulations. **B)** Frequently microtubules in the GFP-MAP4 line feature neck to neck connections forming circumferential hoops at the shank of lobes (pair of arrows). **C)** and **D)** Microtubules underlying the outer and inner periclinal walls, respectively, of pavement cells in GFP-TUB6 line. The images are single channel maximum projections of confocal Z-stacks, with a single slice containing the cell borders merged in post-processing as a red channel to mark the borders. Scale bar = 10 μm. **E-I)** Cellulose in pavement cells of *Arabidopsis thaliana* cotyledons 3 to 5 DAG stained with calcofluor white. **E)** and **F)** Cellulose microfibrils labeled with calcofluor white, as also observed in staining with PFS (see supplemental information), are concentrated in the necks from where they radiate into the periclinal wall. **G)** Comparison of cellulose orientation in outer and inner periclinal walls of the same cell. **H)** Bundles of cellulose microfibrils demonstrated in early stage, pavement cells of cotyledon extracted from the seed coat even at slight curvatures. The sample is stained with calcofluor white. Same pavement cells of wild-type *Arabidopsis thaliana* cotyledons treated with **I)** and **J)** DMSO and **K)** and **L)** CGA visualized at 2 and 4 DAG. While the DMSO-treated cells showed increase in surface area, perimeter and lobe number the CGA-treated cells developed only a very few lobes and necks (see supplemental information). **M)** Oblique view of a z-stack 3D reconstruction of pavement cells showing that cellulose microfibrils extend into the depth of the anticlinal wall at neck-lobe pairs. **N)** Schematic representation of typical cellulose orientation depending on the aspect ratio of cells: in elongated cells, the microfibrils form a pattern predominantly perpendicular to the long axis. In cells with an aspect ratio close to one, bundles of cellulose are more centrifugally oriented. Scale bars = 10 μm, 20 μm (H).

is suggested to correlate with altered cell shapes and occurrence of a swollen phenotype (Aouar et al., 2010; Fujita et al., 2013). We grew *Arabidopsis* seedlings in presence of CGA 325'615 (CGA), shown to reduce cellulose crystallinity (Crowell et al., 2009; Peng et al., 2001), and monitored shape parameters over 4 DAG. At 2 DAG, cells in samples grown in media containing CGA (treated cell hereafter) and the control cells had the same perimeter and area (supplemental information). However, lobe formation in treated cells was significantly altered. Following the same cells over a period of 4 first days after germination showed that control cells had an average of 9.1 (± 0.7) lobes, whereas treated cells only developed 3.3 (±0.5) at 2 DAG. Over the two subsequent days (at 4 DAG), control cells formed 6-7 additional lobes, whereas treated cells only added 1-2 lobes (see data in Fig. 4-15S). These results indicate a significant reduction in lobe formation when cellulose is affected from early stages of epidermal cell development (Fig. 4-6I-L). This further supports the significance of cellulose in development of wavy cell borders by restriction of expansion in the neck regions. Further, this emphasizes that

the present model is not limited to cells that are already highly wavy but this mechanism is also essential for cells to form any lobes at earlier stages of development

Acquiring images of the cellulose orientation in the inner periclinal walls proved challenging due to the thickness of the samples and the fact that the signal from the inner periclinal walls was challenging to distinguish from the signal deriving from the directly adjacent mesophyll cell walls. However, in some cases, we succeeded and observed that regarding enrichment at necks the cellulose orientation on the inner periclinal wall seems to follow similar trends as the outer periclinal wall (Fig. 4-6G). This motivated us to analyze the cellulose status of the anticlinal walls since they might serve as mechanical links between the inner and outer faces of pavement cells.

4.4.15 Cellulose microfibrils and microtubules form bundles at the undulations that extend in depth of the anticlinal walls coupling the inner and outer walls

3D reconstruction of confocal images of cotyledons stained with calcofluor white revealed that in neck regions cellulose extends down the anticlinal walls (Fig. 4-6M). This can also be observed by re-slicing the Z-stack and acquiring max projections for a few slides before and after the occurrence of an undulation, from two sides (Figs. 4-12SF1 and F2). These observations provide support for the predictions made by the finite element model incorporating alternate placement of stiffness on periclinal walls. As the finite element simulations show, the anticlinal extension of cellulose microfibrils at the undulation can act as a lever, increasing the magnitude of undulations.

Regardless of the mechanical contribution of the anticlinal reinforced bands in the development of undulations, they might transmit the mechanical signal from the inner periclinal wall up to the outer periclinal wall. To visualize this, we used the finite element model with the extension of stiffening in the depth of the anticlinal wall but without stiffened regions on the periclinal wall (Fig. 4-7A). Although this configuration does not generate any undulation in the anticlinal wall, the stress can be partly transmitted to the periclinal wall at its junction with the anticlinal bands. This can mark the position, attract further bundling of cortical microtubules in a positive feedback loop, and lead to deposition of cellulose under the outer periclinal wall.

Since the stress due to local stiffening of the inner periclinal wall can be transmitted to the anticlinal walls (Fig. 4-7B), these bands of anticlinal stiffening can originate from the stress generated from the inner periclinal wall. This may explain why if one of the periclinal walls develops a particular pattern of anisotropy, the other wall is triggered to mirror this through the microtubule-mediated addition of cellulose microfibrils. The stress pattern would be propagated from one periclinal wall to the other by way of the anticlinal walls.

Interestingly, after removal of the optical slices pertaining to upper and lower periclinal walls to isolate the anticlinal wall, 3D reconstruction of the confocal stack shows that cortical microtubules assume a preferentially vertical (Z direction) orientation on the anticlinal walls. Moreover, the bundles appear to be thicker near the tips of undulations (Figs. 4-7C and D, arrows).

4.4.16 Mechanical buckling may precede polarization and symmetry breaking

We observed that microtubules appear to be bundled in necks in regions with an already established curvature, while they are scarce in lobes and only occasionally do cortical microtubule arrays seem to reach the tip of lobes (Fig. 4-7E). This confirms microtubule behavior in pavement cells observed by Armour et al. (2015). In smaller, less developed cells or regions of developed cells with walls with smaller bends, however, the difference in microtubule density on two sides of the wall between lobes and necks appears to be significantly less pronounced compared to later stages (Fig. 4-7F). This is consistent with the notion proposed here, that microtubule bundling and consequent wall reinforcement can amplify the amplitude of undulations in a positive feedback loop. However, it may also imply that lobe initiation can precede the focal bundling of microtubules and cell content polarization. In such a scenario, the initial bundling of microtubules at necks, which we demonstrated to experience higher stresses, would initially imply a correlation rather than a causality in lobe formation.

Our simulations suggested that while the anticlinal walls experience large positive (tensile) stresses in Z-direction due to the shape and dimensions of the inflated cells, the stress along the length of the anticlinal wall can become locally zero or negative (compressive). This is interesting as the plant cell wall in turgid cells is commonly presumed to be ubiquitously

under tension. Based on our observations, we hypothesize that in the anticlinal walls and consequently in the connected periclinal walls, local compression and buckling may occur. For proof of concept, we developed an FE model of a closed-box rectangular cell geometry subject to internal pressure (Fig. 4-7G-1) (see supplemental information). Positive eigenvalues were found from the linear buckling analysis suggesting that compressive stress and buckling can arise due to cell geometry and internal pressure. A buckling mode for this model is depicted in Fig. 4-7G-2. Interestingly, the model also suggests the periclinal wall at site of indentations to locally bulge out (magnified view 4-7G-2). This is consistent with the microscopic observations showing the cell wall on neck side of undulations bulging out of plane (Fig. 4-1A and orthogonal view in Fig. 4-5B). These results indicate that the cell walls have the potential to buckle due to cell geometry and internal pressure.

4.5 Discussion

Unlike animal cells, in plant cells actin-myosin based actuators are not directly involved in generating the forces required to move or to alter cell shape (Geitmann, 2016). In this study, we show that complex cell shaping in plants is accomplished through other means such as growth-driven buckling, stress-driven cell wall reinforcement by the organization of cellulose microfibril orientation, and selective modulation of local properties of the pectin matrix under application of the turgor pressure. The formation of interlocking protrusions and indents in pavement cells on the leaf epidermis of many plants has attracted much attention since neither the underlying events in genesis of these shapes nor their purpose is understood. The analysis of the underlying genetic pathways and mechanistic processes regarding cytoskeletal activities and cell wall biosynthesis have presented a formidable challenge to biologists and modelers (Belteton et al., 2017; Fu et al., 2005; Majda et al., 2017; Panteris and Galatis, 2005; Sampathkumar et al., 2014a; Sapala et al., 2018; Sotiriou et al., 2018; Xu et al., 2010; Zhang et al., 2011). Until now, the focus of research has predominantly been on the role of the cytoskeletal arrays, whereas experimental evidence for events occurring in the cell wall and a validated mechanical explanation for the formation of lobes and necks have been elusive. A mechanistic study by Sampathkumar et al. (2014a) analyzed the effect of a pre-determined pavement cell shape on intracellular stresses and microtubule organization revealing crucial

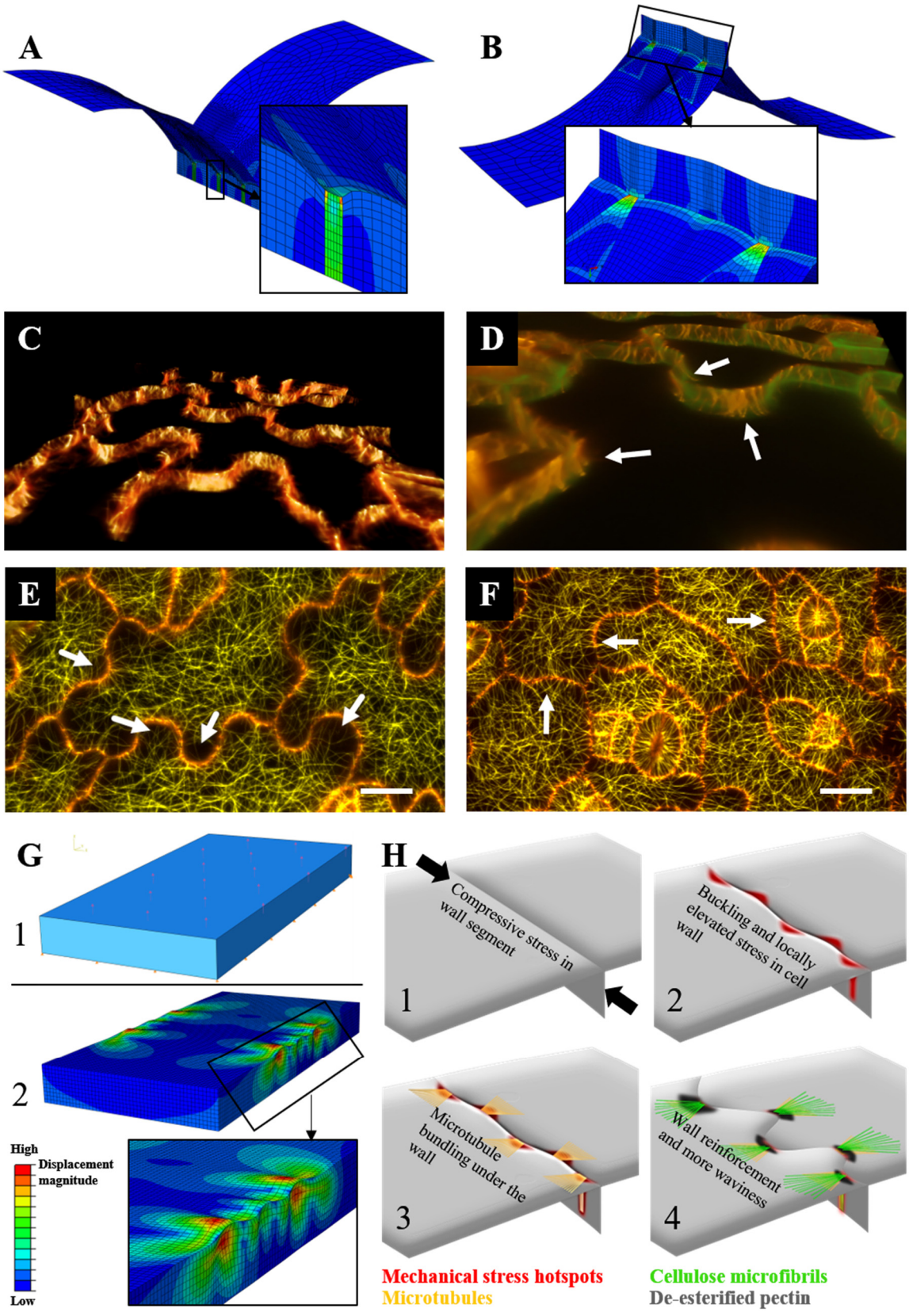
A
B
C
D
E
F
G
1
2
High
Displacement magnitude
Low
H
Compressive stress in wall segment
1
Buckling and locally elevated stress in cell wall
2
Microtubule bundling under the wall
3
Wall reinforcement and more waviness
4
Mechanical stress hotspots
Microtubules
Cellulose microfibrils
De-esterified pectin

Figure 4-7. Patterns of mechanical stress and microtubule orientation. Models containing a segment of anticlinal and periclinal walls under turgor pressure show that **A)** anticlinal bands of stiffened cell wall material and homogeneous isotropic periclinal wall or **B)** material inhomogeneity in the periclinal wall can cause locally elevated stress in the connected wall transmitting the stresses between the inner and outer cell walls. **C)** Oblique view of a z-stack 3D reconstruction of pavement cells from *Arabidopsis thaliana* GFP-MAP4 line excluding periclinal walls demonstrating cortical anticlinal microtubules. **D)** Dual channel image of propidium iodide (green) and GFP-MAP4 (orange) showing that cortical anticlinal microtubules appear more abundantly on the neck side of the undulations. **E** and **F)** Cortical periclinal microtubules visualized in cotyledons of the *Arabidopsis thaliana* GFP-MAP4 line 4 (**E**) and 1 DAG (**F**). At both stages, microtubule density on the opposite sides of corresponding lobe-neck pairs is different with higher density at the neck side. However, this difference is less pronounced in earlier developmental stages (white arrows in **F)**. At 4 DAG microtubules appear to be bundled in necks while they are scarce in lobes. Occasionally microtubule bundles reach the tips of a lobe. The images do not correspond to the same cotyledon. Scale bars = 10 μm. **G) G-1)** A closed-box model of a hollow cell with turgor pressure applied to inner face of the outer periclinal wall. Turgor pressure was not applied to lateral walls as equal pressures were shown in previous models to cancel each other out from two sides in a multicell context and only result in compression of the wall thickness. Inner periclinal wall was prevented from out or inward displacement to simulate attachment to mesophyll layer. **G-2)** A buckling mode from the linear buckling analysis demonstrating folding of the cell border in both periclinal and anticlinal walls. Interestingly, the model suggests the location of indentation on periclinal walls to bulge out of plane which is consistent with microscopic observations of pavement cells. **H)** A schematic of the model with mechanical buckling acting as a morphogenetic cue initiating the mechanical and growth anisotropy. **H-1)**. Compressive stress in anticlinal walls arises due to internal pressure bulging out periclinal walls or from the growth in the cellular environment such as by matrix swelling. **H-2)** Stress inhomogeneities arisen due to buckling mark stress hotspots that trigger local bundling of microtubules (**H-3)** and reinforcement of the cell wall by cellulose deposition and alterations in pectin esterification in necks. This further develops the protrusions at undulating borders (**H-4)**.

pieces of information relevant to stresses experienced in walls of cells with already established shapes. Here, we investigated early processes by asking how cell shapes are formed *de novo* and how these shapes are further developed. Based on our experimental data and numerical simulations we propose that the development of cell shape is a product of initially minute and subsequently amplified material inhomogeneity in a stress-dependent manner. We also show that, inversely, stress depends on the evolving geometry of cells, even when the material used in simulations was isotropic and homogeneous. From these and the observation of the stress state in the cell wall and the gradual development of polarization in cortical microtubule

contents, we surmise that the stress anisotropy precedes the material inhomogeneity and acts as a morphogen shaping the cells.

Our initial simulations based on isolated anticlinal walls predict that the generation of local protrusions would require either the differential expansion behavior of the attached anticlinal wall layers, or differential turgor pressures in adjacent cells. Both predictions are hard to reconcile with the biology of the system. The differential expansion behavior generates curvatures in the opposite direction of what is expected, and differential turgor in neighboring cells is a requirement that would be difficult to meet in the complex mosaic of the epidermis. The concept of differential turgor would also be difficult to reconcile with cell morphology at later developmental stages when single wall sections can form multiple alternating protrusions and indents. We also showed that the stretch-based model of isolated anticlinal wall proposed by Majda et al. (2017) is not able to produce pronounced bends, and that periclinal walls virtually eliminate the minute bends in the anticlinal walls. Further, the model of stretch-induced wave formation cannot produce simple bends since the mechanism conceptually can only produce second and higher order curvatures. Lastly, while Majda et al. (2017) did not report the wall stresses arising from their model, our simulations of their proposed mechanism shows the stresses to be higher in lobes. Our static analysis of turgor-driven stress as well as the study by Sampathkumar et al. (2014a) confirm that the geometry of indentation and protrusions dictate a higher stress on indentation side of the cell walls. This is consistent with the accumulation of microtubules in these locations, a behavior that is known to be guided by stress fields (Landrein and Hamant, 2013; Uyttewaal et al., 2012). Together, these results point at the limitations of models focusing solely on the anticlinal wall to explain the morphogenesis in pavement cells through bending. In fact, simulations including the periclinal walls generate crucial and non-intuitive observations. When the turgor pressure is applied to all existing walls in a complete 3D model, the out-of-plane swelling of the periclinal wall (in the Z direction) forces the anticlinal walls to move toward the center of the cell reducing the projected cell surface. This occurs despite the presence of the same pressure on the anticlinal walls. The reason for this is that due to difference in surface areas the combined forces resulting from the turgor pressure are higher on the periclinal walls than those acting on the anticlinal wall surface. These simulations

also imply that for a cell to grow in-plane, selective and isotropic softening of the anticlinal walls is not sufficient and changes in mechanical properties of periclinal walls are required.

In stress analysis of inflated 3D cell models, we found that the anticlinal walls experience high stresses vertically (in the Z direction) compared to the in-plane directions (Figs. 4-3B and C). Therefore, in a stress-stiffening feedback mechanism, it is expected that these walls become transversely reinforced at very early stages of their formation. Interestingly, we observed that this expected stress pattern matches the observed net orientation of cortical microtubules underlying the anticlinal walls. This behavior is consistent with the fact that microtubules have been found to reorient with respect to stress fields (Landrein and Hamant, 2013; Uyttewaal et al., 2012).

Our simulations suggest that the formation of alternately located regions of stiffening on periclinal walls in a growing cell suffices to develop necks and lobes. Such an alternating pattern of stiffness distribution is consistent with our observation of bundling of microtubules, deposition of cellulose and de-esterification of pectin in neck regions. Extension of the stiffening in the depth of the anticlinal wall results in increased wave magnitude. It is important to note that the anticlinal wall stiffening can only amplify but cannot form indentations in the absence of periclinal stiffening. However, we showed that if the stiffening is initiated in any of these walls, it can extend to the other ones due to transmitted stresses. Our simulations predict that softening of the periclinal wall in regions of incipient lobes facilitates the elongation of lobes in a trend similar to alternating stiffening. As long as there is a difference in the stiffness along the periclinal cell wall, the undulations can develop. Simulations suggest that both phenomena, stiffening and softening, work similarly and promote growth of waves. Therefore, the model can mechanically explain why inhibition of either cortical microtubule bundling or formation of fine actin microfilaments have the potential to affect the pavement cell phenotype (Armour et al., 2015; Fu et al., 2005; Mathur, 2004). In the positive mechanical feedback loop between wall stress and local stiffness values, we demonstrated that developing lobes and necks can initiate from infinitesimally small stiffness differentials. However, unless a simultaneous inhibition mechanism is implemented, the stress and therefore the stiffness differential eventually becomes smoothened out due to geometrically-driven stresses being able to suppress the small stress anisotropy arising from material inhomogeneity. The existence of such a lateral inhibition

mechanism is consistent with the proposed antagonism and competition between microtubule and actin regulation pathways (Chen et al., 2015; Fu et al., 2005; Fu et al., 2002; Xu et al., 2010). Since microtubules are associated with guided deposition of cellulose and actin filaments are thought to deliver the new, and presumably softer, wall material such a scenario would cause lateral inhibition of stiffening predicted by our model. The antagonistic pathways and specifically the exclusivity of microtubules and actin to necks and lobes, respectively, are not uncontested, however (Armour et al., 2015; Belteton et al., 2017). For instance, Armour et al. (2015) did not observe any obvious association between lobes and actin microfilaments at least in early stages of cell shape development. The role of the cytoskeletal elements warrants further investigation. Our simulations showed that after the initiation of lobes and necks, the geometry itself will cause higher stresses at the neck side, even if isotropic material properties are used. The anisotropic stress pattern from the static simulations closely match the experimental observations of cortical microtubule orientation (Figs. 4-4D and 4-6A). This result is consistent with previous suggestions by Sampathkumar et al. (2014a) on the influence of geometry on the stress state of the cell wall.

Further away from the tip of the lobes, bundles of microtubules radiating from two neighboring necks form transverse connections on the shank of the tube-like lobe (Figs. 4-6A and B). These arrays seem to connect regions of greatest stress which develop in the necks according to the finite element model (Fig. 4-4D). If this particular orientation and bundling of cortical microtubules result in increased cellulose deposition at these locations, the widening of lobes is restricted so that the material incorporated into the wall can promote elongation of the lobe instead (Fig. 4-14SH). Recently, Sapala et al. (2018) suggested that this might serve as a mechanism to control the diameter of pavement cells, to control the surface area under turgor pressure and minimize the stresses arising on the cell wall. 3D reconstruction of the confocal stacks shows that at the anticlinal walls, cortical microtubules assume a preferentially vertical (in the Z direction) orientation. They appear to be more abundant near the tip of the undulations on the neck side. This result is consistent with previous findings (Zhang et al., 2011) (Figs. 4-7C, D and 4-12SG). This spatial distribution and orientation of microtubules at the anticlinal walls, followed by deposition of cellulose microfibrils with the same net orientation, can orchestrate a mechanical communication between the inner and outer periclinal walls so that

shaping signals and/deformations are transmitted and possibly mirrored in both inner and outer periclinal walls. Importantly, this orientation of microtubules, and consequently that of cellulose microfibrils, renders the anticlinal walls transversely isotropic. In this way, the anticlinal walls can grow in-plane by separation of more or less parallel cellulose microfibrils, similar to an accordion, allowing growth of pavement cells in plane while preventing their out-of-plane expansion (Figs. 4-14SF-H). This orientation of microtubules follows maximal stress direction in the anticlinal walls.

Staining the cotyledons with propidium iodide and COS^{488} shows pectin in pavement cells to be weakly esterified at the neck sides of undulations. De-esterified pectin can enhance the mechanical stiffness of the pectic network when cross-linked by calcium. Therefore, changes to the pectin status in the neck region could locally stiffen the cell wall. Variations in the esterification status of pectin have been implied in other plant tissues related to the polar growth of cells and organogenesis (Bidhendi and Geitmann, 2016; Palin and Geitmann, 2012; Peaucelle et al., 2015; Wolf et al., 2009). For instance, studies have shown that pectin at the growing tip of pollen tubes are highly esterified while at the non-growing shank the pectin is weakly esterified (Chebli et al., 2012; Vogler et al., 2013). It is possible that de-esterification of pectin in these regions locally decreases cell wall deformability by preventing slippage and separation in the xyloglucan-cellulose network required for cell wall growth (Abasolo et al., 2009; Bidhendi and Geitmann, 2016).

Staining cotyledons with Calcofluor white and PFS revealed super-bundles of cellulose microfibrils (Bidhendi and Geitmann, 2016) radiating from the neck side of the undulations. Accumulation and bundling of cellulose microfibrils in these regions can be interpreted as locally elevated stiffness of the cell wall. The tip of lobes on the periclinal walls showed considerably less fluorescent signal and generally seemed devoid of organized cellulose microfibrils. However, similar to the organization of microtubules, microfibrils seemed to connect neighboring or opposite necks (Fig. 4-6F). In some observations, the neck-neck connections in the inner periclinal walls appeared to be more pronounced, and bundles of cellulose seemed packed tighter compared to their corresponding outer periclinal wall (Fig. 4-6G). Therefore, the inner periclinal wall may be more determinant in dictating the augmentation of undulations while the outer periclinal wall may loosely mimic the cellulose pattern of the

inner wall. Such harmonization is possible by stress and deformation coupling through the formation of anticlinal strips of cellulose reinforcement. Alternatively, the observed stronger neck to neck associations and tighter bundling in the inner periclinal walls may merely reflect a temporal order of events with the development of anisotropic reinforcement in the inner wall of a cell preceding that in the outer periclinal wall. The loss of fluorescence signal in deeper tissue regions combined with signals from the underlying mesophyll layer precluded a more meticulous and quantitative analysis of the inner periclinal walls for the time being.

Armour et al. (2015) report that the regions of the anticlinal wall where microtubules form the cortical anticlinal bundles mark the position of incipient necks. However, our observations and a closer analysis of images provided by Armour et al. (2015) suggest that even the earliest evidence of microtubules focally marking a region of the anticlinal wall is associated with an already existing local change of curvature, even if the curvature is not pronounced. The diffraction limit of the optical microscope may be responsible for the inability to detect these curvatures at their very early stages. Therefore, the available studies cannot indicate whether there was a change in the cell wall composition/stress that caused bundling of the microtubules in those regions or whether it was the microtubule accumulation that predicted the site of future lobes. Higher temporal and spatial resolution study of straight walls prior to the focal bundling of microtubules can shed light on this matter.

Buckling has been suggested in various tissue level contexts, e.g., in leaf blades (Dumais, 2007; Liang and Mahadevan, 2009). Here we suggest this mechanical phenomenon to act at subcellular level as a morphogenetic step preceding emergence of complex shapes. We provide a proof of concept that buckling in the walls is possible resulting simply from turgor induced stress and we demonstrate that it would induce spontaneous and stochastic local stress and stiffness inhomogeneity (Figs. 4-3B and C, 7G and H). The local stress triggers microtubule bundling (Eng and Sampathkumar, 2018), and through a feedback loop results in cell wall reinforcement. A schematic of the morphogenetic steps initiating from buckling of isotropic cell walls and resulting in anisotropic mechanical properties and growth of waves at pavement cell borders is depicted in Fig. 4-7H. We conjecture that compressive forces result in buckling of the anticlinal and periclinal walls (Fig. 4-7H-1). As discussed, the compressive forces can arise due to geometry-dictated local contraction resulting from the application of internal pressure.

Independently and compounding this effect, external compressive stresses may, of course, also arise due to conditions such as variations in growth rates between neighboring cells and matrix swelling such as by wall loosening or changes in pectin esterification status and free calcium available (Tibbits et al., 1998). Indeed Armour et al. (2015) and Elsner et al. (2012) demonstrated that the growth rates of the walls of pavement cells can vary considerably both at subcellular and tissue scales. The notion of buckling as a mechanical event preceding cytoskeletal and cell wall biochemical polarization also matches observations made in mutants and plants treated pharmacologically. Interference with the regulators of microtubule functioning such as brassinosteroids, regulators of ROPs such as RhoGDIs, mutations in microtubule-associated or microtubule-severing proteins such as IQD, CLASP or KATANIN considerably decrease lobe depth, but in no case do they completely eliminate cell border waviness (Akita et al., 2015; Ambrose et al., 2011; Fu et al., 2005; Han et al., 2015; Kirik et al., 2007; Kotzer and Wasteneys, 2006; Liang et al., 2018; Lin et al., 2013; Liu et al., 2018; Mitra et al., 2018; Möller et al., 2017; Wu et al., 2013). The same applies to mutations affecting the actin cytoskeleton (Le et al., 2006; Rosero et al., 2016) or cellulose synthesis or crystallinity such as *any1* (Fujita et al., 2013; Ivakov and Persson, 2013). This further corroborates the notion that microtubules and subsequent cellulose reinforcement of necks, while crucial in pavement cell development, do not initiate the cell border waviness. We suggest that these shallow waves result initially from buckling of the cell wall and that the depth of the lobes fail to further deepen due to the lack of a functional feedback mechanism involving the microtubule cytoskeleton and spatially confined cellulose microfibril deposition. To what degree the external forces arising due to growth-rate mismatch and the resulting constrained growth of the cell wall contributes to the buckling and shaping procedure in pavement cells warrants further studies. Stress hotspots arise due to buckling (Fig. 4-7H-2) triggering subcellular polarization of the cell contents such as microtubules. Pectin de-esterification, and microtubule bundling with the consequent cellulose reinforcement associated with localized microtubule bundles, inhibit the expansion of the necks in a positive feedback loop developing the interdigitating cellular extensions (Fig. 4-7H-3 and 4). The quality of the buckling as a morphogenetic factor triggering local cell wall material anisotropy and inhomogeneity is subject of our further studies.

4.6 Experimental Procedures

4.6.1 Plant growth conditions

Arabidopsis thaliana ecotype Col-0 seeds were germinated in sterile Petri plates containing 1x MS (Murashige and Skoog, 1962) media with 1% sucrose and 0.8% plant agar under long-day lighting condition (16 hours of light and 8 hours of darkness). The seeds for GFP-expressing line GFP-TUB6 (Nakamura et al., 2004) was obtained from Arabidopsis Biological Resource Center under stock number CS6550. The GFP-MAP4 line (Marc et al., 1998) was also used to verify the observations with GFP-TUB6. The GFP-MAP4 was generously provided by Dr. Charles T. Anderson.

4.6.2 Staining

Staining procedures were carried out mostly in dark condition. For pectin, seedlings were stained with either propidium iodide or COS^{488}. COS^{488} was generously provided by Dr. William George Tycho Willats (University of Copenhagen). For visualizing cellulose, calcofluor white and PFS, a dye with high affinity to cellulose, were used. Calcofluor was used at a concentration of 2 mg/mL in ddH_2O. PFS staining was carried out with a 14 mg/mL solution of PFS in PBS buffer (Na_2HPO_4 3.2 mM, KH_2PO_4 0.5 mM, NaCl 135 mM, KCl 1.3 mM, pH 7.3).

4.6.3 CGA treatment and time-lapse study of pavement cell growth

Cotyledon samples from *Arabidopsis* were treated with the herbicide CGA (CGA 325'615) at 0.9 nM prepared from a 10 μM stock solution dissolved in DMSO. CGA is suggested to inhibit the synthesis of and reduce the cell wall content of crystalline cellulose (Peng et al., 2001). The same concentration of DMSO (v/v) was used for the control experiment. The solutions were added to the ½ x MS (Murashige and Skoog, 1962) growth media. The samples were labeled with propidium iodide (0.01 mg/ml) for 20 min, followed by three washes with distilled water before observation. Propidium iodide labeling was applied at each time point prior to observation. Samples were mounted between slide and coverslip at each image acquisition. After each image acquisition, samples were placed immediately back to the in vitro growth

chamber. For tracing the cells over time, at each time point, same cells were located with the help of their recognizable geometrical features and marked manually. The adaxial side of the wild-type *Arabidopsis* was chosen for the study. For statistical analysis, for each time-point, 50-70 cells were studied from 10-12 seedlings.

4.6.4 Fluorescence microscopy

Fluorescence microscopy was carried out on a Zeiss LSM 510 META confocal laser scanning microscope using a Plan Apochromat 63x oil immersion objective with numerical aperture of 1.40. For propidium iodide and PFS, excitation wavelength of 532 nm and bandpass emission filter of 550-615 nm was used. For COS^{488}, 489 nm laser with bandpass filter of 550-615 nm was used. For calcofluor white, excitation wavelength of 405 nm in META mode and bandpass filter of 420-480 nm was used. For GFP lines, either excitation wavelength of 489 nm with emission bandpass of 500-525 nm, or in META mode, the argon laser of 488 nm with bandpass filter of 505-550 nm were used. For time-lapse imaging of CGA-treated and control samples, LSM 5 LIVE was used with 532 nm laser with an emission filter 590-625 nm.

4.6.5 Image analysis and 3D reconstruction software

Analysis of fluorescence intensity was performed on maximum projections of z-stacks using ImageJ (Schneider et al., 2012). 3D reconstruction of confocal z-stacks was carried out using either Amira 5.6.0 (FEI, Visualization Science Group) or Bitplane Imaris 7.5.2 (Bitplane A.G.). For pectin, signal intensities between lobes and necks were compared in t-tests (supplemental experimental procedures).

4.6.6 Modeling

Finite element simulations

Abaqus 6.14-2 finite element package was used for the creation of the geometries, meshing and post-processing. Abaqus/Standard solver was used for quasi-static finite element simulations (see supplemental modeling procedures for more details).

Feedback loop

To implement a feedback loop, a Python script was developed to read and write in the finite element model. After each iteration, the code extracts the deformed geometry from the Abaqus database and reads the stresses for each element. If a specific element has a stress higher than a threshold and does not belong to a list of stiffening-inhibition zone, the new value of stiffness for that element is updated in a stress-stiffening paradigm (see supplemental modeling procedures).

4.7 Author contributions

A.J.B. and A.G. designed the study, A.J.B. performed the modeling and the experiments. B.A provided the CGA treatment results. A.J.B., F.P.G, and A.G. analyzed the data, A.J.B. and A.G. wrote the manuscript.

4.8 Acknowledgments

This project was supported by a Discovery grant from the Natural Sciences and Engineering Research Council of Canada (NSERC) and by the Canada Research Chair Program. We would like to thank Dr. William George Tycho Willats and Dr. Jozef Mravec from the University of Copenhagen for kindly providing us with COS^{488} for pectin staining.

4.9 Supplemental Information

4.9.1 Supplemental Figures

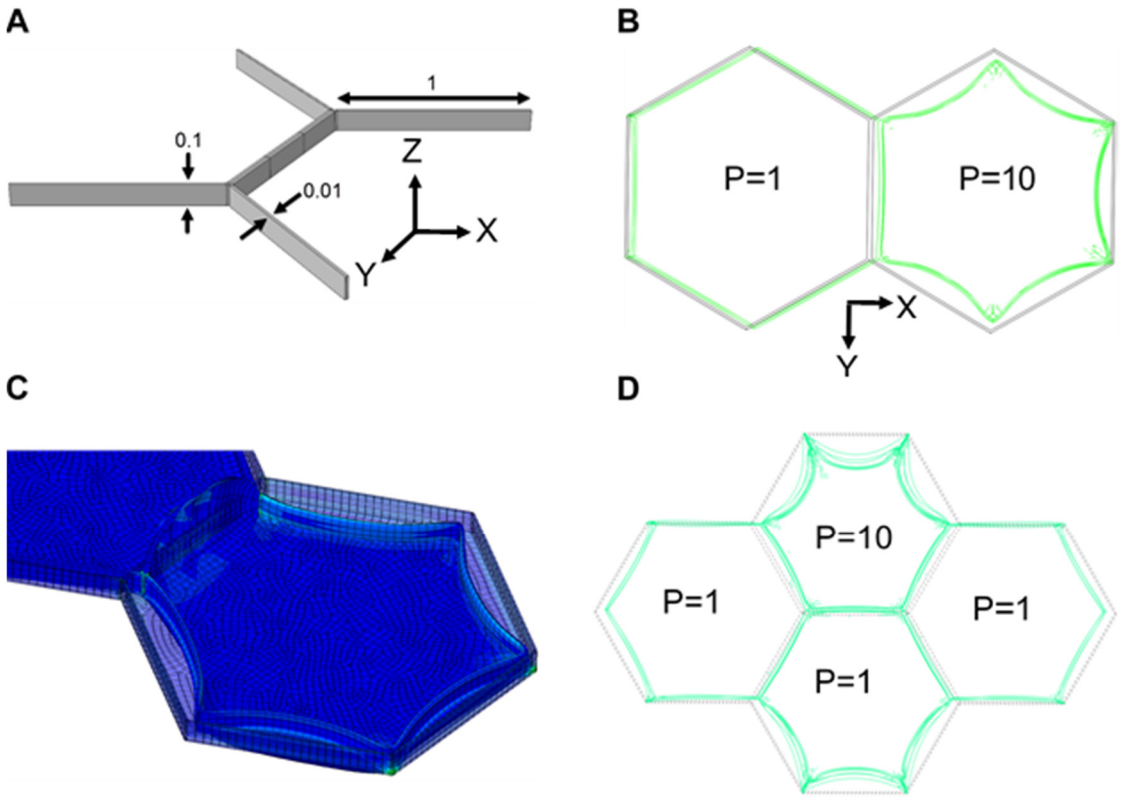

Figure 4-8S. Finite element models designed to investigate the effect of anticlinal wall stiffness modulation and turgor pressure differential on cell shape. **A)** Relative dimensions in the model focusing on anticlinal wall between adjacent cells; only half of each cell is modeled with symmetry boundary conditions. **B)** Deformation of two cells with isotropic material properties and identical stiffness in anticlinal and periclinal walls with different turgor pressures. A pressure difference with ratio of 1:10 was implemented. Upon application of turgor pressure, due to out-of-plane swelling of cells, in-plane cell dimensions contract with the anticlinal wall shared with the neighboring cell displacing and forming a slight curvature toward the cell with a higher turgor pressure. **C)** The shared anticlinal walls between two cells is softened compared to the other walls in the model. The outer periclinal walls are removed from the view to show the status of the anticlinal wall. The softened anticlinal wall forms a bulge toward the cell with a lower pressure but the top and bottom edges with the periclinal walls remain straight. **D)** Model of four cells sharing two tricellular junctions, with different relative values of turgor pressure (P)**.** Turgor induced deformation of the anticlinal walls viewed from the top. The construct of this model is the same as the model in (**B**) but was intended to study the behavior of anticlinal walls embedded in between several cells without free edges.

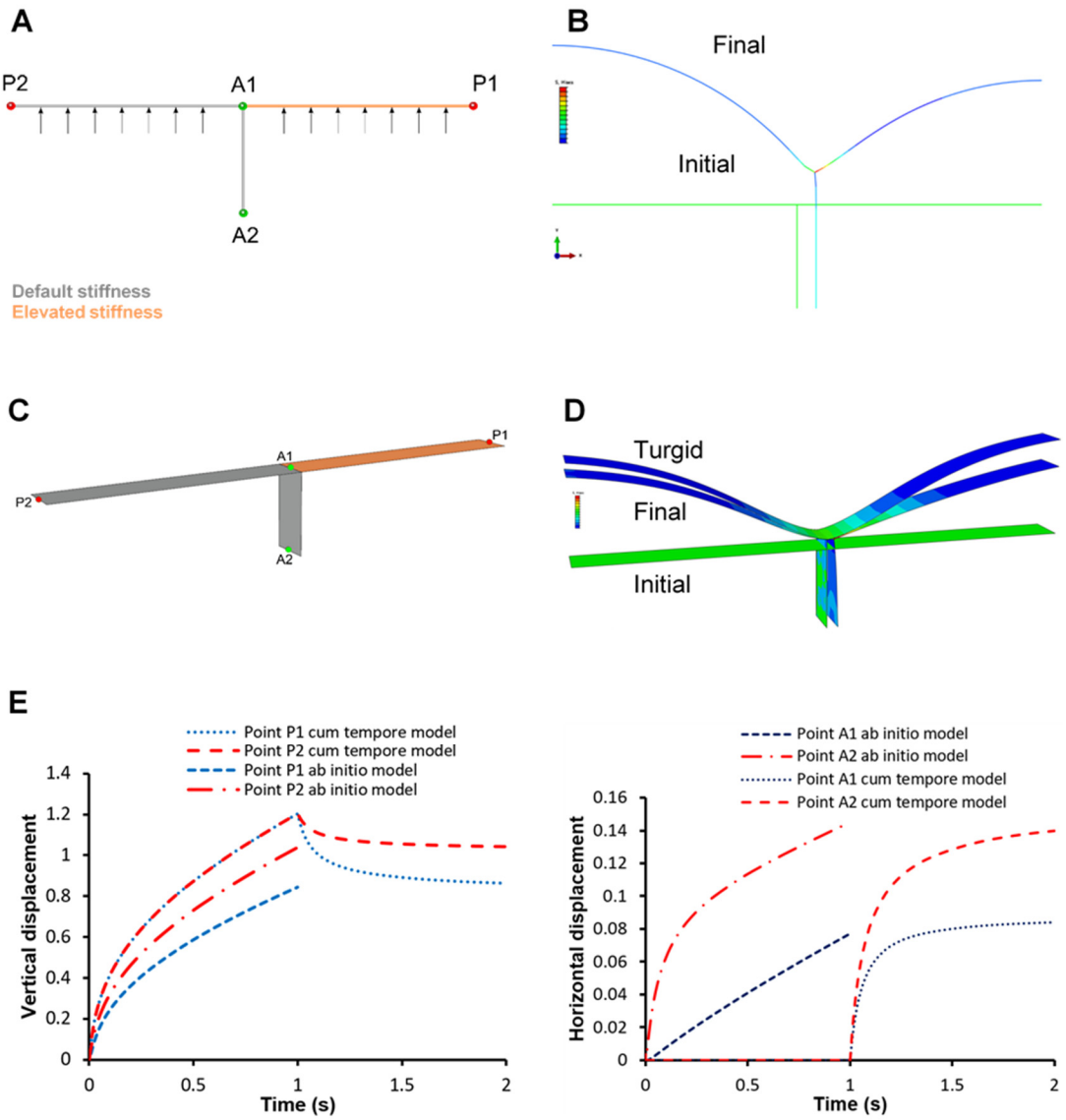

Figure 4-9S. A) 2D beam model of the wall segment demonstrated in Fig. 4-3D. Turgor pressure is applied on internal edges of the beam elements. At the anticlinal wall the effect of equal turgor on both sides cancels each other out, but periclinal wall segments bulge out of the plane of the epidermis. Four points of interest on periclinal and anticlinal walls are identified for recording the resulting displacements. **B)** Initial and deformed shapes of the 2D model showing displacement of the anticlinal wall segment toward the stiffer (neck) side. Finite element models of wall segments implementing *cum tempore* stiffening. The onset of stiffness augmentation is applied when the walls are already under tension due to turgor pressure. **C)** Shell model for *cum tempore* stiffening. Pressure is applied to the inner side of the periclinal walls and the right periclinal wall segment is stiffened after the full application of pressure. **D)** Displacement for the shell model resulting from repeated pressure application with *cum tempore* stiffening. The anticlinal wall is displaced toward the side with the stiffer periclinal wall. **E** and **F)** Comparison of the displacement of fiducial markers on shell model for *ab initio* and *cum tempore* models.

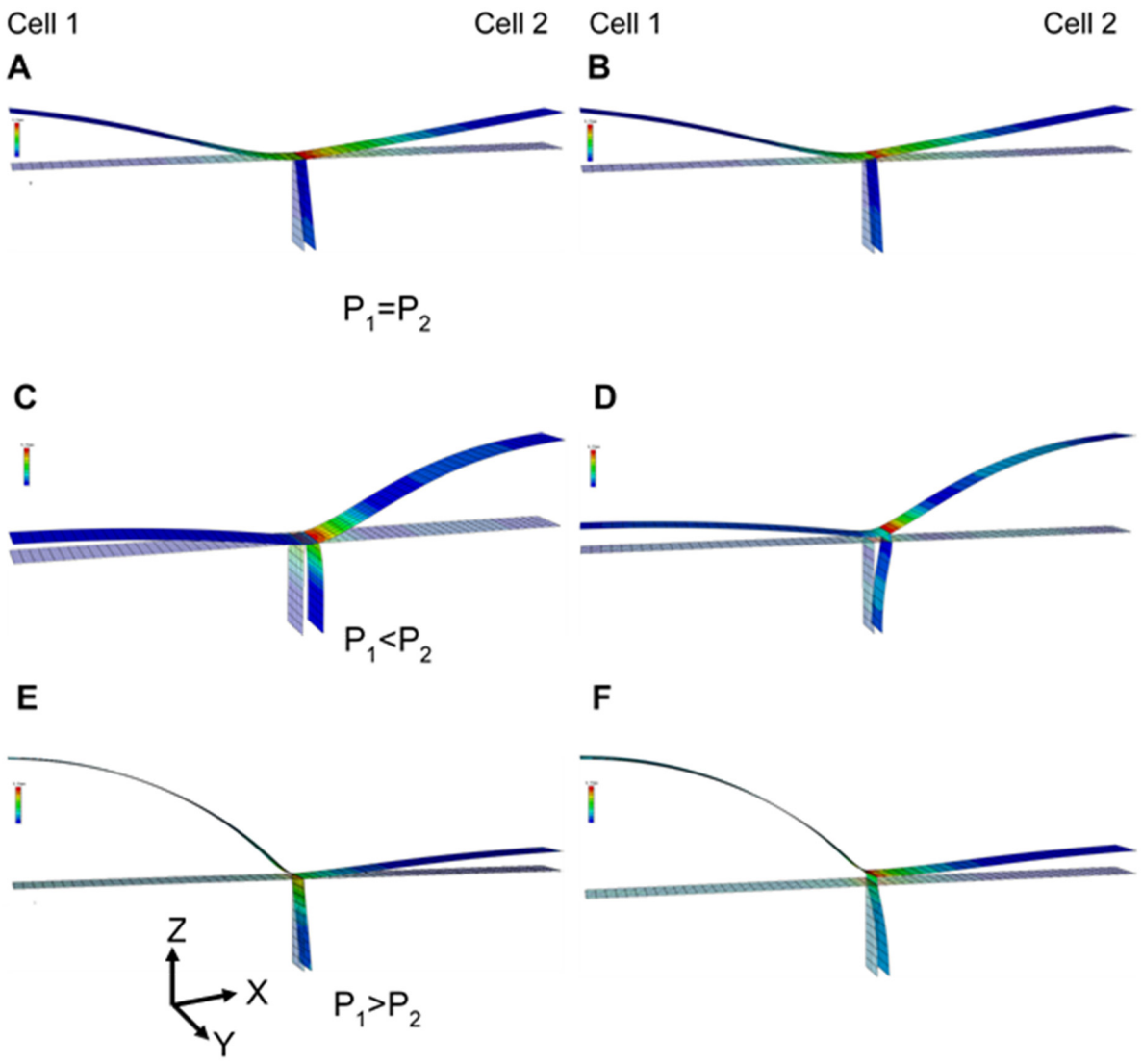

Figure 4-10S. Shell model of segments of periclinal and anticlinal walls with stiffened periclinal wall in cell 2 (normalized, C_{10}=2). Turgor pressure is either identical in both cells (**A, B**), higher in cell 2 (**C, D**) or in cell 1 (**E, F**). Anticlinal wall is either stiffened (C_{10}=2, in **A, C, E**) or has default stiffness (C_{10}=1 in **B, D, F**). In all cases is the anticlinal wall displaced towards cell 2.

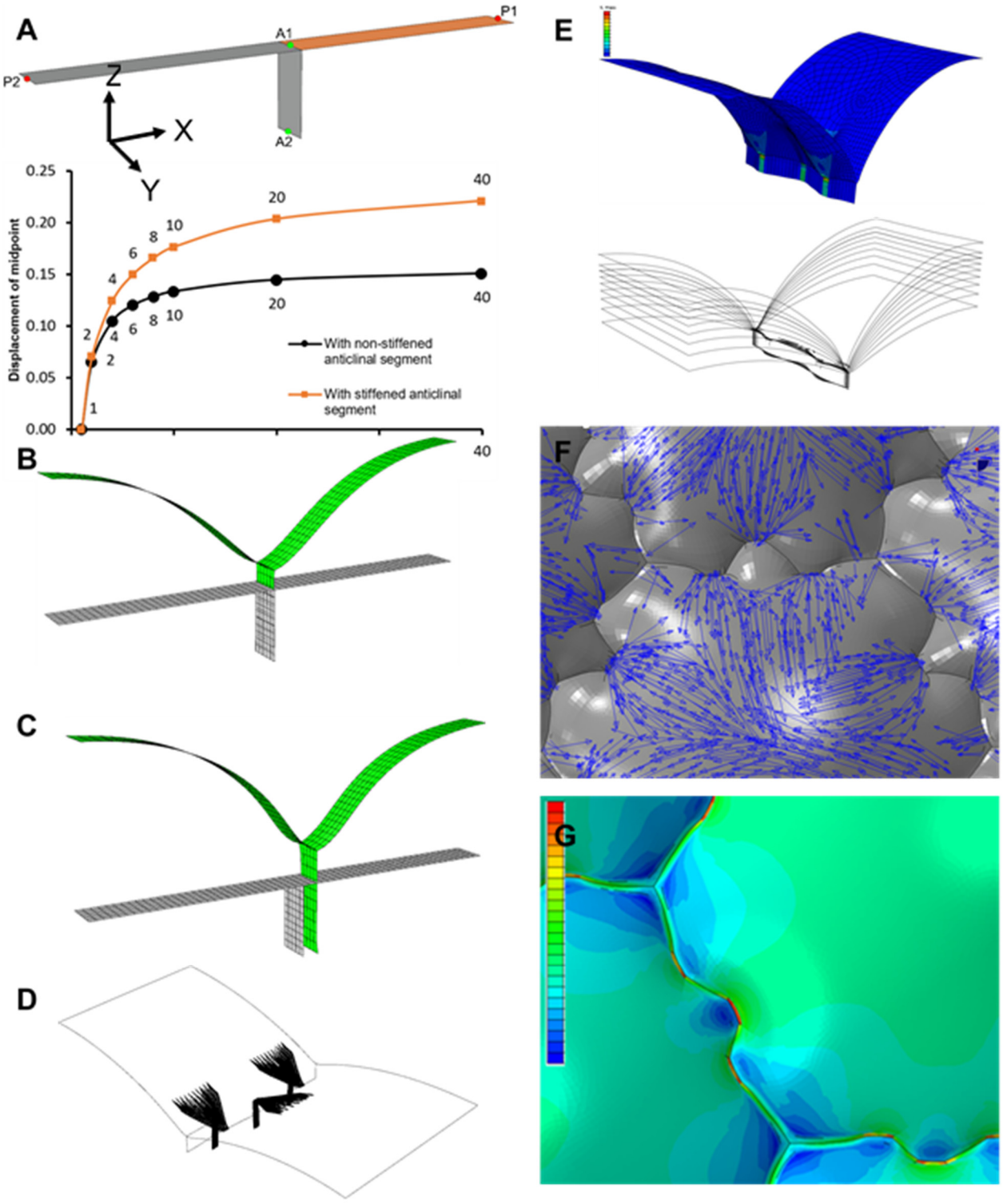
A
P1
A1
P2
Z
X
A2
Y
0.25
0.20
0.15
0.10
0.05
0.00
Displacement of midpoint
40
20
10
8
6
4
2
1
With non-stiffened anticlinal segment
With stiffened anticlinal segment
B
C
D
E
F
G

Figure 4-11S. Partial and whole cell finite element models of cell wall deformation. **A)** Horizontal displacement of Point A2 against the stiffness ratio between the periclinal wall segments with default and increased stiffness, with stiffened and non-stiffened anticlinal wall segment. **B)** Displacement of the anticlinal wall after 3 iterations of load application with stiffness ratio between the right and left periclinal segments equal to 1.02. **C)** Ditto with stiffness ratio equal to 2. **D)** Anisotropic Holzapfel-Gasser-Ogden hyperelastic model allows for definition of cellulose microfibrils stiffness, distribution and orientation (black lines) and matrix stiffness separately. The configuration shown in the image resulted in maximum magnitude of lobes upon application of the turgor pressure compared to other orientations of fibers. **E)** Evolution of undulations for the model with alternative placement of stiffenings on periclinal and anticlinal walls by iterating load application with relieving the wall stress after each iteration. **F)** Stress field reveals stress concentration at necks and cell corners. **G)** Geometry with undulations at cell borders used as an input geometry with isotropic material properties and same stiffness value in all regions of the model. The stresses are higher on the convex side of undulations.

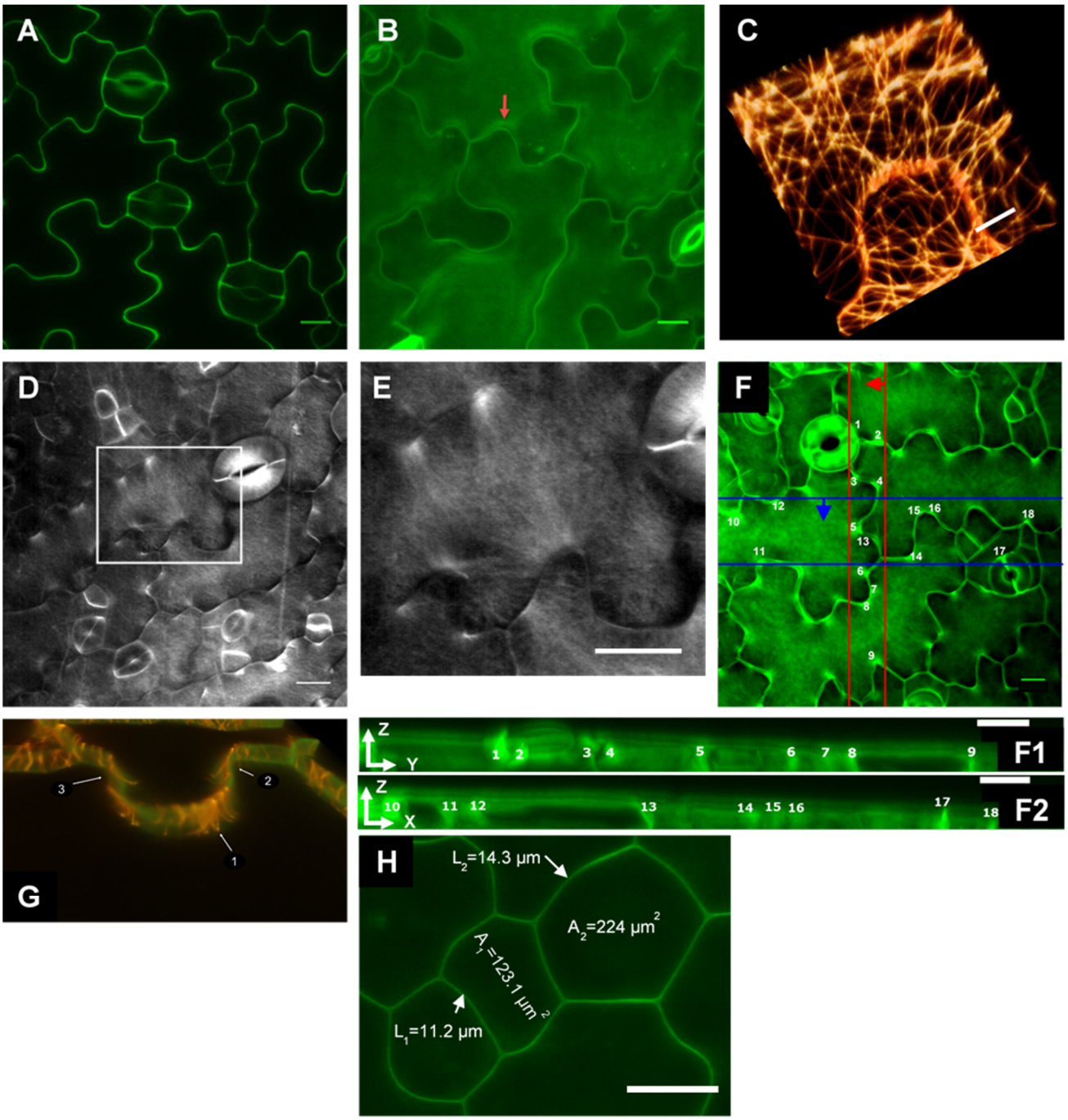
A
B
C
D
E
F
1
2
3
4
5
6
7
8
9
10
11
12
13
14
15
16
17
18
G
3
2
1
Z
Y
F1
Z
X
F2
H
L2=14.3 µm
A2=224 µm2
A1=123.1 µm2
L1=11.2 µm

Figure 4-12S. Fluorescence micrographs of *Arabidopsis thaliana* cotyledons at 3 to 5 days after germination. **A)** Single optical section through middle of the epidermal layer thickness, showing the borders of cells stained with propidium iodide, reveals varying signal intensity along the length of anticlinal walls. Tri-cellular cell junctions typically display high signal. **B)** Maximum projection of z-stack reveals propidium iodide signal intensity in periclinal walls to be higher at neck locations. **C)** Microtubules labeled with GFP-MAP4 show more abundant bundling on the neck side, although the bundles can also occasionally be found extending to the tips of lobes. The image represents a volumetric rendering of a confocal Z-stack. **D)** and **E)** Pontamine fast scarlet 4B reveals localization of cellulose bundles in periclinal walls at neck sides of undulations. **E** shows magnified region from **D** as indicated. **F)** XY maximum projection of Z-stack stained with calcofluor white**: F1)** YZ and **F2)** XZ projections of the cell walls between the lines marked on figure **F**. **G)** 3D reconstruction of partial z-stack excluding periclinal walls, viewed obliquely. Dual channel overlay of propidium iodide (green) and GFP-MAP4 (orange) label. Cortical anticlinal microtubules appear more abundantly on the neck sides of the undulations. **H) I)** Typical dimensions of epidermal cells in the *Arabidopsis* cotyledon. L_1 and L_2 are the lengths of anticlinal walls with corresponding surface areas of 58.24 and 74.36 μm^2, respectively. Their surface was measured based on the depth of the anticlinal wall measured to be 5.2 µm (obtained from the corresponding Z-stack). The areas A_1 and A_2 correspond to the surfaces of outer periclinal walls of the two cells. Scale bars = 5 µm (**C**) and 10 µm (**A**, **B**, **D**, **E**, **F** and **H**).

4.9.2 Supplemental Experimental Procedures

Polysaccharide staining

To visualize pectin status, seedlings were stained with 0.5 mg/mL aqueous solution of propidium iodide in double distilled water (ddH_2O). A drop of propidium iodide was placed on each seedling. The dye was removed after 10-20 minutes with a Kimwipe tissue paper and washed gently with double distilled water (ddH_2O) at least three times before mounting in water for visualization. For COS^{488} staining, the stock was diluted 1:500 in MES buffer (25 mM, pH 5.7). The seedlings were incubated with COS^{488} for 5-15 minutes and washed with MES for 3-5 times for at least 30 seconds. The samples were then mounted in MES before visualization. For visualizing cellulose, calcofluor white and PFS were used. Calcofluor was used at a concentration of 2 mg/mL in ddH_2O. Seedlings were placed in Eppendorf tubes containing calcofluor white and transferred to a vacuum of 20 in Hg (Pelco BioWave 34700) at room temperature. After 45 minutes the tubes were transferred on a rotator in a dark room for an additional 45 minutes. The specimens were then washed gently for 3-5 times with ddH_2O before being mounted in ddH_2O for observation. PFS staining was carried out with a 14 mg/mL solution

of PFS in PBS buffer (Na_2HPO_4 3.2 mM, KH_2PO_4 0.5 mM, NaCl 135 mM, KCl 1.3 mM, pH 7.3). The staining of specimens was performed as described above for an incubation time of 30-60 minutes before washing and mounting in PBS for observation.

Image analysis and 3D reconstruction software

Analysis of propidium iodide signal intensity for pectin staining was carried out observing 5 cotyledons from different staining experiments. Between 3 to 5 cells were chosen from each cotyledon for analysis making up to 19 cells in total from which 101 pairs of lobes and necks were analyzed. To analyze the signal intensities for a pair of lobe and neck, identical rectangular regions were selected near the anticlinal border, and the average signal intensity within these regions of interest was recorded. This procedure was repeated three times for each pair of lobe and neck with changing rectangle sizes and shapes. This was done to eliminate possible bias generated by placement of the location of interest. The average of the three measurements was considered as mean signal intensity for each neck and lobe. Signal intensities were compared in paired T-tests.

Supplemental Modeling Procedures

For all simulations, neo-Hookean hyperelastic material model was used. Two material constants are needed to define a neo-Hookean material model in Abaqus: $C_{10} = \frac{\mu_0}{2}$ and $D_1 = \frac{2}{K_0}$; where μ_0 and K_0 correspond to shear and bulk moduli, respectively. The material constants were normalized by μ_0 of a region with a default stiffness. The material in all models was considered incompressible. It should be noted, however, that compressibility would not affect the behavior of the model if it was assumed otherwise. The turgor was applied as a distributed pressure (the value of which was normalized by μ_0) on surfaces or edges in case of beam models. Boundary conditions were applied to allow free deformation of wall segments under turgor pressure while preventing movement of the whole body in 3D space. The dimensions of the geometries were normalized by half of the height of the anticlinal wall that was considered 12 µm. The base value for cell wall thickness was set to 700 nm which was then normalized to 6 µm.

For the model including only the anticlinal wall, continuum quadratic three-dimensional large strain elements with reduced integration (C3D20RH) were used. The anticlinal walls of

two adjacent cells were tied together in all degrees of freedom. For beam models, linear two-node beam elements were used. In other models, the cell wall was considered as thin shell as the thickness of the cell wall compared to other cell dimensions is negligible. These models were discretized with four-node first order reduced integration shell elements (S4R). In multi-cell models, the geometries of individual cells were merged at their anticlinal walls. To compare deformations in *ab initio* or *cum tempore* stiffening models, the secondary onset of stiffening in a segment of cell walls in the *cum tempore* model was applied indirectly through exploiting a temperature-dependent stiffness scenario. As temperature can be defined to change in time, the stiffness could be made to vary in a time-dependent manner. Quantitative comparisons between *ab initio* stiffening and *cum tempore* stiffening were performed by monitoring the displacement of four fiducial points on the 2D shell model (Fig. 4-9SA). The results indicate that in both cases, similar displacements for anticlinal and periclinal walls result from the application of turgor (Figs. 4-9SC and D).

In simulations, we implemented the effect of cell wall stiffening, resultant of either pectin de-esterification or cellulose bundling, by introducing non-homogeneous stiffness in the neo-Hookean hyperelastic material model for the cell wall. To verify that the generality of the mechanism underlying our model is preserved whether or not anisotropy (and not inhomogeneity) is considered, we repeated the model with periclinal and anticlinal walls using anisotropic hyperelastic Holzapfel-Gasser-Ogden fiber-reinforced material model that is available in Abaqus to account for direction of cellulose microfibrils in regions of restricted growth (necks) (Fig. 4-11SD). This model allows for direct and independent definition of matrix and fiber stiffness values for a transversely isotropic material behavior (Abaqus, 2014; Gasser et al., 2006). The Holzapfel hyperelastic material model was originally proposed to model mechanical behavior of arterial walls with distributed orientations of collagen fibers. In this model, two families of fibers are embedded in a soft matrix and considered with two distinctive mean fiber orientations. Two sets of material and structural parameters are needed as inputs to define this model. The material parameters describing the properties of the base solid matrix, and the stiffness of fibers. The structural parameters of the model are the values for dispersion fibers, the angle of their mean orientations, and the number of the family of fibers. The minimum allowable number of families of fibers in this model is two. In our case, since only family of

fibers was to be defined, the two families of fibers were given identical properties and were adjusted to be aligned with each other to define bundles of cellulose microfibrils. The results of this model confirmed the outcomes presented in this paper and demonstrated that the magnitude of forming lobes is increased when initial orientation of fibers in periclinal and anticlinal walls joining each other are perpendicular to cell borders (Fig. 4-11SD), similar to the observed stress pattern, and microtubule and cellulose orientation in cell walls. Upon this verification, in all other models in this paper, neo-Hookean material model was used.

To implement a feedback loop, a Python script was developed to read and write in the finite element model. After each iteration, the code extracts the deformed geometry from the Abaqus database and reads the stresses for each element. If a specific element has a stress higher than a threshold and does not belong to a list of stiffening-inhibition zone (in model accounting for inhibition of stiffening), the new value of stiffness for that element in terms of C_{10} is updated according to $C_{10_{new}} = C_{10_{old}} + tanh(C_{10_{old}} \times S_{rel})$; where S_{rel} is the von Mises stress of the corresponding element relative to the threshold stress. The threshold stress was calculated in each iteration as average stress of all elements. Otherwise, $C_{10_{new}} = C_{10_{old}}$ was assigned for the element with either a stress below the threshold stress or located in a stiffening-exclusion region. After assigning new stiffness values, the script runs the model keeping all other model parameters such as the turgor pressure and boundary conditions as the previous iteration.

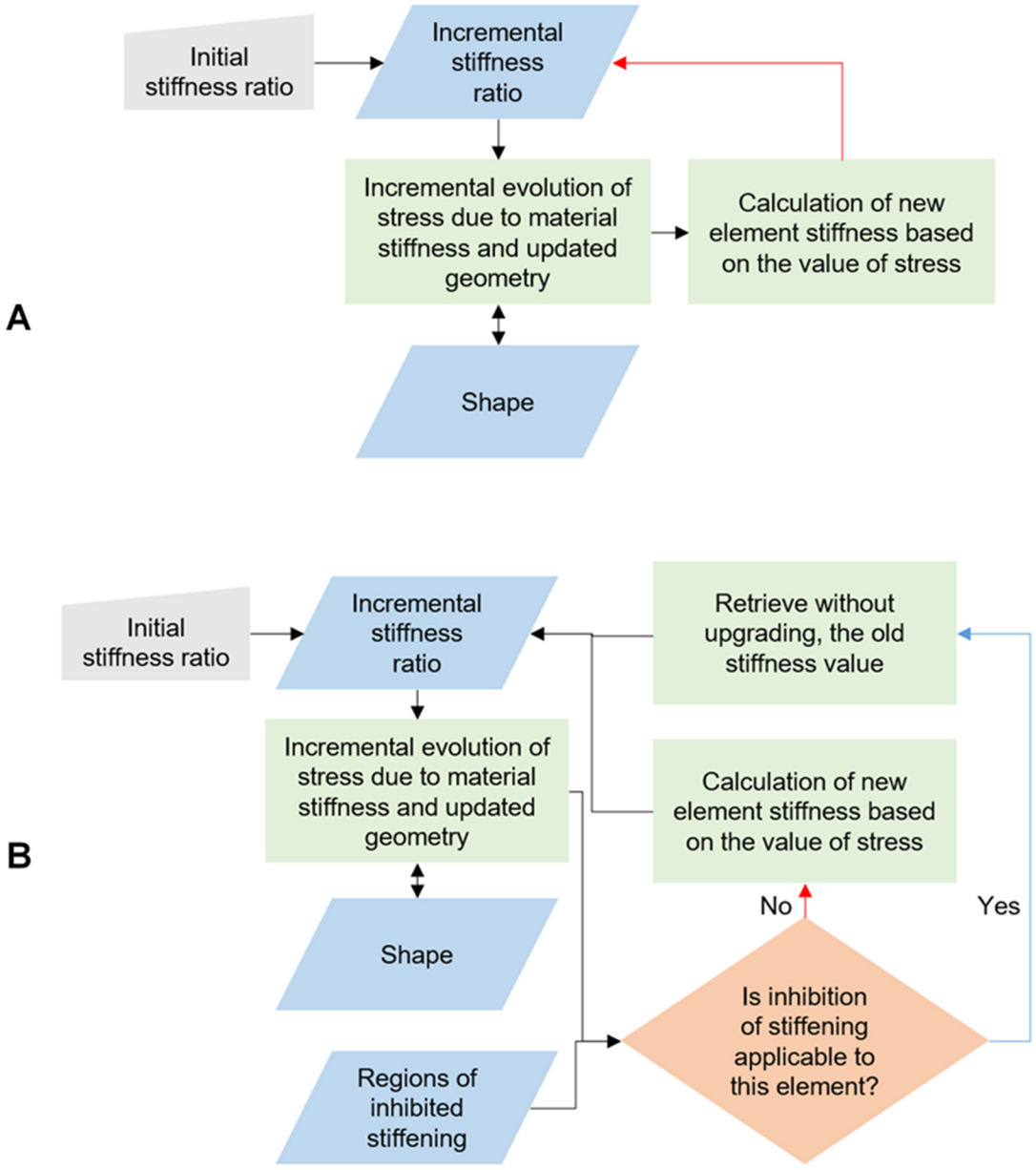

Figure 4-13S. Steps in the positive mechanical feedback model linking the stresses, wall deformation and local stiffness. **A)** Without inhibition of stress-induced stiffening in regions alternating with incipient necks. **B)** Feedback model implementing inhibition of stiffening in regions alternating with incipient necks.

Construction of the stretch-based wave formation and buckling models

To investigate the paradigm suggested by Majda et al. (2017), 3D models of the anticlinal wall and anticlinal and periclinal walls were developed. The anticlinal wall followed a normalized approach as in the other models presented in this paper. The length of the anticlinal wall was considered as unit and the other dimensions were defined as a fraction of the length with height and wall thickness at 0.1 and 0.01, respectively. The anticlinal wall was divided into four contiguous regions along its length and into half in its thickness (Fig. 4-14SA and B). This allowed us to assign alternating material properties along and across the anticlinal all as proposed by Majda et al. (2017). A hyperelastic material model was used as explained previously. One end of the anticlinal wall structure was fixed and the other end was stretched. Two different stiffness ratios for the opposing wall segments were implemented: 2:1 (the ratio used by Majda et al. (2017) and 100:1 (to test extremes). Both isolated anticlinal wall and the anticlinal wall model supported laterally by the periclinal walls were tested. In a separate simulation for the model with the periclinal walls, application of the turgor pressure was attempted prior to application of the stretch along the anticlinal wall. We observed that this preload did not change the magnitude of waves significantly. Further, models were repeated with absolute values for dimensions (e.g., cell wall length, height and thickness were modeled as 100, 10, and 0.01 μm, respectively) and elastic moduli starting from 100 KPa and 50 KPa to higher stiff to soft ratios. Similar results (both trends and values) were obtained as with the models with normalized inputs. The displacement measured for all models were recorded consistently for a specific point in middle of a stiffness segment.

Proof-of-concept buckling models were developed to demonstrate that the cell walls, including both the anticlinal and periclinal walls, can buckle resulting in wavy cell contours. For this, the cell was modeled as a hollow rectangular box. Shell behavior was considered for the cell walls. Linear elastic material was used for linear buckling analysis. We observed that with and without a static preloading step, the structure can buckle under internal pressure and positive eigenvalues for the buckling analysis were found. The eigenvalues of a buckling analysis depend greatly on the geometry, dimensions and material inputs as well as the boundary conditions. The image provided in the manuscript was from a model with dimensions of 100,

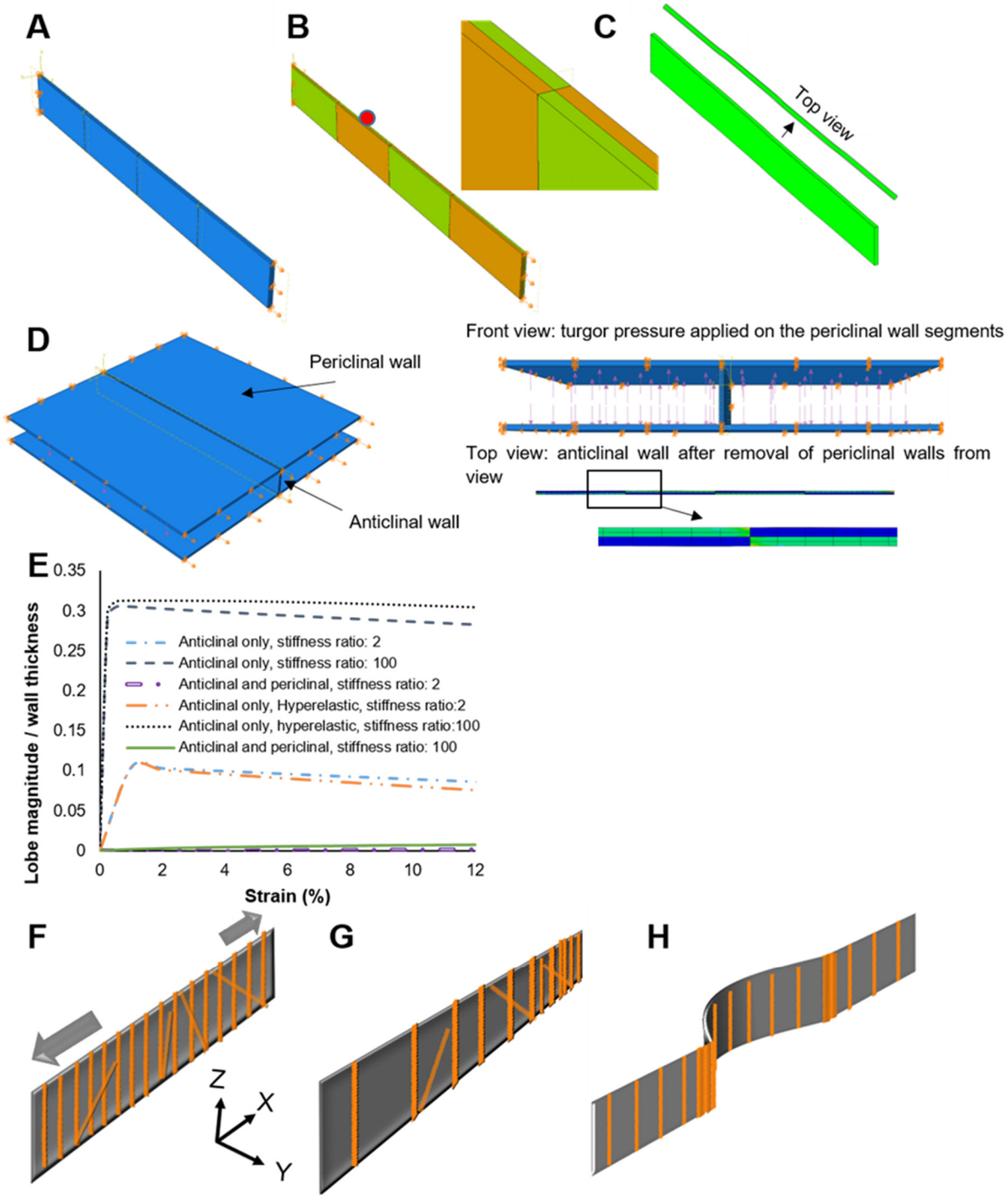
A
B
C
Top view
D
Periclinal wall
Anticlinal wall
Front view: turgor pressure applied on the periclinal wall segments
Top view: anticlinal wall after removal of periclinal walls from view
E
Lobe magnitude / wall thickness
Strain (%)
Anticlinal only, stiffness ratio: 2
Anticlinal only, stiffness ratio: 100
Anticlinal and periclinal, stiffness ratio: 2
Anticlinal only, Hyperelastic, stiffness ratio:2
Anticlinal only, hyperelastic, stiffness ratio:100
Anticlinal and periclinal, stiffness ratio: 100
F
G
H
Z
X
Y

Figure 4-14S. Finite element models of an isolated anticlinal wall (**A-C**). The wall dimensions are normalized by its length with the height and thickness considered as 0.1 and 0.01 ratio to the length. **B)** Material stiffness was alternated along and on two sides of the anticlinal wall. The red dot indicates the position of the control node the displacement of which was read as the lobe magnitude (ΔY). **C)** For a stiffness ratio of 2:1 between the stiff and soft regions, no degree of stretch of the anticlinal wall produced any waviness that was visually discernable, although a minute displacement was measured: The maximum displacement in Y direction was observed approximately at 1% strain and amounted to 0.1 of the wall thickness (see E). In a 1 μm thick wall this would correspond to a displacement of 100 nm. **D)** With the periclinal walls added on two sides of the anticlinal wall with symmetry boundary conditions, lateral deformation virtually disappeared (see E and F). Application of a pre-load (turgor pressure) under the periclinal walls or using non-normalized dimensions and absolute elastic values did not alter the results significantly. **E)** Lateral displacement of tip of a wave (lobe magnitude) expressed as a fraction of cell wall thickness plotted against strain for models with and without the periclinal walls. The graphs show that while increasing the stiffness ratio in the normalized models does somewhat increase lobe magnitude, all values remain negligible and visually not discernable. For models neglecting the periclinal walls, beyond a peak at small strains (~1%), the wall straightened. **F**) Preferential alignment of microtubules along undulations on the anticlinal walls suggesting that subsequent deposition of cellulose microfibrils renders the wall mechanically transversely isotropic. **G**) As a result of microtubule and cellulose orientation, the anticlinal wall can expand similar to an accordion in plane, while out of plane (Z direction) expansion is restricted. **H**) Progression of a lobe is accompanied by marked accumulation of microtubules and presumably increased deposition of cellulose at its two base-points (or necks of the adjacent cell).

10 and 1 μm for length, height and the shell wall thickness, respectively. The material was considered as linear elastic with a Young's modulus of 1 MPa and Poisson's ratio of 0.3. Boundary conditions were applied to prevent the in or out of plane displacement of the inner (lower) periclinal walls (as attached to mesophyll cells). However, further simulations showed that the outcome in terms of feasibility of buckling is not dependent on this particular boundary condition. Turgor load was applied to inner faces of outer periclinal walls. For these inputs, critical buckling load for turgor pressure was found to be as low as 2.8 KPa which is well below the reported range for turgor pressure in plant cells.

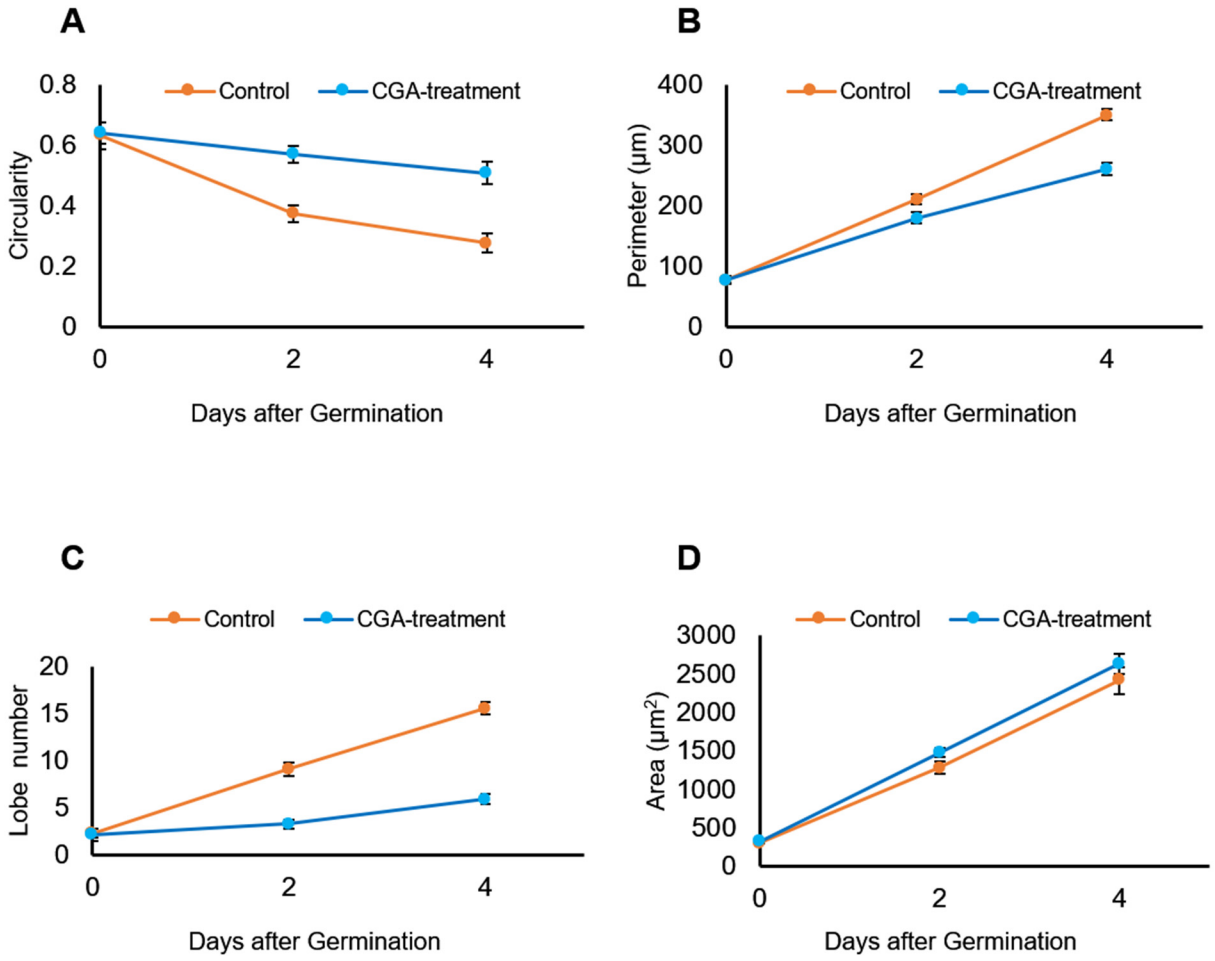

Figure 4-15S. Comparison of the pavement cells on adaxial surfaces of cotyledons of *Arabidopsis thaliana* seedlings grown in presence of CGA to reduce the cellulose crystallinity (control samples contain corresponding amount of DMSO). Pavement cells in treated samples showed reduced ability to form wavy borders **A)** and **B)**. **C)** and **D)** show that both group of samples grow similarly in terms of area and perimeter expansion and the reduced number of lobes was not a consequence of growth arrest in treated samples. The bars indicate standard error.

Chapter 5: Wavy cell shapes protect the epidermis from tear damage

Amir J Bidhendi[1], Bara Altartouri[1], M Shafayet Zamil[2], Frédérick P Gosselin[3], Anja Geitmann[1,2,*]

[1]Institut de Recherche en Biologie Végétale, Département de sciences biologiques

Université de Montréal, Montreal, Quebec, H1X 2B2, Canada

[2]Department of Plant Science, McGill University, Macdonald Campus, 21111 Lakeshore, Ste-Anne-de-Bellevue, Québec H9X 3V9, Canada

[3]Laboratoire de mécanique multi-échelles, Département de génie mécanique, École Polytechnique de Montréal, C.P. 6079, Succ. Centre-ville, Montreal, Quebec, H3C 3A7, Canada

*Address correspondence to: Anja Geitmann (geitmann.aes@mcgill.ca)

Author contributions

A.J.B., A.G. and F.P.G. designed the study. A.J.B. designed the setups and performed the experiments. B.A. provided the confocal micrograph of cellulose orientation in onion cells and performed the genotyping of *any1* mutant. M.S.Z. and A.J.B. built the tensile testing device. A.J.B., F.P.G., and A.G. analyzed the data, A.J.B. and A.G. wrote the manuscript.

Running title: Interlocking cell pattern and epidermis toughness

5.1 Abstract

Pavement cells in leaf epidermis of many plant species form interlocking wavy patterns which have been hypothesized to improve the tensile strength of the epidermis by increasing cell-cell contact. We put this hypothesis to test by stretching strips of the intact wild-type and *any1 Arabidopsis* leaves with reduced pavement cell waviness. To investigate the effect of cell geometry on tear resistance of the epidermis, we performed tear testing on excised strips of leaf epidermis with different cell shapes. The rectangular shape and organized arrangement of onion epidermal cells was associated with considerable anisotropy against tearing with lower force required to tear along the cells' long axes than transverse to them. Tearing along the long axis was associated with cell detachment events while transversely this was absent, presumably due to the staggered placement of cells. In leaf epidermis with wavy epidermal cells, cracks were observed to take a rough zigzag path passing through both cell borders and the periclinal cell walls. We hypothesize that the mixed cell wall and border fracture increases the overall fracture toughness of the tissue. We further corroborated this result with fracture studies performed in macroscopic mock samples made from polymethylmethacrylate laser-etched with patterns adapted from jigsaw puzzle pavement cells. Our results indicate that the wavy interlocking cell patterns increase the tear resistance of the plant epidermis; an ingenious defense strategy at the plants' most exposed surface.

Keywords: cell patterning, epidermis, fracture toughness, interlocking, morphogenesis, nature-inspired design, pavement cells, plant cell mechanics, tear resistance, wavy

5.2 Introduction

Shaping in plant cells must reconcile function and growth requirements of the organ, e.g., local and global growth directions. Involvement of mechanics has been extensively investigated in processes related to cell shaping and growth or turgor-driven movement (for instance see Aouar et al., 2010; Baskin, 2005; Bidhendi and Geitmann, 2016; Bidhendi and Geitmann, 2018a; Braybrook and Peaucelle, 2013; Carter et al., 2017; Cooke et al., 1976; Forterre et al., 2005; Geitmann and Ortega, 2009; Hamant et al., 2008; Majda et al., 2017; Sampathkumar et al., 2014a; Uyttewaal et al., 2012). The epidermis covers plant organs and is composed of cells that

differentiate into strikingly different shapes. The relationship between growth requirement of the organ and the shape of epidermal cells is in many cases intuitive. In organs that predominantly elongate in one direction, such as root or shoot, epidermal cells are often elongated, cylindrical or polyhedral bodies with a principal growth axis aligned with the organ axis. In organs that spread in both dimensions forming a plane, such as many leaves or petals, cells display considerable variation in aspect ratios depending on the growth stage and position within the tissue (Javelle et al., 2011).

Leaves are the primary locations of photosynthesis. Therefore, the integrity of leaves is matter of survival for the plant. Leaves are regularly exposed to mechanical stresses such as those caused by rain, wind or herbivores. Mechanical strength of the leaves is implicated in various studies with regard to stress resistance of the plant or is correlated with food production (Angeles et al., 2013; Aranwela et al., 1999; Balsamo et al., 2006; Niklas, 1992; Onoda et al., 2008; Onoda et al., 2011; Read et al., 2003; Wright and Cannon, 2001). In most species, except for xerophytic plants, leaves have a relatively thin and flat design with a large surface to volume ratio that maximizes exposure to light and gas exchange. However, this design optimization for metabolic functioning is achieved at the price of reduced stability of the thin flat structure against mechanical forces and increased exposure to herbivory.

The leaf of most eudicotyledons consists of four structural layers. Epidermal layers on top and bottom surfaces of the leaf sandwich layers of mesophyll and conductive tissue (Fig. 5-1A and B). Some of the most intricate manifestations of plant cell morphogenesis take place in the leaf epidermis of most dicotyledons, some monocotyledons and ferns (Korn, 1976; Panteris et al., 1994; Panteris and Galatis, 2005). Pavement cells, one of the three types of leaf epidermal cells that cover large portions of the leaf surface, form wavy jigsaw puzzle shapes that interlock (Fig. 5-1C). Molecular studies have investigated the roles of the cytoskeleton and auxin-related pathways in the genesis of the interlocking cell shapes, and recently a mechanical and a mechanistic model for the morphogenesis of wavy pavement cells were suggested (Belteton et al., 2017; Chen et al., 2015; Fu et al., 2005; Lin et al., 2015; Majda et al., 2017; Sapala et al., 2018; Xu et al., 2010; Zhou et al., 2016).

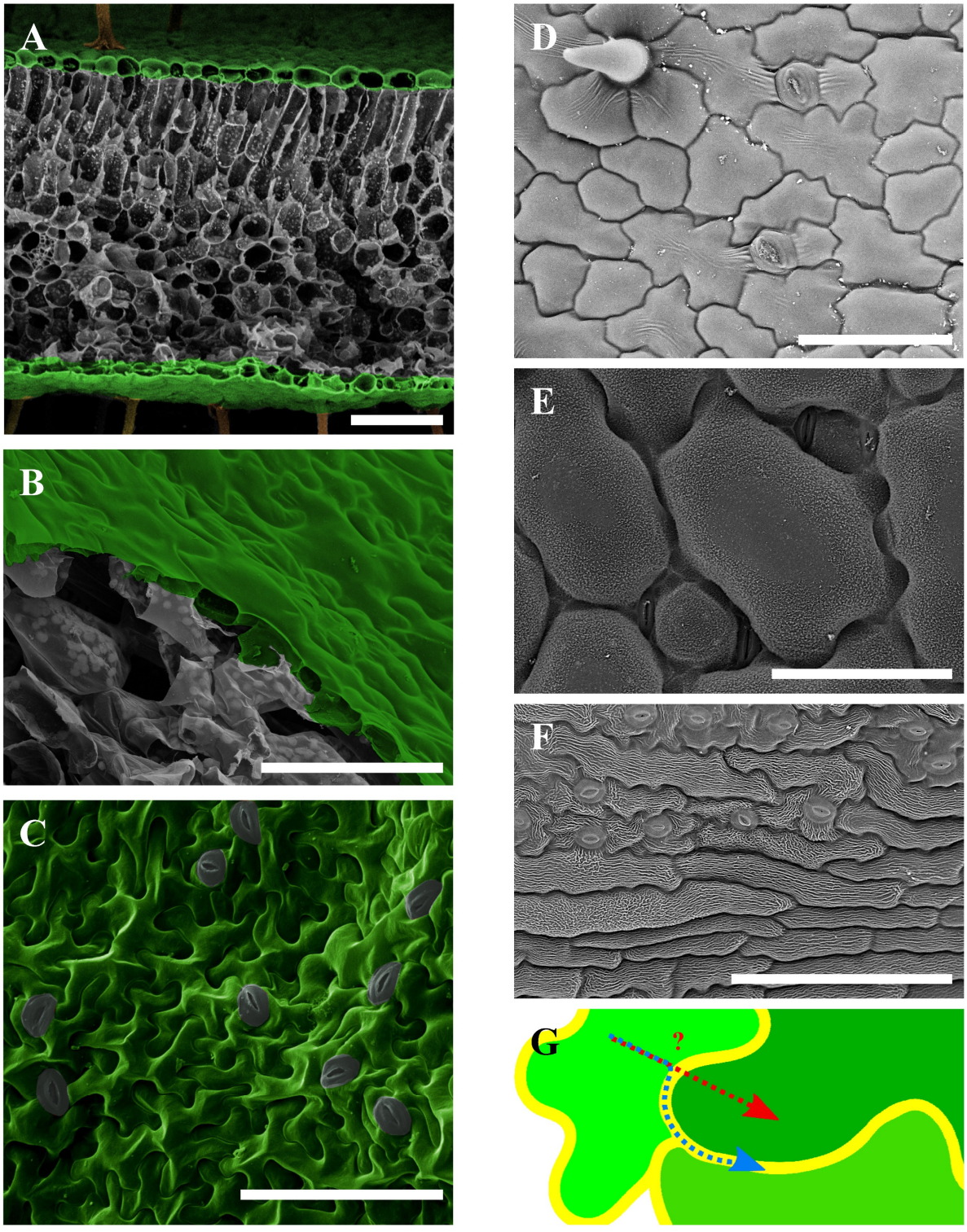
A
B
C
D
E
F
G
?

Figure 5-1. A) Scanning electron micrographs of leaf (*Euphorbia sp.*) cross-section showing upper and lower epidermal layers sandwiching mesophyll layers. **B)** A portion of *Arabidopsis thaliana* leaf cutaway demonstrating the epidermis (green) and underlying mesophyll cells. **C)** Pavement cells (green) in leaf epidermis of *Arabidopsis thaliana* forming interlocking jigsaw puzzle shapes. Epidermal cells on the surface of **D)** *Geranium sp.* leaf**, E)** *Oxalis sp.* leaf and **F)** *Arabidopsis thaliana* pistil. **G)** A tear reaching the border of cells (yellow lines) has two options: passing the border and penetrating into the wall of the neighboring cell (red arrow) which we refer to as wall fracture, or continuing along the border separating the cells (blue arrow) which we refer to as border fracture. Leaf epidermis is assigned a green pseudocolor to facilitate distinction from the mesophyll layers. For image processing and sample preparation see the supplemental information. Scale bars= 100 μm.

These studies have shed light on the mechanism of wavy pavement cell morphogenesis, but while some authors have contemplated possible mechanical advantages of such wavy shapes for the cells and the tissue (Sapala et al., 2018; Sotiriou et al., 2018), the wavy shapes continue to puzzle. Recently, Sotiriou et al. (2018) suggested that the wavy shapes might allow pavement cells to stretch reversibly, with wavy anticlinal walls straightening when being stretched and returning to their original shapes upon unloading, thus increasing the range of elastic tissue deformation. Sapala et al. (2018) suggested the wavy shapes to be a part of a strategy to reduce the turgor-generated stresses on the periclinal cell walls. In said strategy, the cells maintain a narrow width to limit open surface area, and thus less tensile stresses are generated on the periclinal walls. Instead, the cell adds to its volume through outgrowth of lobes. This is an attractive hypothesis and appears to be consistent with cells shapes found in genera such as *Arabidopsis* that have pavement cells forming lobes of significant length at maturity (Fig. 5-1C). However, it remains to be shown whether the concept can be generalized to cells with shallow lobes such as those in the epidermis of *Oxalis sp.* (e.g., Fig. 5-1D-F). In cells with shallow undulations, most of the cell volume derives from the cell body and the waviness does not seem to contribute significantly to the augmentation of cell volume and consequently, as proposed by the mentioned study, to the reduction of stress in the periclinal wall. Similar considerations can be made about epidermal cells that display a high aspect ratio in which slight waviness does not seem to add to the volume (Fig. 5-1F).

Aside from the hypotheses mentioned above, it has been long postulated that the wavy shape of pavement cells results in the increased tensile strength of the leaf. This is thought to be

accomplished by increasing the contact and adhesion surface between the neighboring cells (Glover, 2000; Jacques et al., 2014; Panteris and Galatis, 2005; Sotiriou et al., 2018). However, experimental investigation of this hypothesis and correlation of epidermal cell shape with mechanical failure behavior of the tissue is lacking. Onoda et al. (2015) suggested that the sandwich anatomy of the leaf has an important structural function. The authors suggested the epidermal layers carry the tensile load and the aerenchymatous mesophyll serves as a core spacer thus enhancing overall flexural rigidity at low density. This concept requires the epidermis to have the integrity to tolerate the tensile forces arising in different loading scenarios. While Onoda et al. (2015) did not investigate the failure behavior of the epidermis, their study implies the importance of the epidermis in maintaining tissue integrity. Mesophyll cells, especially the spongy type, form air spaces resulting in reduced cell-cell contacts both within the mesophyll as well as with the epidermal cells. This makes the role of epidermis in maintaining the leaf integrity even more significant. In this study, we investigate the hypothesis that correlates the epidermal cell shape with tissue strength. Moreover, we study whether the shape of the cells correlates with tear and failure of the epidermal tissue upon propagation of existing tears. To investigate these hypotheses, we used *Arabidopsis* and tomato leaves and onion epidermis and complemented microscopic observation with macroscale fracture experiments.

5.3 Materials and methods

5.3.1 Plant material

Arabidopsis thaliana Col-0 wild-type seeds were germinated in sterile Petri plates containing ½ x MS (Murashige and Skoog, 1962) media under long day lighting condition. For tests on true leaves, the seedlings were transplanted one week after germination and were placed in growth chambers until the experiment. Fresh onions (*Allium cepa*) were obtained from a local supermarket. To be consistent, all experiments were conducted with epidermal peels from the white onion variety. The experiments were carried out on epidermis extracted from scales 2, 3 and 4 counting from the most external layers. Other plant types used in the study were obtained from on-campus greenhouses.

5.3.2 Plant sample preparation

For true leaves of *Arabidopsis* or tomato, segments were cut away from the leaf veins to avoid the leaf veins influencing the results. For tensile tests to evaluate the stiffness of adaxial onion epidermis along the two perpendicular directions, the samples were cut into a dogbone shape, using a custom cutter, ensuring that the strain was concentrated in the gauge length. As a result, for classical tension tests, failures occurred consistently in the gauge region. The width and length of the gauge area were 0.65 and 12 mm, respectively. The thickness of the epidermis, 0.08 mm, was averaged using microscopy images as well as a digital caliper independently for n=20 samples. The number of samples for the monotonic tensile test was n=51 from 3 different onions. For tension to the failure of pieces of wild-type and *any1 Arabidopsis* leaves, the samples were cut in dimensions of 1 mm and 8 mm in width and length respectively. For tear test of the middle-notched specimen, the samples were prepared with width and gauge lengths of 12 mm and a 1 mm notch was placed in the middle of the sample with a custom cutter. The end parts were cut wider for improved gripping. In cases that plasmolyzed and non-plasmolyzed samples were compared, the plasmolysis was carried out by placing the samples in 0.8 M mannitol for at least 15 minutes prior to the experiment. The non-plasmolyzed samples were submerged in ddH_2O for the same period. During the experiments involving fresh specimens, the samples were continuously covered with a layer of liquid using the corresponding solution (mannitol for plasmolyzed or ddH_2O for ordinary samples) to avoid dehydration. Samples that were to be observed under the scanning electron microscope (SEM) were fixed using either a formaldehyde or a methanol-ethanol fixation protocol. For formaldehyde fixation, samples were placed in 3.5% formaldehyde, freshly prepared in PBS buffer (pH 7.3, similar to Tirichine et al., 2009), for at least 3 hours in the room temperature. The samples were then rinsed three times thoroughly with PBS buffer. The samples were then gradually dehydrated by submersion in increasing ethanol concentrations from 20%, 50%, 70%, 80%, 90%, for 20 minutes each, followed by a 2-hour submersion in 95% ethanol and three times submersion in 100% ethanol for 30 minutes each. After ethanol graduations, the samples were critical point dried using a Leica EM CPD300 and gold-palladium coated under a Leica EM ACE200 prior to observation under vacuum in the SEM. As an alternative for the formaldehyde fixation, a methanol-ethanol fixation procedure was adopted similar to the study by Talbot and White (2013). The samples

were first submerged in methanol for at least 3 hours before being immediately placed in 100% ethanol for at least 4 hours. For large or thick specimens, the samples were left overnight in fresh ethanol. The samples were then directly critical point dried.

5.3.3 Tensile testing setup for biological samples

Preliminary tensile and fracture tests were carried out on Liveco Vitrodyne V-200, a miniaturized tensile testing setup developed by Lynch and Lintilhac (1997). Complementary tests were carried out on a tensile testing setup developed in-house. In both cases, a linear variable differential transformer (LVDT) measured the displacements of the sample allowing strain computations. Wild-type and *any1 Arabidopsis* leaves were stretched to failure at speeds of 25, 125 and 250 µm/s. Edge-notched and middle-notched onion epidermis specimens were stretched at speeds of 100 and 200 µm/s, respectively. For the classic tensile tests to extract properties such as Young's modulus and tensile strength of the of onion epidermis, the loading speed was set to 20 µm/s, and the samples were stretched to rupture.

5.3.4 Microscopy

Scanning electron microscopy: Samples were fixed, critical point dried and coated as explained in the sample preparation section. FEI Quanta and tabletop microscope Hitachi TM-1000 were used for the observations.

Stereomicroscopy: Tensile tests and, specifically real-time observations of tear propagation in onion epidermis were carried out using Zeiss Discovery V8.

Fluorescence microscopy: To visualize cell borders, samples were stained with propidium iodide and observed using a Zeiss LSM 510 META confocal laser scanning microscope. Propidium iodide staining was performed at a concentration of 250-500 µg/mL at room temperature for approximately 15 minutes. The samples were then thoroughly washed with ddH_2O prior to observation. For propidium iodide staining, the excitation wavelength of 532 nm and bandpass emission filter of 550-615 nm were used. To visualize the cellulose orientation, samples were incubated with 0.5% Pontamine Fast Scarlet 4B (PFS) for one hour. The samples were visualized using a Zeiss Axio observer Z1 platform with excitation wavelength of 561 nm.

5.3.5 Laser engraving and fracture test of PMMA

The engraved patterns of onion and *Arabidopsis* epidermal cells (scaled at approximately 54:1 and 250:1, respectively) were obtained from confocal micrographs as explained in the previous section. Cast polymethylmethacrylate (PMMA) was used for its isotropic properties and being well-suited for laser engraving. The thickness of the sheet was 5.58 mm (0.22 inch). A Trotec Speedy 300 laser-engraved the patterns and cut the compact tension (CT) samples. For engraving, the device was set at the 100% and 10% of maximum laser power and speed, respectively. The frequency of 1000 PPI, and the resolution of 600 dpi were used, and the laser passed over each line three times. The CT sample dimensions were originally adopted from ASTM D5045-99. The sample dimensions were then slightly modified to accommodate the engraving pattern. After engraving of the pattern and cutting out the CT sample, a microcrack was induced at the tip of the laser-cut notch by gentle tapping using a snap-off blade knife. The fracture tests of acrylic CT samples were carried out on an MTS Insight machine at jaw separation speed of 4 μm/s (Fig. 5-8 and Supplemental Fig. 5-12S).

5.3.6 Image processing

General processing of microscopy images was carried out using ImageJ (Schneider et al., 2012). To extract the cell borders for laser engraving, micrographs of pavement cells of *Arabidopsis* and onion obtained through confocal and stereo microscopes were imported in the open source Inkscape software (Inkscape.org). Cells lines were traced and vectorized. 3D reconstructions of Z-stacks for visualization of cracks in *Arabidopsis* embryo (Fig. 5-6) were developed using Amira image analysis software (Visage Imaging). Pseudocoloring of SEM micrographs was performed using GIMP (GNU Image Manipulation Program, Gimp.org). Background of some images (Figs. 2C and D, Figs. 5D and E) was removed for ease of interpretation. For originals please see the Supplemental Materials (S5-S7).

5.4 Results

5.4.1 Under tension, intact epidermis does not fail by cell separation

It has been long conjectured that the wavy interlocking shapes of pavement cells increase the cell-cell contacts, the adhesion surface and consequently the tensile strength of the epidermis. In this study, we first attempted to investigate the link between the failure of an intact tissue under tension and the shape of its epidermal cells. For this, thin strips of leaves were prepared from wild-type and *any1 Arabidopsis.* The mutant *any1* possesses an altered cellulose crystallinity and demonstrates a less interdigitated and rather swollen pavement cell phenotype (Fujita et al., 2013). The strips were mounted on the tensile device, clamped and stretched until rupture (Fig. 5-2B shows a ruptured leaf strip). Only samples that failed in the gauge area were kept for subsequent steps. The samples were then fixed and observed under the scanning electron microscope. Our observations indicated that, in both wild-type and *any1*, the failure seems to cross the sample width going through the periclinal cell walls and no cell separation was observed near the rupture edges (Fig. 5-2C and D). Since periclinal mechanics determines the mechanical strength of the tissue in this case, cell waviness does not necessarily translate to increased epidermis strength. Similar behavior was observed in both wild-type and the *any1* mutant. Nonetheless, we observed that the fracture surfaces curve strongly, presumably due to elastic recoil upon rupture as well as deformations occurring during the fixation and dehydration processes. This curvature obscures the free fracture edges and renders the precise observation of the tear path in the cells challenging.

Using the samples above, we detected that in both wild-type and *any1*, away from the ruptured edges, the damage can propagate into cell borders (Fig. 5-2E). From this observation, we hypothesized that the shape of cell borders and cell orientation can affect the tear resistance of the epidermis. Tear resistance is a measure of the extent that epidermis resists propagation of tears. However, as mentioned, the artifacts occurring upon fracture and fixation of the sample was prohibitive of investigation of fracture surfaces by tearing of fresh leaves with wavy cells. The small size of epidermal cells of *Arabidopsis* and especially the existence of multiple layers beneath the epidermis dispersing the light render stereomicroscopy of the real-time tearing in

jigsaw puzzle pavement cells challenging. Therefore, we chose onion epidermis as an accessible alternative for tear tests.

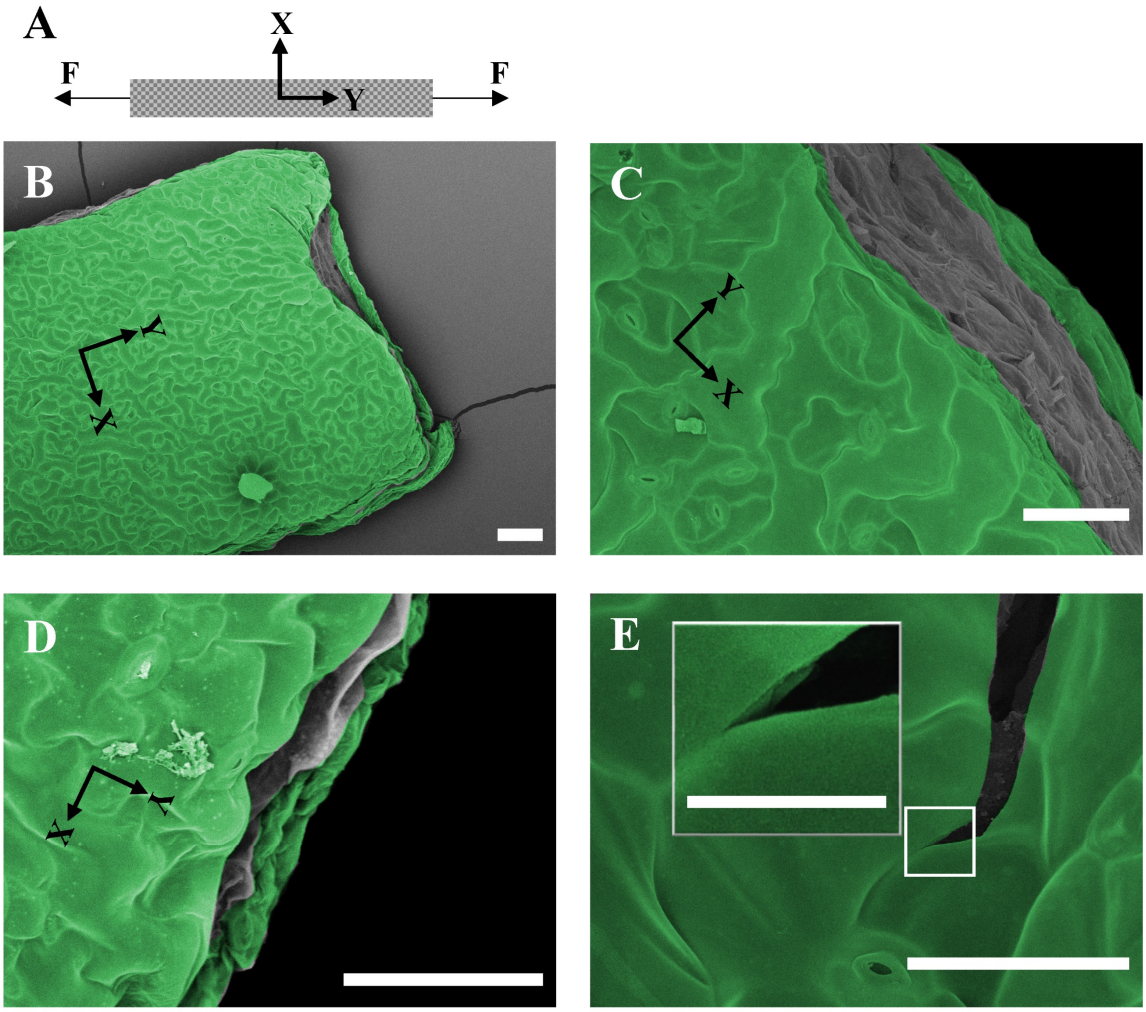

Figure 5-2. A) Schematic of the leaf strip samples. Forces are applied at two ends of samples. The Y direction demarcates the long axis of the sample while X is in width direction in all subsequent images. **B)** A thin strip of *Arabidopsis any1* leaf stretched to fracture. Tear surfaces do not show cell-cell separation in **C)** *any1* or **D)** wild-type *Arabidopsis thaliana*. Tear edges warp. **E)** Close-up of damage away from tear edges in an *any1* leaf demonstrating crack in the cell deviating and propagating into the interface, the middle lamella. Scale bars= 100 (A, B), 30 (C, D) and 10 (D inset) µm. Green pseudocolor demarcates regions perceived to be the epidermis.

5.4.2 The orientation of onion epidermal cells directs tear propagation in the epidermis

To study tear propagation in the epidermis in correlation with cell shape, real-time observation of tear trajectory is crucial. This is mainly due to artifacts that obscure the fracture surfaces and occur in samples observed after tearing and dehydration. Onion epidermis can be separated readily without considerable damage and has large cells that can be easily observed using a stereomicroscope, allowing for real-time observation of tissue tearing.

Further, since the epidermal cells in onion epidermis are relatively well-aligned brick shapes with respect to a single axis, it makes studying the influence of cell orientation on tissue mechanics considerably easier compared to tissues without geometrical bias. For simplicity, in this text, we refer to fracture as "border fracture" when the tear separates the cell bodies without going through the cell wall and breaking the cell (Fig. 5-1G). This is regardless of whether it occurs due to debonding at the interface between the middle lamella and the cell wall (adhesive fracture) or due to the fracture of the middle lamella itself (cohesive fracture). When the crack occurs in the cell wall (cohesive fracture of the wall) and not in the border, we use the term "cell wall fracture".

Specimens were made from adaxial onion epidermis with a custom cutter with an edge-notch forming a trousers-like specimen. The samples were then torn by pulling the trouser legs away from each other in-plane or out of plane (Figs. 5-3A and B). Tear tests were performed using the tensile device under the microscope and were also repeated manually. We observed that tear seems to deflect and rotate when propagating in the epidermis (Fig. 5-3C). If the tear was initially oriented along the long axes of cells, it typically followed a relatively straight line along the cells (Fig. 5-3D). However, the tear showed difficulty crossing perpendicular to the cells axis. In some cases, we observed that upon pulling of the sample's legs, the cut made with the blade immediately rotated 90° with respect to the original orientation and oriented itself along the cell axis (Fig. 5-3E). Note the location of the stars). In some cases, this 90° angle was preserved, or it later turned into an oblique angle traversing the cells (Mov. 1, Fig. 5-3E). Relatedly, in many cases, the oblique angle of a tear turned into a 90° angle with respect to the original transverse orientation resulting in the tear following the cells' major axes (Fig. 5-3F

and G). This seemed to be especially the case at sharp tear angles with respect to cell borders. However, we did not quantify the tear angle-deviation relationship and did not rule out the edge effect for tears getting close to edges of the sample. However, as mentioned above, the 90° turning to orient along the cells long axis was even observed in the middle of the samples and thus not merely an edge effect (Fig. 5-3E). In rare cases, the tear initially placed transverse to the long axis of cells did not deviate from its path and continued a relatively straight path perpendicular to cells major axes. However, even in these cases, considerably rough tear edges were observed with pieces of epidermis protruding in the tear path, a behavior similar to crack-bridging (Fig. 5-3H).

As mentioned above, in transverse samples, the tear deviated from the straight path and in many cases assumed an oblique orientation. Staining the specimens with Pontamine Fast Scarlet 4B (PFS), a dye with a high affinity to cellulose bundles (Anderson et al., 2010; Bidhendi and Geitmann, 2016), we observed an oblique orientation of cellulose in adaxial onion epidermal cells (Fig.5-4). The angle of mean cellulose orientation in adaxial onion epidermal cells (Fig. 5-4) seems to be close to the angle of deviated tear path in some samples (Fig. 5-3E-G). This suggests that the deviation of the tear from a transverse orientation to an oblique angle may occur within the cell before reaching the borders and because of the oblique axis of anisotropy and orientation of the cellulose bundles in the cell wall. However, we did not further investigate the material anisotropy in relation to the tear propagation in this study and focused instead on the geometrical aspects of the cells and the cell borders. While we mainly used adaxial onion epidermis, trials with abaxial epidermis showed similar results, but we continued the experiments with the adaxial epidermis of onion. Abaxial onion epidermal cells split open during detachment from the underlying tissues. This makes obtaining intact samples from this layer challenging. To rule out any substantial contribution from the turgor pressure to tear behavior observed in the epidermis, we carried out some tests on plasmolyzed specimens and observed the same trends as demonstrated above. Therefore, the tearing behavior mainly arises from the material properties and geometrical aspects and not the effect of the internal pressure of the closed cells.

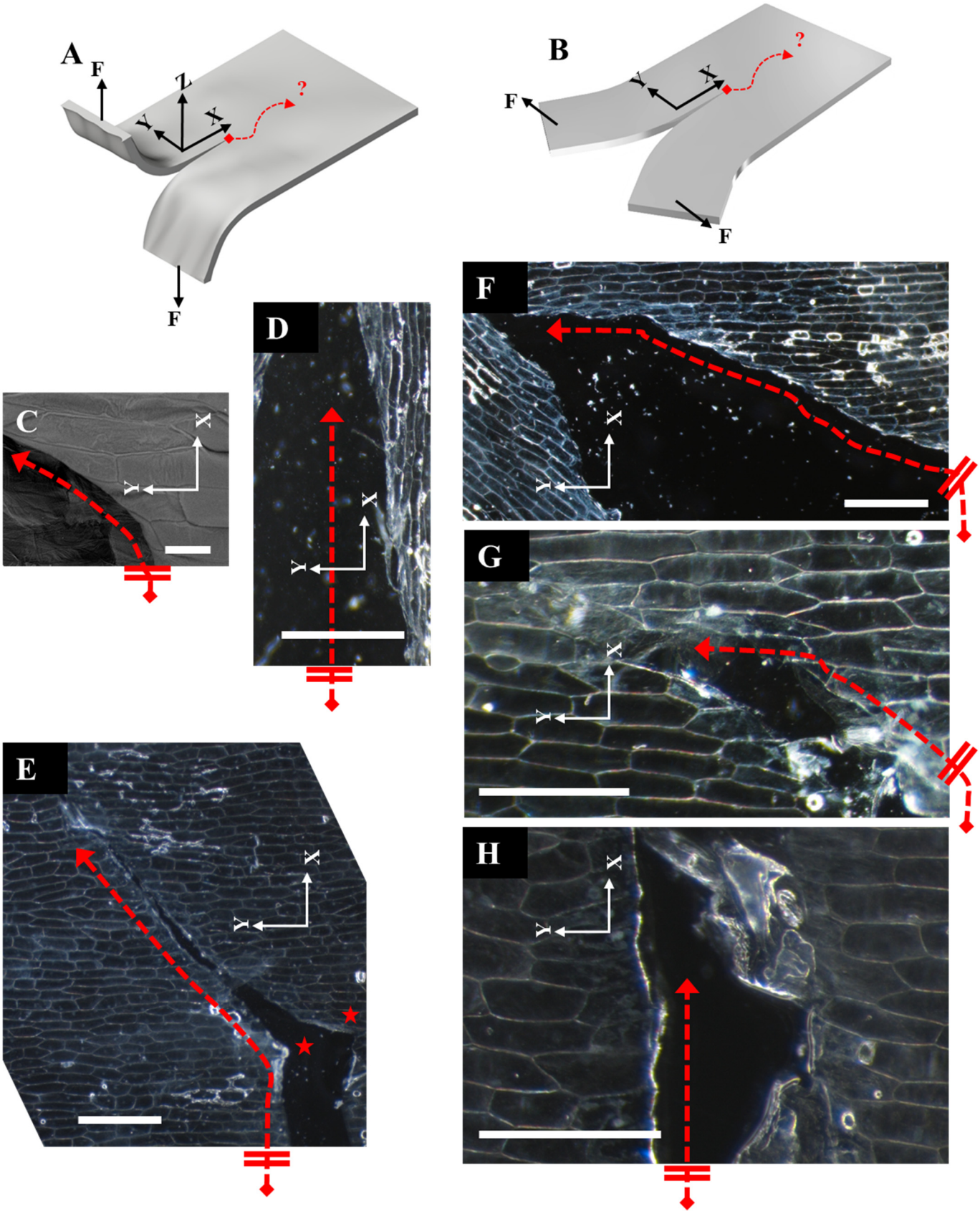
A
F
Z
Y
X
?
F
B
F
Y
X
?
F
C
X
Y
D
X
Y
E
X
Y
F
X
Y
G
X
Y
H
X
Y

Figure 5-3. Geometry and loading of the edge-notched specimen with **A)** out-of-plane and **B)** in-plane loading. F denotes the force applied to the legs of the trousers-like specimens to propagate the tear. The X direction demarcates the orientation of the original blade-cut notch in all the following figures. For the out-of-plane loading, the load is in the Z direction, perpendicular to the plane of the tear. For in-plane loading, the load is in the Y direction, perpendicular to the original cut. All following figures are for type (A) loading scenario, although similar outcomes were observed in type (B) loading. **C)** SEM micrographs showing a local change of tear path from transverse (to cell axis) to longitudinal. **D)** Tear oriented along the cell axis continues a fairly straight path. **E)** Micrograph depicting a transverse blade notch immediately turning close to 90° and then continuing in an oblique path. **F)** and **G)** Transverse tear becoming oblique and later aligning with cells long axis. **H)** In a few rare cases, transverse tears did not deviate or reorient but continued a straight path transversely to cell axes. In these cases, a rough tear surface could be observed with tissue segments bridging the crack. The dotted red arrows mark the tear path. The beginning of the arrows marked with a red-rhombus show the direction, orientation but not the exact distance of the original blade-cut with respect to the image frame. The stars in (E) mark the location of a sharp tear reorientation. Scale bars = 1 mm except for (G, H) = 500 µm and (C) = 100 µm.

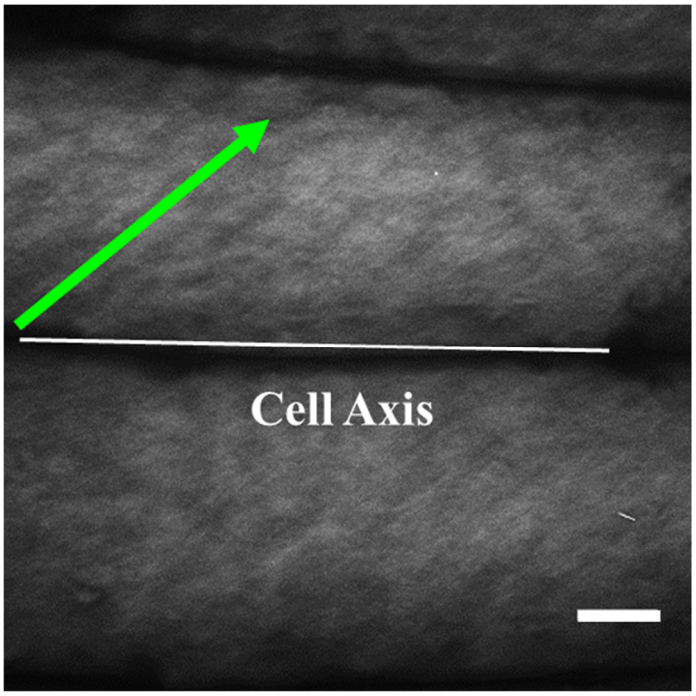

Figure 5-4. Staining of adaxial onion epidermal cells with Pontamine Fast Scarlet 4B (PFS). Predominant cellulose orientation (green arrow) seems to be oblique to the long axis of the cells (white line). Scale bars = 20 µm.

5.4.3 Cell orientation determines the tear resistance of the epidermis

In previous sections, we observed that the onion epidermis behaves anisotropically against propagating tears. Tears perpendicular to the direction of the long axis of cells tend to deviate from their path. To further investigate the influence of cell orientation, and to quantitatively compare the tear resistance of the onion epidermis along the two principal cell axes, tear tests were conducted on middle-notched specimens. The edge-notched specimen used in the previous section was observed to occasionally warp out of the plane, hang loose and make creases in front of the tear path when the legs were pulled apart because of its negligible flexural rigidity. These artifacts can affect the magnitude of the forces being read at the force sensors. Placing the notch in the middle of the specimen and stretching the specimen at its two ends, however, can mitigate these issues and can keep the specimen relatively flat until the tear in the middle reaches the edges. Further, as this type of sample does not allow the tear to run freely choosing the path of minimum resistance, it is better suited to compare the forces required to tear across the specimen. For this test, using a custom cutter, samples were cut consistently with a fissure that was placed in the middle of the specimen and oriented perpendicular to the stretching direction (Fig. 5-5C). The tearing force was recorded. Two groups of samples were tested: middle notch oriented either along or perpendicular to the cells major axis (longitudinally or transversally notched, respectively). On average, the force in stretch tests reached higher values for transversely-notched samples while the longitudinally-notched specimen endured higher strains (Fig. 5-5A and B. For all experimental curves see Supplemental Fig. 5-10S). We thought that these behaviors could partly stem from the fundamental behavior of the intact tissue exhibiting a stiffness anisotropy along the two different axes as was suggested previously (e.g., see Vanstreels et al., 2005; Zamil and Geitmann, 2017). We performed several sets of experiments to identify the elastic moduli of the onion epidermis along and transverse to the cells axis. The result of these classic tensile tests indicates that the onion epidermis appears slightly stiffer in the longitudinal direction (Supplemental Fig. 5-11S). The area under the force-displacement curve, work or energy, can be used as a measure of tear resistance.

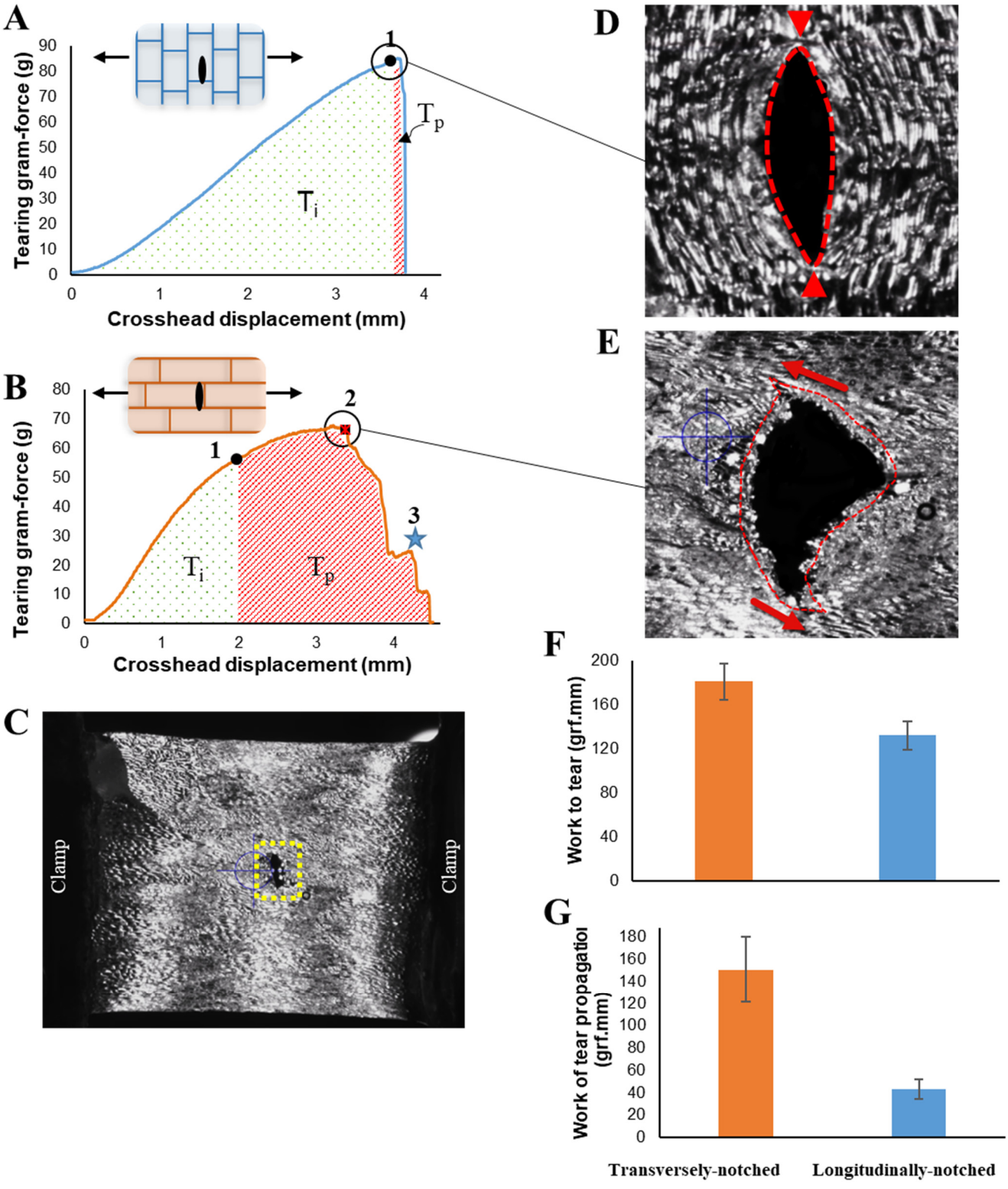
A
Tearing gram-force (g)
Crosshead displacement (mm)
1
T_p
T_i
B
Tearing gram-force (g)
Crosshead displacement (mm)
1
2
3
T_i
T_p
C
Clamp
Clamp
D
E
F
Work to tear (grf.mm)
G
Work of tear propagation (grf.mm)
Transversely-notched
Longitudinally-notched

Figure 5-5. A sample tearing force versus displacement of the tensile device jaw for **A)** longitudinally- and **B)** transversely-notched specimen. The notch was placed in the middle of the specimen. Point 1 corresponds to the onset of tear growth. Point 2 in (B) corresponds to peak force after which the tear seems to turn toward longitudinal direction slightly (see E). Although tear does not freely propagate in the longitudinal direction, this point marked the peak force. Point 3 exemplifies step-wise tearing force with local increases. The green-dotted zone refers to the period of increase in force for tear initiation (T_i). The red-hashed zone belongs to the period of tear propagation (T_p). In the sample graphs, it can be seen that tear propagation zone in longitudinally-notched specimens is negligible. **C)** Middle-notched specimen of adaxial onion epidermis stretched to complete tear while forces to propagate the tear are recorded. The dotted rectangle marks the location of the middle notch. **D)** Tear in longitudinal direction retains its sharp tips (arrows). **E)** Tear shape in transversely-notched specimen becomes relatively elliptical. In some cases, the progressing tips of tear rotate away from the direction of progression (arrows). **F)** Work of tear (T_i+T_p) for transversely- and longitudinally-notched specimens. **G)** Work to propagate the tear (T_p) in transversely- and longitudinally-notched specimens. This data indicates the work to be done to rupture across the sample after tear propagation has begun. The bars indicate standard error.

This area was larger for the transversely-notched specimens meaning more energy is spent to rupture the same width of the specimen by propagating a tear in this direction (Fig. 5-5F) ($p<0.05$). The mechanical anisotropy of the tissue, e.g., different apparent stiffness values in longitudinal and transverse directions, however, confounds the comparison of work of tearing (area under the curve) between the two directions if to isolate only the contribution of cell orientation is intended. A closer look at the real-time tearing experiments and tearing force data, however, reveals some interesting details. In both cases, it was observed that the force (and consequently the stress) needs to build up before any perceivable increase in the length of tear could be observed (point 1 on Figs. 5-5A and B). This can be termed as tear initiation period (T_i). In the longitudinally-notched specimens, this in most cases coincided with the peak force, followed by a catastrophic and abrupt failure afterward (Fig. 5-5A and Mov. 2). In transversely-notched specimens, on the other hand, as the tear starts to grow (point 1 on Fig. 5-5B, Mov. 3), the force continues to rise (tear propagation period T_p). The peak force in the diagrams of this type of samples (point 2 on Fig. 5-5B) does not coincide with the tear initiation. Instead, the peak force was observed to be associated with a tilt of the tear edges toward the long axis of cells (Fig. 5-5E). However, it should be noted that, unlike the edge-notched tearing of specimens, due to loading constraints of the middle-notched tearing tests the tear cannot freely deviate toward an arbitrary path with minimum resistance. The loading geometry prefers the

shortest path across the width of the sample to rupture it. As a result, while the tear traverses the specimen, minor local deviations might occur that, as shown, coincide with drops in tearing force. Further reduction of the tearing force is in part due to a decreased cross-section of the sample bearing the tensile force. Moreover, in the step-wise force reduction associated with transversely-notched samples, we observed an occasional increase in the tear force indicating the continued resistance of the tissue to tear (for instance see point 3 in Fig. 5-5B). Comparing the work for propagation of tear between the longitudinal and transverse configurations demonstrated that in comparison, more than three times the energy is required to rupture the same width of the specimen transversely (Fig. 5-5G) ($P<0.005$). Together, the results indicate that tear propagation is hindered transverse to the main axis of cells, with tear tips becoming blunt and rounded (Fig. 5-5E) while when aligned with cell orientation, the tears remain sharp (Fig. 5-5D) and the tissue fails catastrophically.

5.4.4 Tears can run along the cell borders separating the cells

In the propagation of a crack in the cellular tissue, two scenarios are possible. The fracture can occur in the cell wall, either away or close to the borders. We refer to both cases as cell wall fracture. The other scenario is a clean separation of cells. This can occur either due to adhesive or interfacial fracture resulting in separation of the middle lamella from one of the cell walls on its two sides or due to cohesive failure, fracture of the middle lamella itself. We refer to both of these cases resulting in clean separation of cells as border fracture, regardless of their adhesive or cohesive natures. The propagation of tears along the cell lines in edge-notched specimens and the significant difference between the tear resistance of longitudinally- and transversely middle-notched specimen motivated us to investigate how the tear propagates when reaching borders. To this end, we closely monitored tear propagation in the edge-notched specimens under the stereomicroscope. The results indicate that tears along the cell lines can find their way and travel along borders (Mov. 4). Propagation of tear into the border was observed to be associated with the sudden release of strain energy and a drop in the force required to propagate. This can explain the catastrophic failure of the longitudinally-notched specimen in the previous section. Major border fracture was not observed in transversely-notched specimens. This is at least in part due to the staggered placement of cells (Mov. 5), forcing the tear to pass through both the borders and the periclinal cell walls. Moreover, as seen in previous sections, in jigsaw pavement cells

of *Arabidopsis,* we observed cracks propagating in the middle lamella. The results in this section corroborate the idea that the border fracture is not limited to the *Arabidopsis* tissue or possible merely due to dehydration events, because it occurs in fresh onion epidermis as well. An *Arabidopsis* embryo freshly extracted from the seed coat was placed in a drop of water between a glass slide and a coverslip. Serendipitously, we observed that the stresses due to pressing and rotating the coverslip between the finger resulted in rows of epidermal cells undergoing border fracture in the root (Fig. 5-6A, C) and the cotyledon (Fig. 5-6B, D), a potentially fatal failure. This confirmed that border fracture can occur in various fresh *Arabidopsis* tissues with straight well-aligned cell borders.

5.4.5 Fractures in wavy pavement cells include both the cell wall and border fractures

In previous sections we observed that fractures can propagate into the cell borders, separating the cells. In tissues such as onion epidermis, specifically, we observed that along the main axis of cells, due to border fracture, propagating tears can cause the tissue to fail the tissue catastrophically. In tensile testing of intact segments of *any1* and wild-type *Arabidopsis* leaves, we observed occasional border away from the main site of rupture. To investigate the behavior of tears in jigsaw puzzle-shaped pavement cells, we attempted to repeat the tear experiments done with the onion epidermis. Since the pavement cells of the *Arabidopsis* are considerably smaller than what can be observed in detail using a stereomicroscope, after the tearing the edge notched specimens, the samples were fixed and observed under an SEM. However, as observed before in rupture of intact leaf tensile samples, the free edges demonstrating tear surfaces severely curve and prevent studying of tear trajectory and the newly created tear surfaces (see Fig. 5-7A). Therefore, we decided to study the fracture behavior of the dehydrated edge-notched samples instead. Due to the fragile nature of the dehydrated samples, we performed these tests manually using tweezers. SEM observation of crack paths in wavy pavement cells of *Arabidopsis* and tomato showed that cracks did not propagate in a straight path (Fig. 5-7B-D). Still, the tear did not seem to follow the cell borders predominantly by border fracture. While in some regions the cracks penetrated the middle lamella and followed the cell borders detaching the cells, they did not continue in the border and penetrate the periclinal cell wall (Fig. 5-7E-H).

It seems that tears and cracks do not follow the borders when the curvatures make a wide angle with regard to the tear path and when the lobes become too deep (for instance see Fig. 5-7H).

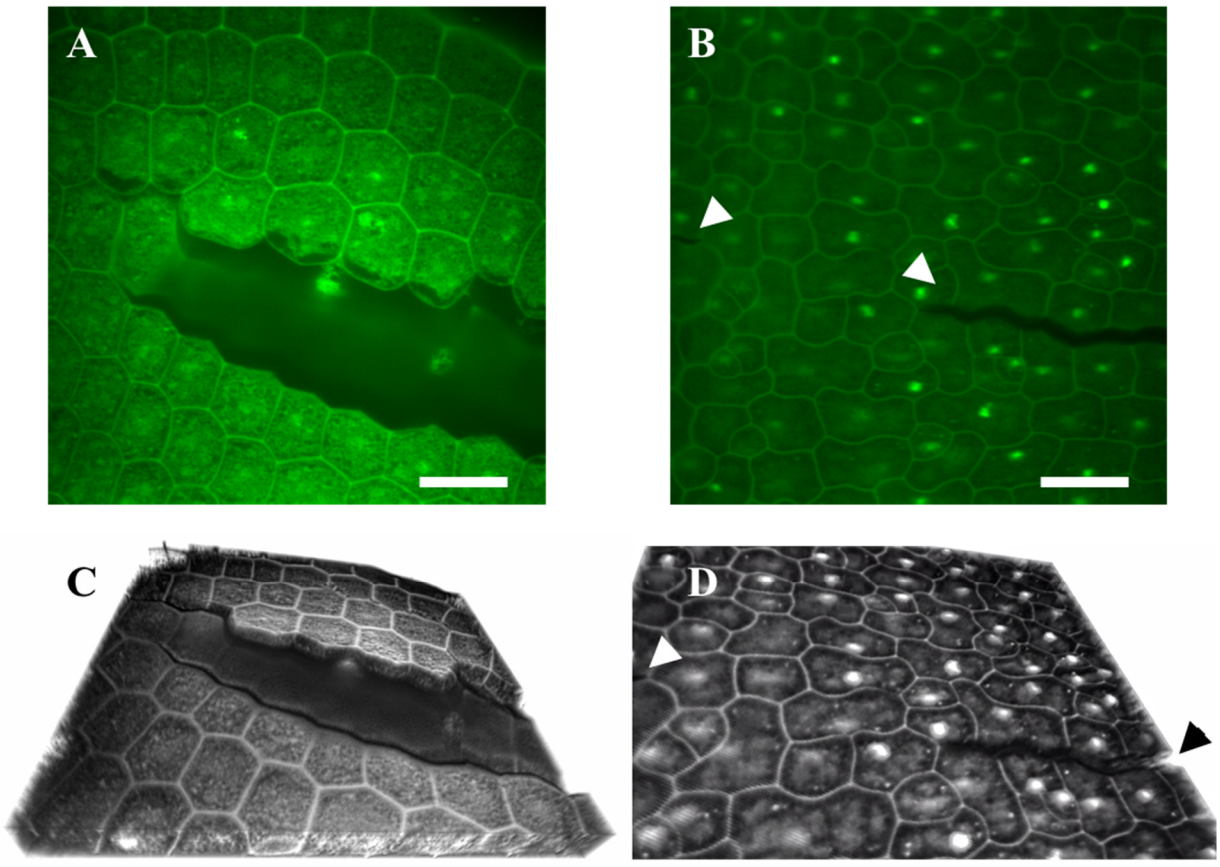

Figure 5-6. Confocal micrographs of a propidium stained fresh *Arabidopsis* embryo squeezed between a glass slide and coverslip demonstrates cell-cell separation in **A)** root and **B)** leaf epidermal cells. **C)** and **D)** are 3D reconstructions of (A) and (B) respectively. Scale bars = 20 µm.

5.4.6 Perpendicular and wavy cell borders increase the fracture toughness of the tissue

In previous sections, we showed that alignment of cells can guide propagation of tears in the onion epidermis. This was shown to be in part due to the difficulty of tears to cross the cells. On the other hand, border fracture at the middle lamella was shown to occur with the potential to provide a low resistance path resulting in catastrophic tissue failure. By studying fracture in dehydrated leaves of *Arabidopsis* and tomato, we realized that cracks formed in eudicot

epidermis with wavy cells tend to take a rough path inducing both border and cell wall fractures. This potentially increases the tear resistance of the epidermis compared to straight borders and aligned cells. However, tear tests to evaluate the influence of wavy cell geometry in tear resistance of the leaf epidermis are challenging. Aside from challenges related to isolation of the intact epidermis from the leaf or conducting experiments on fresh samples that result in curved tear edges, mechanical anisotropy adds a confounding factor. This is because both the geometry and wall mechanics can affect the outcome. Additionally, a meaningful comparison can hardly be made between the tear resistance of wild-type *Arabidopsis* epidermis and epidermis of an *Arabidopsis* mutant or onion. This is because they can have significantly different cell wall parameters such as biochemical composition or thickness. Therefore, to study the effect of the geometrical features on the propagation of tears in the epidermis, we envisaged the use of a physical model to study the pattern-dependent crack propagation. For this, we engraved epidermal cell shapes on compact tension (CT) specimens made from cast PMMA sheets using a laser engraver. Cast PMMA is expected to have isotropic properties, eliminating the material parameter from the problem. The removal of material by laser was intended to create weaker interfaces mimicking the observed tendency of tears to penetrate the cell borders. Two types of cell patterns were engraved. The staggered brick-shaped pattern of an onion epidermis and the interlocking jigsaw puzzle cell pattern of an *Arabidopsis* cotyledon obtained from confocal micrographs (Figs. 5-8A and B).

Two additional patterns were also engraved by rotation of these patterns. This was to study how the orientation of cells affects the fracture toughness, specifically to produce data for transverse and longitudinal onion patterns that could be compared with the tear tests carried out earlier on fresh onion epidermis. CT samples were fractured using an MTS Insight tensile testing machine (Figs. 5-8 and Supplemental Fig. 5-12S).

Fracture in control CT samples (no pattern) took straight lines without a significant deviation confirming proper alignment and symmetry in loading and the sample. In transverse onion pattern, the cracks took relatively straight paths with only occasionally entering the cell borders when aligned with their path (Fig. 5-8C). A similar result was observed in samples

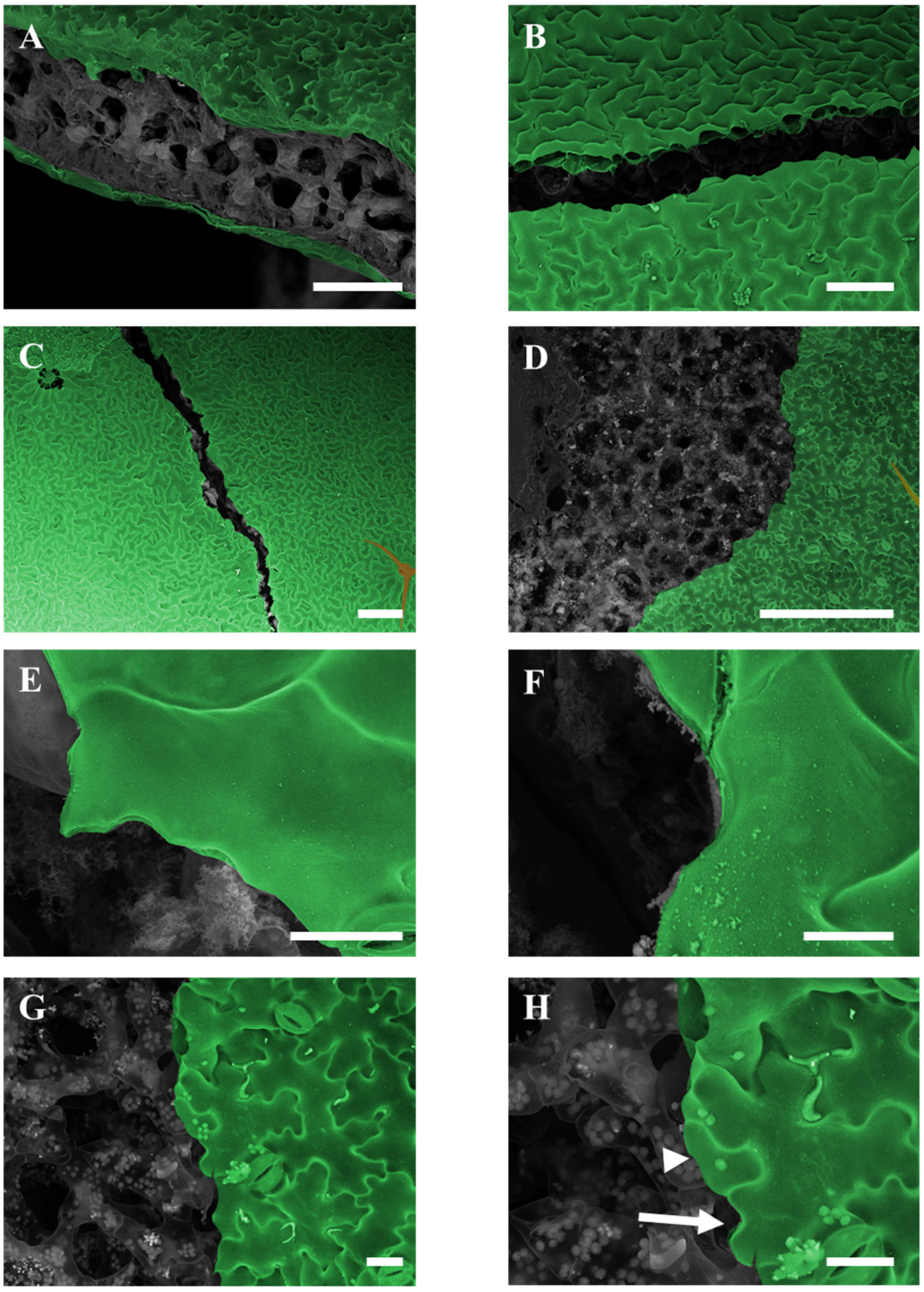
A
B
C
D
E
F
G
H

Figure 5-7. A) Tomato leaf specimen torn prior to dehydration. Tear edges warp obscuring the fracture details. Post-dehydration fracture in **B)** and **C)** *Arabidopsis* and **D)** tomato epidermis with wavy pavement cells follows a jagged path at both cell and tissue scales. **E)** and **F)** Fracture separating the cells in the border in some shallower lobes. **G)** Fracture of the epidermis of tomato leaf demonstrates both border and wall fracture. **H)** Close-up micrograph in (G). The arrowhead points to a deeper lobe that was not separated by crack delamination and was severed instead. Arrow shows shallower lobes that seem to be cleanly separated. Green pseudocolor demarcates the epidermis. Scale bars = 100 μm (A, B), 200 μm (C, D), 20 μm (E and F, G, H).

with longitudinal onion cell pattern, with the only difference that the fracture in the border could occur over longer length paths due to the alignment of the long axis of cells (Fig. 5-8D). In samples with interlocking cell patterns, the cracks propagated intermittently in the borders and the cells (Figs. 5-8E-H). These results closely resemble the observations made previously on cracks in dehydrated *Arabidopsis* leaves (compare Figs. 5-8G and H with Fig. 5-7E-H). A factor affecting whether the crack penetrates the border or continues into the cell wall seemed to be the depth of the interlocking waves. Shallower waves were observed to be more frequently separated at the border (cell-cell separation) while deeper lobes were fractured in the wall instead (see Figs. 5-8E, F, and H). The force-displacement graphs for different patterns revealed some more interesting details (Figs. 5-9A and 5-13S). The fracture of control CT specimen (no pattern) was brittle with sample failing abruptly. A similar pattern was observed for crack propagating along the main axis of the onion cells. In other cases, and especially for transverse onion pattern, the force-displacement curves were step-wise indicating the increased resistance of the PMMA sheet against propagating cracks. These results are comparable with the force of tear patterns observed in tearing tests of middle-notched specimens (Figs. 5-5A and B, Supplemental Fig. 5-10S). From real-time observation of crack growth in PMMA specimen, a local increase in the fracture force (e.g., see asterisk Fig. 5-9A) was associated with the arrest of the crack before reaching a border. Finally, calculating the work of fracture (area below the force-displacement curves) for various patterns clearly demonstrated toughening of the PMMA sheet by the transverse orientation of cells or introducing wavy borders compared to control or longitudinal patterns (Fig. 5-9B).

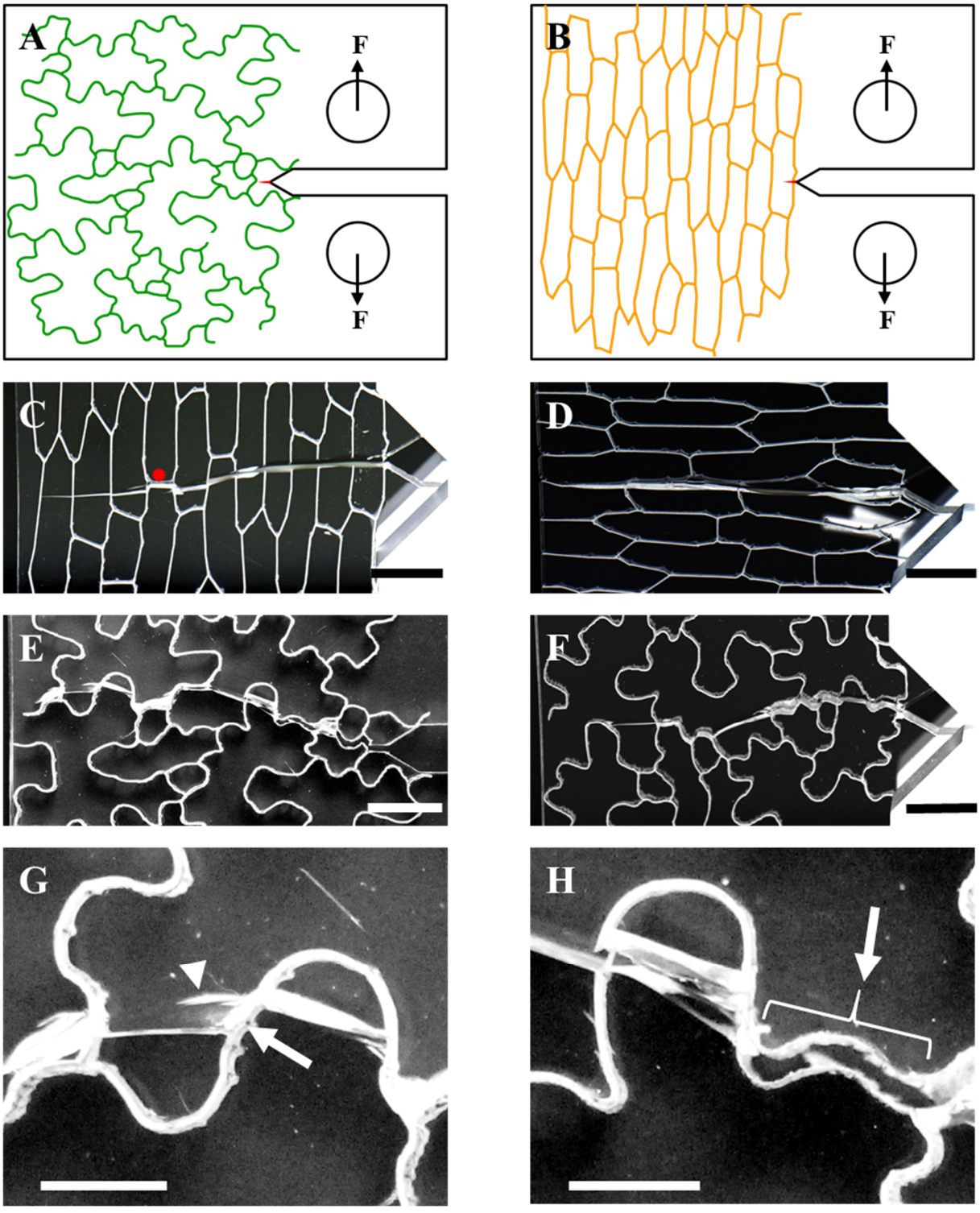
A
F
F
B
F
F
C
D
E
F
G
H

Figure 5-8. Outlines of **A)** *Arabidopsis* and **B)** onion epidermal cells extracted from confocal micrographs are laser engraved on compact tension (CT) specimens cut out of cast polymethylmethacrylate. Two other patterns were also generated by rotating these patterns by 90° for comparison. A microcrack was induced at the tip of the notch (small red triangle) by a blade. CT specimens were pulled apart at the holes for the crack to grow. **C)** Example of crack propagation transverse to the long axis of engraved cells. Cracks took relatively straight paths and only entered the cell borders occasionally (asterisk). **D)** Crack along the engraved cells' main axis took a relatively straight path. However, in samples and regions that the crack entered the cell borders, it continued along the interface. **E)** and **F)** Crack propagation in the wavy pavement cell patterns took ragged paths going through both borders and the cell walls evenly. **G)** and **H)** Close-up views of crack inducing both border and the cell wall domains. It was observed that shallower lobes and necks more frequently experienced border fracture and cell-cell separation while deeper interdigitations experienced fractures in the wall. This corresponds to previous SEM observations demonstrating both intermittent interfacial and cell wall cracks. The arrowhead marks a secondary crack that was arrested. Instead, the crack chose to travel briefly in the border (arrow) before entering the body of the neighboring cell. Scale bars = 1 cm, except for (G, H) = 5 mm.

5.5 Discussion

The wavy interlocking shape of cells in the leaf epidermis has intrigued researchers for decades as they raise developmental and evolutionary questions: How are these shapes formed and what are the potential advantages of such shapes for the plant tissue? (Jacques et al., 2014; Korn, 1976). The molecular mechanisms and the mechanics underlying shape formation in wavy pavement cells have been subject of several studies (Chen et al., 2015; Fu et al., 2005; Majda et al., 2017; Panteris and Galatis, 2005; Sampathkumar et al., 2014a; Sotiriou et al., 2018; Xu et al., 2010). Sotiriou et al. (2018) argue that such shapes increase the range of reversible deformation of the tissue with the wavy walls straightening and falling back into their shape upon unloading. Sapala et al. (2018), on the other hand, proposed that the wavy cell shapes of pavement cells serve to minimize the stress generated on the periclinal walls. Both hypotheses are plausible and demonstrate potential benefits of wavy cell shapes. There are some questions left to speculation regarding these hypotheses, however, such as how the stress minimization strategy relates to cells that produce only shallow waviness, for example in Fig. 5-1. Nevertheless, these hypotheses remain as valuable additions to our understanding of practical aspects of shape formation in plant cells.

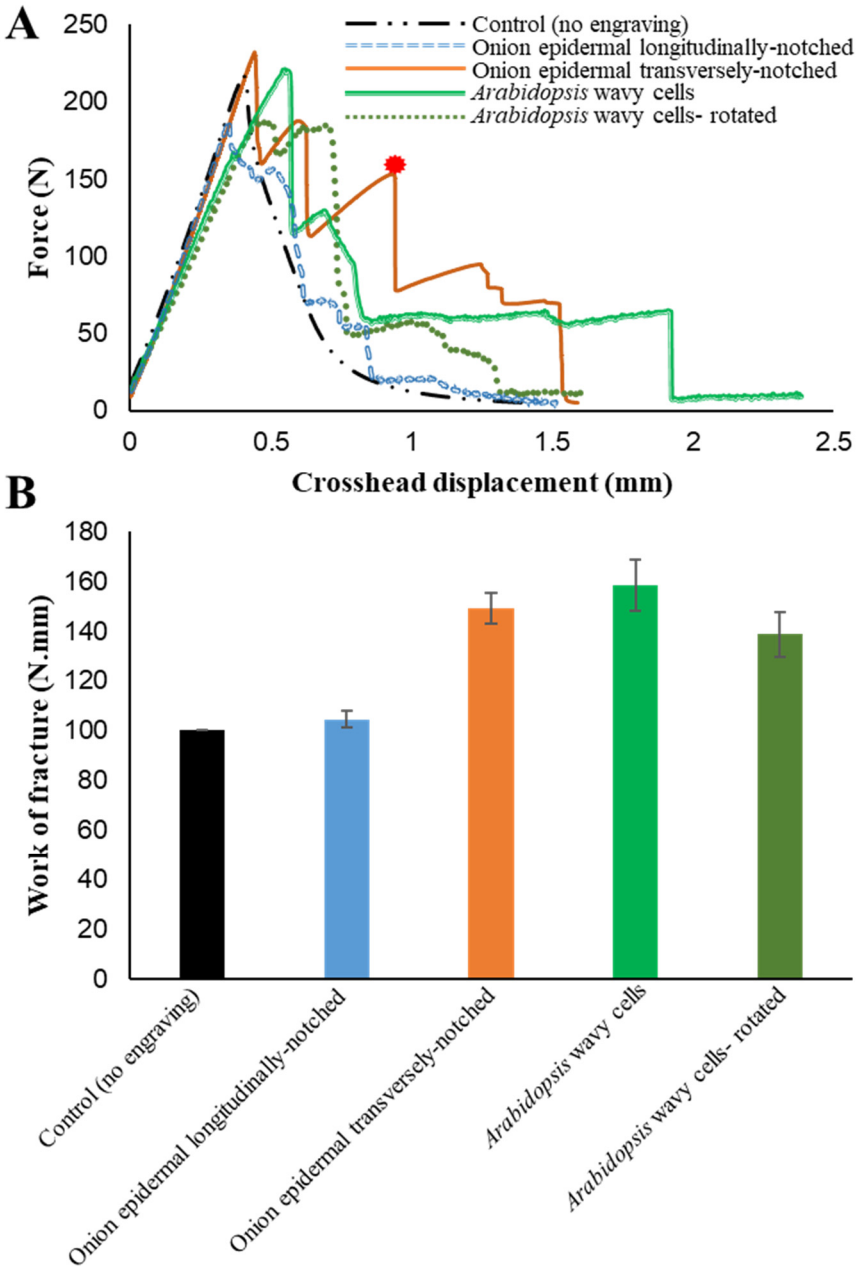

Figure 5-9. A) Sample force-opening graphs for specimens with onion-like and wavy epidermal cell patterns. It could be seen that the control specimen (no engraving) experiences a brittle fracture. The onion patterns with crack propagating along the main axis of cells were also relatively brittle. The samples with onion pattern and the crack perpendicular to main cell axis and the rotations of jigsaw puzzle cell patterns, however, continued to take the load as the crack progressed. Local maxima (e.g., asterisk) correspond to crack arrest when reaching borders. **B)** Comparison of the work of fracture between different engraving patterns and a CT specimen without engraving. While the onion-like pattern was tough in the transverse direction, along the cell lines it did not significantly differ from the specimens without engraving. Jigsaw pavement cell patterns were shown to be nearly as tough in both perpendicular directions. Bars are standard errors.

It has long been hypothesized that by the formation of interlocking digits, wavy pavement cells increase their contact surface, their adhesion and thus increase the tensile strength of the epidermis (Jacques et al., 2014; Sotiriou et al., 2018). This hypothesis, however, is inherently based on the assumption that the epidermis fails by border fracture. This assumption may have roots in the fact that the middle lamella is largely comprised of pectins, and that pectin is generally thought to be comparatively softer and more "fluid" relative to the other cell wall constituents. Nevertheless, this hypothesis was not experimentally evaluated so far.

In preliminary tests, we stretched samples of intact *Arabidopsis* epidermis of wild-type and *any1* with reduced cell waviness. In either type, cells did not seem to separate near the rupture edges. The nature and behavior of the middle lamella—the "glue" material attaching the neighboring cells—is complex and not very well understood (Zamil and Geitmann, 2017). Nevertheless, under normal conditions, the middle lamella seems sufficiently robust to keep the cells together. However, the curving of the tear edges made precise observation of fracture surfaces impossible. Future studies conducting stretch to failure under highspeed cameras may enable further elaboration of these results.

Some studies have suggested that failure in plant tissues with primary cell walls occurs predominantly by cell wall and not border fracture (or by clean cell-cell separation) (Khan and Vincent, 1993; Zamil et al., 2014). In a scenario that the failure does not occur in the borders, whether and how waviness in jigsaw epidermal cell borders would affect the tissue's resistance to failure becomes more perplexing. Away from the rupture zone, we observed evidence of border fracture. We speculated that, if borders fractures are possible, cell shape and orientation can affect the resistance of the tissue against propagating tears. Experimenting with onion epidermis, we observed that the tissue is highly anisotropic in terms of resistance against tear. Under tension, tears along the cell lines propagate catastrophically, while transversely they are arrested or deflected. We observed that along the cell lines, the tear retains its sharp tips while in the transverse direction, the tear gets blunted each time it reaches a new cell. The existence of such tear anisotropy about the epidermal cell lines resembles the property of human skin with respect to Langer's lines (Abyaneh et al., 2014; Annaidh et al., 2012). These lines mark the orientation of collagen fibers in the skin. The orientation of a cut or an incision in the skin with respect to these lines can determine the healing process and the appearance of the outcome. Cuts

made parallel to these lines are less visible while the incisions perpendicular to them remain puckered and may heal more slowly. Our results suggest that cell orientation in tissues with primary cell walls may act similarly to the Langer's lines of the skin. A recent study showed that mechanisms such as fibril straightening and reorientation in the skin under tension dull the tear tips in the skin rendering the tissue extremely tear resistant (Yang et al., 2015). While network and specifically cellulose reorientation toward the stretch direction is suggested to occur at subcellular scale in cell walls being stretched (Kafle et al., 2017; Zhang et al., 2017), such a mechanism does not seem to exist at the tissue scale in the primary plant tissue. In plant epidermis with aligned cells with straight borders, while tears oriented transverse to cell lines seem to experience difficulty in crossing the cells, they propagate catastrophically along the cell lines in the absence of mechanisms that may prevent propagation of tears, such as those in animal skin (Yang et al., 2015). SEM observation of fractures in fixed and dehydrated leaves with wavy epidermal cells indicated a combination of border and cell wall fractures occurring in the epidermis. This effect acts as an ingenious design feature that toughens the epidermis and prevents unstable and catastrophic tear propagation. Fracturing macroscale samples with onion and wavy pavement cell patterns engraved clearly demonstrated increased toughness for specimens with cell borders perpendicular to the crack propagation. While the specimen without engraving or with cell lines parallel to the crack exhibited brittle fractures, unlike the onion pattern, the wavy cells patterns toughened the specimen omnidirectionally. This result is interesting since the cell borders in this case were replicated by removal and weakening of the material at the borders using a laser. Several recent studies have suggested that a nonhomogeneity in the material such as a periodic mismatch in the elastic modulus can serve as a crack-arresting mechanism (Bechtle et al., 2010; Fratzl et al., 2007; Murali et al., 2011). Biological materials incorporate ingenious approaches to increase the toughness. Here we observed that this can be achieved by material weakening at the borders. The waviness of the borders on the other hand, seems to serve to prevent the crack from taking a straight path resulting in frequent switching between the border and material fracture.

5.6 Acknowledgments

Research in the Geitmann lab is funded by Discovery Grant from the National Science and Engineering Research Council of Canada and by the Canada Research Chair Program.

5.7 Supplemental Figures

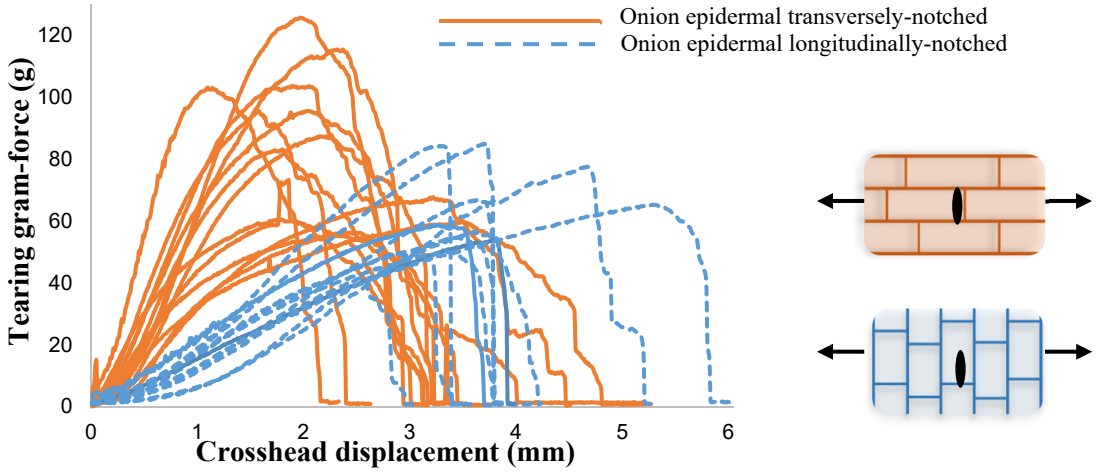

Figure 5-10S. Force-displacement graphs of tear test of adaxial onion epidermis for samples middle-notched longitudinally (along cells main axis, blue) and transversely (brown). The displacement shows the opening of the jaw of the tensile testing device.

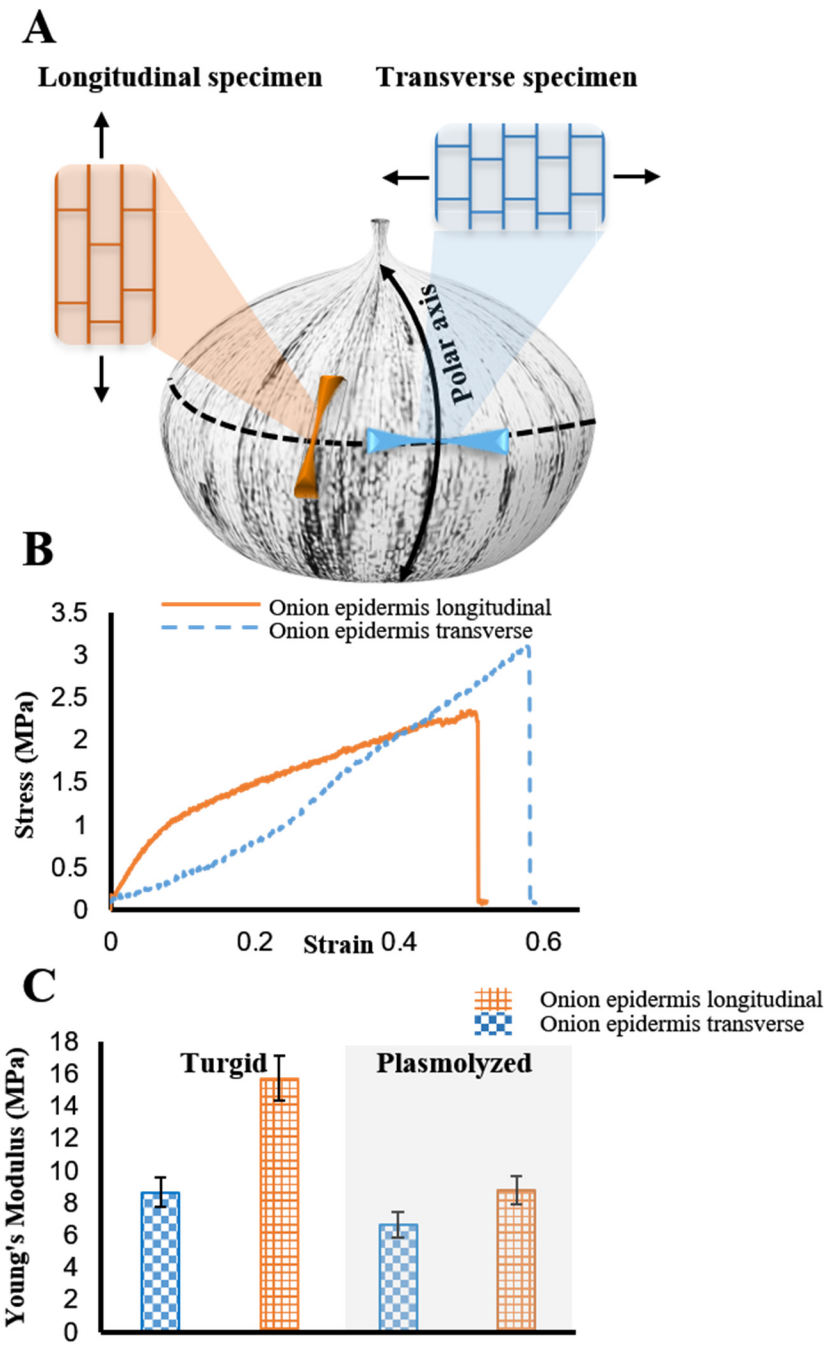

Figure 5-11S. A) Classic tensile tests were carried out on adaxial onion epidermis samples taken from near the equator region of the onion scales, along and transverse to major cell axis. **B)** Stress-strain graphs of turgid adaxial onion epidermis samples stretched along and transverse to main cell axis, demonstrating the anisotropic behavior of the epidermis in two perpendicular directions. **C)** Young's modulus of onion samples calculated from linear part (or strains below 20%) of the stress-strain curves. The stiffness showed to be slightly higher along the cells axis compared to the transverse orientation. In plasmolyzed cells, the difference was reduced. Bars show the standard error.

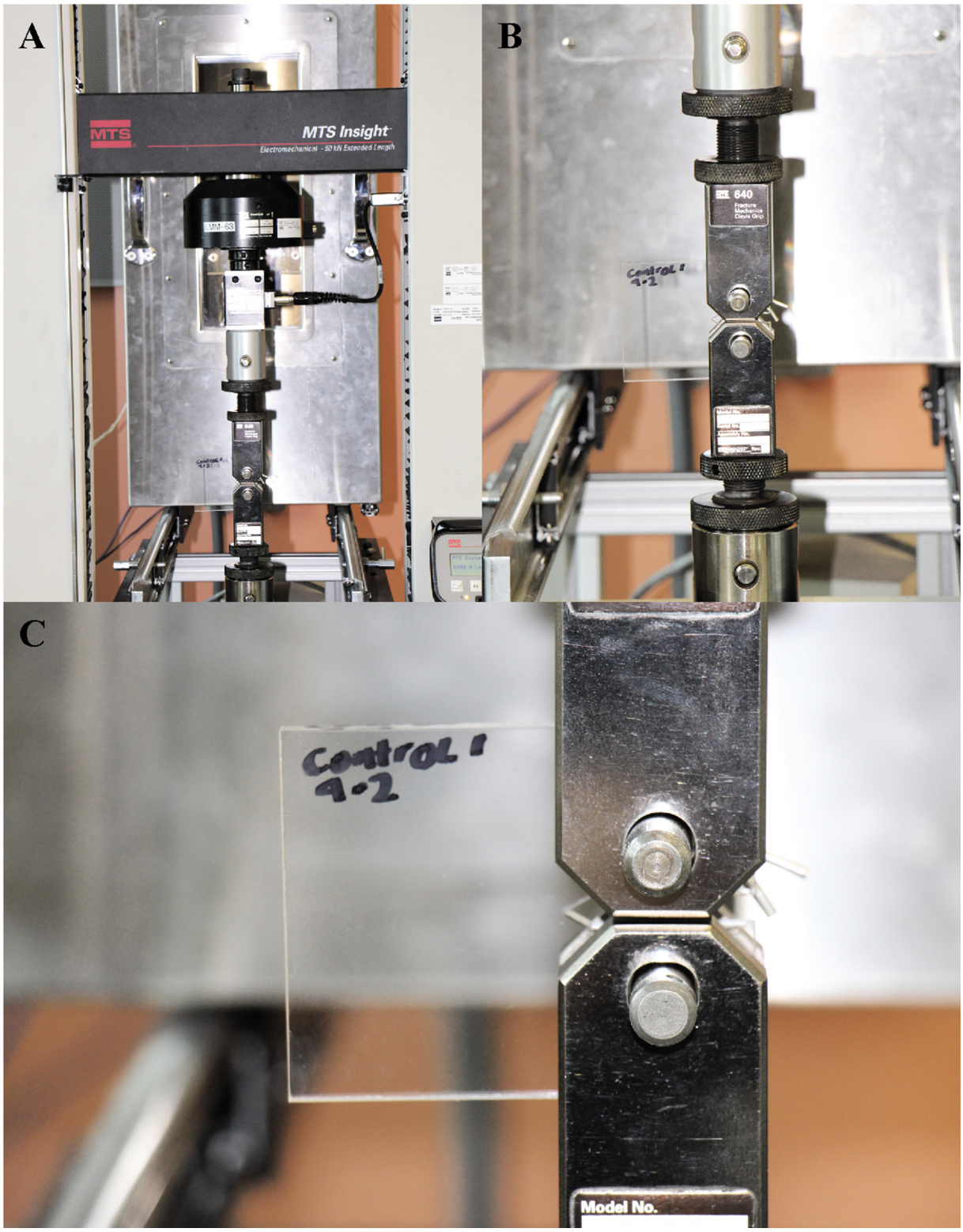

Figure 5-12S. A) MTS Insight tensile testing device. **B)** and **C)** Close-up view of the grips and the CT specimen. Pins inserted in grip-specimen-grip hold the specimen. With the upper grip moving upward, the CT sample is fractured.

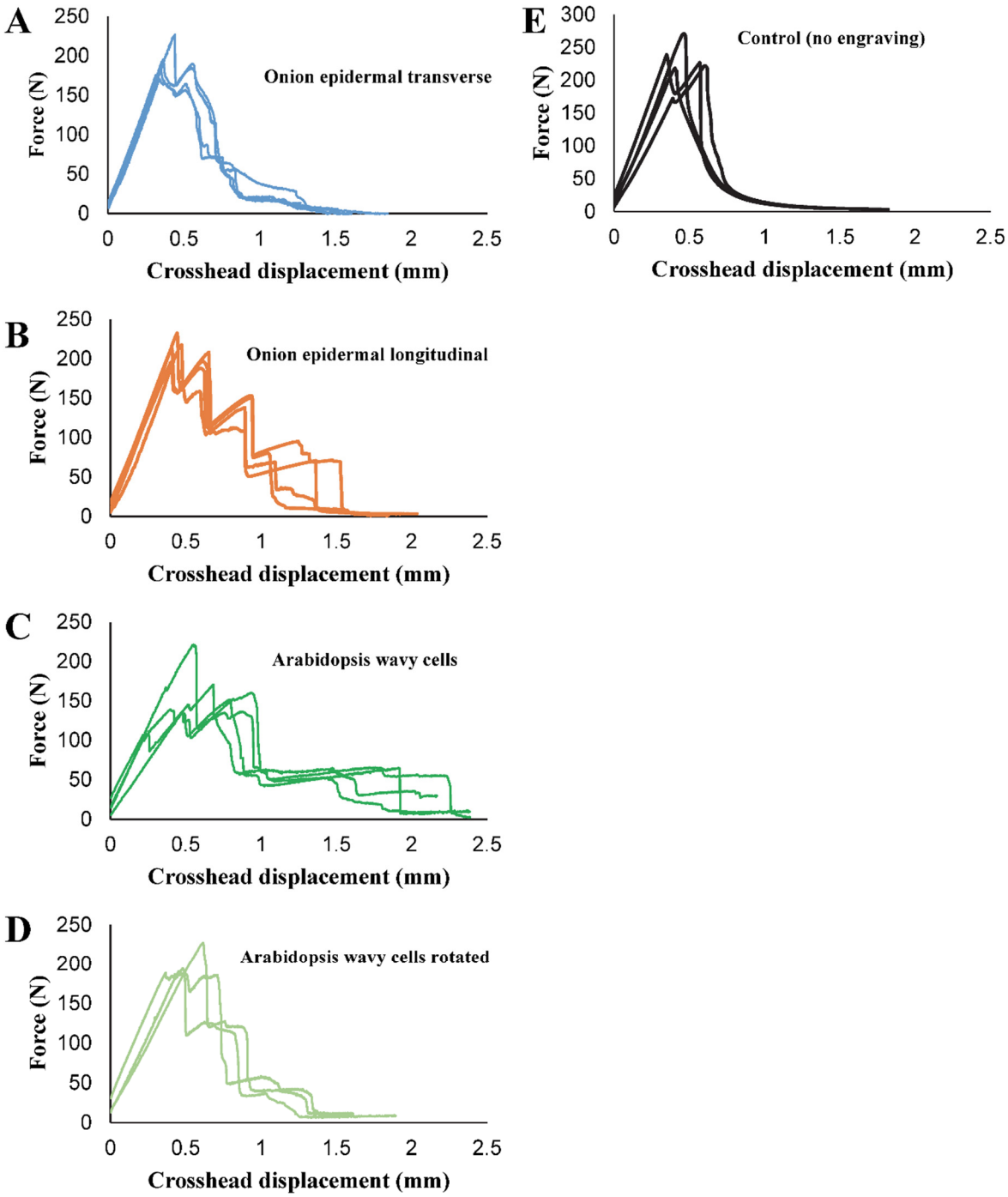

Figure 5-13S. Fracture force-clamp displacement graphs for compact tension (CT) specimens with an adaxial onion epidermal cells pattern in **A)** Longitudinal **B)** Transverse directions and for *Arabidopsis* wavy pavement cell patterns in **C)** and **D).** The engraved pattern in (D) was obtained by 90° rotation of (C). **E)** The force-displacement for the control CT samples with no engraving.

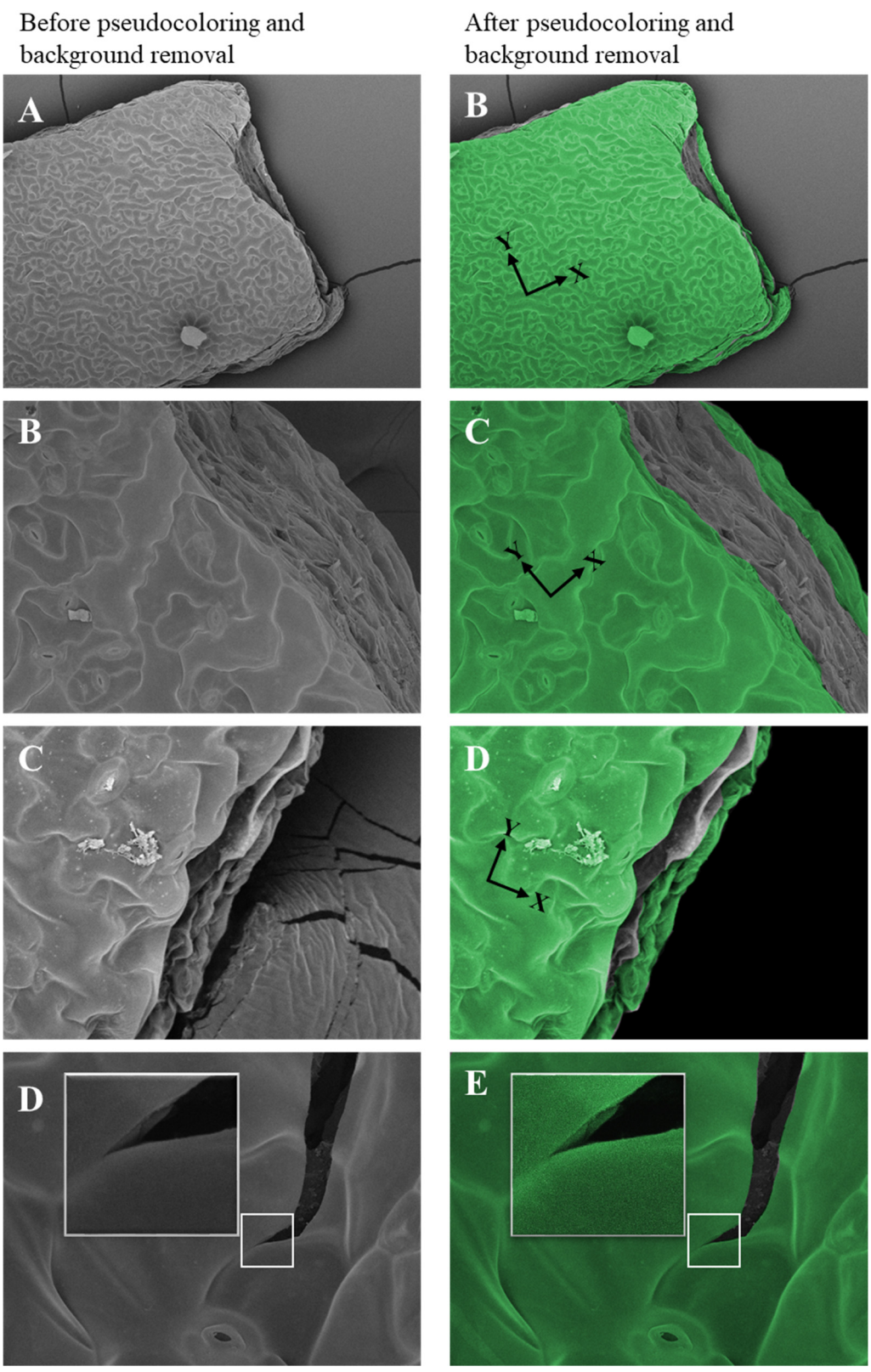

Figure 5-14S. Original versions of micrographs shown in Fig. 5-2 disclosing the effects of pseudocoloring and background removal (C, D).

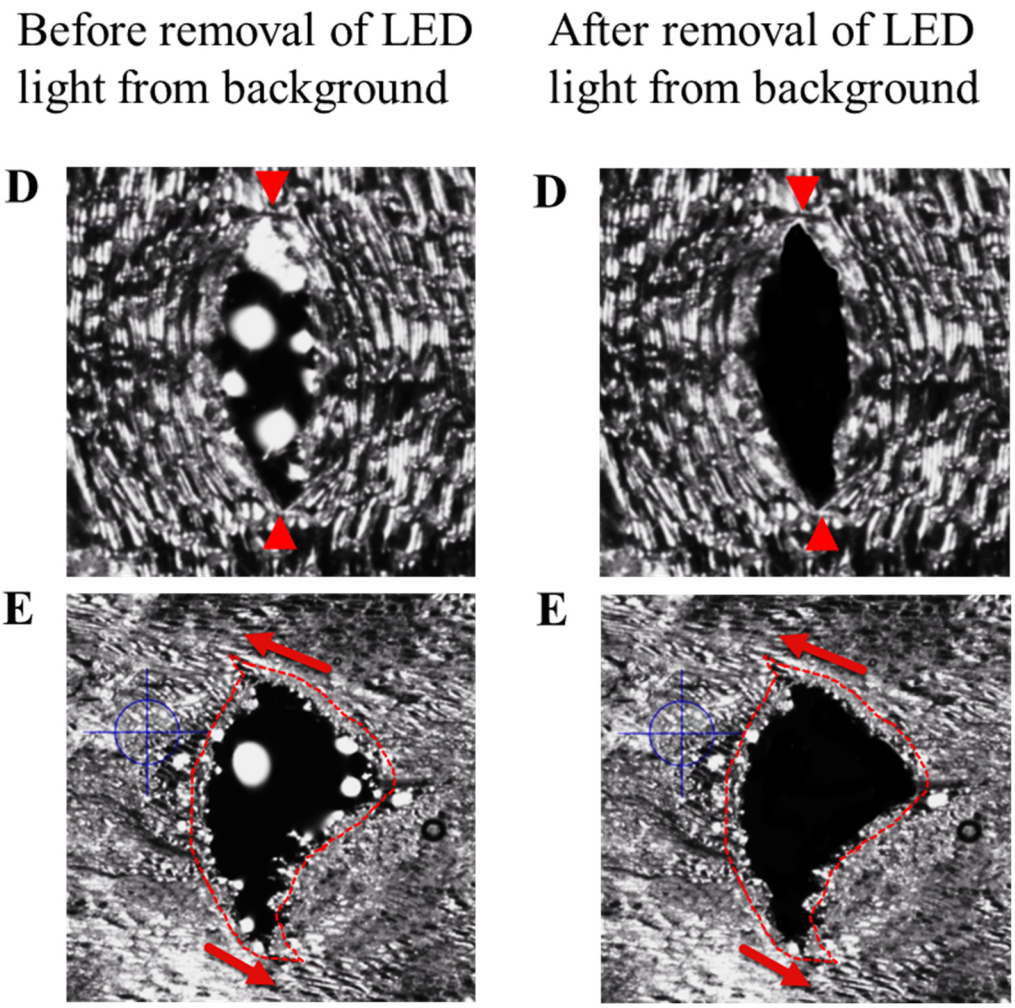

Figure 5-15S. Originals of micrographs shown in Fig. 5-5 depicting the tear shape prior to and after removal of the LED light background.

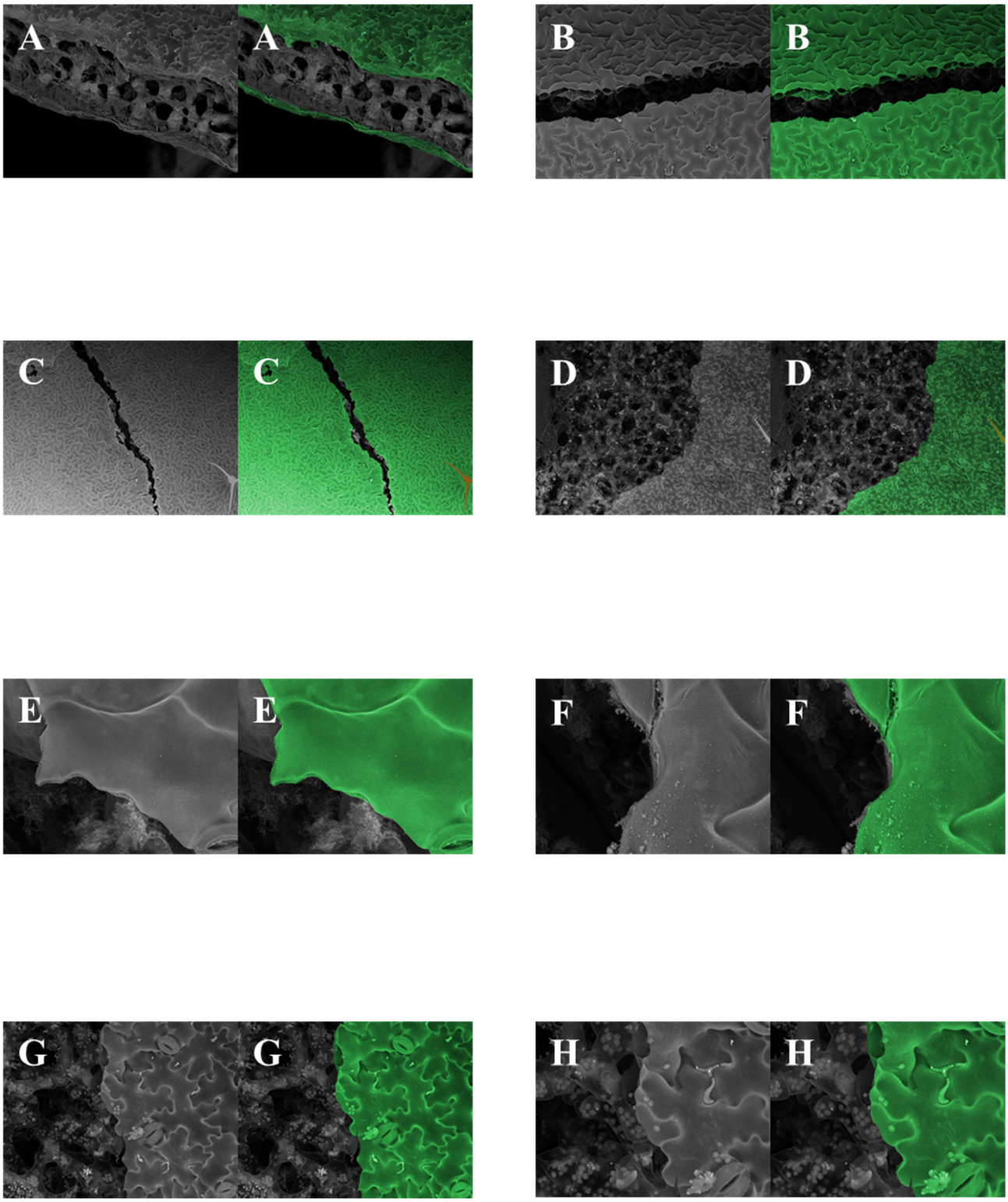

Figure 5-16S. Original micrographs shown in Fig. 5-7 showing effect of pseudocoloring the epidermis in green.

Chapter 6: Discussion and future perspectives

The study of development and morphogenesis in plant cells has evolved into a fast-growing field combining expertise from biology, material science, engineering and computer science. This multidisciplinary approach to analyze a biological phenomenon has been particularly fruitful for the investigation of processes that have a mechanical component. This clearly is the case for plant cells which achieve their functional shape or move by modulating their cell wall mechanics and harnessing the hydraulic pressure generated by turgor. For example, sperm delivery by the pollen tube is accomplished by outgrowth of a protuberance that can travel up to several centimeters to discharge the sperm cells at their target destination. The process is known to be driven by turgor and permanent deformation of the cell wall that is controlled by its assembly and biochemistry. Opening and closure of the stomatal pores, on the other hand, is a reversible mechanism achieved through the peculiar shape and mechanics of the guard cells wall. In both cases, there is a close liaison between the cell shape, function and cell wall mechanics.

Meristematic cells differentiate into specific cell types, each of which has a characteristic and functional shape. Pavement cells are particularly complex as they acquire wavy borders in some plant tissues. The waviness of epidermal cells is most conspicuous in organs such as the leaf or pistil. Looking at the meandering borders of epidermal cells on the surface of leaves of many dicotyledons, one can observe interlocking protrusions (lobes) and indents (necks). This has given rise to developmental and evolutionary questions. A class of studies concentrates on understanding the events controlling the shape formation in these cells (Fu et al., 2005; Higaki et al., 2016; Majda et al., 2017; Panteris and Galatis, 2005; Xu et al., 2010). Another focus is directed towards understanding whether these particular cell shapes benefit the epidermis and the plant mechanically (Jacques et al., 2014; Sapala et al., 2018; Sotiriou et al., 2018). In my Ph.D. research, I investigated both the morphogenesis and the potential evolutionary advantage of epidermal cell shapes.

Previous studies had revealed that locations of protrusions and indents in wavy pavement cells coincide with particular cytoskeletal activities. While observations on the arrangement of the actin network with regard to lobes and necks remain conflicting, there is substantial evidence

for the association of microtubules with the site of cell border indentations (Armour et al., 2015; Fu et al., 2005). Microtubules are thought to associate with and direct the trajectory of the cellulose synthase units (Li et al., 2012b). Previous studies on plants such as maize had suggested aggregated deposition of cellulose in the site of indentation (Panteris and Galatis, 2005). A dominant conceptual model for the wavy shape formation suggests the sites of indentations to be locations of limited growth due to cellulose deposition. At the protruding lobes, the growth is thought to be promoted by the provision of wall loosening and wall building materials (Panteris and Galatis, 2005). However, a mechanical validation of this perspective has not been presented hitherto.

I used the model plant *Arabidopsis* for studying the mechanisms underlying wavy shape formation in pavement cells. Staining the *Arabidopsis* cotyledons with Pontamine Fast Scarlet 4B and Calcofluor White showed clear patterns of arrangement of cellulose bundles in the neck regions at both the anticlinal and periclinal walls. Staining with COS^{488} also displayed higher signal in the neck, suggesting more de-esterified pectin in these regions. Cellulose is recognized as the main load-bearing component of the primary cell wall. Further, pectin de-esterification can reinforce the cell wall rigidity either directly by calcium bridging or by prevention of slippage or separation between the bundles of cellulose (Abasolo et al., 2009; Bidhendi and Geitmann, 2016). A study by Sampathkumar et al. (2014a), employing atomic force microscopy to probe the stiffness on the surface of the periclinal walls, showed a higher apparent stiffness in the neck regions. This accords well with the interpretations of the biochemical observations in the current study. Therefore, I translated the "superbundling" of cellulose and pectin de-esterification into an increased stiffness in the input of the mechanical models developed to study the cell wall deformation.

Next, I developed several finite element models to scrutinize cell wall deformation, starting from models focusing on the anticlinal wall progressing to full 3D models of the cell. It was observed that models consisting of only the anticlinal walls are not able to reproduce the waviness at the cell borders under biologically relevant conditions. The mechanical influence of the periclinal wall was found to be significant due to considerable lateral support it provides to the anticlinal wall restricting its free movement. In models considering the periclinal walls, the regions of increased stiffness were placed alternatingly along and across the two periclinal

walls joining a piece of anticlinal wall in the middle. It was observed that upon applying the turgor pressure, the less-deforming regions with enhanced stiffness marked the regions of indentations forming an interlocking pattern. Further, it was observed that these regions experienced higher stress upon application of turgor. This is consistent with the stress distribution pattern reported in the study by Sampathkumar et al. (2014a). Using only the periclinal wall outlines of cells with fully formed lobes and fixed borders, Sampathkumar et al. (2014a) had reported the regions of indentation to experience higher stress. Here we established that even for an isotropic material, the cell wall at the side of indentations that are being developed *de novo* experiences higher stresses. Using *Arabidopsis* lines with tagged microtubule-associated proteins, consistent with earlier reports, I noted a considerable bundling of microtubules at necks. Microtubules are known to respond to and align with the maximal mechanical stress. Therefore, the observation of the increased stress at necks and abundance of cortical microtubules can be well correlated. The possible linkage between the mechanisms orchestrating pectin de-esterification and microtubule bundling in the necks is still not clear and warrants further studies. Further, from these observations, we hypothesized that a positive stress-stiffness feedback mechanism to be involved in the shaping process of the pavement cells. Since in reality, change in wall stiffness is expected to occur progressively in contrast to the implementation of a significant stiffness difference *ab initio*, I explored whether a positive feedback loop with an initially negligible stiffness difference ratio between the wall regions could result in the occurrence of waves at the cell border. A positive feedback loop was integrated with the finite element model. The algorithm was set to update the stiffness of each finite element with respect to its stress. Thus, higher stress regions were being assigned a higher stiffness in each iteration of the model. It was observed that the stiffening resulting from the geometrically driven stress overrides the slight stiffness differences in few first iterations preventing the evolution of any waviness. With the implementation of lateral inhibition of stiffening, however, the effect of geometrically driven stresses was overcome, and waves could be generated starting with infinitesimally small differences in stiffness on the periclinal walls. Therefore, a lateral inhibition of stiffening is required if a positive stress-stiffening feedback mechanism is to shape the waves. This notion is biologically relevant as some former studies have suggested the existence of an antagonism between the pathways regulating events in lobes and necks. These pathways, at the downstream, result in a lateral inhibition between the

accumulation of microtubules and actin microfilaments (Fu et al., 2005; Xu et al., 2010). Using *Arabidopsis* lines with fluorescently tagged microtubules, I observed that well-developed necks with pronounced curvatures are rich in organized microtubules and the corresponding lobes are relatively bereft of it. However, it was observed that this distinction is hardly evident at earlier stages of lobe formation when the curvature is not pronounced yet, and the segment of the border is relatively straight. This supports the notion of a positive feedback mechanism. Further, this indicates that a separate event might precede the microtubule polarization across the lobes and necks. Mathematical and physical models allow investigation of parameters that are experimentally impossible to determine otherwise. For instance, the finite element models of the cell wall deformation allowed for determination of regions in the cell wall with higher stresses. Mechanical stress has been shown to be vital in both plant and animal cell mechanics as it is suggested to affect the intracellular dynamics, polarization and cytoskeletal rearrangement (Hamant et al., 2008; Srivastava and Robinson, 2015). However, the pattern and distribution of mechanical stress are not always easy to predict due to complex interplay between forces, the material and the geometry of the structure. In addition to local stress distribution, the finite element models in this study unveiled a rather robust and yet somewhat unexpected patterning mechanism at the cell level by providing evidence for the possibility of buckling in turgid cells.

The mechanical models and microscopic observation of the cell wall components in this study present a congruent paradigm of patterning in cells with wavy borders. A recent model by Majda et al. (2017) suggests the waviness in borders of the cell wall to arise from the stretch of the anticlinal wall with alternatingly placed stiffness along and across it. However, this model does not consider the periclinal walls. It also reports higher stresses and stiffness on the lobe side of the wall curvature. This is in contrast to my model, as well as experimental data such as the enrichment of cellulose and de-esterified pectin, the stiffness of the periclinal walls and microtubule aggregation on the neck side. Further, while the model proposed by Majda et al. (2017) can produce higher order curvatures, it cannot reproduce simple lower level curves with only a single bend observed in many cells at earlier stages. Moreover, since the mechanism suggested by Majda et al. (2017) is based on a moment (turning effect) generated by stiffness difference along and across the glued anticlinal walls, it requires the two anticlinal walls to be

in contact with each other. As a result, this model is unable to explain lobe formation in cells such as those of aerenchymatic mesophyll where lobes and necks are placed opposite to each other rather than alternatingly (Panteris and Galatis, 2005). In these cells, the indented regions in each cell separate from the opposing region of the neighboring mesophyll cell creating an air space. My model, on the other hand, can simulate these situations corroborating its generality and validating the roles of cellulose and potentially pectin de-esterification in neck formation. My mechanical model indicates that even individual cells can form wavy borders by alternate placement of stiffness along their periclinal walls without a need to be connected to a neighboring cell. The model also provides a suggestion on a putative mechanical cue as the initiator of this mechanical anisotropy of the cell wall. I hypothesize that stochastic buckling of the cell wall can result in the stress (tension and compression) hotspots in the cell wall that mark the location of microtubule bundling and formation of incipient necks in a positive feedback loop. I am currently developing finite element models to further investigate this phenomenon. Buckling occurs under compression which is not commonly an expected stress state for the walls of turgid cells. Interestingly, however, our 3D finite element models of closed turgid cells showed the anticlinal walls to be prone to buckling due to zero or even negative stresses emerging as a result of lateral contraction of cells when pressurized. This sets another example of how models not incorporating all walls surrounding the cell may neglect critical mechanical aspects resulting in inaccurate interpretations. A buckling mechanism is consistent with our knowledge of the stress and deformation state of the cell wall and can reproduce any order of curvature. However, in itself, proving the occurrence of buckling is challenging. If molecular fluorescent markers for compressive stress were available, direct evidence of negative stress and buckling of the cell wall prior to lobe formation could be obtained. In an alternative approach, using further finite element models, I am currently investigating whether the curvature patterns in the cell walls over a region can be correlated. If possible, this can help to differentiate the buckling events from simple random bends. My finite element model results also imply that if the surface of anticlinal walls becomes larger than that of periclinal walls, the chance of buckling in the anticlinal walls due to cell pressure decreases. For prospective studies, we are collecting information on the epidermis of different plant genera with different cell wall dimensions and degree of waviness.

In the second part of the project, I investigated whether a mechanical advantage arises from the wavy cell shapes. Specifically, I was motivated to verify the existing hypothesis correlating the tensile strength of the epidermis with cell border waviness. Stretching strips of *Arabidopsis* leaf on a tensile testing apparatus did not reveal any indication of cell detachment. Therefore, even if middle lamella is the weakest link in the cellular material, the placement of cells and loading conditions in a tensile test would not allow cell detachment, even for cells of the mutant *any1* with reduced cell border waviness. However, I hypothesized the cell shape to influence the propagation of damage in the epidermis. Tear tests on fresh onion epidermis demonstrated that the work to propagate the tear across the alignment of the main axis of the cells to be more than three times the work for the longitudinal tear propagation. Real-time observation of tear propagation in onion epidermis indicated that decreased resistance in the longitudinal direction is due to cell detachment ahead of the tear. From this, I hypothesized that border waviness would preclude such ease in the travel of the crack in the cell borders that seemed to require considerably less force. Precise observation of tear path in fresh samples with wavy pavement cells of *Arabidopsis* proved to be very challenging. This was because their minute size and the light dispersion from the underlying tissues prohibited the real-time observation of tearing experiments of fresh samples under a stereomicroscope. Study of the tear induced in the fresh specimens was also not satisfactory if the specimens were fixed and dehydrated after tearing and before observation. Curving of free fracture edges during the process would obscure the precise path of the tear. As a result, I observed the crack propagation induced in the specimens after they were fixed and dehydrated so that the fracture edges remain straight. I observed that crack alternated between the cell border and the cell wall in wavy cells of *Arabidopsis* and tomato leaf epidermis. I hypothesized this would increase the fracture toughness of the epidermis since the uninterrupted distances the crack could travel in only one type of material is reduced. This is not to mention the minimization of border fracture and cell separation, seemingly less energy consuming than breaking the cell wall. However, as mentioned above, due to reasons such as the delicate nature of the epidermis containing wavy cells, accurate tear force measurement experiments or real-time observation of the outcome were deemed impractical. In future studies, I intend to build a miniaturized version of our existing tensile testing device that can wirelessly operate inside the chamber of an environmental scanning electron microscope. This would allow scrutiny of the failure behavior in real-time and

measurement of the forces required to propagate the damage in the wavy pavement cells of fresh leaves. Due to these challenges and to untangle the material anisotropy from the geometrical effect of cells on the fracture behavior of the epidermis, I used a macroscopic physical representative of the epidermis. I engraved the cell patterns on isotropic polymethylmethacrylate. This allowed me to study the influence of cell patterns on fracture toughness in the macroscale. The control sample with no engraving showed a very brittle fracture with no considerable resistance upon initiation of a crack. The case with cell lines parallel to the crack direction also showed similar behavior and low fracture toughness. When the fracture was attempted in wavy cell patterns acquired from *Arabidopsis* cotyledons or perpendicular to the main axis of onion cells, I observed an increase in the fracture toughness of the samples and the fracture behavior changed from a brittle to a non-brittle behavior. These observations show that the cell borders, even when modeled by material removal, result in hindrance and deflection of the propagating cracks. This is consistent with previous studies on fracture propagation in materials with periodic structures. It has been suggested that a mismatch in the material stiffness can result in crack arrest (Murali et al., 2011). Altogether, these results indicate that introducing waviness in the epidermal cells increases the resistance of the epidermis against the propagation of cracks, a damage minimization strategy at one of the most exposed plant organs. Since we were able to increase the fracture toughness of polymethylmethacrylate by designing patterns on it, these results can also serve as examples of a nature-inspired design with applications in other fields. In an extended experiment, I sought to image in real-time the leaf damage by an insect herbivore. However, establishing a favorable environment for simultaneous feeding and high-resolution imaging of the insect proved very challenging, and the experiment was halted. Further, the nature of cell detachment observed in this study is still not clear, whether the border cracks occur in the middle lamella by cohesive failure or at the interface of the cell wall and the middle lamella. Future studies using electron microscopy can shed light on this question and improve our perception of the middle lamella and the quality of the linkages it forms with the cell wall.

References

Abaqus V. 2014. 6.14 Documentation. *Dassault Systemes Simulia Corporation*.

Abasolo W, Eder M, Yamauchi K, Obel N, Reinecke A, Neumetzler L, Dunlop JW, Mouille G, Pauly M, Höfte H. 2009. Pectin may hinder the unfolding of xyloglucan chains during cell deformation: implications of the mechanical performance of *Arabidopsis* hypocotyls with pectin alterations. *Molecular Plant* **2**, 990-999.

Abyaneh M, Griffith R, Falto-Aizpurua L, Nouri K. 2014. Famous lines in history: Langer lines. *JAMA Dermatology* **150**, 1087-1087.

Agudelo CG, Sanati Nezhad A, Ghanbari M, Naghavi M, Packirisamy M, Geitmann A. 2013. TipChip: a modular, MEMS-based platform for experimentation and phenotyping of tip-growing cells. *The Plant Journal* **73**, 1057-1068.

Akita K, Higaki T, Kutsuna N, Hasezawa S. 2015. Quantitative analysis of microtubule orientation in interdigitated leaf pavement cells. *Plant Signaling & Behavior* **10**, e1024396.

Alcaraz J, Buscemi L, Grabulosa M, Trepat X, Fabry B, Farré R, Navajas D. 2003. Microrheology of human lung epithelial cells measured by atomic force microscopy. *Biophysical Journal* **84**, 2071-2079.

Ali O, Mirabet V, Godin C, Traas J. 2014. Physical models of plant development. *Annual Review of Cell and Developmental Biology* **30**, 59-78.

Altartouri B, Geitmann A. 2015. Understanding plant cell morphogenesis requires real-time monitoring of cell wall polymers. *Current Opinion in Plant Biology* **23**, 76-82.

Amada G, Onoda Y, Ichie T, Kitayama K. 2017. Influence of leaf trichomes on boundary layer conductance and gas-exchange characteristics in Metrosideros polymorpha (Myrtaceae). *Biotropica* **49**, 482-492.

Ambrose C, Allard JF, Cytrynbaum EN, Wasteneys GO. 2011. A CLASP-modulated cell edge barrier mechanism drives cell-wide cortical microtubule organization in *Arabidopsis*. *Nature Communications* **2**, 430.

Amsbury S, Hunt L, Elhaddad N, Baillie A, Lundgren M, Verhertbruggen Y, Scheller HV, Knox JP, Fleming AJ, Gray JE. 2016. Stomatal function requires pectin de-methyl-esterification of the guard cell wall. *Current Biology* **26**, 2899-2906.

Anderson CT, Carroll A, Akhmetova L, Somerville C. 2010. Real-time imaging of cellulose reorientation during cell wall expansion in *Arabidopsis* roots. *Plant Physiology* **152**, 787-796.

Angeles G, Lascurain M, Davalos-Sotelo R, Zarate-Morales RP, Ortega-Escalona F. 2013. Anatomical and physical changes in leaves during the production of tamales. *American Journal of Botany* **100**, 1509-1521.

Annaidh AN, Bruyère K, Destrade M, Gilchrist MD, Otténio M. 2012. Characterization of the anisotropic mechanical properties of excised human skin. *Journal of the Mechanical Behavior of Biomedical Materials* **5**, 139-148.

Anssari-Benam A, Legerlotz K, Bader DL, Screen HR. 2012. On the specimen length dependency of tensile mechanical properties in soft tissues: Gripping effects and the characteristic decay length. *Journal of Biomechanics* **45**, 2481-2482.

Antonacci G, Braakman S. 2016. Biomechanics of subcellular structures by non-invasive Brillouin microscopy. *Scientific Reports* **6**, 37217.

Aouar L, Chebli Y, Geitmann A. 2010. Morphogenesis of complex plant cell shapes: the mechanical role of crystalline cellulose in growing pollen tubes. *Sexual Plant Reproduction* **23**, 15-27.

Arancibia RA, Motsenbocker CE. 2006. Pectin methylesterase activity in vivo differs from activity in vitro and enhances polygalacturonase-mediated pectin degradation in tabasco pepper. *Journal of Plant Physiology* **163**, 488-496.

Aranwela N, Sanson G, Read J. 1999. Methods of assessing leaf-fracture properties. *New Phytologist* **144**, 369-383.

Argatov I, Mishuris G. 2015. *Contact mechanics of articular cartilage layers: asymptotic models*. Cham: Springer International Publishing, 335.

Armour WJ, Barton DA, Law AM, Overall RL. 2015. Differential growth in periclinal and anticlinal walls during lobe formation in *Arabidopsis* cotyledon pavement cells. *The Plant Cell* **27**, 2484-2500.

Ashraf MW, Tayyaba S, Afzulpurkar N. 2011. Micro electromechanical systems (MEMS) based microfluidic devices for biomedical applications. *International Journal of Molecular Sciences* **12**, 3648-3704.

Aylor DE, Parlange J-Y, Krikorian AD. 1973. Stomatal mechanics. *American Journal of Botany* **60**, 163-171.

Baker AJ. 2012. *Finite elements: computational engineering sciences*. New Jersey: John Wiley & Sons, 288.

Ballmann CW, Meng Z, Traverso AJ, Scully MO, Yakovlev VV. 2017. Impulsive Brillouin microscopy. *Optica* **4**, 124-128.

Balsamo R, Vander Willigen C, Bauer A, Farrant J. 2006. Drought tolerance of selected Eragrostis species correlates with leaf tensile properties. *Annals of Botany* **97**, 985-991.

Bargel H, Spatz H-C, Speck T, Neinhuis C. 2004. Two-dimensional tension tests in plant biomechanics-sweet cherry fruit skin as a model system. *Plant Biology* **6**, 432-439.

Bascom CS, Hepler PK, Bezanilla M. 2018. Interplay between ions, the cytoskeleton, and cell wall properties during tip growth. *Plant Physiology* **176**, 28-40.

Baskin TI. 2005. Anisotropic expansion of the plant cell wall. *Annual Review of Cell and Developmental Biology* **21**, 203-222.

Baskin TI, Beemster GT, Judy-March JE, Marga F. 2004. Disorganization of cortical microtubules stimulates tangential expansion and reduces the uniformity of cellulose microfibril alignment among cells in the root of *Arabidopsis*. *Plant Physiology* **135**, 2279-2290.

Baskin TI, Jensen OE. 2013. On the role of stress anisotropy in the growth of stems. *Journal of Experimental Botany* **64**, 4697-4707.

Baskin TI, Wilson JE, Cork A, Williamson RE. 1994. Morphology and microtubule organization in *Arabidopsis* roots exposed to oryzalin or taxol. *Plant and Cell Physiology* **35**, 935-942.

Bassel GW, Stamm P, Mosca G, de Reuille PB, Gibbs DJ, Winter R, Janka A, Holdsworth MJ, Smith RS. 2014. Mechanical constraints imposed by 3D cellular geometry and arrangement modulate growth patterns in the *Arabidopsis* embryo. *Proceedings of the National Academy of Sciences of the United States of America* **111**, 8685-8690.

Beauzamy L, Derr J, Boudaoud A. 2015. Quantifying hydrostatic pressure in plant cells by using indentation with an atomic force microscope. *Biophysical Journal* **108**, 2448-2456.

Bechtle S, Fett T, Rizzi G, Habelitz S, Klocke A, Schneider GA. 2010. Crack arrest within teeth at the dentinoenamel junction caused by elastic modulus mismatch. *Biomaterials* **31**, 4238-4247.

Bell DJ, Lu TJ, Fleck NA, Spearing SM. 2005. MEMS actuators and sensors: observations on their performance and selection for purpose. *Journal of Micromechanics and Microengineering* **15**, S153.

Belteton S, Sawchuk MG, Donohoe BS, Scarpella E, Szymanski DB. 2017. Reassessing the roles of PIN proteins and anticlinal microtubules during pavement cell morphogenesis. *Plant Physiology* **176**, 432-449.

Bernal M, Urban MW, Rosario D, Aquino W, Greenleaf JF. 2011. Measurement of biaxial mechanical properties of soft tubes and arteries using piezoelectric elements and sonometry. *Physics in Medicine and Biology* **56**, 3371.

Bidhendi AJ, Geitmann A. 2016. Relating the mechanics of the primary plant cell wall to morphogenesis. *Journal of Experimental Botany* **67**, 449-461.

Bidhendi AJ, Geitmann A. 2018a. Finite element modeling of shape changes in plant cells. *Plant Physiology* **176**, 41-56.

Bidhendi AJ, Geitmann A. 2018b. Tensile testing of primary plant cells and tissues. In: Geitmann A, Gril J, eds. *Plant Biomechanics*. Cham: Springer 321-347.

Bidhendi AJ, Korhonen RK. 2012. A finite element study of micropipette aspiration of single cells: effect of compressibility. *Computational and Mathematical Methods in Medicine* **2012**.

Blamey F, Asher C, Edwards D, Kerven G. 1993. In vitro evidence of aluminum effects on solution movement through root cell walls. *Journal of Plant Nutrition* **16**, 555-562.

Boitier G, Chermant J, Vicens J. 2000. Understanding the creep behavior of a 2.5 D Cf–SiC composite: II. Experimental specifications and macroscopic mechanical creep responses. *Materials Science and Engineering: A* **289**, 265-275.

Bolduc J-F, Lewis LJ, Aubin C-É, Geitmann A. 2006. Finite-element analysis of geometrical factors in micro-indentation of pollen tubes. *Biomechanics and Modeling in Mechanobiology* **5**, 227-236.

Bosch M, Hepler PK. 2005. Pectin methylesterases and pectin dynamics in pollen tubes. *The Plant Cell* **17**, 3219-3226.

Boudaoud A. 2010. An introduction to the mechanics of morphogenesis for plant biologists. *Trends in Plant Science* **15**, 353-360.

Boudon F, Chopard J, Ali O, Gilles B, Hamant O, Boudaoud A, Traas J, Godin C. 2015. A computational framework for 3D mechanical modeling of plant morphogenesis with cellular resolution. *PLoS Computational Biology* **11**, e1003950.

Bozorg B, Krupinski P, Jönsson H. 2014. Stress and strain provide positional and directional cues in development. *PLoS Computational Biology* **10**, e1003410.

Braybrook SA, Peaucelle A. 2013. Mechano-chemical aspects of organ formation in *Arabidopsis thaliana*: the relationship between auxin and pectin. *PLoS One* **8**, e57813.

Bringmann M, Bergmann DC. 2017. Tissue-wide mechanical forces influence the polarity of stomatal stem cells in *Arabidopsis*. *Current Biology* **27**, 877-883.

Bringmann M, Li E, Sampathkumar A, Kocabek T, Hauser M-T, Persson S. 2012. POM-POM2/CELLULOSE SYNTHASE INTERACTING1 is essential for the functional association of cellulose synthase and microtubules in *Arabidopsis*. *The Plant Cell* **24**, 163-177.

Brulé V, Rafsanjani A, Pasini D, Western TL. 2016. Hierarchies of plant stiffness. *Plant Science* **250**, 79-96.

Brummell DA. 2006. Cell wall disassembly in ripening fruit. *Functional Plant Biology* **33**, 103-119.

Buckingham SD, Kidd JF, Law RJ, Franks CJ, Sattelle DB. 2005. Structure and function of two-pore-domain K^+ channels: contributions from genetic model organisms. *Trends in Pharmacological Sciences* **26**, 361-367.

Burgert I, Dunlop JW. 2011. Micromechanics of cell walls. In: Wojtaszek P, ed. *Mechanical Integration of Plant Cells and Plants*. Berlin, Heidelberg: Springer, 27-52.

Burgert I, Fratzl P. 2009. Plants control the properties and actuation of their organs through the orientation of cellulose fibrils in their cell walls. *Integrative and Comparative Biology* **49**, 69-79.

Burgert I, Frühmann K, Keckes J, Fratzl P, Stanzl-Tschegg SE. 2003. Microtensile testing of wood fibers combined with video extensometry for efficient strain detection. *Holzforschung* **57**, 661-664.

Burgert I, Keplinger T. 2013. Plant micro- and nanomechanics: experimental techniques for plant cell-wall analysis. *Journal of Experimental Botany* **64**, 4635-4649.

Bursa J, Zemanek M. 2008. Evaluation of biaxial tension tests of soft tissues. *Studies in Health Technology and Informatics* **133**, 45-55.

Caffall KH, Mohnen D. 2009. The structure, function, and biosynthesis of plant cell wall pectic polysaccharides. *Carbohydrate Research* **344**, 1879-1900.

Camacho-Cristóbal JJ, Martín-Rejano EM, Herrera-Rodríguez MB, Navarro-Gochicoa MT, Rexach J, González-Fontes A. 2015. Boron deficiency inhibits root cell elongation via an ethylene/auxin/ROS-dependent pathway in *Arabidopsis* seedlings. *Journal of Experimental Botany*, erv186.

Cameron C, Geitmann A. 2018. Cell mechanics of pollen tube growth. *Current Opinion in Genetics & Development* **51**, 11-17.

Campàs O, Mahadevan L. 2009. Shape and dynamics of tip-growing cells. *Current Biology* **19**, 2102-2107.

Campàs O, Mammoto T, Hasso S, Sperling RA, O'connell D, Bischof AG, Maas R, Weitz DA, Mahadevan L, Ingber DE. 2014. Quantifying cell-generated mechanical forces within living embryonic tissues. *Nature Methods* **11**, 183-189.

Carew E, Patel J, Garg A, Houghtaling P, Blackstone E, Vesely I. 2003. Effect of specimen size and aspect ratio on the tensile properties of porcine aortic valve tissues. *Annals of Biomedical Engineering* **31**, 526-535.

Carter R, Woolfenden H, Baillie A, Amsbury S, Carroll S, Healicon E, Sovatzoglou S, Braybrook S, Gray JE, Hobbs J, Morris RJ, Fleming AJ. 2017. Stomatal opening involves polar, not radial, stiffening of guard cells. *Current Biology* **27**, 2974-2983.

Casson S, Gray JE. 2008. Influence of environmental factors on stomatal development. *New Phytologist* **178**, 9-23.

Cavalier DM, Lerouxel O, Neumetzler L, Yamauchi K, Reinecke A, Freshour G, Zabotina OA, Hahn MG, Burgert I, Pauly M, Raikhel NV, Keegstra K. 2008. Disrupting two *Arabidopsis thaliana* xylosyltransferase genes results in plants deficient in xyloglucan, a major primary cell wall component. *The Plant Cell* **20**, 1519-1537.

Chanliaud E, Burrows KM, Jeronimidis G, Gidley MJ. 2002. Mechanical properties of primary plant cell wall analogues. *Planta* **215**, 989-996.

Chatterjee M, Tabi Z, Galli M, Malcomber S, Buck A, Muszynski M, Gallavotti A. 2014. The boron efflux transporter ROTTEN EAR is required for maize inflorescence development and fertility. *The Plant Cell* **26**, 2962-2977.

Che S, Guduru P, Nurmikko A, Maris H. 2015. A scanning acoustic microscope based on picosecond ultrasonics. *Ultrasonics* **56**, 153-159.

Chebli Y, Kaneda M, Zerzour R, Geitmann A. 2012. The cell wall of the *Arabidopsis* pollen tube—spatial distribution, recycling, and network formation of polysaccharides. *Plant Physiology* **160**, 1940-1955.

Chen AS, Matthews FL. 1993. A review of multiaxial/biaxial loading tests for composite materials. *Composites* **24**, 395-406.

Chen J, Wang F, Zheng S, Xu T, Yang Z. 2015. Pavement cells: a model system for non-transcriptional auxin signalling and crosstalks. *Journal of Experimental Botany* **66**, 4957-4970.

Cheng Q, Wang S. 2008. A method for testing the elastic modulus of single cellulose fibrils via atomic force microscopy. *Composites Part A: Applied Science and Manufacturing* **39**, 1838-1843.

Cheng S, Clarke EC, Bilston LE. 2009. The effects of preconditioning strain on measured tissue properties. *Journal of Biomechanics* **42**, 1360-1362.

Cheung AY, Boavida LC, Aggarwal M, Wu H-M, Feijó JA. 2010. The pollen tube journey in the pistil and imaging the in vivo process by two-photon microscopy. *Journal of Experimental Botany* **61**, 1907-1915.

Chimungu JG, Loades KW, Lynch JP. 2015. Root anatomical phenes predict root penetration ability and biomechanical properties in maize (Zea mays). *Journal of Experimental Botany* **66**, 3151-3162.

Chormova D, Messenger DJ, Fry SC. 2014. Boron bridging of rhamnogalacturonan-II, monitored by gel electrophoresis, occurs during polysaccharide synthesis and secretion but not post-secretion. *The Plant Journal* **77**, 534-546.

Cintrón MS, Johnson GP, French AD. 2011. Young's modulus calculations for cellulose Iβ by MM3 and quantum mechanics. *Cellulose* **18**, 505-516.

Cooke JR, De Baerdemaeker JG, Rand RH, Mang HA. 1976. A finite element shell analysis of guard cell deformations. *Transactions of the ASAE* **19**, 1107-1121.

Cooke JR, Rand RH, Mang HA, De Baerdemaeker JG, LEE JY. 2008. Shell analysis of elliptical guard cells in higher plants: a review. In: Abel JF, Cooke JR, eds. *Proceedings of the 6th international Conference on Computation of Shell and Spatial Structures IASS-IACM 2008: "Spanning Nano to Mega"*. Cornell University, Ithaca, NY, USA.

Cosgrove DJ. 1989. Characterization of long-term extension of isolated cell walls from growing cucumber hypocotyls. *Planta* **177**, 121-130.

Cosgrove DJ. 1993. Wall extensibility: its nature, measurement and relationship to plant cell growth. *New Phytologist* **124**, 1-23.

Cosgrove DJ. 1997. Relaxation in a high-stress environment: the molecular bases of extensible cell walls and cell enlargement. *The Plant Cell* **9**, 1031-1041.

Cosgrove DJ. 1998. Cell wall loosening by expansins. *Plant Physiology* **118**, 333-339.

Cosgrove DJ. 2005. Growth of the plant cell wall. *Nature Reviews Molecular Cell Biology* **6**, 850-861.

Cosgrove DJ. 2014. Re-constructing our models of cellulose and primary cell wall assembly. *Current Opinion in Plant Biology* **22**, 122-131.

Cosgrove DJ. 2015. Plant cell wall extensibility: connecting plant cell growth with cell wall structure, mechanics, and the action of wall-modifying enzymes. *Journal of Experimental Botany* **67**, 463-476.

Cosgrove DJ. 2018. Diffuse growth of plant cell walls. *Plant Physiology* **176**, 16-27.

Cretin B, Sthal F. 1993. Scanning microdeformation microscopy. *Applied Physics Letters* **62**, 829-831.

Cross SE, Jin Y-S, Rao J, Gimzewski JK. 2007. Nanomechanical analysis of cells from cancer patients. *Nature Nanotechnology* **2**, 780-783.

Crowell EF, Bischoff V, Desprez T, Rolland A, Stierhof Y-D, Schumacher K, Gonneau M, Höfte H, Vernhettes S. 2009. Pausing of Golgi bodies on microtubules regulates secretion of cellulose synthase complexes in *Arabidopsis*. *The Plant Cell* **21**, 1141-1154.

Crowell EF, Timpano H, Desprez T, Franssen-Verheijen T, Emons A-M, Höfte H, Vernhettes S. 2011. Differential regulation of cellulose orientation at the inner and outer face of epidermal cells in the *Arabidopsis* hypocotyl. *The Plant Cell* **23**, 2592-2605.

Dahl JB, Lin J, Muller SJ, Kumar S. 2015. Microfluidic strategies for understanding the mechanics of cells and cell-mimetic systems. *Annual Review of Chemical and Biomolecular Engineering* **6**, 293-317.

Dehoux T, Ghanem MA, Zouani O, Rampnoux J-M, Guillet Y, Dilhaire S, Durrieu M-C, Audoin B. 2015. All-optical broadband ultrasonography of single cells. *Scientific Reports* **5**, 8650.

DeMichele DW, Sharpe PJ. 1973. An analysis of the mechanics of guard cell motion. *Journal of Theoretical Biology* **41**, 77-96.

Deng Y, Sun M, Shaevitz JW. 2011. Direct measurement of cell wall stress stiffening and turgor pressure in live bacterial cells. *Physical Review Letters* **107**, 158101.

Derbyshire P, Findlay K, McCann MC, Roberts K. 2007. Cell elongation in *Arabidopsis* hypocotyls involves dynamic changes in cell wall thickness. *Journal of Experimental Botany* **58**, 2079-2089.

Dick-Pérez M, Zhang Y, Hayes J, Salazar A, Zabotina OA, Hong M. 2011. Structure and interactions of plant cell-wall polysaccharides by two-and three-dimensional magic-angle-spinning solid-state NMR. *Biochemistry* **50**, 989-1000.

Dick-Perez M, Wang T, Salazar A, Zabotina OA, Hong M. 2012. Multidimensional solid-state NMR studies of the structure and dynamics of pectic polysaccharides in uniformly 13C-labeled *Arabidopsis* primary cell walls. *Magnetic Resonance in Chemistry* **50**, 539-550.

Diddens I, Murphy B, Krisch M, Müller M. 2008. Anisotropic elastic properties of cellulose measured using inelastic X-ray scattering. *Macromolecules* **41**, 9755-9759.

Dintwa E, Jancsók P, Mebatsion H, Verlinden B, Verboven P, Wang C, Thomas C, Tijskens E, Ramon H, Nicolai B. 2011. A finite element model for mechanical deformation of single tomato suspension cells. *Journal of Food Engineering* **103**, 265-272.

Doblin MS, Kurek I, Jacob-Wilk D, Delmer DP. 2002. Cellulose biosynthesis in plants: from genes to rosettes. *Plant and Cell Pysiology* **43**, 1407-1420.

Dordas C, Brown P. 2005. Boron deficiency affects cell viability, phenolic leakage and oxidative burst in rose cell cultures. *Plant and Soil* **268**, 293-301.

Dumais J. 2007. Can mechanics control pattern formation in plants? *Current Opinion in Plant Biology* **10**, 58-62.

Dumais J. 2013. Modes of deformation of walled cells. *Journal of Experimental Botany* **64**, 4681-4695.

Dumais J, Shaw SL, Steele CR, Long SR, Ray PM. 2006. An anisotropic-viscoplastic model of plant cell morphogenesis by tip growth. *International Journal of Developmental Biology* **50**, 209–222.

Dumont M, Lehner A, Bouton S, Kiefer-Meyer MC, Voxeur A, Pelloux J, Lerouge P, Mollet J-C. 2014. The cell wall pectic polymer rhamnogalacturonan-II is required for proper pollen tube elongation: implications of a putative sialyltransferase-like protein. *Annals of Botany* **114**, 1177-1188.

Dupuy L, Mackenzie J, Haseloff J. 2010. Coordination of plant cell division and expansion in a simple morphogenetic system. *Proceedings of the National Academy of Sciences of the United States of America* **107**, 2711-2716.

Durachko DM, Cosgrove DJ. 2009. Measuring plant cell wall extension (creep) induced by acidic pH and by alpha-expansin. *Journal of Visual Experiments*, e1263.

Durand-Smet P, Chastrette N, Guiroy A, Richert A, Berne-Dedieu A, Szecsi J, Boudaoud A, Frachisse J-M, Bendahmane M, Hamant O. 2014. A comparative mechanical analysis of plant and animal cells reveals convergence across kingdoms. *Biophysical Journal* **107**, 2237-2244.

Dyson R, Band L, Jensen O. 2012. A model of crosslink kinetics in the expanding plant cell wall: yield stress and enzyme action. *Journal of Theoretical Biology* **307**, 125-136.

Dyson R, Jensen O. 2010. A fibre-reinforced fluid model of anisotropic plant cell growth. *Journal of Fluid Mechanics* **655**, 472-503.

Eder M, Arnould O, Dunlop JW, Hornatowska J, Salmén L. 2013. Experimental micromechanical characterisation of wood cell walls. *Wood Science and Technology* **47**, 163-182.

Edwards M, Meidner H, Sheriff D. 1976. Direct measurements of turgor pressure potentials of guard cells: II. The mechanical advantage of subsidiary cells, the spannungsphase, and the optimum leaf water deficit. *Journal of Experimental Botany* **27**, 163-171.

Eichhorn S, Young R. 2001. The Young's modulus of a microcrystalline cellulose. *Cellulose* **8**, 197-207.

Elliott A, Shaw SL. 2018. Update: plant cortical microtubule arrays. *Plant Physiology* **176**, 94-105.

Elsayad K, Werner S, Gallemí M, Kong J, Guajardo ERS, Zhang L, Jaillais Y, Greb T, Belkhadir Y. 2016. Mapping the subcellular mechanical properties of live cells in tissues with fluorescence emission–Brillouin imaging. *Science Signaling* **9**, rs5.

Elsner J, Michalski M, Kwiatkowska D. 2012. Spatiotemporal variation of leaf epidermal cell growth: a quantitative analysis of *Arabidopsis thaliana* wild-type and triple cyclinD3 mutant plants. *Annals of Botany* **109**, 897-910.

Eng RC, Sampathkumar A. 2018. Getting into shape: the mechanics behind plant morphogenesis. *Current Opinion in Plant Biology* **46**, 25-31.

Fabry B, Maksym GN, Butler JP, Glogauer M, Navajas D, Fredberg JJ. 2001. Scaling the microrheology of living cells. *Physical Review Letters* **87**, 148102.

Farzadi A, Solati-Hashjin M, Asadi-Eydivand M, Osman NAA. 2014. Effect of layer thickness and printing orientation on mechanical properties and dimensional accuracy of 3D printed porous samples for bone tissue engineering. *PLoS One* **9**, e108252.

Fayant P, Girlanda O, Chebli Y, Aubin C-É, Villemure I, Geitmann A. 2010. Finite element model of polar growth in pollen tubes. *The Plant Cell* **22**, 2579-2593.

Fernandes AN, Thomas LH, Altaner CM, Callow P, Forsyth VT, Apperley DC, Kennedy CJ, Jarvis MC. 2011. Nanostructure of cellulose microfibrils in spruce wood. *Proceedings of the National Academy of Sciences of the United States of America* **108**, E1195-E1203.

Fernández V, Guzmán-Delgado P, Graça J, Santos S, Gil L. 2016. Cuticle structure in relation to chemical composition: re-assessing the prevailing model. *Frontiers in Plant Science* **7**, 427.

Fleischer A, O'Neill MA, Ehwald R. 1999. The pore size of non-graminaceous plant cell walls is rapidly decreased by borate ester cross-linking of the pectic polysaccharide rhamnogalacturonan II. *Plant Physiology* **121**, 829-838.

Fletcher DA, Mullins RD. 2010. Cell mechanics and the cytoskeleton. *Nature* **463**, 485-492.

Footer MJ, Kerssemakers JW, Theriot JA, Dogterom M. 2007. Direct measurement of force generation by actin filament polymerization using an optical trap. *Proceedings of the National Academy of Sciences of the United States of America* **104**, 2181-2186.

Forouzesh E, Goel A, Mackenzie SA, Turner JA. 2013. In vivo extraction of *Arabidopsis* cell turgor pressure using nanoindentation in conjunction with finite element modeling. *The Plant Journal* **73**, 509-520.

Forterre Y. 2013. Slow, fast and furious: understanding the physics of plant movements. *Journal of Experimental Botany* **64**, 4745–4760.

Forterre Y, Skotheim JM, Dumais J, Mahadevan L. 2005. How the Venus flytrap snaps. *Nature* **433**, 421-425.

Foster J, Rugar D. 1983. High resolution acoustic microscopy in superfluid helium. *Applied Physics Letters* **42**, 869-871.

Franks P, Farquhar G. 1998. A study of stomatal mechanics using the cell pressure probe. *Plant, Cell & Environment* **21**, 94-100.

Franks PJ, Buckley TN, Shope JC, Mott KA. 2001. Guard cell volume and pressure measured concurrently by confocal microscopy and the cell pressure probe. *Plant Physiology* **125**, 1577-1584.

Franks PJ, Farquhar GD. 2007. The mechanical diversity of stomata and its significance in gas-exchange control. *Plant Physiology* **143**, 78-87.

Fratzl P, Gupta HS, Fischer FD, Kolednik O. 2007. Hindered crack propagation in materials with periodically varying Young's modulus—lessons from biological materials. *Advanced Materials* **19**, 2657-2661.

Freundthal AM. 1968. Statistical approach to brittle fracture. In: Lievowitz H, ed. *Fracture: an Advanced Treatise*, Vol. 2. New York: Academic Press, 591-619.

Fu Y, Gu Y, Zheng Z, Wasteneys G, Yang Z. 2005. *Arabidopsis* interdigitating cell growth requires two antagonistic pathways with opposing action on cell morphogenesis. *Cell* **120**, 687-700.

Fu Y, Li H, Yang Z. 2002. The ROP2 GTPase controls the formation of cortical fine F-actin and the early phase of directional cell expansion during *Arabidopsis* organogenesis. *The Plant Cell* **14**, 777-794.

Fujita M, Himmelspach R, Ward J, Whittington A, Hasenbein N, Liu C, Truong TT, Galway ME, Mansfield SD, Hocart CH. 2013. The anisotropy1 D604N mutation in the *Arabidopsis* cellulose synthase1 catalytic domain reduces cell wall crystallinity and the velocity of cellulose synthase complexes. *Plant Physiology* **162**, 74-85.

Funakawa H, Miwa K. 2015. Synthesis of borate cross-linked rhamnogalacturonan II. *Frontiers in Plant Science* **6**, 223.

Gadalla A, Dehoux T, Audoin B. 2014. Transverse mechanical properties of cell walls of single living plant cells probed by laser-generated acoustic waves. *Planta* **239**, 1129-1137.

Gallenmüller F, Feus A, Fiedler K, Speck T. 2015. Rose prickles and Asparagus spines–different hook structures as attachment devices in climbing plants. *PLoS One* **10**, e0143850.

Galli M, Comley KS, Shean TA, Oyen ML. 2009. Viscoelastic and poroelastic mechanical characterization of hydrated gels. *Journal of Materials Research* **24**, 973-979.

Gasser TC, Ogden RW, Holzapfel GA. 2006. Hyperelastic modelling of arterial layers with distributed collagen fibre orientations. *Journal of the Royal Society Interface* **3**, 15-35.

Geitmann A. 2010. Mechanical modeling and structural analysis of the primary plant cell wall. *Current Opinion in Plant Biology* **13**, 693-699.

Geitmann A. 2016. Actuators acting without actin. *Cell* **166**, 15-17.

Geitmann A, Dyson R. 2014. Modeling of the primary plant cell wall in the context of plant development. In: Assmann S, Liu B, eds. *Cell Biology*. New York, NY: Springer, 1-17.

Geitmann A, Hush J, Overall R. 1997. Inhibition of ethylene biosynthesis does not block microtubule re-orientation in wounded pea roots. *Protoplasma* **198**, 135-142.

Geitmann A, Ortega JK. 2009. Mechanics and modeling of plant cell growth. *Trends in Plant Science* **14**, 467-478.

Gershlak JR, Hernandez S, Fontana G, Perreault LR, Hansen KJ, Larson SA, Binder BY, Dolivo DM, Yang T, Dominko T. 2017. Crossing kingdoms: Using decellularized plants as perfusable tissue engineering scaffolds. *Biomaterials* **125**, 13-22.

Gianola D, Eberl C. 2009. Micro-and nanoscale tensile testing of materials. *JOM Journal of the Minerals, Metals and Materials Society* **61**, 24-35.

Glover BJ. 2000. Differentiation in plant epidermal cells. *Journal of Experimental Botany* **51**, 497-505.

Goldberg R, Pierron M, Bordenave M, Breton C, Morvan C, du Penhoat CH. 2001. Control of mung bean pectinmethylesterase isoform activities Influence of pH and carboxyl group distribution along the pectic chains. *Journal of Biological Chemistry* **276**, 8841-8847.

Goriely A, Tabor M. 2003. Self-similar tip growth in filamentary organisms. *Physical Review Letters* **90**, 108101.

Grédiac M, Toussaint E, Pierron F. 2002. Special virtual fields for the direct determination of material parameters with the virtual fields method. 1—Principle and definition. *International Journal of Solids and Structures* **39**, 2691-2705.

Green PB. 1960. Multinet growth in the cell wall of Nitella. *The Journal of Cell Biology* **7**, 289-296.

Green PB. 1962. Mechanism for plant cellular morphogenesis. *Science* **138**, 1404-1405.

Green PB. 1968. Growth physics in Nitella: a method for continuous in vivo analysis of extensibility based on a micro-manometer technique for turgor pressure. *Plant Physiology* **43**, 1169-1184.

Gu Y, Kaplinsky N, Bringmann M, Cobb A, Carroll A, Sampathkumar A, Baskin TI, Persson S, Somerville CR. 2010. Identification of a cellulose synthase-associated protein required for cellulose biosynthesis. *Proceedings of the National Academy of Sciences of the United States of America* **107**, 12866-12871.

Guhados G, Wan W, Hutter JL. 2005. Measurement of the elastic modulus of single bacterial cellulose fibers using atomic force microscopy. *Langmuir* **21**, 6642-6646.

Guilak F, Butler DL, Goldstein SA, Baaijens FP. 2014. Biomechanics and mechanobiology in functional tissue engineering. *Journal of Biomechanics* **47**, 1933-1940.

Guilak F, Tedrow JR, Burgkart R. 2000. Viscoelastic properties of the cell nucleus. *Biochemical and Biophysical Research Communications* **269**, 781-786.

Guo J, Sachs F, Meng F. 2014. Fluorescence-based force/tension sensors: a novel tool to visualize mechanical forces in structural proteins in live cells. *Antioxidants & Redox Signaling* **20**, 986-999.

Gutierrez R, Lindeboom JJ, Paredez AR, Emons AMC, Ehrhardt DW. 2009. *Arabidopsis* cortical microtubules position cellulose synthase delivery to the plasma membrane and interact with cellulose synthase trafficking compartments. *Nature Cell Biology* **11**, 797-806.

Guz N, Dokukin M, Kalaparthi V, Sokolov I. 2014. If cell mechanics can be described by elastic modulus: study of different models and probes used in indentation experiments. *Biophysical Journal* **107**, 564-575.

Haag K, Müssig J. 2016. Scatter in tensile properties of flax fibre bundles: influence of determination and calculation of the cross-sectional area. *Journal of Materials Science* **51**, 7907-7917.

Haase K, Pelling AE. 2015. Investigating cell mechanics with atomic force microscopy. *Journal of The Royal Society Interface* **12**, 20140970.

Hall LN, Tucker GA, Smith CJS, Watson CF, Seymour GB, Bundick Y, Boniwell JM, Fletcher JD, Ray JA, Schuch W, Bird CR, Grierson D. 1993. Antisense inhibition of pectin esterase gene expression in transgenic tomatoes. *The Plant Journal* **3**, 121-129.

Hall SA, Muir Wood D, Ibraim E, Viggiani G. 2010. Localised deformation patterning in 2D granular materials revealed by digital image correlation. *Granular Matter* **12**, 1-14.

Hamant O, Heisler MG, Jönsson H, Krupinski P, Uyttewaal M, Bokov P, Corson F, Sahlin P, Boudaoud A, Meyerowitz EM. 2008. Developmental patterning by mechanical signals in *Arabidopsis*. *Science* **322**, 1650-1655.

Hamant O, Meyerowitz EM, Traas J. 2011. Is cell polarity under mechanical control in plants? *Plant Signaling & Behavior* **6**, 137-139.

Hamant O, Traas J. 2010. The mechanics behind plant development. *New Phytologist* **185**, 369-385.

Han B, Chen L, Wang J, Wu Z, Yan L, Hou S. 2015. Constitutive expresser of pathogenesis related genes 1 is required for pavement cell morphogenesis in *Arabidopsis*. *PLoS One* **10**, e0133249.

Han C-S, Sanei SH, Alisafaei F. 2016. On the origin of indentation size effects and depth dependent mechanical properties of elastic polymers. *Journal of Polymer Engineering* **36**, 103-111.

Hancock BC, Clas S-D, Christensen K. 2000. Micro-scale measurement of the mechanical properties of compressed pharmaceutical powders. 1: the elasticity and fracture behavior of microcrystalline cellulose. *International Journal of Pharmaceutics* **209**, 27-35.

Hannon A, Tiernan P. 2008. A review of planar biaxial tensile test systems for sheet metal. *Journal of Materials Processing Technology* **198**, 1-13.

Haque M, Saif M. 2002. In-situ tensile testing of nano-scale specimens in SEM and TEM. *Experimental Mechanics* **42**, 123-128.

Harley R, James D, Miller A, White J. 1977. Phonons and the elastic moduli of collagen and muscle. *Nature* **267**, 285-287.

Hayot CM, Forouzesh E, Goel A, Avramova Z, Turner JA. 2012. Viscoelastic properties of cell walls of single living plant cells determined by dynamic nanoindentation. *Journal of Experimental Botany* **63**, 2525–2540.

Heisler MG, Hamant O, Krupinski P, Uyttewaal M, Ohno C, Jönsson H, Traas J, Meyerowitz EM, Goldfarb T, Lichten M. 2010. Alignment between PIN1 polarity and microtubule orientation in the shoot apical meristem reveals a tight coupling between morphogenesis and auxin transport. *PLoS Biology* **8**, e1000516.

Hepler PK, Winship LJ. 2010. Calcium at the cell wall-cytoplast interface. *Journal of Integrative Plant Biology* **52**, 147-160.

Hervy M, Santmarti A, Lahtinen P, Tammelin T, Lee K-Y. 2017. Sample geometry dependency on the measured tensile properties of cellulose nanopapers. *Materials & Design* **121**, 421-429.

Higaki T, Takigawa-Imamura H, Akita K, Kutsuna N, Kobayashi R, Hasezawa S, Miura T. 2016. Exogenous cellulase switches cell interdigitation to cell elongation in an RIC1-dependent manner in *Arabidopsis thaliana* cotyledon pavement cells. *Plant and Cell Physiology* **58**, 106-119.

Hild F, Roux S. 2006. Digital image correlation: from displacement measurement to identification of elastic properties–a review. *Strain* **42**, 69-80.

Hoffman BD, Crocker JC. 2009. Cell mechanics: dissecting the physical responses of cells to force. *Annual Review of Biomedical Engineering* **11**, 259-288.

Hofhuis H, Moulton D, Lessinnes T, Routier-Kierzkowska A-L, Bomphrey Richard J, Mosca G, Reinhardt H, Sarchet P, Gan X, Tsiantis M, Ventikos Y, Walker S, Goriely A, Smith R, Hay A. 2016. Morphomechanical innovation drives explosive seed dispersal. *Cell* **166**, 222-233.

Holdaway-Clarke TL, Weddle NM, Kim S, Robi A, Parris C, Kunkel JG, Hepler PK. 2003. Effect of extracellular calcium, pH and borate on growth oscillations in *Lilium formosanum* pollen tubes. *Journal of Experimental Botany* **54**, 65-72.

Hu C, Munglani G, Vogler H, Fabrice TN, Shamsudhin N, Wittel FK, Ringli C, Grossniklaus U, Herrmann HJ, Nelson BJ. 2017. Characterization of size-dependent mechanical properties of tip-growing cells using a lab-on-chip device. *Lab on a Chip* **17**, 82-90.

Hu S, Eberhard L, Chen J, Love JC, Butler JP, Fredberg JJ, Whitesides GM, Wang N. 2004. Mechanical anisotropy of adherent cells probed by a three-dimensional magnetic twisting device. *American Journal of Physiology-Cell Physiology* **287**, C1184-C1191.

Hua T, Xie H, Pan B, Qing X, Dai F, Feng X. 2007. A new micro-tensile system for measuring the mechanical properties of low-dimensional materials—Fibers and films. *Polymer Testing* **26**, 513-518.

Huang H, Kamm RD, Lee RT. 2004. Cell mechanics and mechanotransduction: pathways, probes, and physiology. *American Journal of Physiology-Cell Physiology* **287**, C1-C11.

Huang R, Becker A, Jones I. 2012. Modelling cell wall growth using a fibre-reinforced hyperelastic–viscoplastic constitutive law. *Journal of the Mechanics and Physics of Solids* **60**, 750-783.

Huang R, Becker AA, Jones IA. 2015. A finite strain fibre-reinforced viscoelasto-viscoplastic model of plant cell wall growth. *Journal of Engineering Mathematics* **95**, 121-154.

Hwang J-U, Gu Y, Lee Y-J, Yang Z. 2005. Oscillatory ROP GTPase activation leads the oscillatory polarized growth of pollen tubes. *Molecular Biology of the Cell* **16**, 5385-5399.

Ivakov A, Persson S. 2013. Plant cell shape: modulators and measurements. *Frontiers in Plant Science* **4**, 439.

Iwai H, Hokura A, Oishi M, Chida H, Ishii T, Sakai S, Satoh S. 2006. The gene responsible for borate cross-linking of pectin Rhamnogalacturonan-II is required for plant reproductive tissue development and fertilization. *Proceedings of the National Academy of Sciences of the United States of America* **103**, 16592-16597.

Iwamoto S, Kai W, Isogai A, Iwata T. 2009. Elastic modulus of single cellulose microfibrils from tunicate measured by atomic force microscopy. *Biomacromolecules* **10**, 2571-2576.

Jackman RL, Stanley DW. 1995. Perspectives in the textural evaluation of plant foods. *Trends in Food Science & Technology* **6**, 187-194.

Jacques E, Verbelen J-P, Vissenberg K. 2013. Mechanical stress in *Arabidopsis* leaves orients microtubules in a'continuous' supracellular pattern. *BMC Plant Biology* **13**, 163.

Jacques E, Verbelen J-P, Vissenberg K. 2014. Review on shape formation in epidermal pavement cells of the *Arabidopsis* leaf. *Functional Plant Biology* **41**, 914-921.

Jäger A, Bader T, Hofstetter K, Eberhardsteiner J. 2011. The relation between indentation modulus, microfibril angle, and elastic properties of wood cell walls. *Composites Part A: Applied Science and Manufacturing* **42**, 677-685.

Janmey PA, McCulloch CA. 2007. Cell mechanics: integrating cell responses to mechanical stimuli. *Annual Review of Biomedical Engineering* **9**, 1-34.

Javelle M, Vernoud V, Rogowsky PM, Ingram GC. 2011. Epidermis: the formation and functions of a fundamental plant tissue. *New Phytologist* **189**, 17-39.

Johnson KL, Degnan KA, Ross Walker J, Ingram GC. 2005. AtDEK1 is essential for specification of embryonic epidermal cell fate. *The Plant Journal* **44**, 114-127.

Johnston R, Atalar A, Heiserman J, Jipson V, Quate C. 1979. Acoustic microscopy: resolution of subcellular detail. *Proceedings of the National Academy of Sciences of the United States of America* **76**, 3325-3329.

Jones L, Milne JL, Ashford D, McQueen-Mason SJ. 2003. Cell wall arabinan is essential for guard cell function. *Proceedings of the National Academy of Sciences of the United States of America* **100**, 11783-11788.

Jones WR, Ting-Beall HP, Lee GM, Kelley SS, Hochmuth RM, Guilak F. 1999. Alterations in the Young's modulus and volumetric properties of chondrocytes isolated from normal and osteoarthritic human cartilage. *Journal of Biomechanics* **32**, 119-127.

Julkunen P, Kiviranta P, Wilson W, Jurvelin JS, Korhonen RK. 2007. Characterization of articular cartilage by combining microscopic analysis with a fibril-reinforced finite-element model. *Journal of Biomechanics* **40**, 1862-1870.

Kafle K, Park YB, Lee CM, Stapleton JJ, Kiemle SN, Cosgrove DJ, Kim SH. 2017. Effects of mechanical stretching on average orientation of cellulose and pectin in onion epidermis cell wall: A polarized FT-IR study. *Cellulose* **24**, 3145-3154.

Kalidindi S, Abusafieh A, El-Danaf E. 1997. Accurate characterization of machine compliance for simple compression testing. *Experimental Mechanics* **37**, 210-215.

Kashfuddoja M, Ramji M. 2013. Whole-field strain analysis and damage assessment of adhesively bonded patch repair of CFRP laminates using 3D-DIC and FEA. *Composites Part B: Engineering* **53**, 46-61.

Keckes J, Burgert I, Frühmann K, Müller M, Kölln K, Hamilton M, Burghammer M, Roth SV, Stanzl-Tschegg S, Fratzl P. 2003. Cell-wall recovery after irreversible deformation of wood. *Nature Materials* **2**, 810-813.

Keller E, Cosgrove DJ. 1995. Expansins in growing tomato leaves. *The Plant Journal* **8**, 795-802.

Kerstens S, Decraemer WF, Verbelen J-P. 2001. Cell walls at the plant surface behave mechanically like fiber-reinforced composite materials. *Plant Physiology* **127**, 381-385.

Kha H, Tuble SC, Kalyanasundaram S, Williamson RE. 2010. WallGen, software to construct layered cellulose-hemicellulose networks and predict their small deformation mechanics. *Plant Physiology* **152**, 774-786.

Khan A, Vincent J. 1993. Anisotropy in the fracture properties of apple flesh as investigated by crack-opening tests. *Journal of Materials Science* **28**, 45-51.

Kierzkowski D, Nakayama N, Routier-Kierzkowska A-L, Weber A, Bayer E, Schorderet M, Reinhardt D, Kuhlemeier C, Smith RS. 2012. Elastic domains regulate growth and organogenesis in the plant shoot apical meristem. *Science* **335**, 1096-1099.

Kim J-H, Nizami A, Hwangbo Y, Jang B, Lee H-J, Woo C-S, Hyun S, Kim T-S. 2013. Tensile testing of ultra-thin films on water surface. *Nature Communications* **4**, 2520

Kim K, Yi H, Zamil MS, Haque MA, Puri VM. 2015. Multiscale stress–strain characterization of onion outer epidermal tissue in wet and dry states. *American Journal of Botany* **102**, 12-20.

Kirik V, Herrmann U, Parupalli C, Sedbrook JC, Ehrhardt DW, Hülskamp M. 2007. CLASP localizes in two discrete patterns on cortical microtubules and is required for cell morphogenesis and cell division in *Arabidopsis*. *Journal of Cell Science* **120**, 4416-4425.

Kirmizis D, Logothetidis S. 2010. Atomic force microscopy probing in the measurement of cell mechanics. *International Journal of Nanomedicine* **5**, 137-145.

Klahre U, Becker C, Schmitt AC, Kost B. 2006. Nt-RhoGDI2 regulates Rac/Rop signaling and polar cell growth in tobacco pollen tubes. *The Plant Journal* **46**, 1018-1031.

Köhler L, Spatz H-C. 2002. Micromechanics of plant tissues beyond the linear-elastic range. *Planta* **215**, 33-40.

Kollmannsberger P, Fabry B. 2011. Linear and nonlinear rheology of living cells. *Annual Review of Materials Research* **41**, 75-97.

Korn RW. 1976. Concerning the sinuous shape of leaf epidermal cells. *New Phytologist* **77**, 153-161.

Korn RW, Spalding RM. 1973. The geometry of plant epidermal cells. *New Phytologist* **72**, 1357-1365.

Koshiba T, Kobayashi M, Ishihara A, Matoh T. 2010. Boron nutrition of cultured tobacco BY-2 cells. VI. Calcium is involved in early responses to boron deprivation. *Plant and Cell Physiology* **51**, 323-327.

Kost B. 2008. Spatial control of Rho (Rac-Rop) signaling in tip-growing plant cells. *Trends in Cell Biology* **18**, 119-127.

Kost B, Lemichez E, Spielhofer P, Hong Y, Tolias K, Carpenter C, Chua N-H. 1999. Rac homologues and compartmentalized phosphatidylinositol 4, 5-bisphosphate act in a common pathway to regulate polar pollen tube growth. *The Journal of Cell Biology* **145**, 317-330.

Kotchoni SO, Zakharova T, Mallery EL, Le J, El-Assal SE-D, Szymanski DB. 2009. The association of the *Arabidopsis* actin-related protein2/3 complex with cell membranes is linked to its assembly status but not its activation. *Plant Physiology* **151**, 2095-2109.

Kotzer A, Wasteneys G. 2006. Mechanisms behind the puzzle: microtubule–microfilament cross-talk in pavement cell formation. *Botany* **84**, 594-603.

Kroeger J, Geitmann A. 2011. Modeling pollen tube growth: feeling the pressure to deliver testifiable predictions. *Plant Signaling & Behavior* **6**, 1828-1830.

Kroeger JH, Geitmann A. 2012. Pollen tube growth: getting a grip on cell biology through modeling. *Mechanics Research Communications* **42**, 32-39.

Kroeger JH, Geitmann A, Grant M. 2008. Model for calcium dependent oscillatory growth in pollen tubes. *Journal of Theoretical Biology* **253**, 363-374.

Kuchen EE, Fox S, de Reuille PB, Kennaway R, Bensmihen S, Avondo J, Calder GM, Southam P, Robinson S, Bangham A. 2012. Generation of leaf shape through early patterns of growth and tissue polarity. *Science* **335**, 1092-1096.

Kulasinski K, Keten S, Churakov SV, Derome D, Carmeliet J. 2014. A comparative molecular dynamics study of crystalline, paracrystalline and amorphous states of cellulose. *Cellulose* **21**, 1103-1116.

Kuznetsova TG, Starodubtseva MN, Yegorenkov NI, Chizhik SA, Zhdanov RI. 2007. Atomic force microscopy probing of cell elasticity. *Micron* **38**, 824-833.

Lally C, Reid A, Prendergast P. 2004. Elastic behavior of porcine coronary artery tissue under uniaxial and equibiaxial tension. *Annals of Biomedical Engineering* **32**, 1355-1364.

Landrein B, Hamant O. 2013. How mechanical stress controls microtubule behavior and morphogenesis in plants: history, experiments and revisited theories. *The Plant Journal* **75**, 324-338.

Larsen FH, Byg I, Damager I, Diaz J, Engelsen SB, Ulvskov P. 2011. Residue specific hydration of primary cell wall potato pectin identified by solid-state 13C single-pulse MAS and CP/MAS NMR spectroscopy. *Biomacromolecules* **12**, 1844-1850.

Lautenschläger F, Paschke S, Schinkinger S, Bruel A, Beil M, Guck J. 2009. The regulatory role of cell mechanics for migration of differentiating myeloid cells. *Proceedings of the National Academy of Sciences of the United States of America* **106**, 15696-15701.

Lava P, Cooreman S, Coppieters S, De Strycker M, Debruyne D. 2009. Assessment of measuring errors in DIC using deformation fields generated by plastic FEA. *Optics and Lasers in Engineering* **47**, 747-753.

Lawrence BD, Marchant JK, Pindrus MA, Omenetto FG, Kaplan DL. 2009. Silk film biomaterials for cornea tissue engineering. *Biomaterials* **30**, 1299-1308.

Le J, Mallery EL, Zhang C, Brankle S, Szymanski DB. 2006. *Arabidopsis* BRICK1/HSPC300 is an essential WAVE-complex subunit that selectively stabilizes the Arp2/3 activator SCAR2. *Current Biology* **16**, 895-901.

Lee JM, Courtman DW, Boughner DR. 1984. The glutaraldehyde-stabilized porcine aortic valve xenograft. I. Tensile viscoelastic properties of the fresh leaflet material. *Journal of Biomedical Materials Research Part A* **18**, 61-77.

Lee JY. 1986. A finite element for shell analysis and its application to biological objects, Cornell University, 249.

Li C, Tao J, Zhao D, You C, Ge J. 2012a. Effect of calcium sprays on mechanical strength and cell wall fractions of herbaceous peony (*Paeonia lactiflora* Pall.) inflorescence stems. *International Journal of Molecular Sciences* **13**, 4704-4713.

Li QS, Lee GY, Ong CN, Lim CT. 2008. AFM indentation study of breast cancer cells. *Biochemical and Biophysical Research Communications* **374**, 609-613.

Li S, Lei L, Somerville CR, Gu Y. 2012b. Cellulose synthase interactive protein 1 (CSI1) links microtubules and cellulose synthase complexes. *Proceedings of the National Academy of Sciences of the United States of America* **109**, 185-190.

Li S, Logan Bashline LL, Gu Y. 2014. Cellulose synthesis and its regulation. *The Arabidopsis Book* **12**, e0169.

Liang H, Mahadevan L. 2009. The shape of a long leaf. *Proceedings of the National Academy of Sciences of the United States of America* **106**, 22049-22054.

Liang H, Zhang Y, Martinez P, Rasmussen C, Xu T, Yang Z. 2018. The microtubule-associated protein IQ67 DOMAIN5 modulates microtubule dynamics and pavement cell shape. *Plant Physiology* **177**, 1555-1568.

Liesche J, Ziomkiewicz I, Schulz A. 2013. Super-resolution imaging with Pontamine Fast Scarlet 4BS enables direct visualization of cellulose orientation and cell connection architecture in onion epidermis cells. *BMC Plant Biology* **13**, 226.

Lin D, Cao L, Zhou Z, Zhu L, Ehrhardt D, Yang Z, Fu Y. 2013. Rho GTPase signaling activates microtubule severing to promote microtubule ordering in *Arabidopsis*. *Current Biology* **23**, 290-297.

Lin D, Lopez-Sanchez P, Gidley MJ. 2016. Interactions of pectins with cellulose during its synthesis in the absence of calcium. *Food Hydrocolloids* **52**, 57-68.

Lin D, Ren H, Fu Y. 2015. ROP GTPase-mediated auxin signaling regulates pavement cell interdigitation in *Arabidopsis thaliana*. *Journal of Integrative Plant Biology* **57**, 31-39.

Lintilhac PM, Wei C, Tanguay JJ, Outwater JO. 2000. Ball tonometry: a rapid, nondestructive method for measuring cell turgor pressure in thin-walled plant cells. *Journal of Plant Growth Regulation* **19**, 90-97.

Liu X, Yang Q, Wang Y, Wang L, Fu Y, Wang X. 2018. Brassinosteroids regulate pavement cell growth by mediating BIN2-induced microtubule stabilization. *Journal of Experimental Botany* **69**, 1037-1049.

Loh O, Vaziri A, Espinosa H. 2009. The potential of MEMS for advancing experiments and modeling in cell mechanics. *Experimental Mechanics* **49**, 105-124.

Luczynski KW, Brynk T, Ostrowska B, Swieszkowski W, Reihsner R, Hellmich C. 2013. Consistent quasistatic and acoustic elasticity determination of poly-L-lactide-based rapid-

prototyped tissue engineering scaffolds. *Journal of Biomedical Materials Research Part A* **101**, 138-144.

Luo C, Wightman R, Meyerowitz E, Smoukov SK. 2015. A 3-dimensional fibre scaffold as an investigative tool for studying the morphogenesis of isolated plant cells. *BMC Plant Biology* **15**, 211.

Lynch TM, Lintilhac PM. 1997. Mechanical signals in plant development: a new method for single cell studies. *Developmental Biology* **181**, 246-256.

Maathuis FJ. 2011. Vacuolar two-pore K^+ channels act as vacuolar osmosensors. *New Phytologist* **191**, 84-91.

Machado G, Favier D, Chagnon G. 2012. Membrane curvatures and stress-strain full fields of axisymmetric bulge tests from 3D-DIC measurements. Theory and validation on virtual and experimental results. *Experimental Mechanics* **52**, 865-880.

Maier-Schneider D, Maibach J, Obermeier E. 1995. A new analytical solution for the load-deflection of square membranes. *Journal of Microelectromechanical Systems* **4**, 238-241.

Majda M, Grones P, Sintorn I-M, Vain T, Milani P, Krupinski P, Zagórska-Marek B, Viotti C, Jönsson H, Mellerowicz EJ, Hamant O, Robert S. 2017. Mechanochemical polarization of contiguous cell walls shapes plant pavement cells. *Developmental Cell* **43**, 290-304.e294.

Malik I, Mirkhalaf M, Barthelat F. 2017. Bio-inspired "jigsaw"-like interlocking sutures: Modeling, optimization, 3D printing and testing. *Journal of the Mechanics and Physics of Solids* **102**, 224-238.

Marc J, Granger CL, Brincat J, Fisher DD, Kao T-h, McCubbin AG, Cyr RJ. 1998. A GFP–MAP4 reporter gene for visualizing cortical microtubule rearrangements in living epidermal cells. *The Plant Cell* **10**, 1927-1939.

Marga F, Grandbois M, Cosgrove DJ, Baskin TI. 2005. Cell wall extension results in the coordinate separation of parallel microfibrils: evidence from scanning electron microscopy and atomic force microscopy. *The Plant Journal* **43**, 181-190.

Mariano M, El Kissi N, Dufresne A. 2014. Cellulose nanocrystals and related nanocomposites: Review of some properties and challenges. *Journal of Polymer Science Part B: Polymer Physics* **52**, 791-806.

Martín-Rejano EM, Camacho-Cristóbal JJ, Herrera-Rodríguez MB, Rexach J, Navarro-Gochicoa MT, González-Fontes A. 2011. Auxin and ethylene are involved in the responses of root system architecture to low boron supply in *Arabidopsis* seedlings. *Physiologia Plantarum* **142**, 170-178.

Mathur J. 2004. Cell shape development in plants. *Trends in Plant Science* **9**, 583-590.

Mathur J. 2006. Local interactions shape plant cells. *Current Opinion in Cell Biology* **18**, 40-46.

Mathur J, Hülskamp M. 2002. Microtubules and microfilaments in cell morphogenesis in higher plants. *Current Biology* **12**, R669-R676.

Mathur J, Spielhofer P, Kost B, Chua N. 1999. The actin cytoskeleton is required to elaborate and maintain spatial patterning during trichome cell morphogenesis in *Arabidopsis thaliana*. *Development* **126**, 5559-5568.

Maver U, Velnar T, Gaberšček M, Planinšek O, Finšgar M. 2016. Recent progressive use of atomic force microscopy in biomedical applications. *TrAC Trends in Analytical Chemistry* **80**, 96-111.

McCann MC, Roberts K. 1994. Changes in cell wall architecture during cell elongation. *Journal of Experimental Botany* **45**, 1683-1691.

McCartney L, Ormerod AP, Gidley MJ, Knox JP. 2000. Temporal and spatial regulation of pectic (1→ 4)-β-d-galactan in cell walls of developing pea cotyledons: implications for mechanical properties. *The Plant Journal* **22**, 105-113.

McKenna BA, Kopittke PM, Wehr JB, Blamey F, Menzies NW. 2010. Metal ion effects on hydraulic conductivity of bacterial cellulose–pectin composites used as plant cell wall analogs. *Physiologia Plantarum* **138**, 205-214.

Mechri C, Ruello P, Breteau J, Baklanov M, Verdonck P, Gusev V. 2009. Depth-profiling of elastic inhomogeneities in transparent nanoporous low-k materials by picosecond ultrasonic interferometry. *Applied Physics Letters* **95**, 091907.

Meidner H, Mansfield TA. 1968. *Physiology of stomata*. Maidenhead: McGraw Hill, 178.

Meng Z, Traverso AJ, Ballmann CW, Troyanova-Wood MA, Yakovlev VV. 2016. Seeing cells in a new light: a renaissance of Brillouin spectroscopy. *Advances in Optics and Photonics* **8**, 300-327.

Merced A, Renzaglia K. 2014. Developmental changes in guard cell wall structure and pectin composition in the moss Funaria: implications for function and evolution of stomata. *Annals of Botany* **114**, 1001-1010.

Metraux JP, Taiz L. 1978. Transverse viscoelastic extension in nitella: I. Relationship to growth rate. *Plant Physiology* **61**, 135-138.

Micheli F. 2001. Pectin methylesterases: cell wall enzymes with important roles in plant physiology. *Trends in Plant Science* **6**, 414-419.

Michon C, Chapuis C, Langendorff V, Boulenguer P, Cuvelier G. 2004. Strain-hardening properties of physical weak gels of biopolymers. *Food Hydrocolloids* **18**, 999-1005.

Mikshina P, Petrova A, Faizullin D, Zuev YF, Gorshkova T. 2015. Tissue-specific rhamnogalacturonan I forms the gel with hyperelastic properties. *Biochemistry (Moscow)* **80**, 915-924.

Milani P, Braybrook SA, Boudaoud A. 2013. Shrinking the hammer: micromechanical approaches to morphogenesis. *Journal of Experimental Botany* **64**, 4651-4662.

Milani P, Gholamirad M, Traas J, Arnéodo A, Boudaoud A, Argoul F, Hamant O. 2011. In vivo analysis of local wall stiffness at the shoot apical meristem in *Arabidopsis* using atomic force microscopy. *The Plant Journal* **67**, 1116-1123.

Milani P, Mirabet V, Cellier C, Rozier F, Hamant O, Das P, Boudaoud A. 2014. Matching patterns of gene expression to mechanical stiffness at cell resolution through quantitative tandem epifluorescence and nano-indentation. *Plant Physiology* **165**, 1399-1408.

Miller CJ, Davidson LA. 2013. The interplay between cell signalling and mechanics in developmental processes. *Nature Reviews Genetics* **14**, 733-744.

Miller KS, Edelstein L, Connizzo BK, Soslowsky LJ. 2012. Effect of preconditioning and stress relaxation on local collagen fiber re-alignment: inhomogeneous properties of rat supraspinatus tendon. *Journal of Biomechanical Engineering* **134**, 031007.

Mir M, Ali MN, Sami J, Ansari U. 2014. Review of mechanics and applications of auxetic structures. *Advances in Materials Science and Engineering* **2014**, 753496.

Mirkhalaf M, Dastjerdi AK, Barthelat F. 2014. Overcoming the brittleness of glass through bio-inspiration and micro-architecture. *Nature Communications* **5**, 3166.

Mitchison J, Swann M. 1954. The mechanical properties of the cell surface I. The cell elastimeter. *Journal of Experimental Biology* **31**, 443-460.

Mitra D, Kumari P, Quegwer J, Klemm S, Moeller B, Poeschl Y, Pflug P, Stamm G, Abel S, Bürstenbinder K. 2018. Microtubule-associated protein IQ67 DOMAIN5 regulates interdigitation of leaf pavement cells in *Arabidopsis thaliana*. *BioRxiv*, 268466.

Miura K, Nasu H, Yamamoto S. 2013. Scanning acoustic microscopy for characterization of neoplastic and inflammatory lesions of lymph nodes. *Scientific Reports* **3**, 1255.

Miwa K, Wakuta S, Takada S, Ide K, Takano J, Naito S, Omori H, Matsunaga T, Fujiwara T. 2013. Roles of BOR2, a boron exporter, in cross linking of rhamnogalacturonan II and root elongation under boron limitation in *Arabidopsis*. *Plant Physiology* **163**, 1699-1709.

Mofrad MR. 2009. Rheology of the cytoskeleton. *Annual Review of Fluid Mechanics* **41**, 433-453.

Mohnen D. 2008. Pectin structure and biosynthesis. *Current Opinion in Plant Biology* **11**, 266-277.

Möller B, Poeschl Y, Plötner R, Bürstenbinder K. 2017. PaCeQuant: a tool for high-throughput quantification of pavement cell shape characteristics. *Plant Physiology* **175**, 998-1017.

Money N. 2007. Biomechanics of invasive hyphal growth. In: Howard RJ, Gow NAR, eds. *Biology of the Fungal Cell*, Vol. 8. Berlin, Heidelberg: Springer, 237-249.

Moroni F, Mirabella T. 2014. Decellularized matrices for cardiovascular tissue engineering. *American Journal of Stem Cells* **3**, 1-20.

Mosca G, Sapala A, Strauss S, Routier-Kierzkowska A-L, Smith R. 2017. On the micro-indentation of plant cells in a tissue context. *Physical Biology* **14**, 015003.

Motra H, Hildebrand J, Dimmig-Osburg A. 2014. Assessment of strain measurement techniques to characterise mechanical properties of structural steel. *Engineering Science and Technology, an International Journal* **17**, 260-269.

Mravec J, Kračun SK, Rydahl MG, Westereng B, Miart F, Clausen MH, Fangel JU, Daugaard M, Van Cutsem P, Henrik H. 2014. Tracking developmentally regulated post-synthetic processing of homogalacturonan and chitin using reciprocal oligosaccharide probes. *Development* **141**, 4841-4850.

Murali P, Bhandakkar TK, Cheah WL, Jhon MH, Gao H, Ahluwalia R. 2011. Role of modulus mismatch on crack propagation and toughness enhancement in bioinspired composites. *Physical Review E* **84**, 015102.

Murashige T, Skoog F. 1962. A revised medium for rapid growth and bio assays with tobacco tissue cultures. *Physiologia Plantarum* **15**, 473-497.

Nakamura M, Naoi K, Shoji T, Hashimoto T. 2004. Low concentrations of propyzamide and oryzalin alter microtubule dynamics in *Arabidopsis* epidermal cells. *Plant and Cell Physiology* **45**, 1330-1334.

Nakamura T, Gu Y. 2007. Identification of elastic–plastic anisotropic parameters using instrumented indentation and inverse analysis. *Mechanics of Materials* **39**, 340-356.

Nakayama N, Smith RS, Mandel T, Robinson S, Kimura S, Boudaoud A, Kuhlemeier C. 2012. Mechanical regulation of auxin-mediated growth. *Current Biology* **22**, 1468-1476.

Neggers J, Hoefnagels J, Hild F, Roux S, Geers M. 2014. Direct stress-strain measurements from bulged membranes using topography image correlation. *Experimental Mechanics* **54**, 717-727.

Ng B, Chou S, Krishna V. 2005. The influence of gripping techniques on the tensile properties of tendons. *Proceedings of the Institution of Mechanical Engineers, Part H: Journal of Engineering in Medicine* **219**, 349-354.

Nguyen BV, Wang QG, Kuiper NJ, El Haj AJ, Thomas CR, Zhang Z. 2010. Biomechanical properties of single chondrocytes and chondrons determined by micromanipulation and finite-element modelling. *Journal of The Royal Society Interface* **7**, 1723-1733.

Niklas KJ. 1992. *Plant biomechanics: an engineering approach to plant form and function*. Chicago: University of Chicago Press, 622.

Noguchi K, Yasumori M, Imai T, Naito S, Matsunaga T, Oda H, Hayashi H, Chino M, Fujiwara T. 1997. *bor1-1*, an *Arabidopsis thaliana* mutant that requires a high level of boron. *Plant Physiology* **115**, 901-906.

Norris A. 2006. Extreme values of Poisson's ratio and other engineering moduli in anisotropic materials. *Journal of Mechanics of Materials and Structures* **1**, 793-812.

Nouira H, Salgado J, El-Hayek N, Ducourtieux S, Delvallée A, Anwer N. 2014. Setup of a high-precision profilometer and comparison of tactile and optical measurements of standards. *Measurement Science and Technology* **25**, 044016.

O'Neill MA, Eberhard S, Albersheim P, Darvill AG. 2001. Requirement of borate cross-linking of cell wall rhamnogalacturonan II for *Arabidopsis* growth. *Science* **294**, 846-849.

Oda Y, Iida Y, Nagashima Y, Sugiyama Y, Fukuda H. 2015. Novel coiled-coil proteins regulate exocyst association with cortical microtubules in xylem cells via the conserved oligomeric Golgi-complex 2 protein. *Plant and Cell Physiology* **56**, 277-286.

Oelschlägel B, Gorb S, Wanke S, Neinhuis C. 2009. Structure and biomechanics of trapping flower trichomes and their role in the pollination biology of Aristolochia plants (Aristolochiaceae). *New Phytologist* **184**, 988-1002.

Ogawa E, Yamada Y, Sezaki N, Kosaka S, Kondo H, Kamata N, Abe M, Komeda Y, Takahashi T. 2015. ATML1 and PDF2 play a redundant and essential role in *Arabidopsis* embryo development. *Plant and Cell Physiology* **56**, 1183-1192.

Okada K, Ueda J, Komaki MK, Bell CJ, Shimura Y. 1991. Requirement of the auxin polar transport system in early stages of *Arabidopsis* floral bud formation. *The Plant Cell* **3**, 677-684.

Olsson R. 2011. A survey of test methods for multiaxial and out-of-plane strength of composite laminates. *Composites Science and Technology* **71**, 773-783.

Onoda Y, Schieving F, Anten NP. 2008. Effects of light and nutrient availability on leaf mechanical properties of Plantago major: a conceptual approach. *Annals of Botany* **101**, 727-736.

Onoda Y, Schieving F, Anten NP. 2015. A novel method of measuring leaf epidermis and mesophyll stiffness shows the ubiquitous nature of the sandwich structure of leaf laminas in broad-leaved angiosperm species. *Journal of Experimental Botany* **66**, 2487-2499.

Onoda Y, Westoby M, Adler PB, Choong AM, Clissold FJ, Cornelissen JH, Díaz S, Dominy NJ, Elgart A, Enrico L. 2011. Global patterns of leaf mechanical properties. *Ecology Letters* **14**, 301-312.

Orthner M, Rieth L, Solzbacher F. 2010. High speed wafer scale bulge testing for the determination of thin film mechanical properties. *Review of Scientific Instruments* **81**, 055111.

Osorio S, Castillejo C, Quesada MA, Medina-Escobar N, Brownsey GJ, Suau R, Heredia A, Botella MA, Valpuesta V. 2008. Partial demethylation of oligogalacturonides by pectin methyl esterase 1 is required for eliciting defence responses in wild strawberry (*Fragaria vesca*). *The Plant Journal* **54**, 43-55.

Palin R, Geitmann A. 2012. The role of pectin in plant morphogenesis. *Biosystems* **109**, 397-402.

Pan B, Qian K, Xie H, Asundi A. 2009. Two-dimensional digital image correlation for in-plane displacement and strain measurement: a review. *Measurement Science and Technology* **20**, 062001.

Pang C, Lee G-Y, Kim T-i, Kim SM, Kim HN, Ahn S-H, Suh K-Y. 2012. A flexible and highly sensitive strain-gauge sensor using reversible interlocking of nanofibres. *Nature Materials* **11**, 795-801.

Panteris E, Apostolakos P, Galatis B. 1994. Sinuous ordinary epidermal cells: behind several patterns of waviness, a common morphogenetic mechanism. *New Phytologist* **127**, 771-780.

Panteris E, Galatis B. 2005. The morphogenesis of lobed plant cells in the mesophyll and epidermis: organization and distinct roles of cortical microtubules and actin filaments. *New Phytologist* **167**, 721-732.

Park Y, Best CA, Badizadegan K, Dasari RR, Feld MS, Kuriabova T, Henle ML, Levine AJ, Popescu G. 2010. Measurement of red blood cell mechanics during morphological changes. *Proceedings of the National Academy of Sciences of the United States of America* **107**, 6731-6736.

Parre E, Geitmann A. 2005. Pectin and the role of the physical properties of the cell wall in pollen tube growth of Solanum chacoense. *Planta* **220**, 582-592.

Peaucelle A, Braybrook Siobhan A, Le Guillou L, Bron E, Kuhlemeier C, Höfte H. 2011. Pectin-induced changes in cell wall mechanics underlie organ initiation in *Arabidopsis*. *Current Biology* **21**, 1720-1726.

Peaucelle A, Wightman R, Höfte H. 2015. The control of growth symmetry breaking in the *Arabidopsis* hypocotyl. *Current Biology* **25**, 1746-1752.

Pena MJ, Ryden P, Madson M, Smith AC, Carpita NC. 2004. The galactose residues of xyloglucan are essential to maintain mechanical strength of the primary cell walls in *Arabidopsis* during growth. *Plant Physiology* **134**, 443-451.

Peng L, Xiang F, Roberts E, Kawagoe Y, Greve LC, Kreuz K, Delmer DP. 2001. The experimental herbicide CGA 325′ 615 inhibits synthesis of crystalline cellulose and causes accumulation of non-crystalline β-1, 4-glucan associated with CesA protein. *Plant Physiology* **126**, 981-992.

Perry SS. 2004. Scanning probe microscopy measurements of friction. *MRS Bulletin* **29**, 478-483.

Peters WS, Tomos AD. 2000. The mechanic state of "inner tissue" in the growing zone of sunflower hypocotyls and the regulation of its growth rate following excision. *Plant Physiology* **123**, 605-612.

Pettolino FA, Walsh C, Fincher GB, Bacic A. 2012. Determining the polysaccharide composition of plant cell walls. *Nature Protocols* **7**, 1590-1607.

Pezzulla M, Smith GP, Nardinocchi P, Holmes DP. 2016. Geometry and mechanics of thin growing bilayers. *Soft Matter* **12**, 4435-4442.

Phyo P, Wang T, Kiemle SN, O'Neill H, Pingali SV, Hong M, Cosgrove DJ. 2017. Gradients in wall mechanics and polysaccharides along growing inflorescence stems. *Plant Physiology* **175**, 1593–1607.

Picton J, Steer M. 1983. Evidence for the role of Ca^{2+} ions in tip extension in pollen tubes. *Protoplasma* **115**, 11-17.

Pieczywek PM, Kozioł A, Konopacka D, Cybulska J, Zdunek A. 2017. Changes in cell wall stiffness and microstructure in ultrasonically treated apple. *Journal of Food Engineering* **197**, 1-8.

Pieczywek PM, Zdunek A. 2014. Finite element modelling of the mechanical behaviour of onion epidermis with incorporation of nonlinear properties of cell walls and real tissue geometry. *Journal of Food Engineering* **123**, 50-59.

Prasanna V, Prabha T, Tharanathan R. 2007. Fruit ripening phenomena–an overview. *Critical Reviews in Food Science and Nutrition* **47**, 1-19.

Promma N, Raka B, Grediac M, Toussaint E, Le Cam J-B, Balandraud X, Hild F. 2009. Application of the virtual fields method to mechanical characterization of elastomeric materials. *International Journal of Solids and Structures* **46**, 698-715.

Ptashnyk M, Seguin B. 2016. The impact of microfibril orientations on the biomechanics of plant cell walls and tissues. *Bulletin of Mathematical Biology* **78**, 2135-2164.

Raschke K. 1975. Stomatal action. *Annual Review of Plant Physiology* **26**, 309-340.

Rashid B, Destrade M, Gilchrist MD. 2012. Inhomogeneous deformation of brain tissue during tension tests. *Computational Materials Science* **64**, 295-300.

Raum K, Leguerney I, Chandelier F, Talmant M, Saied A, Peyrin F, Laugier P. 2006. Site-matched assessment of structural and tissue properties of cortical bone using scanning acoustic microscopy and synchrotron radiation μCT. *Physics in Medicine and Biology* **51**, 733.

Raven JA. 2014. Speedy small stomata? *Journal of Experimental Botany* **65**, 1415-1424.

Read J, Gras E, Sanson GD, Clissold F, Brunt C. 2003. Does chemical defence decline more in developing leaves that become strong and tough at maturity? *Australian Journal of Botany* **51**, 489-496.

Redgwell RJ, Melton LD, Brasch DJ. 1990. Cell wall changes in kiwifruit following post harvest ethylene treatment. *Phytochemistry* **29**, 399-407.

Refrégier G, Pelletier S, Jaillard D, Höfte H. 2004. Interaction between wall deposition and cell elongation in dark-grown hypocotyl cells in *Arabidopsis*. *Plant Physiology* **135**, 959-968.

Remmerbach TW, Wottawah F, Dietrich J, Lincoln B, Wittekind C, Guck J. 2009. Oral cancer diagnosis by mechanical phenotyping. *Cancer Research* **69**, 1728-1732.

Renzaglia KS, Villarreal JC, Piatkowski BT, Lucas JR, Merced A. 2017. Hornwort stomata: Architecture and fate shared with 400 million year old fossil plants without leaves. *Plant Physiology* **174**, 788-797.

Richmond PA. 1991. Occurrence and functions of native cellulose. In: Haigler CH, Weimer PJ, eds. *Biosynthesis and Biodegradation of Cellulose* New York: Marcel Dekker, Inc., 5-23.

Richmond PA, Métraux J-P, Taiz L. 1980. Cell expansion patterns and directionality of wall mechanical properties in nitella. *Plant Physiology* **65**, 211-217.

Ridley BL, O'Neill MA, Mohnen D. 2001. Pectins: structure, biosynthesis, and oligogalacturonide-related signaling. *Phytochemistry* **57**, 929-967.

Roelfsema MRG, Hedrich R. 2005. In the light of stomatal opening: new insights into 'the Watergate'. *New Phytologist* **167**, 665-691.

Roelofsen PA, Houwink A. 1953. Architecture and growth of the primary cell wall in some plant hairs and in the *Phycomyces* sporangiophore. *Acta Botanica Neerlandica* **2**, 218-225.

Rojas ER, Hotton S, Dumais J. 2011. Chemically mediated mechanical expansion of the pollen tube cell wall. *Biophysical Journal* **101**, 1844-1853.

Rose JK. 2003. *The plant cell wall: annual plant reviews*. London: Blackwell Publishing, 381.

Rosero A, Oulehlová D, Stillerová L, Schiebertová P, Grunt M, Žárský V, Cvrčková F. 2016. *Arabidopsis* FH1 formin affects cotyledon pavement cell shape by modulating cytoskeleton dynamics. *Plant and Cell Physiology* **57**, 488-504.

Rounds CM, Lubeck E, Hepler PK, Winship LJ. 2011. Propidium iodide competes with Ca^{2+} to label pectin in pollen tubes and *Arabidopsis* root hairs. *Plant Physiology* **157**, 175-187.

Routier-Kierzkowska A-L, Smith RS. 2013. Measuring the mechanics of morphogenesis. *Current Opinion in Plant Biology* **16**, 25-32.

Routier-Kierzkowska A-L, Weber A, Kochova P, Felekis D, Nelson BJ, Kuhlemeier C, Smith RS. 2012. Cellular force microscopy for in vivo measurements of plant tissue mechanics. *Plant Physiology* **158**, 1514-1522.

Rui Y, Anderson CT. 2016. Functional analysis of cellulose and xyloglucan in the walls of stomatal guard cells of *Arabidopsis*. *Plant Physiology* **170**, 1398-1419.

Rupin F, Saïed A, Dalmas D, Peyrin F, Haupert S, Raum K, Barthel E, Boivin G, Laugier P. 2009. Assessment of microelastic properties of bone using scanning acoustic microscopy: A face-to-face comparison with nanoindentation. *Japanese Journal of Applied Physics* **48**, 07GK01.

Ryden P, Sugimoto-Shirasu K, Smith AC, Findlay K, Reiter WD, McCann MC. 2003. Tensile properties of *Arabidopsis* cell walls depend on both a xyloglucan cross-linked microfibrillar network and rhamnogalacturonan II-borate complexes. *Plant Physiology* **132**, 1033-1040.

Saijo Y, Tanaka M, Okawai H, Sasaki H, Nitta S-I, Dunn F. 1997. Ultrasonic tissue characterization of infarcted myocardium by scanning acoustic microscopy. *Ultrasound in Medicine & Biology* **23**, 77-85.

Salmén L, Bergström E. 2009. Cellulose structural arrangement in relation to spectral changes in tensile loading FTIR. *Cellulose* **16**, 975-982.

Sampathkumar A, Krupinski P, Wightman R, Milani P, Berquand A, Boudaoud A, Hamant O, Jönsson H, Meyerowitz EM. 2014a. Subcellular and supracellular mechanical stress prescribes cytoskeleton behavior in *Arabidopsis* cotyledon pavement cells. *ELife* **3**, e01967.

Sampathkumar A, Yan A, Krupinski P, Meyerowitz EM. 2014b. Physical forces regulate plant development and morphogenesis. *Current Biology* **24**, R475-R483.

Sanati Nezhad A, Geitmann A. 2015. Tip growth in walled cells: cellular expansion and invasion mechanisms. In: Cuerrier C, Pelling A, eds. *Cells, Forces and the Microenvironment*. Boca Raton: CRC Press 335-356.

Sanati Nezhad A, Naghavi M, Packirisamy M, Bhat R, Geitmann A. 2013. Quantification of the Young's modulus of the primary plant cell wall using Bending-Lab-On-Chip (BLOC). *Lab on a Chip* **13**, 2599-2608.

Sanders PG, Eastman J, Weertman J. 1997. Elastic and tensile behavior of nanocrystalline copper and palladium. *Acta Materialia* **45**, 4019-4025.

Sandhu APS, Randhawa GS, Dhugga KS. 2009. Plant cell wall matrix polysaccharide biosynthesis. *Molecular Plant* **2**, 840-850.

Sapala A, Runions A, Routier-Kierzkowska A-L, Gupta MD, Hong L, Hofhuis H, Verger S, Mosca G, Li C-B, Hay A. 2018. Why plants make puzzle cells, and how their shape emerges. *ELife* **7**, e32794.

Sasaki H, Saijo Y, Tanaka M, Nitta S, Terasawa Y, Yambe T, Taguma Y. 1997. Acoustic properties of dialysed kidney by scanning acoustic microscopy. *Nephrology Dialysis Transplantation* **12**, 2151-2154.

Savaldi-Goldstein S, Peto C, Chory J. 2007. The epidermis both drives and restricts plant shoot growth. *Nature* **446**, 199-202.

Saxe F, Weichold S, Reinecke A, Lisec J, Döring A, Neumetzler L, Burgert I, Eder M. 2016. Age effects on hypocotyl mechanics. *PLoS One* **11**, e0167808.

Scarcelli G, Yun SH. 2008. Confocal Brillouin microscopy for three-dimensional mechanical imaging. *Nature Photonics* **2**, 39-43.

Scarponi F, Mattana S, Corezzi S, Caponi S, Comez L, Sassi P, Morresi A, Paolantoni M, Urbanelli L, Emiliani C. 2017. High-performance versatile setup for simultaneous Brillouin-Raman micro-spectroscopy. *Physical Review X* **7**, 031015.

Schatzmann L, Brunner P, Stäubli H. 1998. Effect of cyclic preconditioning on the tensile properties of human quadriceps tendons and patellar ligaments. *Knee Surgery, Sports Traumatology, Arthroscopy* **6**, S56-S61.

Schneider CA, Rasband WS, Eliceiri KW. 2012. NIH Image to ImageJ: 25 years of image analysis. *Nature Methods* **9**, 671-675

Sedighi-Gilani M, Navi P. 2007. Experimental observations and micromechanical modeling of successive-damaging phenomenon in wood cells' tensile behavior. *Wood Science and Technology* **41**, 69-85.

Sedighi-Gilani M, Sunderland H, Navi P. 2005. Microfibril angle non-uniformities within normal and compression wood tracheids. *Wood Science and Technology* **39**, 419-430.

Serrano M, Coluccia F, Torres M, L'Haridon F, Métraux J-P. 2014. The cuticle and plant defense to pathogens. *Frontiers in Plant Science* **5**, 274.

Shah DU, Schubel PJ, Clifford MJ, Licence P. 2012. The tensile behavior of off-axis loaded plant fiber composites: An insight on the nonlinear stress–strain response. *Polymer Composites* **33**, 1494-1504.

Sharpe PJ, Wu HI. 1978. Stomatal mechanics: volume changes during opening. *Plant, Cell & Environment* **1**, 259-268.

Sharpe W, Pulskamp J, Gianola D, Eberl C, Polcawich R, Thompson R. 2007. Strain measurements of silicon dioxide microspecimens by digital imaging processing. *Experimental Mechanics* **47**, 649-658.

Shaw SL, Dumais J, Long SR. 2000. Cell Surface Expansion in Polarly Growing Root Hairs ofMedicago truncatula. *Plant Physiology* **124**, 959-970.

Silva S, Sabino M, Fernandes E, Correlo V, Boesel L, Reis R. 2005. Cork: properties, capabilities and applications. *International Materials Reviews* **50**, 345-365.

Small MK, Daniels BJ, Clemens BM, Nix WD. 1994. The elastic biaxial modulus of Ag–Pd multilayered thin films measured using the bulge test. *Journal of Materials Research* **9**, 25-30.

Smith LG. 2003. Cytoskeletal control of plant cell shape: getting the fine points. *Current Opinion in Plant Biology* **6**, 63-73.

Smith LG, Oppenheimer DG. 2005. Spatial control of cell expansion by the plant cytoskeleton. *Annual Review of Cell and Developmental Biology* **21**, 271-295.

Soons J, Lava P, Debruyne D, Dirckx J. 2012. Full-field optical deformation measurement in biomechanics: digital speckle pattern interferometry and 3D digital image correlation applied to bird beaks. *Journal of the Mechanical Behavior of Biomedical Materials* **14**, 186-191.

Sotiriou P, Giannoutsou E, Panteris E, Galatis B, Apostolakos P. 2018. Local differentiation of cell wall matrix polysaccharides in sinuous pavement cells: its possible involvement in the flexibility of cell shape. *Plant Biology* **20**, 223-237.

Spatz H, Kohler L, Niklas K. 1999. Mechanical behaviour of plant tissues: composite materials or structures? *Journal of Experimental Biology* **202**, 3269-3272.

Srikar V, Spearing S. 2003. A critical review of microscale mechanical testing methods used in the design of microelectromechanical systems. *Experimental Mechanics* **43**, 238-247.

Srivastava V, Robinson DN. 2015. Mechanical stress and network structure drive protein dynamics during cytokinesis. *Current Biology* **25**, 663-670.

Stan G, Solares SD. 2014. Frequency, amplitude, and phase measurements in contact resonance atomic force microscopies. *Beilstein Journal of Nanotechnology* **5**, 278-288.

Stansbury JW, Idacavage MJ. 2016. 3D printing with polymers: Challenges among expanding options and opportunities. *Dental Materials* **32**, 54-64.

Strange DG, Fletcher TL, Tonsomboon K, Brawn H, Zhao X, Oyen ML. 2013. Separating poroviscoelastic deformation mechanisms in hydrogels. *Applied Physics Letters* **102**, 031913.

Stubbs CJ, Baban NS, Robertson DJ, Alzube L, Cook DD. 2018. Bending stress in plant stems: models and assumptions. In: Geitmann A, Gril J, eds. *Plant Biomechanics*. Cham: Springer, 49-77.

Sun EQ. 2006. Shear locking and hourglassing in MSC Nastran, Abaqus, and Ansys. *MSC Software Corporation's 2006 Americas Virtual Product Development Conference: Evolution to Enterprise Simulation, MSC Software*. Santa Ana, CA.

Sun W, Sacks MS, Scott MJ. 2005. Effects of boundary conditions on the estimation of the planar biaxial mechanical properties of soft tissues. *Journal of Biomechanical Engineering* **127**, 709-715.

Suslov D, Ivakov A, Boron AK, Vissenberg K. 2015. In vitro cell wall extensibility controls age-related changes in the growth rate of etiolated *Arabidopsis* hypocotyls. *Functional Plant Biology* **42**, 1068-1079.

Suslov D, Vissenberg K. 2018. Cell wall expansion as viewed by the creep method. In: Geitmann A, Gril J, eds. *Plant Biomechanics*. Cham: Springer, 305-320.

Sutton M, Reu PL, eds. 2017. *International Digital Imaging Correlation Society: Proceedings of the First Annual Conference 2016*. Cham: Springer International Publishing, 283.

Szymanski DB. 2014. The kinematics and mechanics of leaf expansion: new pieces to the *Arabidopsis* puzzle. *Current Opinion in Plant Biology* **22**, 141-148.

Szymanski DB, Marks MD, Wick SM. 1999. Organized F-actin is essential for normal trichome morphogenesis in *Arabidopsis*. *The Plant Cell* **11**, 2331-2347.

Szymanski DB, Staiger CJ. 2018. The actin cytoskeleton: functional arrays for cytoplasmic organization and cell shape control. *Plant Physiology* **176**, 106-118.

Takada S, Takada N, Yoshida A. 2013. ATML1 promotes epidermal cell differentiation in *Arabidopsis* shoots. *Development* **140**, 1919-1923.

Talbot MJ, White RG. 2013. Methanol fixation of plant tissue for scanning electron microscopy improves preservation of tissue morphology and dimensions. *Plant Methods* **9**, 36.

Tanaka K, Kitano T, Egami N. 2014. Effect of fiber orientation on fatigue crack propagation in short-fiber reinforced plastics. *Engineering Fracture Mechanics* **123**, 44-58.

Tanguy M, Bourmaud A, Baley C. 2016. Plant cell walls to reinforce composite materials: relationship between nanoindentation and tensile modulus. *Materials Letters* **167**, 161-164.

Teulé F, Miao Y-G, Sohn B-H, Kim Y-S, Hull JJ, Fraser MJ, Lewis RV, Jarvis DL. 2012. Silkworms transformed with chimeric silkworm/spider silk genes spin composite silk fibers with improved mechanical properties. *Proceedings of the National Academy of Sciences of the United States of America* **109**, 923-928.

Thimm JC, Burritt DJ, Ducker WA, Melton LD. 2009. Pectins influence microfibril aggregation in celery cell walls: An atomic force microscopy study. *Journal of Structural Biology* **168**, 337-344.

Thomas LH, Forsyth VT, Šturcová A, Kennedy CJ, May RP, Altaner CM, Apperley DC, Wess TJ, Jarvis MC. 2013. Structure of cellulose microfibrils in primary cell walls from collenchyma. *Plant Physiology* **161**, 465-476.

Tibbits CW, MacDougall AJ, Ring SG. 1998. Calcium binding and swelling behaviour of a high methoxyl pectin gel. *Carbohydrate Research* **310**, 101-107.

Ting T. 2004. Very large Poisson's ratio with a bounded transverse strain in anisotropic elastic materials. *Journal of Elasticity* **77**, 163-176.

Ting T, Chen T. 2005. Poisson's ratio for anisotropic elastic materials can have no bounds. *The Quarterly Journal of Mechanics and Applied Mathematics* **58**, 73-82.

Tirichine L, Andrey P, Biot E, Maurin Y, Gaudin V. 2009. 3D fluorescent in situ hybridization using *Arabidopsis* leaf cryosections and isolated nuclei. *Plant Methods* **5**, 11.

Tissier A. 2012. Glandular trichomes: what comes after expressed sequence tags? *The Plant Journal* **70**, 51-68.

Tittmann BR, Xi X. 2014. Imaging and quantitative data acquisition of biological cell walls with atomic force microscopy and scanning acoustic microscopy. In: Méndez-Vilas A, ed. *Microscopy: Advances in Scientific Research and Education*, Vol. 1. Badajoz: Formatex, 161-172.

Toole GA, Gunning PA, Parker ML, Smith AC, Waldron KW. 2001. Fracture mechanics of the cell wall of *Chara corallina*. *Planta* **212**, 606-611.

Torode TA, O'Neill RE, Marcus SE, Cornuault V, Pose-Albacete S, Lauder RP, Kracun SK, Gro Rydahl M, Andersen MCF, Willats WGT, Braybrook SA, Townsend BJ, Clausen MH, Knox JP. 2017. Branched pectic galactan in phloem-sieve-element cell walls: implications for cell mechanics. *Plant Physiology* **176**, 1547-1558.

Tsuchiya T, Tabata O, Sakata J, Taga Y. 1998. Specimen size effect on tensile strength of surface-micromachined polycrystalline silicon thin films. *Journal of Microelectromechanical Systems* **7**, 106-113.

Turek DE. 1993. On the tensile testing of high modulus polymers and the compliance correction. *Polymer Engineering & Science* **33**, 328-333.

Ulvskov P, Wium H, Bruce D, Jørgensen B, Qvist KB, Skjøt M, Hepworth D, Borkhardt B, Sørensen SO. 2005. Biophysical consequences of remodeling the neutral side chains of rhamnogalacturonan I in tubers of transgenic potatoes. *Planta* **220**, 609-620.

Uyttewaal M, Burian A, Alim K, Landrein B, Borowska-Wykręt D, Dedieu A, Peaucelle A, Ludynia M, Traas J, Boudaoud A. 2012. Mechanical stress acts via katanin to amplify differences in growth rate between adjacent cells in *Arabidopsis*. *Cell* **149**, 439-451.

Vanstreels E, Alamar M, Verlinden B, Enninghorst A, Loodts J, Tijskens E, Ramon H, Nicolaï B. 2005. Micromechanical behaviour of onion epidermal tissue. *Postharvest Biology and Technology* **37**, 163-173.

Vincken J-P, Schols HA, Oomen RJFJ, McCann MC, Ulvskov P, Voragen AGJ, Visser RGF. 2003. If homogalacturonan were a side chain of rhamnogalacturonan I. Implications for cell wall architecture. *Plant Physiology* **132**, 1781-1789.

Vlassak JJ, Nix W. 1994. Measuring the elastic properties of anisotropic materials by means of indentation experiments. *Journal of the Mechanics and Physics of Solids* **42**, 1223-1245.

Vőfély RV, Gallagher J, Pisano GD, Bartlett M, Braybrook SA. 2018. Of puzzles and pavements: a quantitative exploration of leaf epidermal cell shape. *New Phytologist*.

Vogler H, Draeger C, Weber A, Felekis D, Eichenberger C, Routier-Kierzkowska AL, Boisson-Dernier A, Ringli C, Nelson BJ, Smith RS. 2013. The pollen tube: a soft shell with a hard core. *The Plant Journal* **73**, 617-627.

Von Mohl H. 1856. Welche Ursachen bewirken die Erweiterung und Verengung der Spaltöffnungen. *Botanische Zeitung* **14**, 697-704.

Wakabayashi K, Hoson T, Huber DJ. 2003. Methyl de-esterification as a major factor regulating the extent of pectin depolymerization during fruit ripening: a comparison of the action of avocado (*Persea americana*) and tomato (*Lycopersicon esculentum*) polygalacturonases. *Journal of Plant Physiology* **160**, 667-673.

Wang C, Wang L, Thomas C. 2004. Modelling the mechanical properties of single suspension-cultured tomato cells. *Annals of Botany* **93**, 443-453.

Wang G, Mao W, Byler R, Patel K, Henegar C, Alexeev A, Sulchek T. 2013. Stiffness dependent separation of cells in a microfluidic device. *PLoS One* **8**, e75901.

Wang Q-M, Mohan AC, Oyen ML, Zhao X-H. 2014. Separating viscoelasticity and poroelasticity of gels with different length and time scales. *Acta Mechanica Sinica* **30**, 20-27.

Wang YM, Judkewitz B, DiMarzio CA, Yang C. 2012. Deep-tissue focal fluorescence imaging with digitally time-reversed ultrasound-encoded light. *Nature Communications* **3**, 928.

Watson R. 1942. The effect of cuticular hardening on the form of epidermal cells. *New Phytologist*, 223-229.

Weber A, Braybrook S, Huflejt M, Mosca G, Routier-Kierzkowska A-L, Smith RS. 2015. Measuring the mechanical properties of plant cells by combining micro-indentation with osmotic treatments. *Journal of Experimental Botany* **66**, 3229-3241.

Wei C, Lintilhac LS, Lintilhac PM. 2006. Loss of stability, pH, and the anisotropic extensibility of Chara cell walls. *Planta* **223**, 1058-1067.

Wei C, Lintilhac PM, Tanguay JJ. 2001. An insight into cell elasticity and load-bearing ability. Measurement and theory. *Plant Physiology* **126**, 1129-1138.

Weiss EC, Lemor RM, Pilarczyk G, Anastasiadis P, Zinin PV. 2007. Imaging of focal contacts of chicken heart muscle cells by high-frequency acoustic microscopy. *Ultrasound in Medicine & Biology* **33**, 1320-1326.

Willats WG, McCartney L, Mackie W, Knox JP. 2001a. Pectin: cell biology and prospects for functional analysis. *Plant Molecular Biology* **47**, 9-27.

Willats WG, Orfila C, Limberg G, Buchholt HC, van Alebeek G-JW, Voragen AG, Marcus SE, Christensen TM, Mikkelsen JD, Murray BS. 2001b. Modulation of the degree and pattern of methyl-esterification of pectic homogalacturonan in plant cell walls Implications for pectin methyl esterase action, matrix properties, and cell adhesion. *Journal of Biological Chemistry* **276**, 19404-19413.

Williams M, Vincent R, Pinder D, Hemar Y. 2008. Microrheological studies offer insights into polysaccharide gels. *Journal of Non-Newtonian Fluid Mechanics* **149**, 63-70.

Williamson RE. 1990. Alignment of cortical microtubules by anisotropic wall stresses. *Functional Plant Biology* **17**, 601-613.

Wilson RH, Smith AC, Kačuráková M, Saunders PK, Wellner N, Waldron KW. 2000. The mechanical properties and molecular dynamics of plant cell wall polysaccharides studied by Fourier-transform infrared spectroscopy. *Plant Physiology* **124**, 397-406.

Wolf S, Greiner S. 2012. Growth control by cell wall pectins. *Protoplasma* **249**, 169-175.

Wolf S, Mouille G, Pelloux J. 2009. Homogalacturonan methyl-esterification and plant development. *Molecular Plant* **2**, 851-860.

Wolf S, Mravec J, Greiner S, Mouille G, Höfte H. 2012. Plant cell wall homeostasis is mediated by brassinosteroid feedback signaling. *Current Biology* **22**, 1732-1737.

Woolfenden HC, Bourdais G, Kopischke M, Miedes E, Molina A, Robatzek S, Morris RJ. 2017. A computational approach for inferring the cell wall properties that govern guard cell dynamics. *The Plant Journal* **92**, 5-18.

Wright I, Cannon K. 2001. Relationships between leaf lifespan and structural defences in a low-nutrient, sclerophyll flora. *Functional Ecology* **15**, 351-359.

Wu Y, Zhao S, Tian H, He Y, Xiong W, Guo L, Wu Y. 2013. CPK3-phosphorylated RhoGDI1 is essential in the development of *Arabidopsis* seedlings and leaf epidermal cells. *Journal of Experimental Botany* **64**, 3327-3338.

Wymer CL, Wymer SA, Cosgrove DJ, Cyr RJ. 1996. Plant cell growth responds to external forces and the response requires intact microtubules. *Plant Physiology* **110**, 425-430.

Xi X, Kim SH, Tittmann B. 2015. Atomic force microscopy based nanoindentation study of onion abaxial epidermis walls in aqueous environment. *Journal of Applied Physics* **117**, 024703.

Xi X, Li X, Miyasaka C, Kropf M, Tittmann B. 2013. High frequency scanning acoustic microscopy as diagnostic tool in tissue science. *Journal of Biotechnology & Biomaterials* **3**, 1000160.

Xu T, Wen M, Nagawa S, Fu Y, Chen J-G, Wu M-J, Perrot-Rechenmann C, Friml J, Jones AM, Yang Z. 2010. Cell surface-and rho GTPase-based auxin signaling controls cellular interdigitation in *Arabidopsis*. *Cell* **143**, 99-110.

Yakubov GE, Bonilla MR, Chen H, Doblin MS, Bacic A, Gidley MJ, Stokes JR. 2016. Mapping nano-scale mechanical heterogeneity of primary plant cell walls. *Journal of Experimental Botany* **67**, 2799–2816.

Yamaguchi I. 1981. A laser-speckle strain gauge. *Journal of Physics E: Scientific Instruments* **14**, 1270-1273.

Yanagisawa M, Desyatova AS, Belteton SA, Mallery EL, Turner JA, Szymanski DB. 2015. Patterning mechanisms of cytoskeletal and cell wall systems during leaf trichome morphogenesis. *Nature Plants* **1**, 15014.

Yang L, Ettemeyer A. 2003. Strain measurement by three-dimensional electronic speckle pattern interferometry: potentials, limitations, and applications. *Optical Engineering* **42**, 1257-1266.

Yang W, Sherman VR, Gludovatz B, Schaible E, Stewart P, Ritchie RO, Meyers MA. 2015. On the tear resistance of skin. *Nature Communications* **6**, 6649.

Yapo BM. 2011. Rhamnogalacturonan-I: a structurally puzzling and functionally versatile polysaccharide from plant cell walls and mucilages. *Polymer Reviews* **51**, 391-413.

Yeats TH, Rose JK. 2013. The formation and function of plant cuticles. *Plant Physiology* **163**, 5-20.

Yi H, Puri VM. 2012. Architecture-based multiscale computational modeling of plant cell wall mechanics to examine the hydrogen-bonding hypothesis of the cell wall network structure model. *Plant Physiology* **160**, 1281-1292.

Yip AK, Iwasaki K, Ursekar C, Machiyama H, Saxena M, Chen H, Harada I, Chiam K-H, Sawada Y. 2013. Cellular response to substrate rigidity is governed by either stress or strain. *Biophysical Journal* **104**, 19-29.

Yu Y, Jiang Z, Fei B, Wang G, Wang H. 2011. An improved microtensile technique for mechanical characterization of short plant fibers: a case study on bamboo fibers. *Journal of Materials Science* **46**, 739-746.

Yu Z, Xu H, Chen H, Pei Y, Fang D. 2016. Characterization Method of Thick Films Using the Bulge Test Technique. *Experimental Mechanics* **56**, 881-889.

Zamil MS, Geitmann A. 2017. The middle lamella—more than a glue. *Physical Biology* **14**, 015004.

Zamil MS, Yi H, Haque M, Puri VM. 2013. Characterizing microscale biological samples under tensile loading: Stress–strain behavior of cell wall fragment of onion outer epidermis. *American Journal of Botany* **100**, 1105-1115.

Zamil MS, Yi H, Puri VM. 2014. Mechanical characterization of outer epidermal middle lamella of onion under tensile loading. *American Journal of Botany* **101**, 778-787.

Zamil MS, Yi H, Puri VM. 2015. The mechanical properties of plant cell walls soft material at the subcellular scale: the implications of water and of the intercellular boundaries. *Journal of Materials Science* **50**, 6608-6623.

Zamil MS, Yi H, Puri VM. 2017. A multiscale FEA framework for bridging cell-wall to tissue-scale mechanical properties: the contributions of middle lamella interface and cell shape. *Journal of Materials Science* **52**, 7947-7968.

Zemánek M, Burša J, Děták M. 2009. Biaxial tension tests with soft tissues of arterial wall. *Engineering Mechanics* **16**, 3-11.

Zerzour R, Kroeger J, Geitmann A. 2009. Polar growth in pollen tubes is associated with spatially confined dynamic changes in cell mechanical properties. *Developmental Biology* **334**, 437-446.

Zhang C, Halsey LE, Szymanski DB. 2011. The development and geometry of shape change in *Arabidopsis thaliana* cotyledon pavement cells. *BMC Plant Biology* **11**, 1-13.

Zhang T, Mahgsoudy-Louyeh S, Tittmann B, Cosgrove DJ. 2014. Visualization of the nanoscale pattern of recently-deposited cellulose microfibrils and matrix materials in never-dried primary walls of the onion epidermis. *Cellulose* **21**, 853-862.

Zhang T, Vavylonis D, Durachko DM, Cosgrove DJ. 2017. Nanoscale movements of cellulose microfibrils in primary cell walls. *Nature Plants* **3**, 17056.

Zhang T, Zheng Y, Cosgrove DJ. 2016. Spatial organization of cellulose microfibrils and matrix polysaccharides in primary plant cell walls as imaged by multichannel atomic force microscopy. *The Plant Journal* **85**, 179-192.

Zhao R, Boudou T, Wang WG, Chen CS, Reich DH. 2013. Decoupling cell and matrix mechanics in engineered microtissues using magnetically actuated microcantilevers. *Advanced Materials* **25**, 1699-1705.

Zhao X, Akhtar R, Nijenhuis N, Wilkinson SJ, Murphy L, Ballestrem C, Sherratt MJ, Watson RE, Derby B. 2012. Multi-layer phase analysis: quantifying the elastic properties of soft tissues and live cells with ultra-high-frequency scanning acoustic microscopy. *IEEE Transactions on Ultrasonics, Ferroelectrics, and Frequency Control* **59**, 610-620.

Zheng Y-P, Choi A, Ling H, Huang Y-P. 2009. Simultaneous estimation of Poisson's ratio and Young's modulus using a single indentation: a finite element study. *Measurement Science and Technology* **20**, 045706.

Zhou P, Goodson KE. 2001. Subpixel displacement and deformation gradient measurement using digital image/speckle correlation (DISC). *Optical Engineering* **40**, 1613-1620.

Zhou W, Wang Y, Wu Z, Luo L, Liu P, Yan L, Hou S. 2016. Homologs of SCAR/WAVE complex components are required for epidermal cell morphogenesis in rice. *Journal of Experimental Botany* **67**, 4311-4323.

Zhu C, Bao G, Wang N. 2000. Cell mechanics: mechanical response, cell adhesion, and molecular deformation. *Annual Review of Biomedical Engineering* **2**, 189-226.

Zhu C, Ganguly A, Baskin TI, McClosky DD, Anderson CT, Foster C, Meunier KA, Okamoto R, Berg H, Dixit R. 2015. The Fragile Fiber1 kinesin contributes to cortical microtubule-mediated trafficking of cell wall components. *Plant Physiology* **167**, 780-792.

Ziegenspeck A. 1955. Das Vorkommen von Fila in radialer Anordnung in den Schliesszellen. *Protoplasma* **44**, 385-388.

Zou R, Xia Y, Liu S, Hu P, Hou W, Hu Q, Shan C. 2016. Isotropic and anisotropic elasticity and yielding of 3D printed material. *Composites Part B: Engineering* **99**, 506-513.

Zurlo G, Truskinovsky L. 2017. Printing non-Euclidean solids. *Physical review letters* **119**, 048001.

Annex 1

Chapter 7: Potential, challenges and limitations of emerging quantitative tools for plant cell mechanics

Amir J Bidhendi[1], Anja Geitmann[1,2,*]

[1]Institut de Recherche en Biologie Végétale, Département de sciences biologiques

Université de Montréal, Montreal, Quebec, H1X 2B2, Canada

[2]Department of Plant Science, McGill University, Macdonald Campus, 21111 Lakeshore, Ste-Anne-de-Bellevue, Québec H9X 3V9, Canada

*Address correspondence to: Anja Geitmann (geitmann.aes@mcgill.ca)

Running head: Tools for plant cell mechanics

7.1 Abstract

Plant tissues are a crucial source of engineering biomaterial and the microscopic structure of these tissues serves as inspiration for engineering design concepts. At the base of plant tissue architecture is a polymer material with highly complex and dynamic properties—the plant cell wall. The chemical conformation, quality of bonds and hydration state of this polymer network beget an extensive array of mechanical properties that in situ regulates growth and morphogenesis of plants across the length scales and effects passive and active behaviors of plant material in response to intrinsic and environmental cues. In recent years, there has been a joint effort to study the correlation between the mechanics and chemistry in cell wall regulation to gain insight into the cell biology and to exploit the gained knowledge for the design of biomaterials and biotechnology. As a result, a multitude of experimental and theoretical mechanical approaches has been developed or adapted to study the cell wall. However, given the complexity of the material, challenges associated with the mechanics in decreasing dimensions of the cell wall and inherent differences in the nature of the various mechanical tests warrant careful consideration to ensure that results are not only reliable but also comparable between experimental systems and approaches. Here we present a critical evaluation of available and emerging tools and mechanical modeling approaches pertinent to the measurement of plant cell wall mechanics, notably primary cell walls, that can be to some extent applicable to similar thin composites at multiple scales.

7.2 The primary cell wall as a composite material regulated in a two-way feedback loop

Plant cells are amazingly dynamic—they move, take shape, and act as force sensors and actuators, all without contractile protein-powered muscles (Bidhendi and Geitmann, 2016). Such remarkable accomplishments have incited an increasing interest over recent years, not only in the plant sciences but also in engineering and medical research aiming at creating new materials (for instance refer to Gershlak et al., 2017; Luo et al., 2015; Zurlo and Truskinovsky, 2017) that can replace alternative sources (Gershlak et al., 2017; Moroni and Mirabella, 2014)

or enhance existing designs through mimesis (Malik et al., 2017). However, to exploit plant-based concepts in intelligent designs, a better understanding of plant cell mechanics is essential.

The mechanical behavior of cells is a decisive feature that determines their functioning within the tissue and organism. This concept was recognized decades ago (Mitchison and Swann, 1954) and particularly for mammalian cells, the importance of cell mechanics is well established (Fletcher and Mullins, 2010; Hoffman and Crocker, 2009; Huang et al., 2004; Janmey and McCulloch, 2007). Changes in mechanical properties of cells and the underlying structural components, notably the cytoskeleton, have been associated with cell differentiation and fate, function and states of disease (Cross et al., 2007; Lautenschläger et al., 2009; Park et al., 2010; Zhu et al., 2000). Cell mechanics and mechanical forces exerted on cells act both upstream and downstream of cell signaling and gene expression (Miller and Davidson, 2013). In the plant kingdom, the understanding of cell mechanics has benefitted from recently intensified research. A major distinction between plant and animal cells is a relatively stiff exoskeleton encapsulating the plant cell protoplast—the cell wall. The relative stiffness of the plant cell wall compared to protoplasmic components renders it a major feature governing the mechanics of these cells. Therefore, unlike in animal cells where the mechanical behavior of the cytoskeleton governs cell mechanics, the role of these structural proteins in plant cells, while essential, is rather indirect; through their involvement in assembling the cell wall and fine-tuning its mechanics. While many concepts and experimental techniques employed for the investigation of animal cell mechanics are relevant for plant cells, the fundamental differences created by the presence of an exoskeleton warrants particular attention to address the challenges associated with walled cells.

Plant cell walls are built directly on the surface of the plasma membrane, either through exocytosis of structural polysaccharides assembled in the Golgi or through surface-located synthesis by plasma membrane-bound synthases. The type of material incorporated into the wall changes with developmental stages: all plant cell types form the thin primary wall that serves as a flexible envelope allowing the cells to grow. The secondary cell wall is generated during later developmental stages in certain cell types only. It is deposited between the existing primary cell wall and the plasma membrane. Because of its high rigidity, the formation of the secondary cell wall is associated with cessation of cell growth. Secondary walls are responsible for the

mechanics of sclerenchymatous tissues such as wood, for example, and therefore represent an attractive domain for biomechanical studies in the context of resistance to external loads on tissues and organs. However, in this review, we focus on the role of the primary cell wall that governs the developmental processes such as cell growth and morphogenesis. Therefore, unless specified otherwise, we focus on the mechanics of primary plant cell walls.

The primary plant cell wall is a dynamic structure consisting of bundled cellulose microfibrils embedded into and interacting with a matrix of mainly pectins, hemicellulose, and structural proteins (Sandhu et al., 2009). During plant cell growth, this polymeric layer yields to and is stretched by the force driving this process—the turgor pressure. Regulating this process is achieved through tailoring the mechanics of the cell wall to meet the plant developmental requirements. Cellulose is the most abundant biopolymer on Earth. The biochemical composition of this biopolymer and the quality of linkages with other cell wall constituents regulate the mechanical properties of the wall material (Bidhendi and Geitmann, 2016). Crucially, the modulation of the primary cell wall through softening or stiffening, through the selective addition of stiffer or softer material, or the modification of the intermolecular linkages between existing polymers, is associated with the promotion or restriction of plant cell growth. For example, the coordinated deposition of cellulose microfibrils is a means of stiffening the wall material either locally or in a particular orientation or both. Cellulose microfibrils are thought to be deposited and therefore reinforce the cell wall in direction of maximal mechanical stresses, in a process governed by the sensitivity and re-orientation of microtubules along the stress fields. Such preferential orientation of cellulose microfibrils presumably renders the plant cell wall a composite material whose efficient design features are optimized to withstand stresses while using a minimal amount of building materials. We have recently reviewed the major cell wall constituents and their implication for plant cell mechanics and morphogenesis (Bidhendi and Geitmann, 2016).

While the cell can actively modulate its mechanical properties to control growth, inversely, changes in the mechanical properties of the wall can also trigger cellular responses. Changes in cell wall stiffness can promote the local bundling of microtubules, for example. This, in turn, results in localized cellulose deposition which further increases the cell wall stiffness closing the feedback loop (Hamant et al., 2008). How the cell perceives local stress is still poorly

understood. However, the flux of the plant hormone auxin, an agent that regulates plant cell growth seems to play a major role in mediating the signal (Hamant et al., 2011; Heisler et al., 2010; Nakayama et al., 2012).

The mechanics of the cell wall plays a pivotal role in the regulatory mechanism governing plant cell morphogenesis and plant development. The versatility of the plant cell wall enabling it to accommodate a variety of mechanical requirements evokes self-regulating thin films. Other than bearing internal and external loads, the plant cell wall is involved in an astonishing array of functions, ranging from the forceful growth exerted by invasive cells, the rapid closure of the leaves of the Venus flytrap or of stomatal pores in response to external stimuli, to the generation of stresses in tension wood. All this is achieved without muscles and only through a functional anisotropy based on modulation of few types of polysaccharides. An understanding of how the hierarchical structure (Brulé et al., 2016) of this thin film and the arrangement of cells within plant tissues are regulated to enable such diverse functions will lead to developing novel bioinspired materials and biomimetic mechanisms. Quantitative approaches to better understand the mechanical behavior of the plant cell wall have therefore experienced considerable interest in recent years, and a surge of technological development has been dedicated to advancing the field of plant cell mechanics. These techniques are important both for the understanding the behavior of the plant cell walls and that of bio-inspired and bio-based thin films, for example plant-based scaffolds (Gershlak et al., 2017) or those used as graft in tissue engineering or in silk-based protective garments (Lawrence et al., 2009; Teulé et al., 2012).

In this review, we summarize the experimental and computational approaches used to address the need for experimental data, and we elaborate on the challenges associated with each technique. Specific attention is drawn to emerging approaches with significant potential to expand our understanding of plant cell mechanics.

7.3 Plant cell-specific considerations for the choice of experimental techniques

Most cell mechanics methods require the application of a deforming force on the cell and the simultaneous quantification of the cell's response. The deformations are generally administered in form of stretching, compression, bending, or shear and serve to infer the mechanical properties of the specimen. Because of the mechanically dominating cell wall, many of the techniques conventionally used for mammalian cell mechanics such as micropipette aspiration or optical trapping cannot be used for the deformation of walled cells since they do not produce forces that are high enough to deform the cell wall or act against the turgor pressure which typically ranges between 200 kPa to 1 MPa but may even reach 5 MPa in some cases such as in guard cells (Franks et al., 2001; Hayot et al., 2012). Further, plant cells are typically tightly linked to the surrounding tissue and the isolation of the response of a single cell is not trivial. Some of the above-mentioned techniques have been used to investigate plant protoplasts, however (Durand-Smet et al., 2014). Another difference between mammalian and walled cells arises from the wall's macromolecular structure. Mammalian cells can exhibit substantial variations in their local mechanical properties, i.e. heterogeneity, but unlike the extracellular matrix, they typically don't display strong anisotropy, i.e. direction-dependent elasticity. Heterogeneity results from the spatial distribution of intracellular organelles such as the nucleus, or formation of cytoskeletal patches. Anisotropy, when present, can be produced through a preferential arrangement of stress fibers in adherent cells for instance (Hu et al., 2004). This is a special situation, however, and typically the mechanics of animal cells is described by a set of elastic or viscoelastic parameters idealizing the cells as isotropic. In walled cells anisotropy is an important feature generated by the molecular structure of the wall. Through the preferential orientation of structural polysaccharides, the cell wall can behave highly anisotropically. The combination of heterogeneity and anisotropy in the cell wall determines the growth pattern of the individual cell (Sanati Nezhad and Geitmann, 2015). Both parameters, therefore, need to be considered when evaluating plant cell mechanics through load application and when simulating cell behavior in silico.

7.4 More than scratching the surface: Indentation-based techniques in plant cell wall mechanics

Indentation-based methods are among the most widely used techniques to study the mechanics of animal cells (Alcaraz et al., 2003; Li et al., 2008) and plant cells and tissues (Forouzesh et al., 2013; Peaucelle et al., 2011; Peaucelle et al., 2015). The concept behind these techniques relies either on inducing a specific deformation to the specimen with a rigid probe while measuring the reaction forces generated by the sample or on applying a defined force and measuring the deformation of the sample (Fig. 7-1A). The resulting force-indentation curve can be used to derive several mechanical parameters including the indentation modulus (related to elastic modulus), as well as plastic and viscoelastic properties of the specimen. Commonly, the retraction portion of the loading-unloading curve is used to calculate the indentation modulus, to exclude the plastic deformations that may arise during the loading portion. Viscoelastic properties are measured either by dynamic indentation (resulting in measurement of complex modulus that holds information on both elastic and viscous properties of the cell wall) or by keeping the load or indentation depth constant and measuring the subsequent changes in indentation depth or force, respectively. Several excellent reviews describe the fundamentals of indentation techniques in probing the mechanics of biological materials including plant cells (Guz et al., 2014; Haase and Pelling, 2015; Kirmizis and Logothetidis, 2010; Kuznetsova et al., 2007; Maver et al., 2016; Milani et al., 2013; Routier-Kierzkowska and Smith, 2013).

The advantages of indentation techniques include an excellent resolution (spatial and force), minimal sample preparation allowing for *in vivo* studies, and the ability to acquire stiffness maps of surfaces. Based on the size of the indenting tips, depth of deformation or magnitude of measured forces, indentation techniques range from atomic force microscopy (AFM) providing piconewton force resolution to variations of microindentation systems (Cretin and Sthal, 1993; Routier-Kierzkowska et al., 2012). Cell compression methods may be considered as a special case of indentation when the size of the flat indenter becomes considerably large compared to the cell size. Cell compression has been used for tomato cells (Wang et al., 2004) and plant cell protoplasts (Durand-Smet et al., 2014) allowing for the calculation of elastic and time-dependent properties of the cells.

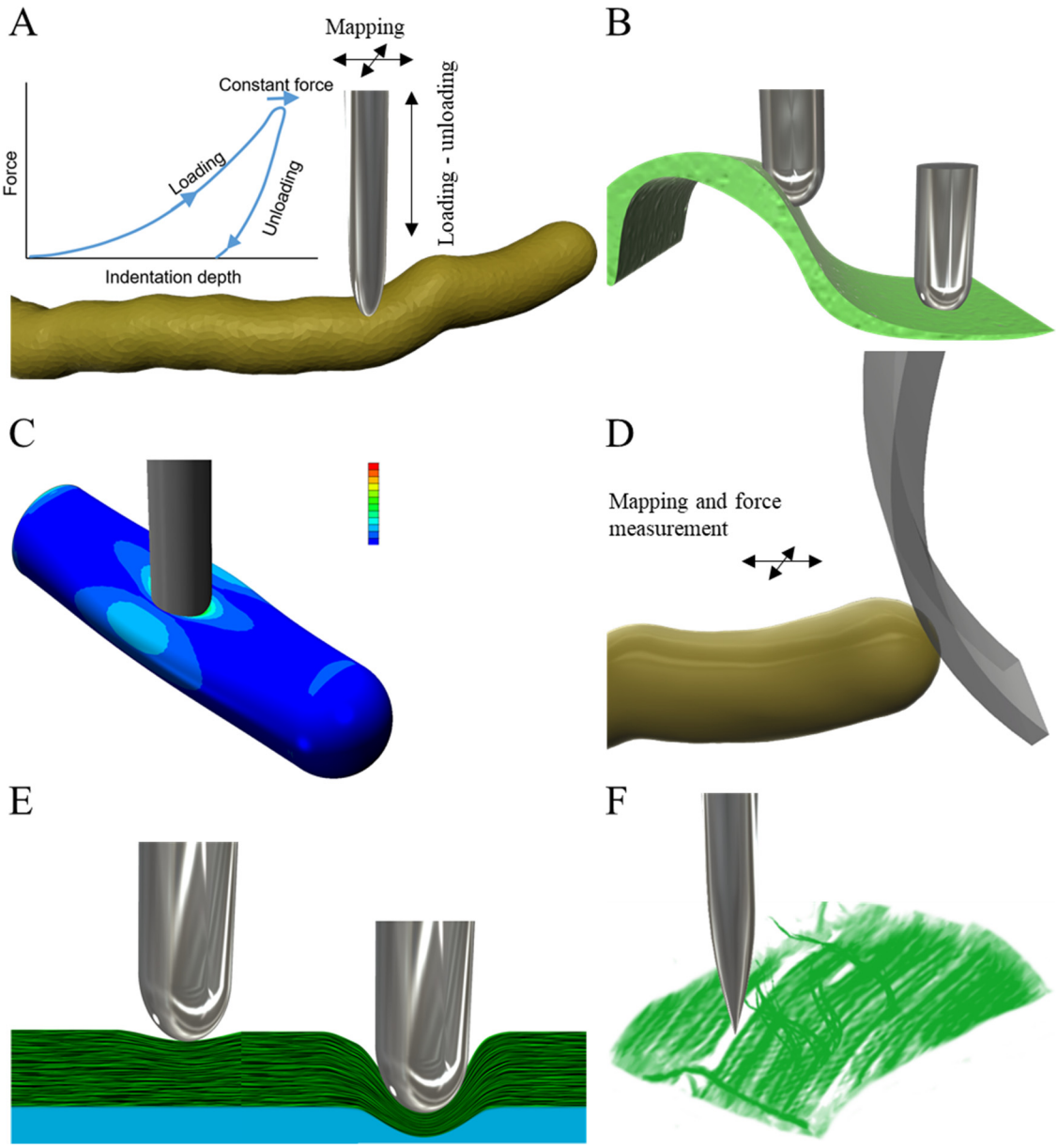

Figure 7-1. A) Schematic of a typical indentation experiment showing loading, constant force (holding) and unloading segments of the force-indentation trace. Surface rastering and indentation/force sensing directions are perpendicular to each other. **B)** Tip geometry and curvature of the specimen influence the contact quality and therefore the measured forces. **C)** Aspect ratio of the sample affects the stress and strain fields under indentation. **D)** Concept of lateral force microscopy. The probing tip or the cantilever deflects or distorts by lateral forces. Rastering is performed parallel to the surface. **E)** The depth of the indentation determines to what extent the inner layers of a single wall, as well as the turgor pressure contribute to the measured forces. **F)** Fibers may move apart by the indentation of a sharp probe. This displacement has the potential to alter the measured stiffness.

Indentation techniques have contributed significantly to our understanding of primary plant cell wall mechanics and cell growth in the past decade. Marga et al. (2005) used nanoindentation combined with scanning electron microscopy to investigate how expansin proteins affect cell wall creep and growth. Microindentation revealed a significant correlation between the changes in the status of the cell wall polymer pectin and the cell wall mechanical properties required for polar growth in plant cells (Parre and Geitmann, 2005; Zerzour et al., 2009). Combining fluorescence microscopy and nanoindentation, Milani et al. (2014) correlated the alterations in stiffness of shoot apex cells in *Arabidopsis thaliana* in response to gene expression. Peaucelle et al. (2015) used nanoindentation to investigate changes in pectin and cellulose orientation related to mechanical anisotropy prior to cell growth symmetry breaking in hypocotyl epidermis, revealing a role for pectin demethylation in regulating cell growth dynamics. Yakubov et al. (2016) exploited nanoindentation to acquire a map of mechanical heterogeneity in the primary cell wall of suspension cultured cells and leaf epidermal cells of *Lolium multiflorum* and leaf epidermal cells of *Arabidopsis thaliana*. Besides the characterization of local mechanical properties of the cells and tissues, indentation techniques enable topographical imaging of the specimen. Such a capability has been used in recent studies to visualize the orientation of cellulose microfibrils. In such an approach, cellulose fibrils must be exposed to be accessible to the indenter. This would require partial removal of substances such as pectin or the cuticle, although reportedly, intact non-treated outer cell wall surfaces seem to have been used in at least one study (Sampathkumar et al., 2014a). Alternatively, the inner face of the wall (closest to the plasma membrane) is investigated after breaking open the cells (Xi et al., 2015; Zhang et al., 2014; Zhang et al., 2016). Since the inner face is the newest layer deposited, it is considered by many to be the most influential in directing the cell growth.

Despite the increasing number of indentation-based studies, significant effort is still being put toward addressing methodological concerns, developing devices and introducing new experimental strategies. This indicates the challenges particular to indentation techniques and especially their application to plant cell walls to be overcome before the techniques reach reproducibility and reliability required for acquisition of absolute rather than comparative data. One of the main challenges in indentation-based measurement of plant cells is posed by the typically high curvature of the outside facing cell walls (outer periclinal walls of the epidermis).

Since the indenter tip measures the forces perpendicular to the surface, the angle between the sample surface and indenter tip in highly curved regions may affect the readings due to a decrease in contact surface (Fig. 7-1B). A potential way to avoid such geometrical complications is to keep the indenter perpendicular to the surface at all times which, however, would require a system that can rotate the tip to match it to the normal axis of the specimen at all subcellular locations. Available systems do not allow for such flexibility. This oblique contact has been reported to be associated with both underestimation and overestimation of the measured value of stiffness. Besides the curvature of the outward facing cell wall, the dimensions of the entire cell can also influence the stress and strain fields and presumably the modulus measurements acquired through indentation (Fig. 7-1C). Several papers have discussed the discrepancies arising from the tip-sample angle of contact (Braybrook and Peaucelle, 2013; Milani et al., 2013; Mosca et al., 2017; Routier-Kierzkowska et al., 2012), but further studies are warranted to overcome the tip-sample angle and geometry problems. We surmise that a promising strategy in the indentation-based study of plant cell wall stiffness would be to measure lateral forces in conjunction with vertical indentations. The deflection or torsion of the tip or the cantilever of known stiffness, depending on the configuration, can measure the stiffness of the sample (Fig. 7-1D). Lateral force microscopy (LFM) is a special application of AFM commonly used in nanotribology to study the frictional forces in materials consisting of varying surface properties. In LFM the tip moves parallel to the surface, and lateral forces are measured. As LFM measures frictional forces (that occur parallel to the plane of the sample), it can potentially provide a measure of in-plane elasticity of the sample (Perry, 2004), although separating frictional forces from the effect of sample topography is not trivial (Maver et al., 2016). Combining perpendicular and lateral scanning modes may provide valuable data on the mechanics of the plant cells in the future.

Another challenge to be considered for indentation-base measurements is the appropriate indentation depth. Many plant tissues are covered by a lipidic layer, the cuticle. In shallow indentations, the effect of this layer might considerably affect the readings. Additionally, in shallow indentations, the mechanical properties measured are those of the outer wall layers (Fig. 7-1E). Given that these outer layers may structurally differ from the inner cell wall layers, extrapolation from outer wall measurements makes assumptions that may not be justified (e.g.,

cellulose orientation may not remain constant in thickness). In measurements with deeper indentations approaching the thickness of the cell wall, the contribution of the turgor pressure and substrate becomes significant. Interestingly, several studies have taken advantage of such an effect solving the system of equations with two variables to measure both the cell wall mechanics and the turgor pressure. This has been accomplished either by combining data from varying indentations depths (Forouzesh et al., 2013) or by combining deep indentations with osmotic treatments (Beauzamy et al., 2015; Weber et al., 2015). Computational modeling has been used previously to determine two or more unknowns from single indentation experiments, such as Young's modulus and Poisson's ratio (Zheng et al., 2009). Indentation approaches provide a minimally-invasive alternative to measure the turgor pressure in plant cells shown to produce values similar to those obtained by other techniques such as pressure probe (Green, 1968) and ball tonometry (Lintilhac et al., 2000; Wei et al., 2001). It should be noted that, regardless of the challenges associated with and specific to plant cell walls, those related to the shape of the indenter tip and indentation depth are inherent to indentation techniques and need to always be considered in the context or tip-sample contact (Han et al., 2016).

Another consideration pertaining to indentation data in the plant cell context is the question how the modulus acquired by the out-of-plane indentation of the specimen corresponds to in-plane properties of the cell wall. Usually, the flexural rigidity of the cell wall is neglected, and the properties measured by indentation are assumed to apply to the tensile properties. However, even if this assumption held, the indentation modulus may not directly correlate with the cell wall properties pertinent to plant cell growth, due to the highly anisotropic nature of cell walls. The modulus measured by indentation is commonly an average modulus for the longitudinal and transverse directions. For anisotropic materials, since the strain is applied in all directions, the indentation modulus is an average of the stiffness in different directions not directly related to the directional stiffness of the material (Eder et al., 2013). Therefore, the data acquired by indentation techniques must be reconciled with the in-plane tensile properties of the plant cell wall and some degree of directional information must be integrated. In a recent study, Tanguy et al. (2016) measured the elastic modulus of plant fibers used in reinforcement of composite materials and compared the values acquired by tensile and nanoindentation methods. The results obtained for various fibers such as sisal and Eden flax fibers indicated a considerable

underestimation of the elastic modulus of the samples obtained using indentation compared to tensile testing. These results clearly suggest that the indentation modulus may differ greatly from the elastic modulus of the cell wall corresponding to the in-plane resistance against tension along the main orientation of the fibers. This begs for caution using indentation techniques for evaluation of strongly anisotropic materials such as plant cell walls. As another source of this discrepancy, Tanguy et al. (2016) suggest that by pushing the nanoindenter into the sample, the fibers can slightly separate (Fig. 7-1F) thus contributing to the underestimation of the computed value for the indentation test. The authors tried to establish a relationship between the nanoindentation and tensile estimated values for elasticity. However, it was suggested that such a ratio might vary from tissue to tissue due to variations in microfibrillar angles. In fact, the higher the degree of anisotropy, the larger the difference between the outcome of tensile tests and nanoindentation. However, by application of a correction coefficient, reasonable estimates can be found. This is useful when other techniques such as tensile testing prove difficult or impossible because of the small size of the sample. To circumvent the challenges associated with correlating the modulus obtained by indentation to the tensile modulus, Nakamura and Gu (2007) used two indenter tip geometries to induce different strain fields. This allowed acquiring more data of the samples used in this study—thermally sprayed coatings for which transverse isotropy was assumed. The authors used an inverse search method to obtain the elastic properties of the thin films along the two perpendicular directions. Similar methods may be promising in the investigation of cell walls with high anisotropy. Several works have provided the theoretical and experimental basis of anisotropic indentation providing the framework for potential adaptation to the anisotropic walls of growing plant cells. Importantly, the conceptual framework will allow extraction of a complete description of the elastic tensor rather than reducing the properties to a single Young's modulus (refer to Jäger et al., 2011; Vlassak and Nix, 1994). We posit that combining these measurements with monitoring the strain pattern using fluorescent markers would also allow obtaining an estimate of the anisotropy factor (modulus along and transverse to the fibers). This concept is not without technical challenges since the appropriate procedure to place fluorescent markers would have to be established, and 3D data analysis would be time and resource-intensive (for instance refer to Kim et al., 2015).

Progress in experimental strategies will require development and incorporation of the material models to interpret the indentation test data adequately. The intricate nature of the cell wall network, the contact properties, and deformation complexities require sophisticated analytical or computational modeling to extract the mechanical parameters that need to be addressed in future studies. We will take up this point in the modeling section.

7.5 Listening through walls: acoustic measurements of cell mechanics

Acoustics are employed in various types of imaging and elastography techniques. These include types of atomic force microscopy, specifically ultrasonic atomic force microscopy and atomic force acoustic microscopy in which the acoustic waves are employed to either vibrate the cantilever or the sample at a frequency (for instance refer to Stan and Solares, 2014). Ultrasonic encoding of light in ultrasound-modulated optical or fluorescence imaging has been demonstrated to enable acquiring deep-tissue images of biological materials beyond the ballistic regime used in conventional light microscopy techniques (Wang et al., 2012). However, here we would like to discuss the direct use of acoustic waves for imaging and mechanical testing of biological materials particularly focusing on plant cells. Sound waves can be employed for mechanical characterization of a specimen either by recording the changes in frequency and amplitude of sound upon interacting with the sample such as in scanning acoustic microscopy or registering the energy shift of photons upon interacting with the acoustic phonons—spontaneous or stimulated acoustic waves—in sample structure. Importantly, the acoustic-based techniques allow for evaluation of elastic and viscoelastic properties of the cell at various depths rather than only probing the surface, and have the potential to provide subcellular resolution. Further, the non-destructive nature of the acoustic approaches for mechanical characterization makes them suitable for *in vivo* studies which is essential for the real-time analysis of the morphogenetic dynamics of plant cells (Altartouri and Geitmann, 2015; Bidhendi and Geitmann, 2016).

Acoustic microscopy can be used for non-destructive imaging and mechanical characterization at the surface and subsurface of biological materials. Scanning acoustic microscopy is a current version of acoustic microscopy. In this technique, the electric signal

received by a piezoelectric transducer is converted to an acoustic wave focused into an acoustic beam by a lens. The modes of scanning are categorized into transmission and reflection depending whether which type of waves are collected by the receiver (Fig. 7-2A, B). Acoustic waves can be generated in either pulse or continuous modes. The transmission mode can work in either configuration, whereas the reflection mode only operates in pulse mode as the transducer and receiver are the same (pulse-echo mode). Depending on the scanning method and reconstruction of the image in terms of point, plane or 3D scanning, several modes have been developed such as the commonly applied C-mode scanning acoustic microscopy (for instance refer to Zhao et al., 2012). Passing through the coupling fluid, the acoustic beam enters the sample. The acoustic wave can be reflected, scattered or attenuated. The portion of the acoustic wave reflected off the specimen is collected back at the transducer that is in listening mode and converted into an electric signal. Alterations in amplitude and frequency between the probing and reflected signals are recorded. The coefficient of reflection of the sound wave at interfaces present in the specimen is correlated to their acoustic impedance mismatch. By using homogeneous calibration materials of known acoustic impedance, the acoustic impedance of the scanned planes can be assessed from the pixel data. The acoustic impedance is correlated with the mass density and longitudinal elastic modulus (in direction of sound propagation) of the specimen. Therefore, the data acquired from the reflected sound can be used to reconstruct the stiffness map of the specimen (Rupin et al., 2009). The range of resolution for scanning acoustic microscopy is versatile and extends from a few nanometers in superfluid helium to several micrometers (Foster and Rugar, 1983; Xi et al., 2013), depending on several parameters including the acoustic beam spot size and the frequency. The resolution and depth of imaging have an inverse relationship. By increasing the frequency, higher resolution of imaging is possible (Rayleigh criterion) while the depth of imaging is forfeited. At a frequency of 2 GHz and room temperature using deionized water submicrometric resolutions have been achieved (Johnston et al., 1979). For embryonic chicken heart muscle cells, at a sub-gigahertz frequency and room temperature, subcellular compartments were resolvable with a resolution close to a micrometer (Weiss et al., 2007), which reconfirms the potential of the technique to acquire stiffness map of living cells at the microscale.

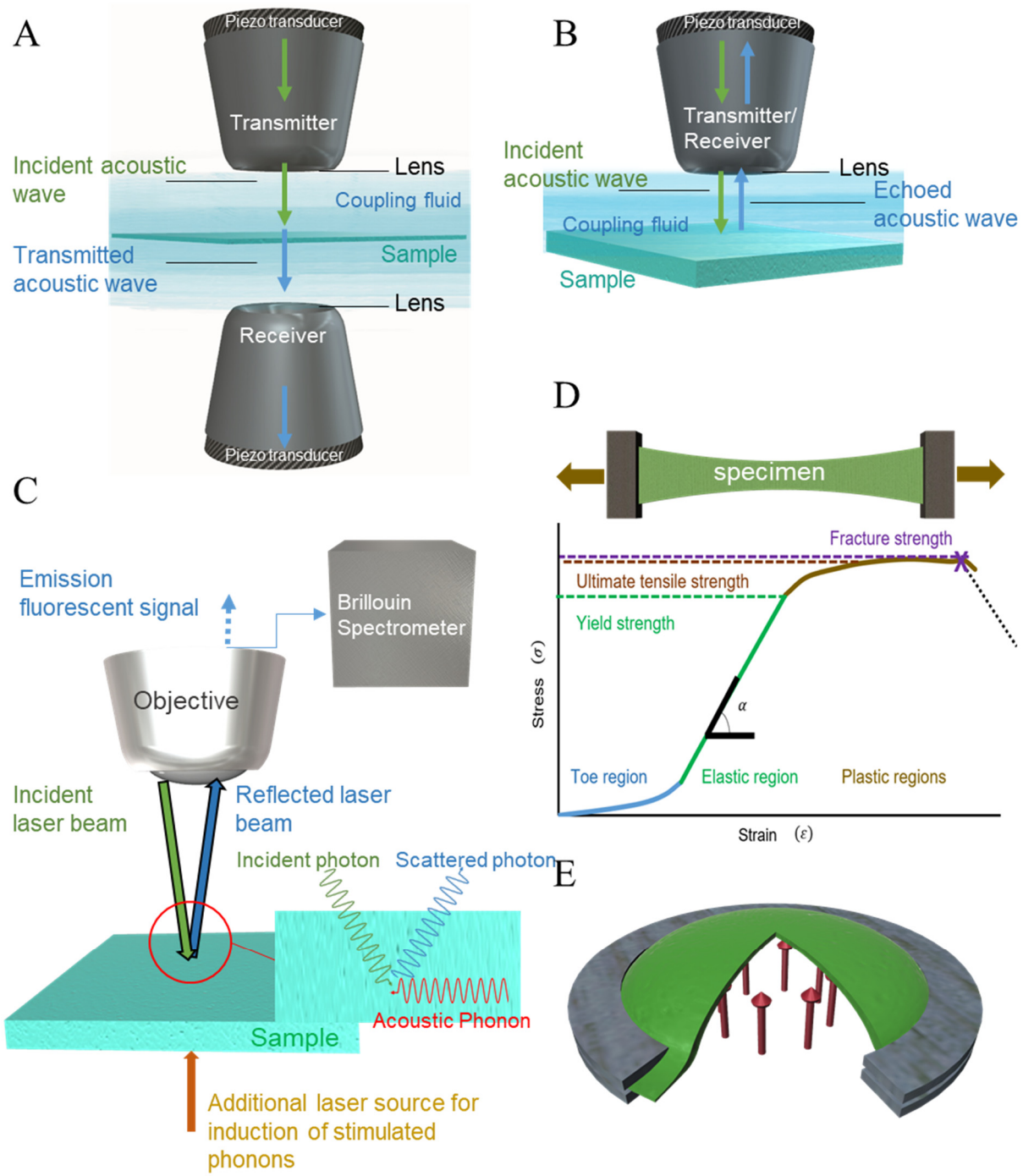

Figure 7-2. Concept of scanning acoustic microscopy in **A)** transmission **B)** reflection modes. **C)** Illustration of the use of Brillouin scattering of light for mechanical imaging in conjunction with fluorescence microscopy. An additional beam can be used for induction of stimulated phonons. **D)** Generic stress-strain graph for the loading portion of a tensile testing. In case of a linear elastic behavior, the slope of the elastic region is used to calculate the Young's modulus of the material. **E)** Cutaway view of thin membrane specimen fixed between two rings and stretched by hydraulic pressure in a bulge test.

Application of scanning acoustic microscopy in mechanical testing ranges from non-destructive detection of subsurface flaws and cracks in products, evaluation of food texture, to detection of mechanical changes indicative of pathology in tissues such as myocardium or kidney (Saijo et al., 1997; Sasaki et al., 1997). Application of scanning acoustic microscopy to study mammalian cell mechanics has become relatively common. For instance, it has recently been suggested as a means for stain-free rapid diagnosis of cancer cells based on their altered properties compared to normal cells in speed and attenuation of sound (Miura et al., 2013). Regarding the mechanics of plant cells, acoustic elastography is perhaps the most underused technique that holds great potential. Tittmann and Xi (2014) used high-frequency scanning acoustic microscopy to investigate the feasibility of its application to investigate primary plant cell wall mechanics. They showed that onion epidermal cells can be imaged with a high-frequency scanning acoustic microscope and this technique can discriminate changes in elastic properties of the cell wall upon application of the enzyme pectinase. Modulation of pectin in the epidermis cell walls was revealed by a reduction in velocity of reflected waves implying a reduced stiffness of the structure (suggesting an increase in attenuation owing to changes in the pectic network) (Tittmann and Xi, 2014; Xi et al., 2013).

Mechanical investigation of primary plant cell walls using scanning acoustic microscopy is not well explored, and potential challenges for plant cell applications are largely unknown. In the short paper published by Tittmann and Xi on imaging of onion epidermal cells using high-frequency scanning acoustic microscopy, the contrast images seem to emphasize the cell borders (i.e. anticlinal walls) and reveal little information on the variation of stiffness in periclinal (outer) walls. Interestingly, however, the technique has revealed details at the cell-cell interfaces potentially providing information on the middle lamella—a pectin-rich layer responsible for cell-cell adhesion in plant tissues. The typical output of scanning acoustic microscopy is acoustic impedance information not directly comparable to results of other types of measurements, typically expressed as Young's modulus. Therefore, a challenge is to develop appropriate analytical and computational models to express the results in conventional mechanical terms. Further, extracting Young’s modulus from the longitudinal stiffness requires a presumption of a set of values such as the Poisson’s ratios in different directions. Since the cell wall material is highly anisotropic in-plane compared to the scanning direction, accurate

extraction of the in-plane properties of the wall based on this technique warrants further studies to provide the supporting theoretical framework. Importantly, while the acoustic impedance map of the specimen is used to interpret its stiffness, the density of the material is presumed to be known or constant over a region. However, this is not necessarily true as cell wall thickness and packing of the porous network can vary. Therefore, use of complementary techniques to assess the spatial and temporal variation of the mass density by techniques such as micro-computed tomography is warranted to acquire elasticity information from the acoustic impedance data (Raum et al., 2006; Rupin et al., 2009). While acquiring nanoscale maps of the cell wall stiffness is theoretically possible using scanning acoustic microscopy, so far the resolution for living cell applications has remained close to a micrometer which is not sufficient for the investigation of cell wall components. However, the resolution of this technique seems improved owing to rapidly developing the technology. Increasing the acoustic frequency *per se* to improve the resolution is not always practical. One reason is the strong attenuation of the sound waves in the coupling fluid that increases with the frequency as the wave propagates. One way to avoid this is to decrease the traveling distance of the sound wave in the media which requires the generation of very short pulses of acoustic waves so the desirable reflected wave is separable from the unwanted reflections. Combining picosecond ultrasonic with scanning acoustic microscopy, Che et al. (2015) used short-pulsed laser wave instead of piezoelectric transducers to generate ultrashort-pulsed acoustic waves and obtained a resolution of 100 nm using reflection mode scanning acoustic microscopy. Another point is to ensure that ultrasonic exposure does not change the cell wall properties thus potentially inducing artifacts. Although acoustic elastography is classified as a non-destructive test, Pieczywek et al. (2017) showed that ultrasound treatment over several minutes could cause the formation of voids in apple tissue. They suggest that the treatment increased the solubilization of pectin in the cell wall, resulting in a dramatic decrease of the measured wall stiffness.

Another form of mechanical imaging, Brillouin scattering microscopy, takes advantage of inelastic scattering of light in interaction with spontaneous or stimulated phonons, *i.e.* acoustic waves (Ballmann et al., 2017; Scarcelli and Yun, 2008). Interaction with compression waves (correlated to mechanical properties of the specimen), results in a shift in frequency and amplitude (energy) of a part of the scattered light (Brillouin frequency shift) (Fig. 7-2C).

Analysis of these modulations can reveal the acoustic vibrations of the structure and therefore its mechanical properties. The first applications of Brillouin scattering for mechanical characterization of biological materials are not very recent. For instance, Harley et al. (1977) used this technique to study the mechanics of rat tail tendon. Over the years, the hardware and the theories have been considerably improved, however, and the technique has gained a significant popularity with a renaissance in the investigation of mechanics of biological materials (for instance refer to the recent review by Meng et al., 2016).

Brillouin scattering microscopy studies generally report a submicron resolution for measurements of local stiffness moduli, with some variations of the technique reporting a resolution as good as 10 nm that has enabled imaging of the fibrillar structures of cells (Dehoux et al., 2015). Elsayad et al. (2016) combined fluorescence microscopy with Brillouin scattering (Fig. 7-2C) to study onion epidermal cells and *Arabidopsis* hypocotyl and root cell walls. Cell wall stiffness and the influence of turgor pressure on the apparent stiffness of the cell wall were studied at submicrometer resolution. This study shows the potential of combining the two microscopy techniques to investigate modulation of stiffness and turgor pressure in the whole organ with a cellular resolution while optically monitoring the subcellular compartments based on conventional fluorescence techniques. However, some conclusions may require clarification, for example, the relationship between turgor pressure and the measured "cytoplasmic stiffness". As the authors mention, the term "stiffness" used in such a study is more related to the bulk modulus of the material rather than its Young's modulus and therefore reflects material compressibility than actual stiffness. Eventually, from the images so far published for these techniques, like acoustic microscopy, these optoacoustic techniques also focus on cell borders (presumably due to vertical anticlinal walls) rather than providing information on the periclinal walls excluding the shape and structural stiffness. In this context, from the images, the technique reports a higher "stiffness" for the nucleus than the periclinal cell wall. This might be due to placement of the focal plane in Z (axial) direction. However, considering that stiffness of the nucleus is in the range of kPa (for example see Guilak et al., 2000) while cell wall stiffness is typically in the MPa range, further studies on the periclinal wall mechanics with this class of techniques is certainly warranted to explain this phenomenon. Picosecond ultrasonics allows for a range of closely related optoacoustic configurations that take advantage of Brillouin scattering

of incident light for acquiring mechanical images of the sample. However, in this technique that can be broadly considered as "stimulated" Brillouin scattering microscopy, a second laser beam is used (in heating a thermoacoustic generator) to induce short-pulsed acoustic vibrations into the specimen rather than relying only on inherent phonons. This strategy increases the efficiency of the Brillouin scattering and allows for resolvable scanning of smaller regions (Dehoux et al., 2015; Mechri et al., 2009). Gadalla et al. (2014) used this approach, to study the wall of onion cells with a submicron lateral and a nanometer in-depth resolution. The authors report a stiffness value of 13 GPa for the cell wall in the onion epidermis, which is interestingly close to upper range of the modulus values reported for cellulose microfibrils. Based on the attenuation, they estimate the loss modulus (a measure of viscous effects) as 1.3 GPa. They suggest that the ratio of the loss to storage (stiffness) moduli is close to values for glass-forming polymers at glassy state. Therefore, the authors indicate that the rheology of the cell wall is governed by the glass-like behavior of the pectin-cellulose components. Overestimation of the stiffness, compared to other mechanical techniques measuring the cell wall, is apparently a common issue with acoustic techniques (Antonacci and Braakman, 2016; Rupin et al., 2009). Further, the mechanical properties are tested in direction perpendicular to the onion epidermis rather than in-plane of the epidermis. Since cellulose microfibrils would presumably lie mostly in-plane rather than extend in the thickness of the cell wall, it is, therefore, not clear what is being measured. This is important since eventually, it is the "in-plane" tensile behavior (whether expressed by an elastic modulus, rate dependent viscoelastic parameters or alternative ways to define extensibility, as discussed before) of the cell wall that correlates with the growth of plant cells. The connection with its compressibility in the context of growth is less clear, all the more since this parameter is strongly affected by water in the material. By combining longitudinal and shear phonons, the complete elastic tensor of the material around its axes of symmetry can be calculated. As with acoustic microscopy, to calculate the longitudinal modulus from the Brillouin frequency shift, the density of the material is required (for more details on the theory refer to references presented thus far, e.g. Meng et al., 2016).

Acoustic techniques can be used for noninvasive real-time measurements of elastic and viscoelastic properties of plant cells. Further, they allow visualizing cells embedded within a thicker tissue, thus providing a potential tool to validate the hypothesis that walls within the

tissue might be more important for determining cell morphogenesis and the mechanics of the whole tissue than previously thought (Baskin, 2005). However, the output from these studies such as spectral shifts, reflected wave velocities, or the longitudinal or transverse moduli do not directly translate into a more tangible stiffness matrix or Young's modulus (in case of isotropy) to sufficiently describe the elasticity of the material in all three dimensions, comparable with results of other techniques such as AFM or tensile tests (Elsayad et al., 2016). In most studies, the value for the mass density of the specimen, which is essential for calculation of the stiffness is adopted from the literature. If the on-site measurement of the density of the cell wall is impossible, this lack of tissue-specific data can pose a serious challenge to be addressed by techniques such as micro-computed tomography. While the techniques have come a long way for acoustic characterization of materials, appropriate models are needed to interpret these data. Acoustic microscopy can be coupled with other types of microscopy to simultaneously acquire different types of data from the same samples. The combination of acoustic techniques such as Brillouin scattering and Raman or fluorescence microscopy (see for instance Elsayad et al., 2016) would open the door to the possibility of visualization and correlation of chemistry, mechanics, and development. First steps in this direction have been taken (Scarponi et al., 2017) and we may soon mechanically-image the cell wall while dynamically follow the changes in pectin network, its association with cellulose microfibrils and the effect of their interconnections on cell wall mechanical parameters, in real time.

7.6 The classic test: tensile measurement of cell wall properties

During tensile testing, the sample is stretched, and the force required for the elongation is measured allowing for determination of elastic, viscoelastic and plastic properties. Uniaxial stretching is the most widely applied type of tensile testing in the characterization of biological materials (for instance refer to Abasolo et al., 2009; Cavalier et al., 2008; Pena et al., 2004; Ryden et al., 2003; Wei et al., 2006; Wei et al., 2001). The choice of a uniaxial set-up is mainly due to simpler device configuration, relatively simple sample geometry and straightforward calculations pertaining to this test. The force and displacement measurements are converted into a stress-strain graph, commonly based on:

$\sigma = \frac{F}{A_0}$ and $\varepsilon = \frac{L - L_0}{L_0}$

Where A_0 and L_0 are original cross section area and length respectively. σ and ε are nominal or engineering stress and strain values (as opposed to true stress and strain when actual cross section area and length are used, quantities that continuously change during the elongation). From this curve, several material parameters are extractable. A generic stress-strain curve typically consists of three main regions (Fig. 7-2D), a "toe" region that is potentially indicative of initial straightening of the specimen or rearrangement of its load-bearing fibers, and the elastic regime which is then followed by the plastic deformation zone. The slope of the reversible part of the graph is used to determine the elastic constants of the specimen (Young's modulus for a linearly elastic material). Ultimate tensile strength and fracture strength of the sample can also be calculated from this graph. As with other modes of mechanical testing, plastic deformation of the sample must be excluded in the calculation of the elastic constants (Young's modulus). Tensile testing may be performed in a loading and unloading manner, and the latter can be used to this end (Luczynski et al., 2013). In many applications, especially in small deformations, the reversible deformation remains linear. However, material nonlinearity may arise in tensile testing of biological samples due to their highly complex structure and because of large strains. Therefore, appropriate material models must be used to describe the behavior of the samples when such effects are not negligible. Nonlinear elastic models such as various hyperelastic functions can be fitted to the stress-strain curves to extract the elastic constants (for instance see Rashid et al., 2012). It should be noted that, while the generic strain-stress curve presented here, typical of ductile metals, is useful to introduce a number concepts, actual tensile graphs of biological tissues including plant specimens usually deviate greatly from this behavior (for example refer to Spatz et al., 1999). This may include a sudden failure at maximum stress rendering the tensile strength and fracture stress to overlap, and sometimes an absence of any perceivable linear zone even at small strains (see the black line in Fig. 7-2D from tensile test on a piece of onion epidermis).

Tensile testing of conventional materials at macroscale is relatively well defined by various standards (such as American Society for Testing and Materials (ASTM) standards). In most standard tensile tests, the sample shape and dimensions, boundary and loading conditions are standardized, such as a dogbone shape for flat specimens. This shape ensures a uniform (homogeneous) strain, and that maximum stresses and fracture occur in the mid-region or gauge

area of the specimen rather than near the clamp region. In non-uniform strains, the values found might greatly deviate from the actual overall properties of the tissue. Additionally, such standardization allows for results of various studies to be comparable. Calculation of material properties for these standard samples is relatively straightforward. However, tensile testing of biological materials, such as plant tissues is inevitably associated with challenges, and the solutions are often custom tailored and require outside-the-box approaches. Because of the delicate and miniature nature of certain plant cell materials, preparing predefined standard shapes is often not possible. Tensile tests of plant specimens have often been limited to tissue scale rather than using cell-sized samples. Few exceptions are giant internode cells of algae (Metraux and Taiz, 1978; Toole et al., 2001) or single fibers of the secondary wall (Burgert and Keplinger, 2013; Sedighi-Gilani et al., 2005) where the single-celled or subcellular sample strips were large enough for conventional tensile testing configurations. In higher plants, the cells are much smaller in size and extraction and handling of samples containing a few cells or subcellular fragments is a considerable challenge. Even samples at the tissue scale pose certain concerns to be accounted for. Tensile testing of specimens with dimensions below millimeter width requires manipulation and handling strategies pertinent to the fragile nature of these specimens (refer to an in-depth discussion of available techniques for manipulation, gripping and force/strain measurement at increasingly smaller length scales in Gianola and Eberl, 2009).

One challenge associated with handling is related to sample alignment regarding force axis. Deviation from parallel alignment can cause a considerable error in measurements. This is especially critical in case of plant tissues with pronounced anisotropy due to cellulose fibers. Usually, establishing the orientation and degree of anisotropy cannot be done ad hoc but requires separate studies and a misalignment resulting from the lack of information on this parameter can only further confound the results. Another critical factor is the aspect ratio of the samples. In plant research, sample dimensions are often limited by the dimensions of the organ under study (which is a considerable constraint with small model plants such as *Arabidopsis thaliana*). Determining the dimensions of the tensile sample in the absence of well-established standards requires justifiable choices and adequate interpretation of the results. This need is illustrated by various studies showing the significant dependence of the measured tensile modulus on aspect ratios of the tensile specimen. Carew et al. (2003) conducted a comparative study on porcine

tissue and found a considerable dependence of the measured stiffness on sample aspect ratio. Interestingly, their results also indicate that the measurements can vary among specimens of different size even if the aspect ratios are kept constant. Similar size effect issues have been discussed in other studies pertaining to tensile properties of soft tissues (e.g., refer to Anssari-Benam et al., 2012). Therefore, comparing tensile properties of samples at different stages of growth must be approached with care as the results can be size-dependent. Calibration and comparison studies to allow for better understanding of this phenomenon in plant tissues and to establish standards for dimensions of plant specimens are deemed crucial.

Preparation of samples poses another significant challenge for tensile testing. Cutting of sample strips needs to be accurate without tears and flaws at edges that would lead to stress concentration and premature failure. Rapid dehydration of specimens can alter the rheology of pectin and that of the cell wall (Bidhendi and Geitmann, 2016). Measurement of initial length and cross-section area is also not without challenges. Saxe et al. (2016) studied the effect of age on the mechanics of the elongated zone (below the growth zone) in etiolated *Arabidopsis* hypocotyls. They correlated the mechanics of this zone to material density, geometry and cellulose content. Their results suggest that the tensile stiffness of the samples increased from one developmental stage to the next. However, interestingly, a biochemical analysis showed a decrease in cellulose content of the cell walls over the same period. These interesting yet confounding results may indicate that cell wall stiffness is not solely governed by its cellulose content but can also be modified by the reorientation of these fibers and other wall polymers such as pectin. On the other hand, this study also highlights the necessity to carefully account for all parameters such as the cross-sectional area of samples. Judging from the published figures, the hypocotyls measured in this particular study exhibited slightly higher cross section in some samples harvested at the earlier developmental stage and, unless this parameter was incorporated in the calculation, it may have caused the deduced tensile stiffness properties to be underestimated. This indicates one of the significant challenges faced in the tensile testing of plant tissues—the quantitative determination of initial parameters, and it emphasizes the necessity to establish protocols enabling consistent measurements of sample dimensions (Burgert et al., 2003; Haag and Müssig, 2016; Sedighi-Gilani and Navi, 2007).

Gripping of the specimens at the stretching ends is yet another critical technical consideration for tensile testing. Challenges arise due to the possibility of slippage and damage near the grips, that can significantly affect the readings in seemingly successful experiments (Ng et al., 2005; Sun et al., 2005). Glues, wires, and abrasive papers have been used to attach samples to the load or displacement extensions to avoid or reduce slippage (Eder et al., 2013). Glue such as cyanoacrylate or dental cement has been used, and epoxy has been suggested to alleviate the stress concentration in the attached end regions (Eder et al., 2013; Saxe et al., 2016; Yu et al., 2011). However, application of glue can cause the generation of prestress in the specimen upon curing to be released prior to the experiment. The gripping challenge is exacerbated in experiments with slow load application such as in creep tests in which the specimens have a higher tendency to slip. Due to stress concentration and microscopic damages induced by the grip, many specimens break prematurely near the grip and sample interface. Such occurrences must be excluded from the data pool.

While measurements of elastic modulus or failure strength typically rely on the administration of a continuously increasing force till fracture, the application, and maintenance of a constant pre-failure force or elongation is employed for evaluation of time-dependent properties. These cases denote the relaxation or creep tests, respectively. Applying a constant load is performed either by attaching a constant weight to one side of the sample or by establishing a force feedback loop that ensures a constant force as the sample is stretched between the load sensors. Creep tests are of particular interest in plant cell mechanics and morphogenesis since they can shed light on the expansion of the cell wall under a constant turgor-driven load. Creep tests have contributed significantly to our understanding of the regulation of cell wall expansion by wall modifying enzymes (Cosgrove, 1989; Durachko and Cosgrove, 2009; Keller and Cosgrove, 1995). The outcome of such experiments is often expressed as “extensibility” in cell wall loosening studies, which may be defined as dynamic creep of the cell wall as it is being modified by wall modifying enzymes or other factors. The subtle difference with a traditional view of creep may be explained by ongoing enzymatic modifications of the wall properties pertaining to the extensibility while creep properties of an inactive material is not modulated over time (for a further discussion of this matter refer to Cosgrove, 1993; Cosgrove, 2015). In this context, it is worth drawing the attention of the reader

to the existence of two apparently parallel views on cell growth. While in many studies, the mechanics of the cell wall has been explicitly or implicitly considered to be associated with a form of influence on cell growth, some researchers have expressed doubts on this issue. This second argument is that growth is controlled by cell wall loosening, such as by act of expansins, and such action may not be sufficiently addressed with reporting alterations in Young's modulus of the wall. This alternative view does not dismiss the importance of cell wall mechanics, but questions the extent of the relevance or mechanical parameters of the cell wall material, such as Young's modulus to the cell growth. This alternative view is prominently and extensively discussed recently by Cosgrove (2015). We think that the cell wall as a material is bound by rules of mechanical physics and although describing the growth of the cell wall by a single parameter such as an elastic modulus may be oversimplification, any changes in the cell wall due to enzymatic modifications can be somehow reflected by a set of pertinent mechanical parameter. Nonetheless, further studies are warranted to assess these two paradigms and potentially link the apparently diverging views.

Uniaxial testing is the simplest tensile test condition but does not correlate well with the stress pattern the cell wall experiences *in vivo*. The stress exerted on plant cell walls by the turgor pressure is biaxial, although the relative stress experienced in the different directions depends on cell geometry. To simulate the *in vivo* loading conditions, multiaxial tension tests may, therefore, reveal new and more relevant aspects of wall behavior. Biaxial loading also eliminates the Poisson's effect generated in uniaxial testing by contraction of the specimen in the direction transverse to the elongation (Fig. 7-2D). Since the cross-section of the specimen is reduced, this contraction can lead to the underestimation of the elastic modulus when the initial cross-section of the specimen is used (definition of engineering stress). This is specifically important for the cell wall as the Poisson's effect can cause different magnitudes of narrowing depending on the alignment of cellulose microfibrils with regard to sample axis. Contraction can cause the irreversible alignment of microfibrils and produces strains prior to rupture that would not occur under biaxial stress *in vivo* (Chanliaud et al., 2002). Loading the sample in all directions can eliminate such effects. Biaxial stress can be applied by many methods, depending on factors such as specimen geometry (for example, refer to Bursa and Zemanek, 2008; Chen and Matthews, 1993; Olsson, 2011). A simple and *in vivo* way of biaxial tension test for intact

cells is to record the changes in cell dimension with and without turgor pressure. For instance, Sanati Nezhad et al. (2013) measured the diameter and length of the pollen tube before and after the release of turgor through bursting and thus identified the moduli of the wall in both longitudinal and transverse directions.

A more technically demanding type of biaxial tensile test especially suited to flat specimens is the hydraulic bulge test that is based on applying a pressure gradient on the two faces of a thin film specimen held in a circular frame. This generates a spherical bulge towards the lower pressure side (for instance see Bargel et al., 2004; Chen and Matthews, 1993) (Fig. 7-2E). The pressure and displacement of the emerging semi-spherical cap are used to plot the stress-strain graph. The system can also be used for creep or relaxation experiments. Several studies have attempted to develop the mathematical grounds for relating the stress-strain relationship of this test to mechanical parameters of the specimen. Alternatively, finite element method can be used to this end, as done by Chanliaud et al. (2002) who employed uni- and biaxial tension tests to study the mechanical behavior of the cell wall under turgor pressure. In this study *Acetobacter xylinus* based cellulose served as plant cell wall analog. Pure cellulose and its composite with pectin or xyloglucan were tested. The results demonstrated that addition of pectin to cellulose causes a decrease in the modulus while providing more extensibility. While the cellulose network had a high modulus, a low extensibility, and a brittle fracture behavior, adding xyloglucan to the network was found to increase compliance and time-dependent viscoelastic behavior.

Deducing the mechanical properties of individual cell walls from the apparent tensile modulus determined through tissue scale mechanical characterization must be interpreted with caution. A load applied to a strip of tissue is not necessarily carried equally by all cell walls composing the tissue. Variations in cell size and geometry and the contraction of the cells during stretching modify the load carrying contribution of individual wall segments. Further, the intercellular interface material, the middle lamella, also contributes to the tensile properties of the tissue (Zamil and Geitmann, 2017). The putative non-uniform strain fields arising in tissue samples due to these features may compromise the ability of the values measured by force-displacement sensors to directly reflect the average mechanical properties of the sample. Using videomicroscopy in conjunction with tensile testing can provide information on the strain field

and non-uniform strain conditions through digital image correlation techniques (Hild and Roux, 2006; Pan et al., 2009). Full-field measurements of the strain acquired by imaging (such as by monitoring the displacement of fluorescent fiduciary markers) combined with a reverse finite element analysis (will be discussed later) can be used to quantitatively determine the local material data (for an example of this approach in plant context refer to Kim et al., 2015). Using this strategy allows determination of tissue level and subcellular stress and strains from a heterogeneous strain field. This allows for a closer scrutiny of properties of individual cell walls under tension. Further, with hydrated tissue samples, the contribution of turgor pressure in the apparent stiffness must be accounted for (for example by measuring the tensile properties under various osmotic conditions). Furthermore, as with all other mechanical testing techniques, the rate dependency must be accounted for. The rate at which a force is applied to stretch the sample is important as at slow loading rate time-dependent properties can emerge which will be superimposed on the ideally elastic (instantaneous) values. Moreover, depending on the speed the measured behavior may reflect the properties of different populations of fibers. Tensile testing is a classic, yet powerful mechanical test of great relevance to reveal in-plane properties of cell walls. However, clearly assigning the mechanical properties measured at multicellular scale to the wall of individual cells is an averaging exercise at best and demands robust protocols for determining a multitude of variables that have the potential to influence the measured data.

7.7 Application of MEMS and microfluidics in mechanical characterization of plant cells

Advances in micromachining techniques in integrated circuits have enabled the fabrication of microelectromechanical systems (MEMS), miniature sized devices with components in the range of a few to hundreds of micrometers. MEMS either consist of passive mechanical microstructures such as cantilevers, or they can incorporate transducers and microelectronics integrated on or off chip. MEMS transducers can be classified as either actuators or sensors. With these components, MEMS can sense and manipulate their physical environment. For example, forces can be measured by quantifying the deflection of calibrated cantilevers. MEMS also enable the incorporation of force or displacement controlled actuators (Loh et al., 2009). The working mechanisms of MEMS transducers exploit the physical properties of materials

such as electrostatic, magnetic, piezoelectric or thermal effects, chosen based on considerations for the particular application such as required maximum displacement, force or resolution (Bell et al., 2005). The nature of MEMS-based tests typically falls in categories described in previous sections such as tensile testing or indentation (Bell et al., 2005; Loh et al., 2009), but allows the miniaturization of the testing framework to enable single cell or subcellular manipulation and simultaneous microscopic visualization, either by light or electron microscopy.

One of the promising examples of a MEMS approach to quantify the mechanics of growing tissues is exemplified in work by Zhao et al. (2013). The authors developed a MEMS-based culture system to study tensile properties of a microtissue construct of fibroblasts and type-I collagen. The system consists of miniature PDMS wells each accommodating two vertical microcantilevers. The deflection of beams was induced by an external off-chip magnetic field and visualized using optical microscopy. Knowing the deformation behavior of the cantilevers based on their material and geometry, the forces applied by the tip of the cantilevers to the specimen can be calculated. With this MEMS-based tensile device, the authors studied not only microtissue stiffness but also active contractile forces exerted by the microtissue.

MEMS-based devices have only been developed for few plant-based applications, for example for tensile testing of subcellular strips of onion cell wall. Zamil et al. (2013) developed a novel method to perform microtensile tests on plant cell wall fragments–with dimensions of only a few micrometers—using an off-chip piezoelectric actuator with submicron force and displacement resolution (Fig. 7-3A). The advantage of this approach is that it allowed characterization of the tensile properties of the cell wall specimen in many orientations regarding the main axis of cell growth. Using focused ion beam milling, fragments as small as 5×15 μm were excised and mounted on the MEMS-based tensile device adapted from Haque and Saif (2002). The off-chip piezoelectric actuator delivered a controlled displacement to the MEMS chip. The MEMS chip, composed of mechanically compliant structures transferred the displacement in a controlled on-axis manner to the cell wall specimen mounted on the chip. The forces delivered to the sample were calculable by observing the deflection of an on-chip beam (force sensor) integrated perpendicular to the axis of loading, using scanning electron microscopy. Sample gripping was accomplished using focused platinum deposition. Using this

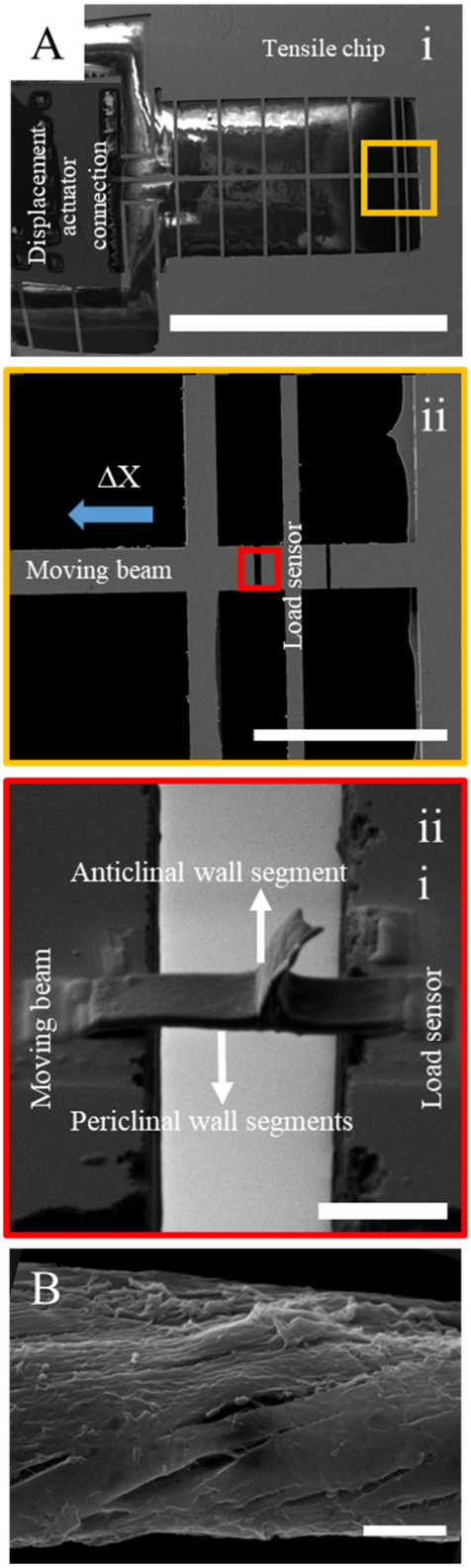

Figure 7-3. A) (i) and (ii): electron micrographs of the MEMS-based tensile device developed by (Zamil et al., 2013). An off-chip displacement transducer moves the horizontal "moving beam" that is stabilized by lateral beams. The force sensor is a beam of known compliance. Displacement of this beam is visually recorded. (iii): a fragment of an abaxial onion cell wall containing the periclinal walls and a portion of the anticlinal wall is being stretched. **B)** Cracks indicating the mechanical anisotropy in Solanum pollen tube wall following removal of pectin and chemical fixation. Scale bars= 4mm (A (i)), 300 µm (A (ii)), 10 µm (A (iii)) and 3 µm (B).

tensile testing configuration, the authors characterized the tensile modulus and the fracture stress and strain of the plant sample. The technique proposed by Zamil et al. has a great potential in understanding the subcellular scale mechanics of the cell wall by eliminating the complexity of the multicellularity of tissue. However, it is only suitable for either dry or rehydrated samples. Since scanning electron microscopy is required to monitor sample deformation, the vacuum in the device has the potential to change the hydration state of the cell wall fragments, thus limiting the slippage of the network components relative to each other potentially resulting in brittle fracture of the specimen as deduced from their results. The results indicated no significant differences in tensile modulus of the cell wall fragments along the major and minor axes of cell growth, although the difference in fracture strengths was significant. Using MEMS at small scales, the physical behavior measured can deviate from macroscale experiments. At smaller scales, other forces such as capillary or surface adhesion forces can become considerable. Zamil et al. (2015) used this to their advantage in another study by exploiting static friction between the hydrated tissue and superpolished surface of the silicon chip to fix the sample on the tensile testing device instead of using glue. When operating at microscale dimensions, water loss can occur rapidly resulting in a significant change in mechanical properties. However, continuous supply of water is impossible when taking advantage of surface adhesion forces. Using this MEMS-based tensile technique Zamil et al. also studied the tensile properties of the middle lamella (Zamil and Geitmann, 2017; Zamil et al., 2014) (Fig. 7-3A (iii)). Interestingly, they found that the middle lamella, and the wall fragments containing middle lamella, are considerably stronger than the wall fragments that lack this interface. Eventually, at microscales, the mechanical properties of the specimens such as Young's modulus can be sensitive to the size and the region of sampling, since the material included in the small specimen can differ substantially from bulk properties of the tissue when tested at a larger scale tensile test. For instance, if a small region with high concentration of aligned cellulose "superbundles" is cut for microtensile testing, the results can differ significantly from an area with lower cellulose aggregation, while neither reflect overall tissue properties. The body of research in this field is scarce for now and warrants further investigation.

Living cells are dynamic structures that sense and modify their mechanical environment and adapt to their surrounding as a result of such interactions. To study the relationship between

the external cues and cell mechanics, devices are needed that can affordably simulate an adjustable physiological environment and measure the mechanical properties of cells with minimal disturbances. Microfluidic devices are designed to enable the control and manipulation of minute volumes of fluids containing living cells. MEMS fabrication techniques can be used in the design of flow sensors, microchannels, microvalves and micropumps to be employed in microfluidic devices with biological applications (Ashraf et al., 2011).

Fabrication of microfluidic devices from transparent materials such as polydimethylsiloxane (PDMS) provides optical properties required for live imaging of cellular events using conventional microscopes. Microfluidic devices have several advantages over conventional macroscopic cell visualization and assessment techniques. Microfluidic devices enable a simulation of the *in vivo* environment regarding fluid flow and physical challenges. They allow precise targeting of live cells by chemical agents such as hormones and growth factors, to study the physical response of cells. By calculated design of the microchannels and controlling the fluid velocity to ensure a very low Reynolds number flow, forces applied to the cell can be fine-tuned (dominated by viscous forces proportional to the square of the fluid velocity). Results obtained by microfluidic devices are highly reproducible, and a high number of cells can be tested in a short period. The high throughput and low cost of production of microfluidic devices enabling many parallel experiments give them an edge in studying the physical properties of cells.

For mammalian cells, microfluidics has been used in cell sorting and mechanical phenotyping including applications in cancer diagnosis (Dahl et al., 2015; Remmerbach et al., 2009; Wang et al., 2013). Agudelo et al. (2013) developed a microfluidic platform that allows manipulating single, tip growing plant and fungal cells for mechanical testing—the TipChip. Sanati Nezhad et al. (2013) used this platform to study the flexural rigidity of growing pollen tubes, the delivery organ of sperm cells in plants. In the study, growing pollen tubes were deflected by a transversely oriented laminar flow of a fluid. The authors used finite element method to model the pollen tube as a thin-walled cylindrical tube exposed to fluid drag and extracted the Young's modulus of the cell wall. The calculations for this bending test showed little sensitivity to absence or presence of a 0.4 MPa turgor pressure assumed for reverse modeling. In another study Sanati Nezhad et al. (2013) used the TipChip to measure the

penetrative forces of growing pollen tubes. The elongating tubes' capacity to deform the elastic PDMS material forming narrow microchannels was used to calculate this parameter. While the elastic PDMS walls of the microchannels represented a passive obstacle, Hu et al. (2017) used active deformation of the pollen tube by compression to calculate the turgor pressure and wall stiffness of lily pollen tubes. Finite element modeling was used to inversely provide a range of geometrical and mechanical parameters that could fit the compression experiment. The solutions of an undetermined system with more unknowns (i.e. wall's Young's modulus and thickness, as well as the turgor pressure) than the equations (modes of experiments) are not unique and were presented as a space of possible solutions. While the changes of turgor pressure resulting from the large deformation during compression were not accounted for in the models, this approach is interesting and exemplifies the potential of microfluidics for cell mechanical studies. The ease of the fabrication process of microfluidic devices and the versatility of the experimental design features can be exploited in many research approaches but have yet to be explored for multicellular plant tissues.

7.8 Insight through failure: tear and fracture to investigate cell wall mechanics and cell-cell adhesion

The mechanical testing techniques reviewed so far, except for the common application of tensile strain, are all rather non-destructive or minimally invasive. However, observing the failure and fracture of a material can provide us with valuable insight on its structural properties. Therefore, we propose that tear and fracture can yield information on plant cell wall mechanics, at both cellular and tissue scales.

Fracture of the tissue material gives us insight on not only the adhesion between cells but also the anisotropic nature of the cell material. In fiber reinforced composite materials, cracks follow the dominant orientation of the fibers. In short-fiber reinforced plastics, a crack applied at an angle to principal fiber orientation changes direction to propagate along the fibers. When fibers are oriented at 0° or 90° to the loading direction, macroscopic observation suggests that the crack path is perpendicular to the loading direction (Tanaka et al., 2014), but microscopically, the crack follows a zigzag path attempting to avoid crossing individual fibers. Consistent with this concept, Aouar et al. (2010) used the orientation of crack propagation in

pollen tubes as a proxy to identify cellulose orientation and overall mechanical anisotropy of the cell wall (Fig. 7-3B). Since cracks involved the entire thickness of the wall, this method provided information that eludes scanning electron microscopic or AFM-based methods, which can only look at the inner- or outer-most layers of the wall. It must be noted that the cracks were obtained by partially removing the pectin network following chemical fixation to reveal the cellulose microfibrils. Actual tensile properties of the native wall might, therefore, be different depending on the relative contribution of pectin to the overall properties. Studies of crack propagation in untreated, hydrated cell wall material will be crucial to investigate the role of pectin chemistry or that of parameters characterizing cellulose such as its crystallinity on the anisotropy of the polymer network.

7.9 The dynamic duo: modeling to gain insight on experimental observation

Models attempting to examine the mechanics of cells fall into two categories: predictive (or forward) and interpretative (or backward) models. Predictive models can be surrogates used to test a concept and study an observed phenomenon by incorporating several rules and constraints, such as those used to simulate cell morphogenesis or the reversible movement of stomatal guard cells that we have reviewed in a different paper (Bidhendi and Geitmann, 2018a). Backward models are fit to series of experimental data to extract unknown quantitative parameters such as elastic moduli. Forward models can be physical or can encompass mathematical and computational models of the plant cell. Physical models allow for reconstruction of the problem at any scale, visualizing the contribution of different structural parameters. Application of physical models related to plant cell and tissue mechanics has remained relatively scarce compared to mathematical models. One of the early examples of this class for plant cells is a physical model simulating the stomatal opening governed by turgor pressure using a pair of balloons locally reinforced by adhesive tapes, representative of radial reinforcement by cellulose (Aylor et al., 1973). Braybrook and Peaucelle (2013) used a silicon replica of the *Arabidopsis* shoot apex to explore the effect of surface curvature on the registered force of indentation. Since a presumably isotropic material is used, changes in indentation force can indicate the influence of surface topology on indentation readings. These physical models of the plant epidermis are

surface mock-ups, however, and cannot inform on details of individual cell behavior or that of internal tissues. Development of additive manufacturing techniques has opened the door to printing 3D physical models (Stansbury and Idacavage, 2016; Zou et al., 2016). Using 3D printing techniques, mock-ups of cells and tissues can be produced for concept tests allowing for a control over the level of details and scaling the sample dimensions. Small dimensions encountered with plant tissues with primary cell walls, often demands custom-made solutions. This ranges from the need for miniaturized testing devices, configurations enabling in situ microscopy of strains, challenges with sample handling, employment of high-end sensors with a reasonable signal to noise ratio and maintaining a proper temperature and humidity control during the test. All these result in a steep increase in expenses as dimensions decrease. 3D printing can provide a way to avoid the otherwise cumbersome testing requirements. If one or a few parameters are of interest to study, such as the effect of cell shape or cell wall anisotropy on tissue response, 3D-printed materials can incorporate only the variable of interest keeping the other factors constant (such as inherent variation between cells within a tissue, temperature or humidity effects etc.). Scaling up the sample dimensions also allows for testing on commonly available universal testing platforms to circumvent the need for costly miniature load cells, vibration isolation and sophisticated imaging set-ups. It is now possible to choose between several materials such as various plastics that can be isotropic or directionally reinforced composites. However, use of 3D printing comes with challenges. For instance, the direction of printing and layer thickness have been shown to affect the mechanical properties of the products (for example see Farzadi et al., 2014). If the printed samples are surrogates for mechanical testing of plant tissues, an important issue to be considered is that even if the material used for 3D printing is isotropic, the layered nature of the construct may render its behavior anisotropic. However, we believe that additive manufacturing techniques such as 3D printing or subtractive manufacturing such as laser cutting and engraving will prove highly useful to investigate the mechanics of plant cell wall, notably because they allow for upscaling the dimensions. Additionally, these techniques can be complementary to in silico simulations not only to provide experimental validation for the simulations but to explore the realms where the constitutive laws or numerical implementation of the materials behavior is missing or physical phenomena are still not well understood such as in exploring the mechanics of failure and fracture (for instance see Mirkhalaf et al., 2014).

Analytical or computational mechanical models have been widely used for both forward and backward models. For recent reviews of models of primary plant cell wall refer to (Bidhendi and Geitmann, 2018a; Geitmann and Dyson, 2014). Analytical solutions are attractive due to their simplicity. However, often, owing to the highly complex behavior of biological materials, sophisticated contact conditions between the experimental device (e.g., AFM probe tip) and the specimen and geometrical nonlinearities, acquiring an analytical solution to extract the mechanical parameters is not practical (Ali et al., 2014). Even if analytical solutions exist, their range of application and reliability is limited to assumptions made in their development. Interpreting material parameters from force-indentation data is often made based on the Hertz model which assumes the material as infinite homogeneous half-space that is linearly elastic, and it accounts only for small depths of indentation compared to the specimen thickness. To overcome these limitations, numerical models can be developed to incorporate more realistic material, geometry, and boundary conditions. The finite element modeling method has been used extensively and represents a promising solution for complex problems of material and geometrical nonlinearity. So far, several finite element models have been developed to either interpret (i.e. quantify) the experimental data (Bolduc et al., 2006; Dintwa et al., 2011; Forouzesh et al., 2013; Hayot et al., 2012; Milani et al., 2011; Routier-Kierzkowska et al., 2012) or to analyze the behavior of plant cells (Cooke et al., 1976; Dupuy et al., 2010; Fayant et al., 2010; Hamant et al., 2008; Kha et al., 2010; Kierzkowski et al., 2012; Sampathkumar et al., 2014a; Yi and Puri, 2012).

To quantitatively analyze experimental data based on modeling, the choice of an appropriate material model is of vital importance. In most finite element studies of plant cell walls, the cell wall material behavior is considered as linearly elastic. However, this assumption only holds for small deformations, inconsistent with the fact that in many tensile experiments the strain may reach 50% or more (Pieczywek and Zdunek, 2014). Further, tensile testing of cell wall material has demonstrated nonlinear behavior and strain-stiffening, which is typical of biological materials (Chanliaud et al., 2002; Pieczywek and Zdunek, 2014; Wang et al., 2004). In plant material, such strain-stiffening may arise from either pectin (Michon et al., 2004; Williams et al., 2008) or cellulose-xyloglucan (Abasolo et al., 2009) networks. Therefore, even in the elastic regime, a linear elastic modulus may not sufficiently describe the material behavior

of the cell wall. Such elastic strain-stiffening behavior may be inherent to the polymeric interaction of the cell wall and differs from the presumably plastic stiffening demonstrated in some of the so-called "biphasic" behavior of the cell wall (Vanstreels et al., 2005). The cell wall, similar to other biological materials, can exhibit strain-rate-dependent deformation behavior. The time or rate dependency can be attributed to either viscoelastic or poroelastic effects. In viscoelastic consideration, the time-dependent behavior of cell wall can result from the viscous behavior of each class of wall biopolymers or their individual interactions due to slippage of the bonds. Poroelastic material behavior, which results from fluid flow through the saturated porous solid structure, can also mimic the time and deformation-rate dependent behavior of the viscoelastic materials closely. In both types of material models, at higher strain rates or short timescales, the material will not have sufficient time to exhibit the viscous properties or those generated by the relatively slow fluid flow through pores. Therefore, at high strain rates, the behavior of the material approaches that of a purely elastic solid. At slower strain rates, the viscoelastic or poroelastic effect will emerge resulting in nonlinear behavior of the material with diminished stiffness. Therefore, the time scale of the deformations, the state of hydration, and the composition of the specimen should dictate whether these perspectives should be incorporated into a model.

In most studies of plant cell wall mechanics, the tested plant tissue is considered a continuum neglecting its cellular nature. However, the shape and orientation of the cells *per se* may affect the apparent mechanical properties of the specimen (this differs from the effect of cell topology on measured forces described in indentation testing). Multiscale modeling approaches can, therefore, be adopted to unravel the cell wall mechanical contribution from the effect of cellularity of the material. Pieczywek and Zdunek (2014) investigated the behavior of onion epidermis tissue under tensile testing by finite element modeling considering realistic geometries of epidermal cells. However, in this study, only the anticlinal walls were modeled (resulting in an open honeycomb-like structure) and the periclinal walls that presumably comprise the dominant portion of the load-bearing body in an epidermis strip were left out. Further studies must incorporate the periclinal walls and hydrostatic pressure to investigate shape and cellularity effects on the mechanical behavior of plant tissues. Such an approach enables the study of cell shape in directional properties of the epidermis. Computation times for

such a geometrically complex model can be reduced by using repetitive units of a representative volume element (RVE) consisting of a small group of adjacent cells that can be assembled in silico to form extended tissues (Ptashnyk and Seguin, 2016; Zamil et al., 2017) (Fig. 7-4C). Finally, aside from geometrical multiscale models of plant tissue and cells, understanding of cell wall behavior would be remarkably enhanced if models could correlate the macroscopic deformation of plant materials to cell wall macromolecular structures such as cellulose orientation and alignment. A few studies have taken this path but are applied only to a spatially limited unit volume of the cell wall (Kha et al., 2010; Yi and Puri, 2012). For these models to be reliable, further information on mechanical properties of individual polysaccharides of the cell wall and their mechanical interactions are needed. Eventually, the availability of ever-improving computing power has provided us with the possibility of building *massively multiscale* models of the cell wall material and geometry to link the observed tissue level behavior to cell wall components—an insight we have so far sought rather indirectly. With such a philosophy in mind, two modeling strategies are of particular interest: substructuring and submodeling which can be considered as bottom-up and top-down approaches, respectively. Substructuring can be broadly defined as the analysis of the behavior of a large-scale system from the behavior of its components (Fig. 7-4A-D). In a submodeling approach, we can zoom in, to study the behavior of a component from the cues generated at the macro scale (e.g., Fig. 7-4A, B, E and F), plasma membrane-level stress and strains from the wind or a water drop on the leaf surface). These procedures are independent of each other although shown in the same figure.

7.10 Conclusion and outlook

Each technique used in the investigation of cell mechanics invariably comes with a set of strengths and limitations. While techniques such as indentation or acoustic technique can provide information on the elastic moduli of the cell wall at a subcellular scale, the measurement of elastic properties needs to be approached with care for correlation of the measured values with in-plane mechanical properties of the material. Further, acoustic techniques are still in their infancy and studies must evaluate their usefulness in determining plant cell wall elastic and viscoelastic properties. Tensile testing allows for a direct measurement of the in-plane properties

B) Finite element models are developed to investigate the cumulative behavior of the macromolecular assembly inferred from (A) (for e.g. refer to Kha et al., 2010; Yi and Puri, 2012). The results of this should be compared against subcellular mechanical tests (e.g., Zamil et al., 2013).

C) Behavior of a cell or a representative volume element (RVE) containing a few cells (e.g., Ptashnyk and Seguin, 2016; Zamil et al., 2017), is derived by incorporating (B) as the material model.

D) Mechanical behavior of the whole tissue under external load is predicted by incorporating (C) to build up a tissue (end result of the substructuring).

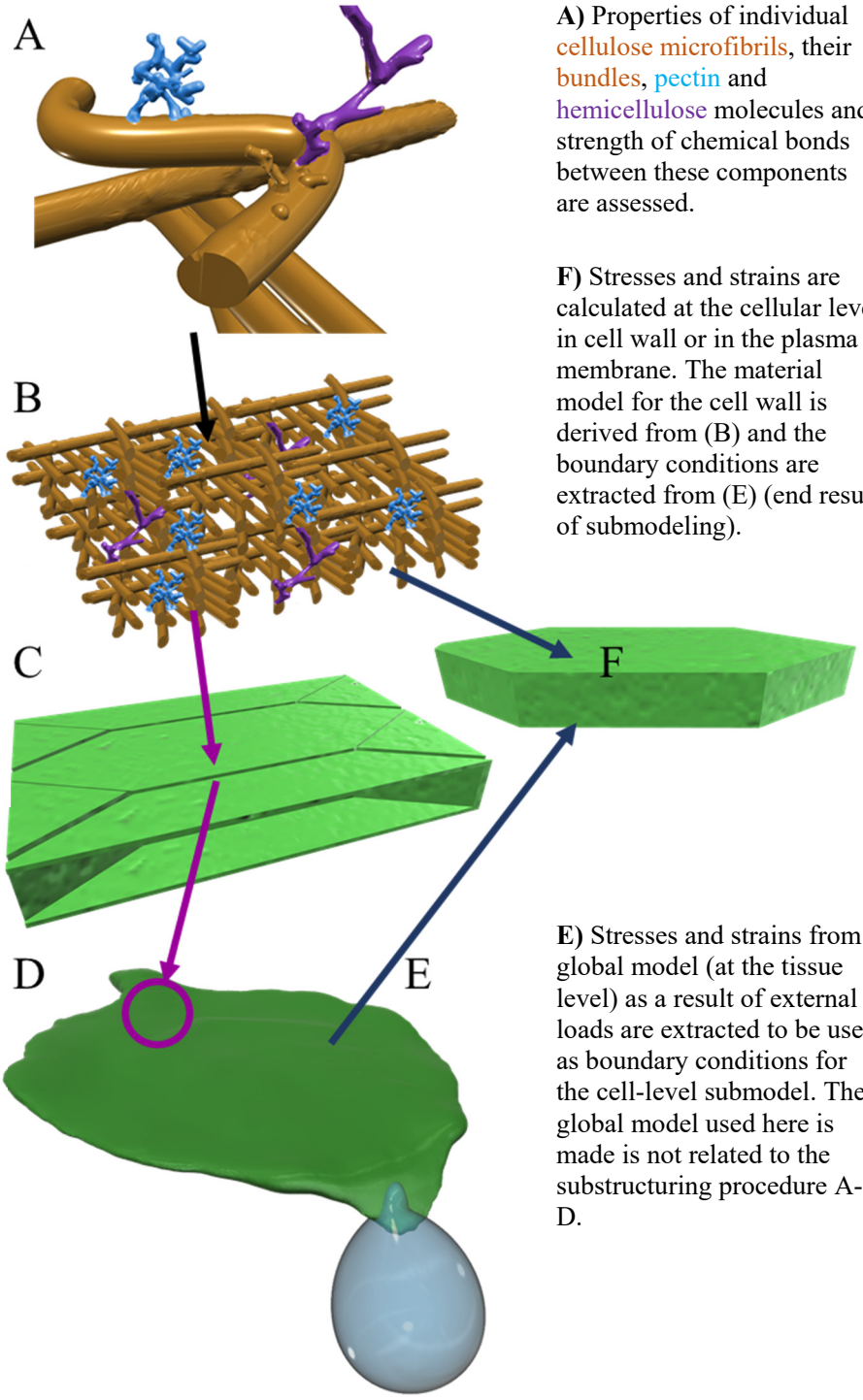

A) Properties of individual cellulose microfibrils, their bundles, pectin and hemicellulose molecules and strength of chemical bonds between these components are assessed.

F) Stresses and strains are calculated at the cellular level in cell wall or in the plasma membrane. The material model for the cell wall is derived from (B) and the boundary conditions are extracted from (E) (end result of submodeling).

E) Stresses and strains from a global model (at the tissue level) as a result of external loads are extracted to be used as boundary conditions for the cell-level submodel. The global model used here is made is not related to the substructuring procedure A-D.

Figure 7-4. Multiscale models can be used to study **(A-D)** the behavior of the plant at tissue level in terms of growth behavior or under external loads such as wind, rain or insects in a substructuring approach (black and magenta arrows) or **(A-B-F** and **E-F)** stresses and strains on a single cell generated by tissue-wide loads due to growth or external forces in a submodeling approach (black and blue arrows).

of the samples, with relatively direct calculations. However, this test is technically rather challenging to perform in a meaningful manner and it is generally invasive, limiting its usefulness for time-course studies requiring repeated measurements of a sample. Further, inferring the subcellular data from tissue level tensile tests using digital image correlation and inverse modeling is experimentally and computationally rather complex. MEMS have shown a great potential to study the cell walls of single cells and can incorporate all other types of mechanical loads and real-time imaging. Fracture and tear of the cell wall allow for the investigation of the cell wall molecular network, mechanical anisotropy and cell adhesions, but it is destructive. In all types of measurements, turgor pressure is a factor that can affect the perceived stiffness of the cell wall, and therefore it must be accounted for. Further, the turgor pressure *per se* can affect the growth of the cell wall and may not be necessarily identical for all cells in a given zone of the tissue. Therefore, measurement of the turgor pressure is warranted in the context of both cell growth and measurements of its viscoelastic properties. We think that studies are needed to compare and benchmark the outcomes of different techniques. This will enhance our understanding of how cell walls behave under different types of loading and allows establishing standard protocols for these tests. Such protocols should define sample dimensions and loading rates to make comparisons across studies possible. Multiscale models can link the modification of the cell wall at the molecular level to cell and tissue behavior, which is important both in the context of cell growth and the cell's ability to sense and respond to the external mechanical cues. Ultimately, while values for strain and stiffness, or visco-elastoplastic properties can be studied experimentally, assessment of the stress distribution in plant cells and tissues is generally done indirectly—through modeling. In recent years, techniques have been developed for animal cell mechanics, such as insertion of microbubbles or introduction of fluorescently tagged reporter proteins, which allow for visualization of mechanical forces between or within cells (Campàs et al., 2014; Guo et al., 2014). Development of similar tools to visualize the stress status in the cell wall or the magnitude of the turgor will be invaluable to study cell growth and plant morphogenesis.

7.11 Acknowledgements

We would like to thank M. Shafayet Zamil for providing us with electron micrographs of the MEMS-based tensile chip depicted in Fig. 7-3A. We would also like to thank Leila Aouar and Youssef Chebli for granting us permission to use their pollen tube micrograph in Fig. 7-3B. Research in the Geitmann lab is funded by Discovery and Accelerator Grants from the National Science and Engineering Research Council of Canada.

7.12 Competing financial interests

The authors declare no competing financial interests.

Annex 2

Chapter 8: Tensile testing of primary plant cells and tissues

Amir J Bidhendi[1], Anja Geitmann[1,2,*]

[1]Institut de Recherche en Biologie Végétale, Département de sciences biologiques

Université de Montréal, Montreal, Quebec, H1X 2B2, Canada

[2]Department of Plant Science, McGill University, Macdonald Campus, 21111 Lakeshore, Ste-Anne-de-Bellevue, Québec H9X 3V9, Canada

*Address correspondence to: Anja Geitmann (geitmann.aes@mcgill.ca)

This is an author-produced version of the book chapter by Bidhendi and Geitmann (2018b) published in Plant Biomechanics. The version of record is available online at: https://link.springer.com/chapter/10.1007/978-3-319-79099-2_15, doi.org/10.1007/978-3-319-79099-2_15

Reprinted by permission from Springer: Plant Biomechanics, A. Geitmann, J. Gril (editors) (2018)

8.1 Abstract

The primary cell wall controls plant growth and morphogenesis but also determines the structural resilience of nonwoody plant organs. The predominant mechanical role of the primary cell wall lies in its ability to resist or conform to tensile forces. Assessing the tensile properties of the cell wall, therefore, is fundamental for both biomechanics and mechanobiology. Tensile testing is a classic approach used for the mechanical characterization of materials. Various loading strategies such as monotonic or, cyclic loading or creep or relaxation allow for analysis of the material response in terms of elastic, viscoelastic, and failure properties. Here, we discuss tensile testing strategies for plant samples with primary cell walls with the aim to provide a practical guide that highlights challenges and offers solutions for the design, execution, and interpretation of such tests.

Keywords: Mechanical characterization, Micromechanics, Cell wall mechanics, Tension test, Uniaxial tensile test, Biaxial testing, Young's modulus, Cellulose, Primary cell wall, Anisotropy, Inverse finite element analysis, Multiscale, *Arabidopsis*

8.2 Introduction

Mechanical testing of material is an essential element in the toolbox of biomechanical research. Understanding how wood breaks, how it resists compression and bending stresses is essential in its use as a construction material or to understand how trees respond to external stresses such as wind and gravity. The resistance to damage of fruit after harvest determines the storage and handling procedures. To be meaningful, mechanical tests should mimic relevant stress types that the biological material experiences during its lifetime. Typical tests for woody plant tissues are three-point bending or compression tests, whereas fruits are typically tested under compression or impact loading.

The mechanical properties of plant tissues are not only relevant for the plant to withstand and respond to externally applied forces but are also involved in internal processes such as plant development and differentiation. The primary cell wall, characteristic of growing cells, is typically between a few tens of nanometers and a few microns depending on the species, the organ of interest as well as cell type (Derbyshire et al., 2007; Zamil et al., 2013). During plant development, at a cellular scale, the forces driving cellular expansion are generated internally by the turgor pressure that acts on the inner face of primary cell walls. As a result of this, a net permanent expansion of the cell wall results under tension that is interpreted as growth. To be consistent with this stress type, the methods used to measure the mechanical properties of plant material in the context of developmental processes need to relate to the tensile behavior of the cell wall. Such pertinent mechanical tests do not only provide information on the mechanical behavior of the plant materials regarding stiffness or failure but also produce vital ingredients for mathematical models. Modeling approaches such as those based on finite element (FE) method attempt to explore phenomena such as cell growth, morphogenesis or organogenesis to elucidate the underlying biology or to guide future experimental strategies (Bidhendi and Geitmann, 2018a). The quality of the predictions made by models is greatly augmented if actual quantitative information can be obtained from mechanical tests. In this chapter, the focus is on tensile testing related to primary plant tissues. The concepts of tensile testing, an introductory guide to tensile experiment components, and the challenges involved in its implementation are discussed.

Woody plant tissues are formed by the secondary xylem, a tissue that depending on the species, comprises only a few different cell types most of which have lignified cell walls. From a macroscopic point of view, wood tissues are, therefore, relatively homogenous. Depending on the scale at which measurements are performed, a block of wood behaves relatively uniformly albeit with significant anisotropy because of the longitudinal arrangements of cells and the presence of growth rings. Interpretation of tensile test results of entire tissues can, therefore, be used to deduce the mechanical properties of single cells in relatively straightforward manner. Herbaceous plant organs, on the other hand, possess different types of tissues including turgid primary tissues such as parenchyma, collenchyma, and sclerenchymatous tissues such as primary xylem. Because of this heterogeneous composition, the analysis of tensile tests administered to whole primary organs needs to consider the spatial variation of mechanical behavior within the organ. Similar considerations are made in the chapter "Bending stress in plant stems: models and assumptions" for bending tests by Stubbs et al. (2018).

The mechanics of woody tissue is dominated by the lignin and cellulose-rich secondary wall of the sclerenchymatous wood cells. Primary plant cell walls, on the other hand, are composed of several types of polysaccharides, proteins, ions, and a significant amount of water. Lignin is absent from the primary wall, and cellulose, while abundant, is less organized and dominant than in the secondary wall. Cellulose is still considered to be a major load-bearing component, however, since due to a low tensile compliance, its spatial arrangement can determine the magnitude and orientation of anisotropy in the cell wall (Baskin, 2005; Cosgrove, 2005). Because of the biochemical complexity of the material, the roles of polymers other than cellulose are rather prominent in defining the mechanics of primary plant cell wall (Bidhendi and Geitmann, 2016). The chemical configuration of pectin, for instance, is associated with the regulation of cell and tissue growth (Bidhendi and Geitmann, 2016; Palin and Geitmann, 2012), organogenesis and the ripening of fruits (Braybrook and Peaucelle, 2013; Prasanna et al., 2007). Therefore, the visualization of cell wall polysaccharides has been an important tool to understand the plant cell structural makeup. However, in many studies, the spatial information on the distribution of cell wall components has been used directly to make inferences on cell mechanics, which, unless accompanied by mechanical testing data, remain inconclusive. The reason is that the relationship between the chemical changes and mechanics is not

straightforward. Highly methylesterified pectin in the tip, where the growth occurs in pollen tubes, is associated with a low stiffness as shown by microindentation techniques (Chebli et al., 2012; Zerzour et al., 2009). Yet, pectin de-esterification is found to be associated with local softening in the shoot apical meristem, where it seems to be a prerequisite for organogenesis or growth anisotropy (Braybrook and Peaucelle, 2013; Peaucelle et al., 2015). This is not to mention the ultrastructural changes in the cell, such as changes in wall thickness or cell shape that are often not accounted for in studies focusing on the chemistry of wall polymer alone (Bidhendi and Geitmann, 2018a). Therefore, visualization of cell wall composition needs to be associated with mechanical tests and in silico experiments to determine the consequence of specific changes in cell wall chemistry (Bidhendi and Geitmann, 2016).

The mechanics of the primary plant cell wall regulate both irreversible and reversible plant processes. Among the reversible processes are those regulating the opening and closing of stomatal pores or the pulvini-driven motion of plant leaves. While in silico modeling has helped to understand the mechanical underpinnings of these mechanisms (Bidhendi and Geitmann, 2018a; Cooke et al., 1976; Forterre et al., 2005), limited experimental work exists to determine the mechanical properties of these structures quantitatively. One of the primary challenges is the type of mechanical test and the scale at which relevant tests should be performed to yield meaningful information.

Mechanical testing is an essential tool for correlating cell wall chemistry and shape to growth and movement in plant cells and tissues. As a result, many mechanical testing techniques have been developed or adapted to study the mechanics of plant cell walls over the past two decades. Micro- and nanoindentation techniques (Bolduc et al., 2006; Milani et al., 2013; Peaucelle et al., 2015; Routier-Kierzkowska et al., 2012; Zerzour et al., 2009), tensile testing (Phyo et al., 2017; Saxe et al., 2016; Zamil et al., 2013), and various forms of acoustics-based microscopy (Gadalla et al., 2014) have been used to this end. These techniques offer a spectrum of force and spatial resolution and each is associated with its own strengths and limitations. For instance, if the deforming force has out-of-plane components with regard to the plane of the specimen, as in indentation experiments, correlating the measured stiffness with in-plane properties of the cell wall is not always straightforward (Eder et al., 2013; Milani et al., 2013). Tensile testing allows for an in-plane stretch of the specimen, and therefore, produces data that

are more tangibly relevant for turgor-induced stretch of the cell wall during cell growth. This aspect makes tensile testing a major mechanical test for the characterization of thin anisotropic primary plant cell walls.

Tensile testing for the assessment of primary plant cell wall mechanics can be classified into two categories. In the first approach, the sample is stretched while either the force (creep test) or the length (relaxation test) is kept constant and the variations in the other parameter are monitored. This approach of tensile testing seeks to identify the time-dependent properties of the specimen. Creep test is the more prevalent type of testing in this category which is also referred to as extensiometry. The creep approach is often employed to investigate the role of enzymes, temperature, and other agents in the modulation of cell wall properties. Important conclusions have been drawn on the roles of agents such as expansins and pH (Cosgrove, 1998; Durachko and Cosgrove, 2009). The second approach in tensile testing is to stretch the specimen until failure with the aim to extract passive mechanical properties such as stiffness, yield or strength. The data from this approach are also relevant for cell growth since they can provide information on the orientation of cellulose and bonding of other wall polymers. For instance, tensile testing of adaxial onion epidermis has shown a higher stiffness parallel to the main axis of cell growth while in the transverse direction the tissue appeared to be more extensible. This tissue behavior is interpreted in terms of the mean longitudinal orientation of cellulose microfibrils in cells of this tissue (Vanstreels et al., 2005). Therefore, this approach of tensile testing can be used to study the cell wall anisotropy which, along with time-dependent enzymatic modification of the cell wall provides a full scenario under which the cell grows or the tissue achieves its functional mechanical properties. The first approach and experiments related to cell wall extensibility are covered in chapter “Cell wall expansion as viewed by the creep method” (Suslov and Vissenberg, 2018).

In this chapter, we focus on the second approach, the classic tensile test. Tensile testing of plant specimens can be exploited to acquire essential information across multiple scales, from the organ-level to the subcellular scale. The plant root, for instance, requires cell wall pliability at the cellular level to grow, yet its overall material and structure should be able to withstand environmental stresses and be rigid enough to penetrate the soil without buckling. Therefore, the mechanical evaluation of root tissue can provide insight into its developmental stages and

identify the parameters that a root should possess for the survival of the plant in a specific soil and environment. Chimungu et al. (2015) observed that the tensile strength of root specimens decreases with the diameter. It was shown that the tensile properties of the stele predominate the overall root tensile strength while the cortical properties such as cell count and thickness were shown to affect the bending and buckling properties of the root. Saxe et al. (2016) studied the effect of age on mechanics of the elongated zone in etiolated *Arabidopsis* hypocotyls. They correlated the mechanics of the elongated zone to material density, geometry, and cellulose content. Their results suggest that the tensile stiffness of the samples may increase over a period of growth with no apparent increase in cellulose content implying a role for other components such as pectin (for related reading refer to Bidhendi and Geitmann, 2016; Phyo et al., 2017). Such an interesting approach combining tensile testing with biochemical analysis enables unraveling the contribution of different wall biopolymers and cell shape to macroscale organ properties.

8.3 Tensile testing parameters and methods

Tensile testing requires gripping a specimen either at two ends (uniaxial testing) or its circumference or along two axes (biaxial testing) and applying a pulling force. Tensile testing can be performed under strain (or displacement) control or force (stress or load) control. In the former, the rate of opening of the device "jaw" or elongation of the specimen is regulated while in the latter the magnitude of the extending force is adjusted. These modes are not to be mistaken with creep or relaxation experiments where either the strain or stress is kept constant. Load application stretches the specimen, and upon release of the force it either returns to its original dimensions immediately (elastic deformation), remains at the stretch-induced dimension (plastic deformation), or slowly returns partially or fully to its original dimensions (viscoelastic or anelastic). During stretching, the force corresponding to the elongation is recorded. For a uniaxial tension test, the force-displacement data points are used to derive a stress-strain graph as

$\sigma = \frac{F}{A_0}$ and $\varepsilon = \frac{L - L_0}{L_0}$

σ and ε are engineering stress and strain. A_0 and L_0 are original cross-section area and length of the specimen prior to onset of the experiment. A typical engineering stress-strain graph is depicted in Fig. 8-1A. The curve may consist of three main zones. A transient "toe" region may indicate initial straightening of the specimen or rearrangement of its load-bearing components. The elastic regime in which deformations are recoverable is followed by the plastic zone, where elastic and permanent deformations occur in parallel. It should be noted, however, that many biological materials such as plant tissues, can exhibit considerably different stress-strain behaviors with the marked zones either hard to distinguish or entirely absent (see the engineering stress–strain curve from a tensile test on onion epidermis in Fig. 8-1B). From this graph, several mechanical parameters of the sample can be obtained. These parameters include the Young's modulus E, the yield strength σ_Y, the engineering ultimate strength σ_U and fracture strength σ_F. The Young's modulus indicates the material's resistance to deform linearly and is determined from the slope of the linear reversible portion of the stress-strain curve. Yield strength corresponds to the stress values at which the specimen begins to deform permanently. This measure is often difficult to pinpoint precisely since plastic deformations can occur even at low strains. Ultimate engineering tensile strength or simply engineering tensile strength corresponds to the highest stress in the engineering stress-strain graph. This corresponds to maximum force occurring prior to fracture divided by the original cross-section area. If the cross-section changes dramatically over the experiment, sometimes an average cross-section is used. Fracture strength corresponds to the stress at fracture point. For materials exhibiting brittle fracture, tensile and fracture strengths can be close to each other. However, for ductile failure, the fracture strength is lower than the ultimate strength on a tensile testing graph based on "engineering" stress and strains. Other than engineering stress-strain curves, true stress-strain calculation accounts for changes in cross-section area of the specimen (generally a reduction) to calculate the stresses. This becomes more prominent in the plastic zone, at least for ductile materials with a tendency for necking (a phenomenon characterized by narrowing and a decrease in the cross-section of the specimen prior to failure; this is not to be confused with reversible lateral contraction of the material referred to as the Poisson's effect that occurs even in the small deformations in the elastic regime. However, necking does not seem to be a characteristic of plant materials) (Fig. 8-1A). True stresses and strains can be calculated as

$\sigma_T = \sigma\,(1+\varepsilon)$ and $\varepsilon_T = ln\,(1+\varepsilon)$

In small strains, despite the lateral contraction of the specimen, the difference between the engineering and true graphs is negligible. However, beyond yielding and especially necking, the difference can be more dramatic. While the engineering stress in the specimen decreases after necking due to decrease in force required to stretch the sample, the true stress continues to increase since the effective cross-section is getting smaller in sample. Tensile tests allow for evaluation of the fracture behavior of the material and determination of fracture toughness. Fracture toughness is a measure of the resistance of the material against the propagation of existing cracks and tears. Such experiments can be carried out, for instance, by tension of a tissue with a preexisting notch. The area below the engineering stress-strain curve up to the elastic limit indicates the strain energy per volume stored and relates to "resilience", while if the curve is considered up to fracture, the area relates to tensile "toughness". Poisson's ratio, ν, measured at the elastic zone, provides information on the extent of the material shrinkage in directions perpendicular to that of the applied stress. Poisson's ratio can be determined based on

$$\nu = -\frac{\varepsilon_{lateral}}{\varepsilon_{axial}}$$

$\varepsilon_{lateral}$ and ε_{axial} correspond to strains in perpendicular to and along the stress direction, respectively. Note that since most common materials contract laterally when stretched, $\varepsilon_{lateral}$ is negative, and therefore the Poisson's ratio holds a positive value. Most isotropic elastic materials hold a Poisson's ratio between 0 and 0.5. In case of a near 0 Poisson's ratio, the material does not considerably strain laterally when strained axially. This applies, for example, to cork and is exploited in its application to seal bottles (Silva et al., 2005). When squeezed, cork does not expand in other directions which facilitates its insertion into and removal from the bottle's neck. A Poisson's ratio of 0.5 refers to an incompressible material behavior, where the volume changes through longitudinal increase and lateral contraction cancel each other out. For anisotropic materials, the Poisson's ratio differs based on the direction and, unlike for isotropic materials, the value is not confined to a particular range (Norris, 2006; Ting, 2004; Ting and Chen, 2005). It might be interesting to note that Poisson's ratio can even hold negative values. "Auxetic" materials with a negative Poisson's ratio, counterintuitively, expand in the transverse

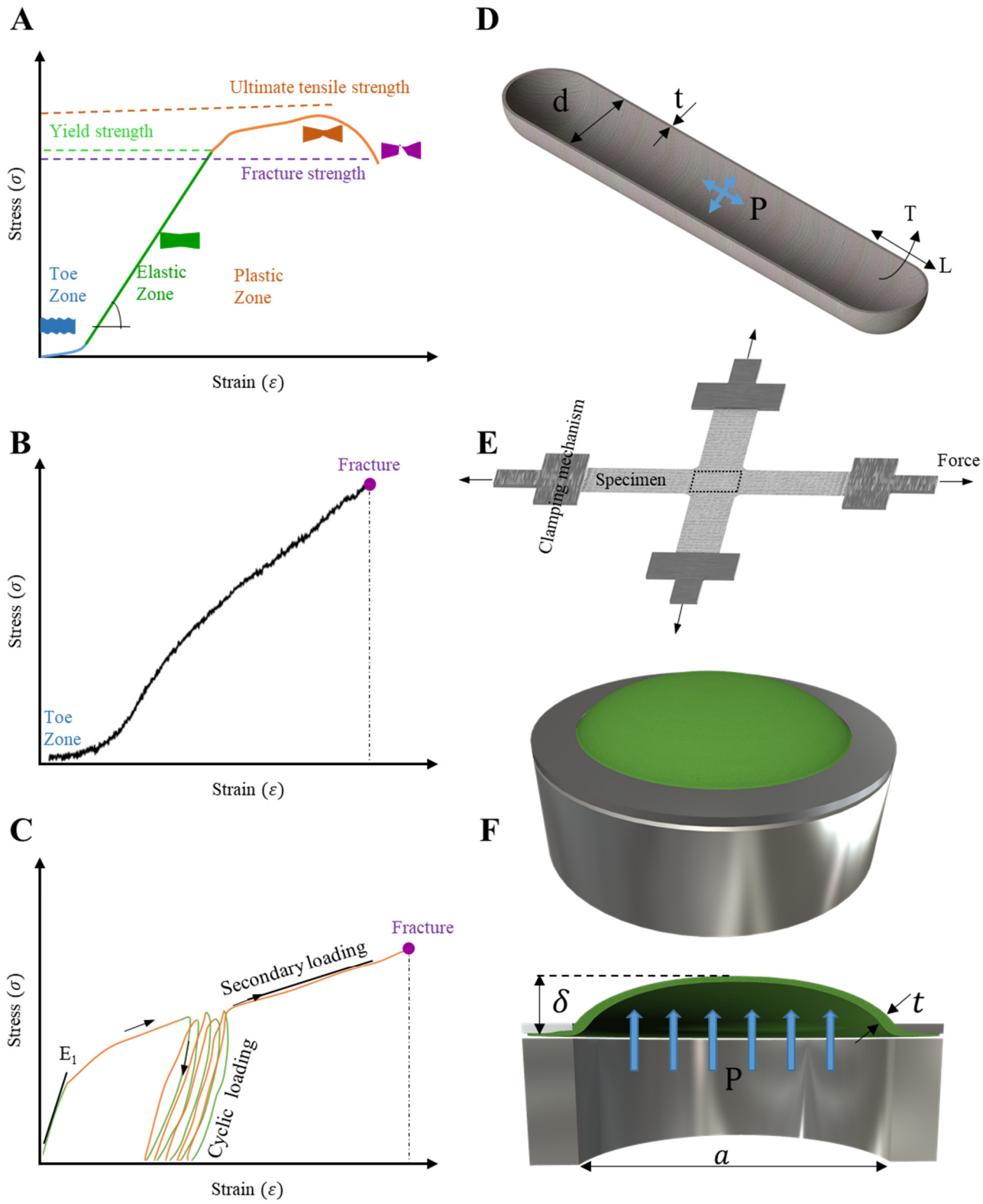
A
Ultimate tensile strength
Yield strength
Fracture strength
Stress (σ)
Toe Zone
Elastic Zone
Plastic Zone
Strain (ε)
B
Fracture
Stress (σ)
Toe Zone
Strain (ε)
C
Fracture
Secondary loading
E1
Cyclic loading
Stress (σ)
Strain (ε)
D
d
t
P
T
L
E
Clamping mechanism
Specimen
Force
F
δ
t
P
a

Figure 8-1. A) Schematic of a typical strain–stress graph obtained from the tensile test. Various zones of material behavior are indicated. **B)** Graph of experimental tensile test carried out on an onion tissue up to failure. **C)** A generic cyclic tensile testing pattern applied to onion epidermal specimen similar to the study conducted by Vanstreels et al. (2005). The initial loading is followed by a number of loading–unloading cycles. The specimen is eventually loaded up to failure. **D)** Cutaway view of a thin-walled cylindrical vessel under pressure (P), with a thickness of (t) and a diameter (d). T and L represent transverse and longitudinal directions, respectively. **E)** Schematic of a biaxial tensile test cruciform specimen. **F)** Bulge test of a flat specimen. The pressure gradient working on the specimen results in a hemispherical bulge of the sample. The displacement of the specimen at the center (δ), thickness (t), diameter (a) and the hydraulic pressure (P) are used to derive the material behavior of the specimen.

dimensions while being stretched uniaxially. This is often due to a particular internal structure, for example, that of the polymer network or shape of unit cells (Mir et al., 2014). Auxetic materials are, however, rare in nature and are mostly synthetic. Most common materials including plant materials contract to compensate for elongation in the other dimension to preserve the volume. The magnitude of this contraction is correlated with the microstructure but also with the state of hydration. The presence of water in the porous network renders the material less compressible if the short force exertion time or impermissible solid network prevents any water movement through the sample microstructure.

When plastic and elastic behaviors occur combined, the components need to be distinguished to correctly deduce the mechanical properties. Experimentally, this can be achieved by closing the "jaw" of the tensile tester until the force read from the sensor reaches zero. The difference between the length at which the force becomes zero upon unloading and the mechanical zero at which the experiment started constitutes the permanent deformation. If further recovery eventually occurs, but not instantly, the material exhibits viscoelastic behavior. Most biological materials do exhibit viscoelastic behavior if given enough time. Therefore, whether to account for viscous effects is a matter of the time frame of the experiment and whether such a time frame is of biological relevance (*i.e.*, may occur *in vivo*).

Uniaxial testing is experimentally easiest to execute, and the obtained data are informative, certainly for plant organs that primarily grow longitudinally such as stems or roots. However, it is important to realize that even in uniaxially growing cells, the stress applied to the cell wall by the turgor pressure, and by the contact with other cells, is biaxial. Furthermore, a

considerable mechanical anisotropy exists in the cell wall of elongating cells that promotes growth in a preferential direction in the first place. Therefore, the mechanical characterization of plant materials and specifically plant cell wall by uniaxial testing may result in an incomplete representation of their overall mechanical behavior. Further, it has been shown for biological material such as arterial wall tissue—a collagen fiber-reinforced composite—that in uniaxial tests fibers can reorient toward the stress direction. This results in altered stiffness measurements in that direction when compared with biaxial tension test (Zemánek et al., 2009). Indeed, recent studies on onion epidermis have demonstrated that during the uniaxial stretch of the sample, cellulosic bundles passively reorient toward the main direction of the stretch (Kafle et al., 2017; Zhang et al., 2017). A similar result was shown for cellulose microfibrils in wood cells (Keckes et al., 2003). Another complicating factor in uniaxial tensile testing occurs when the stress is applied in a direction that does not align with one of the principal anisotropy axes. This can be the case when the anisotropy is not structurally evident, i.e., not correlated to the cell geometry. Off-axis loading of the anisotropic material results in the development of shear forces between the matrix components (e.g., between fibers and the matrix) in addition to tension. While this effect is also useful for the determination of shear strength of composite materials, it has been shown in a flax fiber composite that the failure mechanism of the sample may vary dramatically based on the angle between the loading and the direction of anisotropy (Shah et al., 2012). Therefore, the elastic modulus and failure parameters derived without knowledge of the tissue anisotropy require further attention.

Biaxial tension tests, in general, comprise two pairs of coaxially applied forces. Biaxial tension tests allow several important experiments such as the application of equal or different tension in two perpendicular directions or a stretch in one direction while the other direction is constrained. An *in vivo* way of applying biaxial tension to the walls of intact cells is to record the changes in cell dimension with and without turgor pressure. The changes in diameter and length of the cell can bear the elastic modulus (or moduli for anisotropic wall properties assumption) of the cell wall. For a thin shell pressure vessel ($\frac{t}{d} \ll 1$) (Fig. 8-1D), the resulting stresses along the two principal axes are

$\sigma_L = \frac{Pd}{4t}$ and $\sigma_T = \frac{Pd}{2t}$

Where P is the internal (e.g., hydrostatic) pressure, t and d are the wall thickness and the diameter of the vessel, and σ_L and σ_T are longitudinal and transverse (hoop) stresses, respectively. It can be seen that the transverse stress is two times greater than the longitudinal stress simply due to the shape (for the same reason barbeque sausages split along their axis). From the inverse of the Hooke's law in three dimensions for a linear isotropic material and with plane stress assumption (variation in stress in thickness of the wall is negligible), it can be shown that

$$\varepsilon_L = \frac{1}{E}(\sigma_L - \nu\sigma_T) \text{ and } \varepsilon_T = \frac{1}{E}(\sigma_T - \nu\sigma_L)$$

Where ε_L and ε_T re longitudinal and transverse strains. The strains can be determined from changes in dimension from microscopic images. The Poisson's ratio, however, needs to be measured separately or adopted from the literature. Approaching an incompressible behavior ($\varepsilon_L + \varepsilon_T + \varepsilon_{th} = 0$ with the subscript *th* denoting the direction of the wall thickness) corresponds to a Poisson's ratio of $\nu = 0.5$. However, as mentioned before, elongated cells rarely have an isotropic wall. In most cases, there exists a preferential orientation of cellulose microfibrils in the circumferential direction, although this may later change to a longitudinal direction due to passive reorientation during cell growth (Anderson et al., 2010; Green, 1960). In such a case, the strains cannot be explained with a single Young's modulus. A special case of anisotropy, the transverse isotropy that corresponds to unidirectional composites can be relevant to the composition of plant cell walls with a relatively well-organized direction of fibers. Simplifying the inverse of Hooke's law written in form of strains for transverse isotropy and plane stress assumptions, the longitudinal and transverse strains can be written as

$$\varepsilon_L = \frac{1}{E_L}(\sigma_L - \nu_{TL}\sigma_T) \text{ and } \varepsilon_T = \frac{1}{E_T}(\sigma_T - \nu_{LT}\sigma_L)$$

Where ν_{LT} and ν_{TL} are the Poisson's ratios. The subscript LT, for instance, denotes the Poisson's ratio effect in the transverse direction due to the strain in the longitudinal direction. In case of incompressible transverse isotropy, it can be shown that

$$\nu_{LT} = \frac{1}{2} \text{ and } \nu_{TL} = 1 - \frac{E_L}{2E_T}$$

Therefore, the strain relationships can be further simplified to (for a more in-depth reading refer to classic books on the theory of elasticity or, for instance, see Argatov and Mishuris, 2015; Bernal et al., 2011)

$E_L = \frac{\sigma_T}{2\varepsilon_L + \frac{4}{3}\varepsilon_T}$ and $E_T = \frac{3}{4}\frac{\sigma_T}{\varepsilon_T}$

Therefore, having measured the axial and transverse strains, Young's moduli in two directions can be calculated based on the above relationships. While this method allows for measurement of the elastic moduli of the cell wall along the two axes, it requires a measurement or a justified assumption of the turgor pressure. In the absence of quantitative information on turgor, the ratio of anisotropy ($\frac{E_L}{E_T}$) can be evaluated using this approach.

A common way of performing biaxial tension test for planar materials is to prepare square or cruciform shapes of the sample to be stretched by a pair of perpendicularly positioned actuators (Hannon and Tiernan, 2008; Lally et al., 2004) (Fig. 8-1E). The elastic and plastic deformations are then analyzed in the midsection of the specimen which should remain stationary by proper adjustment of displacement actuators. Bulge testing is yet another common technique for tensile characterization of both thin and thick films (Small et al., 1994; Srikar and Spearing, 2003; Yu et al., 2016). It has the advantage of not requiring preparation of complex sample shapes or dealing with complex stress distributions in specimens. In the bulge test, the sample can be of circular or square shapes. The specimen is fixed at the open end of a tube and pressure is applied on one side (Fig. 8-1F). Usually, a positive pressure is applied, for instance, by using a viscous silicone oil that does not permeate the specimen (Chanliaud et al., 2002), resulting in the outward bulge of the specimen into a hemispherical profile. Depending on the shape of the membrane specimen, various analytical solutions have been developed to correlate the parameters such as pressure (P), the maximum deflection of the specimen (δ), its diameter (a) and thickness (t) (for instance, refer to Maier-Schneider et al., 1995). Alternatively, inverse FE modeling can be employed to identify the unknown parameters. The maximum deflection at the center of the specimen and the sample thickness can be measured using either tactile techniques or, without contact, through optical methods such as 3D digital image correlation (DIC), and plotted against the pressure of the fluid in the chamber (Machado et al., 2012; Neggers et al., 2014; Nouira et al., 2014; Orthner et al., 2010). This technique also allows for

the determination of the Poisson's ratio of the sample. If the pressure is kept constant, the increase in the bulge size versus time can be used as a creep test to acquire viscoelastic properties of the specimen. Adopting this strategy, Chanliaud et al. (2002) performed uni- and biaxial tension tests to study the mechanical behavior of the cell wall under turgor pressure using *Acetobacter xylinus* based cellulose as plant cell wall analog. Cellulose, cellulose/pectin, and cellulose/xyloglucan composites were tested under tension and compared with FE modeling used to interpret the pressure-displacement test data.

8.4 Tensile testing setup

The tensile setup generally consists of two distinct compartments: sensors and actuator units. In this section, we describe the essentials of a simple uniaxial tensing device. For biaxial testing, a significant number of considerably different configurations have been developed over the years (for instance, refer to a review by Hannon and Tiernan, 2008). However, the concepts remain similar to a great extent. The displacement is generated by a displacement transducer. A wide range of actuators can be used to this end such as mechanical, piezoelectric or pneumatic mechanisms (Fig. 8-2). In motorized lead screw actuators, for instance, rotation of the lead screw by a stepper motor causes linear displacement, similar to the driving mechanism of many syringe pumps. Finely threaded screws in conjunction with precise stepper motors allow for the production of displacements of several centimeters in range and submicrometer in resolution well-suited to displacements required in many micromechanical tensile tests. Several methods exist for measurement of displacement or strain in the specimen. The simplest method is to rely on the displacement values given as inputs to the displacement transducer. However, different sources such as the existence of backlash in the gear system can cause a lag and result in the actual displacement to deviate from the input. As a result, the use of displacement input is not ideal, and instead, the device's "crosshead" or "jaw" motion which is equivalent to the actual displacement of the actuator and the gripping ends can be measured and used. Using gripping end displacement as a measure of sample strain is usually accomplished by readings from a position sensor such as a linear variable differential transformer (LVDT). LVDTs consist of a ferromagnetic core that can move freely without contact in a hollow cylinder equipped with an assembly of primary and secondary coils. The primary coil fed with an AC or DC input voltage

induces a voltage in the secondary coils. The movement of the core, connected from one side to the displacement actuator or a gripping end, in or out of the hollow cylinder changes the amplitude and phase of the voltage induced in secondary coils which constitutes the output signal from the LVDT enabling measurement of that displacement. However, this reading does not take into account the compliance of the loading frame. The loading part of the device including the force sensor, extensions and fixtures can deform along with the specimen during the loading and result in an underestimation of the elastic modulus of the specimen (Sanders et al., 1997). The frame compliance can be corrected by using a rigid mock-sample of known elastic modulus (Turek, 1993). Most times, the device compliance is considered to be a constant, meaning that a linear relationship between the force and the deformation of the loading apparatus is presumed (Sanders et al., 1997). However, this might not always be the case, and nonlinearity might exist resulting in deviation of the measurements based on the specimen being used (Kalidindi et al., 1997). Another method for strain measurements in tensile testing is the use of strain gauges. Strain gauges often but not always refer to thin film patches with an electrical resistance that changes when the patch is deformed (for an example of such a design refer to Pang et al., 2012). Generally, strain gauges refer to the use of such contact patches although sometimes the term is also used for noncontact strain measurement approaches (e.g., see Yamaguchi, 1981). There are numerous types of strain gauges based on their working mechanisms and the working environment they are intended for. However, the contact nature of the strain gauge requires it to be mounted and bonded to the surface of the specimen at various locations. The need for bonding to the specimen and the miniature size of most plant specimens render the use of strain gauges in plant tensile studies challenging. Further, the presence of strain gauges on the sample can affect the behavior of the specimen due to reinforcement or due to the weight of the patch and the connecting wires. Despite all these challenges, they only provide limited information on strains in the whole sample as the information is limited to the location of their installment. Therefore, strain fields and possible inhomogeneities and hotspots outside the installment zones remain undetected (Motra et al., 2014; Soons et al., 2012).

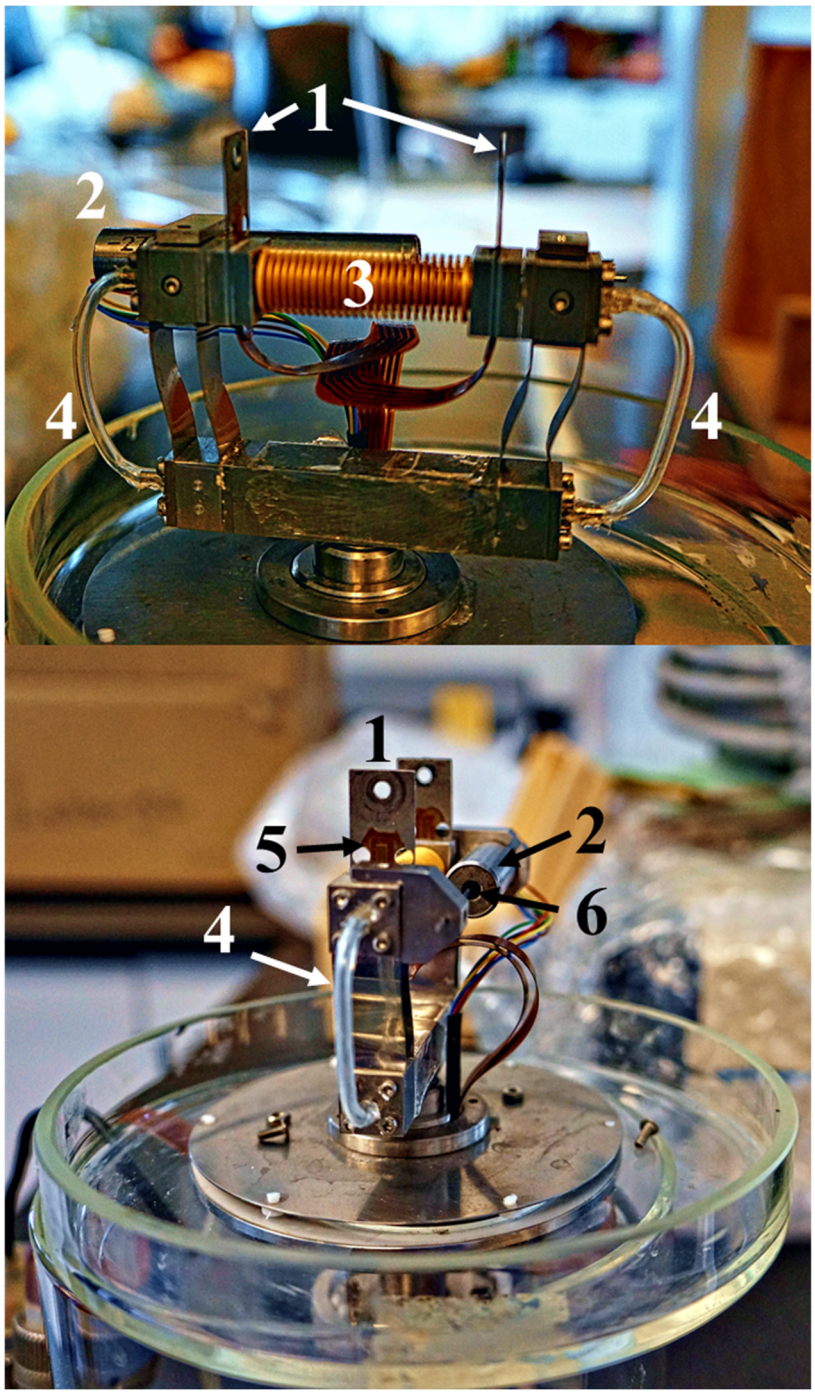

Figure 8-2. A miniaturized tensile testing device developed by Lynch and Lintilhac (1997) allowing for mechanical testing in air and liquid conditions. The testing chamber consists of (1) load shims, (2) LVDT (tube) (3) pneumatic bellows that act as displacement actuator opening or closing the frame driven by air flow (4) adjusted by a control unit based on displacement or force feedback. The deformation of the strain gauges (5) adhered to the load shims is read as the change in the output voltage and translated to forces acting to bend the shims. The displacement of the LVDT core (6) inside the tube reads the displacements.

Extensometers can also make another class of strain measurement techniques. Basic contact extensometers rely on the attachment of a pair of "sensing arms" to two ends of the gauge length of the specimen averaging the strain over this region (for an example of its application refer to Boitier et al., 2000). For plant applications, this method suffers from similar shortcomings as the strain gauges in that it affects the delicate sample and that only average strain data are produced. Noncontact extensiometry approaches, on the other hand, seem very promising for specimens of various texture and sizes, especially in micro- and nanomechanical characterization. Two broad classes of these methods rely on either image matching algorithms or optical interferometry. Matching algorithms such as DIC (Digital Image Correlation) or differential digital image tracking (DDIT) techniques (Sharpe et al., 2007) are based on analysis of consecutive images taken from the sample during the deformation. This is accomplished by means of one or more cameras (2D, 3D or volumetric) or by other techniques such as scanning electron microscopy (Kashfuddoja and Ramji, 2013). A sufficient number of speckles or patterns, either artificial or digital, for DIC (Lava et al., 2009) or intensity peaks on the image for the DDIT are required for comparison and correlation of successive images to carry out full-field measurement of strains in the sample (e.g., Pan et al., 2009; Sutton and Reu, 2017). DIC can provide a subpixel displacement/strain resolution (Hua et al., 2007; Zhou and Goodson, 2001). Another advantage of an image processing-based approach is that rigid body motion (such as that occurring due to slippage of the specimen at clamps) can be accounted and corrected for. Various interferometry techniques have been developed for strain measurement. Electronic speckle pattern interferometry (ESPI), for instance, is one of the common interferometry methods for strain or displacement measurements. In this technique, the sample surface is illuminated with a coherent laser beam. The reflected laser forms a pattern on the image recording setup. Topographical information of the specimen can be acquired based on changes in the phase difference between the reflected and original laser beams that is caused by sample deformation or displacement (Soons et al., 2012; Yang and Ettemeyer, 2003).

Other than displacement actuator and sensors, force sensors comprise another compartment of the tensile device. Forces are measured by one or two load cells that are installed on the gripping ends. Load cells are commonly based on one or more strain gauges. The deflection of the load cell beam results in changes in the electrical resistance of the strain gauge

incorporated into it and, in turn, to a change in the output voltage that is read through an amplifier. The compliance of the load cells can be measured for different loads during the calibration stage and prior to the experiment and be accounted for in the displacement measurements. It is good practice to calibrate the device for force and displacement after mounting all the extensions on which the sample will be fixed, or in case of any change in environmental temperature or humidity. Excluding the weight of the extensions and loading frame from the force and displacement measurements is even more important in vertical setups.

8.5 Common challenges associated with tensile testing

While some mechanical tests such as nanoindentation are relatively easy to perform, correlating the force-displacement data from these tests to in-plane properties of the cell wall, and accounting for complex probe-sample interactions is not straightforward and sometimes demands cumbersome calculations. Tensile testing, on the other hand, is considered a test requiring relatively simple calculations for extraction of the parameters from the experimental data. However, carrying out the experiment itself can be accompanied by many challenges that begin with sample preparation and handling and extend to sample alignment and gripping. Some of these challenges are briefly discussed.

8.6 Measurement of the original values

Obtaining the mechanical parameters of the sample in a tensile test relies on the measurement of several independent variables such as displacement, force, and dimensions of the specimen that serve as inputs for the calculations. The eventual outputs of the tensile test, i.e., stresses and strains, can be only as accurate as the measurements of the independent values allow. Above, we commented on the practical aspects of the force and strain measurements. An important set of input variables used to calculate the tensile testing parameters includes the original length and cross-section area (through diameter or width and thickness) of the specimen. With minute plant specimens such as roots or shoots of *Arabidopsis*, measurements of the original dimensions are typically carried out using optical techniques such as microscopic visualization. The issue here is that other than the considerable biological variability among samples, the errors in measurement of these dimensions can dramatically alter the conclusions of the study. This

becomes significant in situations where small changes in the mechanics of the cells or tissues are being investigated through tensile testing. The changes in mechanical properties of the material over close time points might not be dramatic and could be masked by errors or uncertainties in the measurement of original dimensions. An example of how important the measurement of the initial dimensions can be, even if they add complexity, is provided in a study by Saxe et al. (2016), which tested *Arabidopsis* hypocotyls for their tensile properties. In this study, a subset of hypocotyl samples exhibited decreasing cross-sections with age while in other datasets, no significant age-dependency was observed. The environmental and growth parameters such as humidity and temperature, while able to affect the length of the growing hypocotyls, were shown to not significantly affect the cross-section. The authors calculated the stress based on dividing the force by the cross-section of hypocotyls, as it should be done. However, the biologically atypical reduction in diameter, whether caused by biological variation or other, may significantly influence the determined stress values, thus making a clear-cut interpretation more difficult. An increase in the number of biological replicates will increase the reliability of the conclusions drawn from experimental data. It will also be helpful to define methods and protocols that ascertain precise, consistent and reproducible quantification of dimensions and other parameters with potential influence on the measured mechanical values.

8.7 Gripping

One of the prominent technical challenges associated with tensile testing, particularly for soft and small tissue specimens, is fixing the ends of the sample. Stress concentration and damage near the grip can result in premature failure of the specimen near the gripping ends. With cylindrical samples such as root, shoot or hook structures such as prickles and spines, the ends of the specimen can be tied using a resistant nondeforming thread such as Kevlar (for instance, refer to Gallenmüller et al., 2015). However, this requires a certain minimum size of the sample and the thread compliance needs to be accounted for in calculations. Clamping or grips are one of the common methods to hold the ends of the tensile specimen. Various grades of sandpaper can be used between the specimen and the clamp to prevent slippage. Sometimes, a layer of a softer material is placed between the sample and camping mechanism to reduce the risk of specimen damage (Hervy et al., 2017). Clamp gripping methods tend to induce damage and are

particularly prone to slippage, due to reasons such as the non-flat geometry of the samples and moisture. Further, in case of the model plant *Arabidopsis*, the minute size of its organs makes solutions such as tying unviable. Piercing structures such as fishing hooks have also been used for tensile testing of soft tissue such as porcine arterial specimens (Lally et al., 2004). More invasive gripping techniques such as fishing hooks inevitably result in failure of the tissue around the fixture and are better suited for determination of tensile modulus and not strength. Due to these reasons, application of fast-curing glues such as cyanoacrylate can represent an attractive alternative. A high viscosity glue is preferable to prevent diffusion into the specimen as it can dramatically alter the mechanical properties of the tissue. Still, using a glue is not without its challenges. The glued area tends to shrink upon curing which causes a prestress in the sample. This is easily observable as the force sensors begin to register increasing tensile forces as the glue is curing. Therefore, it is necessary to release this tension prior to the onset of the tensile test. This can be done by closing the "jaw" of the device up to a point that the force reads zero which can be set as the mechanical zero for displacement. Further, moisture on the hydrated tissue can hinder curing of the glue. Since the tissue needs to be kept constantly hydrated, if not thoroughly submerged in liquid, acquiring a perfect fusion in a reasonable time may not be trivial. As the dimensions get smaller in micromechanical tests, the importance of applying glue droplets small enough to prevent bleeding into the gauge length of the specimen becomes significant. In such scenarios, techniques such as platinum deposition have been used to fix the microscale specimen on the loading frame, for instance, to study a subcellular patch of the onion cell wall under the scanning electron microscope (Zamil et al., 2013). Handling and mounting thin film specimens such as an epidermis is challenging since they are prone to wrinkles and folding that can affect the stress distribution in the sample. Water surface provides a substrate to hold the specimen without wrinkles until mounting. In a recent study on tensile testing of ultrathin films, it was shown that stiction forces such as van der Waals could constitute a gripping mechanism (Kim et al., 2013), a promising approach for ultrathin plant layers.

8.8 Biphasic behavior, effects of the loading rate and preconditioning of the cell wall

An interesting note related to the tensile behavior of the plant cell wall is a reported "biphasic" or "bilinear" behavior in the stress-strain curve. Such behavior is described as the existence of two different slopes in the stress-strain curve that in some cases are associated with a primary and a secondary Young's moduli (Pieczywek and Zdunek, 2014; Spatz et al., 1999; Vanstreels et al., 2005) (Fig. 8-1C). While the existence of a strain-dependent and nonlinear elasticity in the plant cell wall, as also observed in mammalian cells and tissues (e.g., refer to Fabry et al., 2001; Guilak et al., 2014; Kollmannsberger and Fabry, 2011; Mofrad, 2009), is expected, the approach adopted to demonstrate this "bilinear" behavior seems unclear. As seen in Fig. 8-1C depicting a generic form of such graphs, in these studies the second Young's modulus suggesting a secondary elastic behavior is defined after a turning in the graph (likely due to yielding) and on the loading (as opposed to unloading) part of the stress-strain curve. First, the slope of engineering stress-strain curves obtained through tensile testing of many materials does change after yielding. The existence of a slope change in the graph *per se* does not indicate a secondary elastic modulus. Further, Young's modulus is defined based on relatively small strains prior to yielding or upon separating the plastic deformations from the total strain (thus using the unloading data) and is strictly indicative of deformations that are elastic, ε_e (where total strain $\varepsilon_t = \varepsilon_e + \varepsilon_p$). However, in these studies, the loading path is marked for the secondary Young's modulus during a monotonic loading and the deformation seems to be associated with considerable plastic strains. For regions that are not purely elastic, fitting of appropriate elastoplastic models or presenting the data in terms of moduli other than Young's modulus such as tangent modulus, therefore, is more appropriate. Second, while in some studies the transition between the primary and secondary elastic behavior is demonstrated under relatively small strains (less than 5% strain in Spatz et al., 1999), others have demonstrated these two values in a range of over 20% strains (Vanstreels et al., 2005). Besides the monotonic tensile loading, cyclic loading is performed in some studies and seems to suggest that when unloading paths are considered, the slope of the stress-strain curve remains relatively unaffected and comparable to initial cycles (Vanstreels et al., 2005). Therefore, the existence of such bilinearity in the stress-strain behavior of the wall material needs further assessment through analysis of

reversible deformations. Moreover, studies are required to look into underlying wall composition and structures that result in such a putatively biphasic behavior.

Viscoelastic materials exhibit a rate dependency in their deformation behavior. This means, the faster the deformation is applied, the stiffer the tissue appears to be. Such a strain-rate dependency can affect the measurement of stiffness, but also the strength and maximum strain at fracture. Higher loading rates can result in increased apparent stiffness, increased stress, but less strain at fracture (the specimen appears less extensible). It is therefore interesting to investigate to what extent the results obtained by stretching the plant cell wall at different loading rates are comparable. Further, in many cases involving tensile testing of soft tissues, the specimen is preconditioned prior to actual data collection. In many animal tissues, it can be observed that the loading and unloading paths do not coincide (hysteresis). The area between them corresponds to the dissipated energy due to viscous or plastic effects. Further, for some materials, the peak load for the same amount of strain appears to differ in each cycle. Therefore, to obtain reproducible results, the specimen is sometimes "preconditioned" prior to measurements, for calculation of the elastic modulus and tensile strength. This is not to be confused with preconditioning term used in other contexts such as cold acclimation of the plant or removal of turgor pressure before tensile testing. The preconditioning is carried out by repeating the loading and unloading cycles for a certain number of times to reduce the peak force variations and also to some degree the hysteresis prior to actual measurements (Lee et al., 1984). For tendons and ligaments, it has been shown that preconditioning results in an increase in both stiffness and strength of the samples. This has been suggested to be due to an increase in recruitment or reorientation of collagen fibers resisting the tensile loads toward the force field (Miller et al., 2012; Schatzmann et al., 1998). To verify whether preconditioning has caused damage or a permanent deformation in the sample, the toe region of the force-displacement curve can be analyzed. An increase in the length of the toe region (i.e., the existence of some strain without a corresponding force) may indicate permanent deformations in the specimen. The reorientation of fibers that might also depend on their initial distribution, to begin with, may render the preconditioning a questionable practice if original properties of the tissue are of interest. There is a considerable variation between the strains used to precondition the samples among various studies. While some advocate a fraction of the real testing strains for

preconditioning strains, others suggest a full experimental strain to be used before actual data collection and, obviously, this treatment must be reported along with other experimental conditions (Cheng et al., 2009). In case that preconditioning strains were observed to induce damage, either due to fatigue (failure in the material at stresses significantly lower than the ultimate and fracture strengths of the material due to repetitive loading) or simply exceeding the fracture strength, there is a need to settle for lower strains in the actual experiments.

Tensile testing of onion epidermis was also demonstrated to exhibit hysteresis in loading-unloading paths (Vanstreels et al., 2005). The existence of such a load history dependency of the plant tissue is suggested to stem from the presence of wrinkles or adhesion of other structures on the onion sample that unfold and resolve over a number of cycles (Wei et al., 2001). However, in addition to these potential artifacts, the hysteresis and rate dependency seem to be an inherent part of most biological tissues, including plant materials. Tensile testing of onion epidermis has also shown a considerable transient response in the first cycle; a significant difference in stress-strain values between the initial and later loading cycles (Kerstens et al., 2001; Vanstreels et al., 2005; Wei et al., 2001). This phenomenon that might be due to plastic deformations of the matrix occurring in the first cycle, becomes even more interesting when considering the contrasting results reported for the onion epidermis. From the work of Wei et al. a more significant transient response is observable in onion epidermal strips stretched perpendicular to the cell axis compared to the longitudinal one. Other (e.g., Kerstens et al., 2001) report the opposite. Since in these studies, this behavior is correlated with the composite material behavior of the cell wall, e.g., the orientation of cellulose microfibrils, further studies are required to address these different observations.

8.9 Effect of cellularity

A major factor that distinguishes the use of tensile testing for the mechanical characterization of plant specimens from common industrial materials is that plant tissues are made up of cells. Whether the aim is to determine tissue-level mechanical properties or to deduce the cell-level mechanical properties, the cellularity of the material incorporates a number of factors that need to be accounted for when interpreting the experimental data. An immediate consequence of the cellularity is the difference between the effective and geometrical cross-sections of samples.

The effective cross-section is the one that bears the loads. For plant tissues, this area is not the same as the tissue cross-section. If cell wall-level properties are to be deduced from the results, measuring only the portion containing the cell walls by subtracting the void space of cell lumina and intercellular spaces from geometrical (tissue-level) cross-section can be beneficial. However, instead, this is often avoided and the whole cross-section is used in the calculations. In cases where factors such as cell type, cell size, and cell wall thickness are expected to be identical between samples, this is probably an acceptable simplification. In cases where any of these factors are different, a more granular approach should be considered. Saxe et al. (2016) estimated the cell wall density based on the hypocotyl's dry weight and its volume in the hydrated state.

Aside from the measurement of the effective cross-section outlined above, inferring the mean mechanical properties of individual cell walls from tissue-level tensile testing is not straightforward. First, due to the shape of the specimen, cellularity, and presence of borders in the material, the stresses may not be distributed uniformly across the cells. This means that different cells in the tissue can experience different levels of stresses and strains. As a result, the properties of some cells may affect the calculations disproportionately, and the outcome of the tensile test may be a weighted rather than the arithmetic average of the properties of all cells. Additionally, even within a single cell, not all the walls experience the same share of stresses and can be stressed to a varying degree depending on their orientation with regard to the stress field and the cell geometry (Fig. 8-3). To what extent the mechanical properties of individual cells of different shapes and locations affect the overall elasticity of the tissue warrants further studies. Nevertheless, a study on onion epidermal cells has suggested that the growth anisotropy of the cells is correlated with tissue stiffness, with tissue samples with more elongated, higher aspect ratio cells appearing stiffer (Vanstreels et al., 2005). While such differences are generally attributed to the anisotropic composition of the cell wall, it might be also due to cell shape. It should be noted that the apparent stiffness of a structure is determined in part by the properties of its building material, e.g., Young's modulus, porosity, and degree of anisotropy, but also by the geometry of the structure. To better illustrate this, consider a beam with a rectangular cross-section under bending. It can be easily illustrated with a plastic ruler that the beam behaves stiffer under bending when placed with the longer edges of its cross-section vertical or parallel

to the force (due to an increase of the second moment of area). Similarly, it is expected that the individual cells with different shapes resist the tissue-level deformation differently due to their geometry and orientation, affecting their contribution to overall mechanical properties of the tissue. This can confound comparison of the mechanical properties of different tissues with considerably different cell geometries if cell-level mechanical properties are to be inferred and

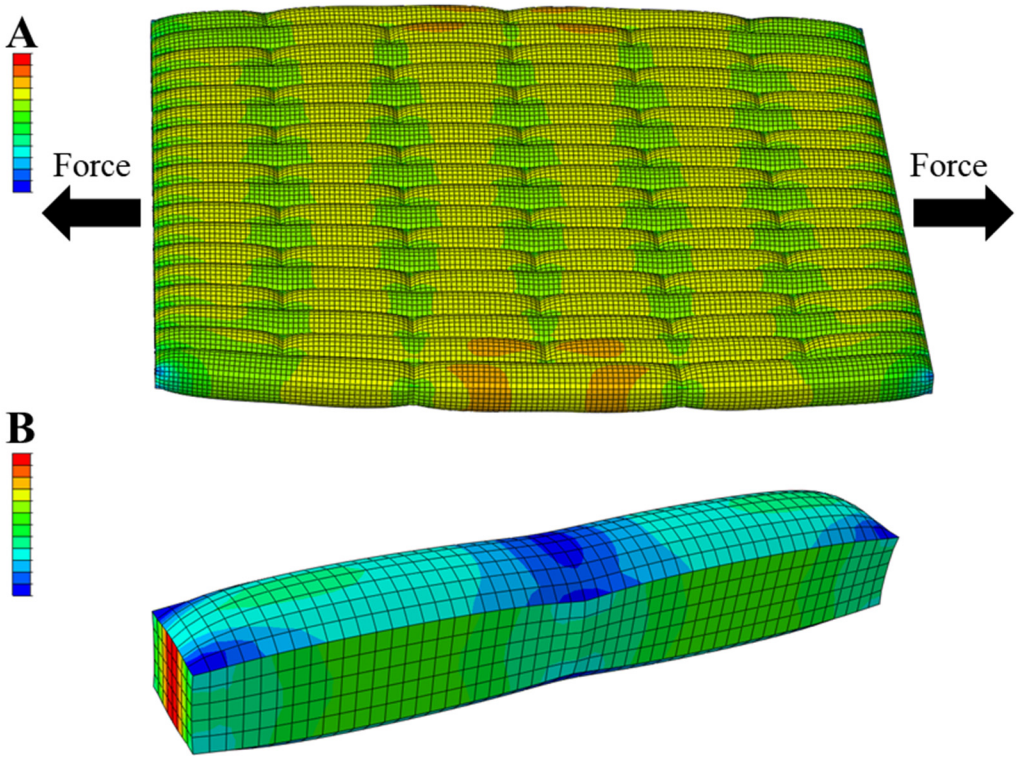

Figure 8-3. Finite element model of a tissue consisting of pressurized elongated cells. The distribution of stresses and strains is not uniform within the tissue **(A)**, and can even vary in different walls of a single cell at subcellular scale **(B)**. Color map represents the magnitude of principal stresses.

correlated to tissue-level behavior. This issue concerns both classes of tensile testing outlined previously. Therefore, studies are required to untangle the contribution of cell geometry and material properties of the cell wall in the mechanical behavior that the tissue exhibits.

Tensile testing can be performed on both turgid and plasmolyzed cells. Turgid tissues are stiffer and reportedly fracture in a brittle manner. On one hand, tensile testing of turgid tissues is interesting since it more closely mimics the state of living plants. On the other hand,

discriminating cell wall properties *per se* from the properties measured when under turgor induced tension requires a comparison between the two hydration states of the sample (Pieczywek and Zdunek, 2014).

Unraveling the mechanical properties of cell walls from the apparent tensile modulus obtained through tissue-scale mechanical characterization requires to also consider the intercellular interface, known as the middle lamella (Pieczywek and Zdunek, 2014; Zamil and Geitmann, 2017). In terms of tensile strength, the role of the middle lamella is intuitive. If tissue failure occurs by the failure at the middle lamella, i.e., cell separation or delamination, the strength of this structure determines the strength of the whole tissue. As explained by the weakest link concept, the fracture of the specimen is determined by the strength of its weakest spot (Freundthal, 1968). If and how the stiffness of the middle lamella also contributes to the tensile stiffness of the whole tissue remains elusive considering its negligible thickness.

To eliminate the compounding features such as cell shape and middle lamella, tensile testing on subcellular patches of the cell wall have been attempted (for instance, refer to Wei et al., 2006; Zamil et al., 2013). Besides the usual technical hurdles, manipulation and observation of the sample while keeping it hydrated are the major challenges at the micron scale. Given the challenges at each length scale, a combination of approaches incorporating macroscale response and micromechanics at the cell level is likely the most promising avenue in many cases. Multiscale experimental and computational strategies that combine tests both at the tissue and subcellular scales, giving consideration to the osmotic status, and integrating the experimental approach with numerical modeling allows for evaluation of the contribution of single cells to tissue-level mechanical properties and, conversely, determination of the cell-level properties from the tissue-level tension experiments. These considerations are equally important in the context of extensiometry and time-dependent studies, where the goal is to infer the effect of cell wall modifying treatments from the creep or relaxation of the whole tissue.

8.10 Nonuniform strain fields and application of optical strain measurement methods

Tensile testing of common industrial materials is often well-documented and protocols regarding dimensions of the testing specimen, mounting and loading conditions are well-defined. These dimensions and proportions are available in various standards provided by organizations such as ISO (International Organization of Standardization) or ASTM (American Society for Testing and Materials). Standards often ask for certain shapes of the specimen such as a so-called “dogbone” geometry or rectangular specimens of certain aspect ratios. The dogbone geometry incorporates a gauge length of a reduced cross-section in the middle part of the specimen and ensures that strains are mainly concentrated and uniform in that region rather than near the clamps. The specimen shape, boundary conditions, and loadings prescribed in these standards ensure accurate, and importantly, reproducible results. In plants, however, the delicate nature of the samples, and the minute dimensions in many cases preclude production of such sample geometries. While some standards exist for tensile testing of thin papers and cardboards such as BS EN ISO 1924, relatively large dimensions, in the order of a few centimeters, are required that do not often correspond well with dimensions of plant tissues (Hervy et al., 2017). Further, if strips need to be prepared, cutting the samples needs to be accurate without tears and flaws at edges that would cause stress concentration, premature failure and influence the mechanical parameters obtained from the test. All samples to be compared should be of same dimensions or at least the gauge length undergoing tension needs to be of same dimensions (Carew et al., 2003; Tsuchiya et al., 1998).

Due to lack of standardized protocols, a great variety of sample shapes (e.g., aspect ratios), often arbitrarily chosen, and even more, variable testing conditions have been used for plant materials. Several studies have demonstrated the sensitivity of tensile testing results to sample dimensions, aspect ratio and geometry (Anssari-Benam et al., 2012; Carew et al., 2003; Hervy et al., 2017). Further, due to errors introduced when measuring the strain based on the motion of the displacement transducer or the crosshead of the tensile device, different sample shapes can result in considerable differences in the calculated tensile modulus even within otherwise standardized samples. Hervy et al. (2017) demonstrated that measurement of stiffness

of cellulose nanopapers shows a considerable dependence on sample geometry. The authors demonstrated that using the optical measurement of strain instead of the opening of the tensile device crosshead reduces the geometry dependence in the estimated mechanical properties. This suggests that size dependence in tensile testing is, at least in part, related to strain measurement (e.g., slippage). The tensile strength defined at failure theoretically does not depend on the specimen size. However, in practice, it has been observed that an increase in sample width can result in a decrease in tensile strength. This can be explained by the weakest link theory. As the width of the specimen increases so does the likelihood of inclusion of weak spots or defects in the sample (Hervy et al., 2017). To add icing on the cake, the cellular nature of the plant tissues, as mentioned previously, and material anisotropy in individual cells, make the strain fields of plant specimens susceptible to inhomogeneity. As a result, the values reported by the force-displacement sensors may not be able to explain directly the phenomena occurring during a tensile test and comparing the mechanical properties of the biological specimens harvested at different stages of development or from tissues featuring intrinsically different cellular arrangement may be problematic. To fully address this concern, noncontact full strain field measurements can be used to acquire local information on the deformation of the sample. Optical extensiometry methods provide an attractive tool for the investigation of deformation within anisotropic and discontinuous materials such as intragranular and boundary movements in granular materials (Hall et al., 2010). The displacement field in subregions of the specimen can be acquired by optical imaging and combined to construct the local strain information. The strain field data can be used to determine the mechanical parameters of the material using approaches such as virtual fields (Grédiac et al., 2002; Promma et al., 2009) or inverse FE method. Through comparing full-field displacement data with the predictions made by the FE model, material parameters can be reverse engineered. An FE model of the tensile test can be developed with inputs of the specimen dimensions (length, width, and thickness) and force recorded from the sensors. The FE-produced displacement field is then compared with the displacement field of the landmarks or fiducial markers. The objective can be defined as the minimization of an error function based on the difference between the in silico and experimentally obtained values which results in the identification of the optimized parameters.

Optical extensiometry techniques are broad in their possible configurations as mentioned for DIC or interferometry approaches (Sutton and Reu, 2017). In the simplest form, they can be carried out by monitoring a few fiducial points on the specimen (such as two pairs of points in axial and transverse directions by Hervy et al., 2017; or four symmetrically placed points in the middle of the square biaxial test specimen by Lally et al., 2004). To increase the number of data points, fiducial markers such as fluorescent beads can be sprayed or fixed on the surface, ideally with a higher density close to the middle and ends of the specimen. The tensile testing device can be placed under a stereo- or confocal microscope to record the displacement of fiducial markers versus the force exerted at two ends of the specimen. Kim et al. (2015)used fluorescent nanobeads as fiducial markers to calculate the microscale deformation of onion epidermis under tension. Application of optical methods in displacement/strain measurements is not limited to tensile testing. For instance, Armour et al. (2015) used fluorescent fiducial markers on the leaf epidermis of *Arabidopsis* to perform a time-lapse study of growth in epidermal pavement cells or Kuchen et al. (2012) used cell corners as landmarks to assess the local growth behavior of leaves.

8.11 Acknowledgements

Research in the Geitmann lab is funded by Discovery and Accelerator Grants from the National Science and Engineering Research Council of Canada and by the Canada Research Chair Program.